New innovative methods for cleaning surfaces using foams based on bio-based surfactants

Carolina Dari

▶ **To cite this version:**

Carolina Dari. New innovative methods for cleaning surfaces using foams based on bio-based surfactants. Food and Nutrition. Université de Lille, 2024. English. NNT : 2024ULILR038 . tel-04846557

HAL Id: tel-04846557

https://theses.hal.science/tel-04846557v1

Submitted on 18 Dec 2024

HAL is a multi-disciplinary open access archive for the deposit and dissemination of scientific research documents, whether they are published or not. The documents may come from teaching and research institutions in France or abroad, or from public or private research centers.

L'archive ouverte pluridisciplinaire **HAL**, est destinée au dépôt et à la diffusion de documents scientifiques de niveau recherche, publiés ou non, émanant des établissements d'enseignement et de recherche français ou étrangers, des laboratoires publics ou privés.

UNIVERSITE DE LILLE – FACULTE DES SCIENCES ET TECHNOLOGIES

École Doctorale de Sciences de la Matière, du Rayonnement et de l'Environnement- SMRE

Unité Matériaux et Transformation- UMET

Thèse préparée et soutenue publiquement par :

Carolina Dari

le 27/09/2024 pour obtenir le grade de :

Docteur de l'Université de Lille

Spécialité : Biotechnologies agroalimentaires, sciences de l'aliment, physiologie

New innovative methods for cleaning surfaces using foams based on bio-based surfactants

Nouvelles méthodes innovantes pour le nettoyage des surfaces à l'aide de mousses à base de tensioactifs biosourcés

Composition du jury :

Présidente :

Mme. Véronique Rataj-Nardello, Professeure, Centrale Lille

Rapporteurs :

Mme. Murielle Rabiller-Baudry, Professeure, Université de Rennes

M. Pierre Bauduin, Directeur de recherche-HDR, CEA, ICSM UMR 5257

Examinateurs :

Mme. Alesia Mikhailovskaia, Chargée de Recherche, Institut de Chimie et des Matériaux Paris-Est

Mme. Florence Rouyer, Maître de conférence-HDR, Université Gustave Eiffel

Directrice :

Mme. Anne-Laure Fameau, Chargée de recherche-HDR, INRAE-UMET

Co-directeur :

M. Thierry Benézech, Directeur de recherche-HDR, INRAE-UMET

Acknowledgements

First, I would like to thank Anne-Laure and Thierry, who trusted me and gave me the opportunity to do this thesis. Special thanks to Anne-Laure, who was there to guide me all along my way, and to whom I would also like to thank for her human qualities, as she was able to help me also outside the workspace.

I would also like to thank all my colleagues at INRAE, Oceane, Angella, Brayan, Helena, Heni, Audrey, Maureen, Amandine, Guillaume, Luisa, Laurent W, Laurent B, Christelle, Thomas, Christine, Maude, Manon, Amelie, Cosmin, Florence, Carolina, Ricardo and Thierry, not only for their help and advice on a scientific level, but also for their friendship and for making every day at INRAE a pleasant and enjoyable place to work.

I would also like to thank my interns, Julien, Laureen and Andrea, who helped me to carry out my work, as well as to test my leadership skills.

I would like to thank my family. Especially my mother, who always cared about my education, as well as giving me self-confidence in life. To my dad, with whom I share a passion for food science. And I would also like to thank my grandmother, my uncles, my brothers and my cousins, for the love they give me, which is the driving force of my life.

Special thanks to Nico Samus, without whom I might not be in Europe doing a thesis. For all the support he gave me during all these years, morally, scientifically and lovingly.

To my Argentinian friends, especially Jupi, Dora, Rama, Juli, for the video calls, the whatsapp messages, that made me feel that I still had them close to me. To my friend Maria, who I made thanks to my stay in Edinburgh.

Last but not least, I want to thank my friends and all the people who made the thesis more than just work at the lab and for whom it is now difficult to leave Lille, especially Nicola, Massimo and Enma.

Table of contents

Table of contents 3

List of figures 8

General Introduction 20

Thesis outputs 24

Chapter 1: Review of literature 26

1.1 Cross-contamination of food by contaminated surfaces 27

1.2 Cleaning of surfaces in food industries 29

1.2.1 Cleaning of open surfaces 31

1.2.2 Cleaning of closed surfaces 32

1.2.3 New eco-friendly cleaning methods in food industries 35

1.3 Foams 36

1.3.1 Foam structure 37

1.3.2 Foam production methods 39

1.3.3 Foam destabilization mechanisms 43

1.4 Surfactants as key foaming agent 44

1.4.1 Surfactant definition and classification 44

1.4.2 Surfactant self-assembly 48

1.4.3 Role of the surfactants on foam production and stability 50

1.5 Foam cleaning 51

1.5.1 Mechanisms involve in foam cleaning 52

1.5.2 Wide range of applications of foams for cleaning purposes 54

1.5.2.1 Foam cleaning in open surfaces (static condition) 54

1.5.2.2 Foam cleaning in closed surfaces (dynamic condition) 58
1.6 Conclusions and objective of the thesis project 64
1.7 References 67
Chapter 2: Foam cleaning in static condition 74
Introduction to chapter 2 75
2.1 Ultrastable and responsive foams based on 10-hydroxystearic acid soap for spores' decontamination 77
2.1.1 Introduction 78
2.1.2 Results and Discussion 80
2.1.2.1 Critical Aggregation Concentration (CAC) of 10-HSA dispersion 80
2.1.2.2 Self-assembled structure and rheological properties at 25°C 81
2.1.2.3 Evolution of the self-assembled structure and rheological properties by increasing temperature 83
2.1.2.4 Foaming properties with time and temperature 85
2.1.2.5 Cleaning of spores contamination on surface by foam imbibition 87
2.1.3 Materials and Methods 90
2.1.3.1 Materials 90
2.1.3.2 Methods 91
2.1.3.3 Viability of spores 94
2.1.4 Conclusions 96
2.1.5 References 98
2.2 Static Foam Cleaning with Sodium Cocoyl Isethionate-Based Foams for Spore Removal from Solid Surfaces 106
2.2.1 Introduction 107

2.2.2 Materials and methods 109
2.2.2.1 Materials 109
2.2.3 Results 115
2.2.3.1 Krafft temperature and Critical Aggregation Concentration of the SCI dispersion 115
2.2.3.2 Characterization of the self-assembled structure at 20 °C and at 50 °C by optical microscopy and SANS 117
2.2.3.3 Characterization of the foams for spores' decontamination 119
2.2.3.4 Foam spores decontamination analysis 122
2.2.4 Conclusions 128
2.2.5 References: 129
Chapter 3: Foam cleaning in dynamic condition 139
Introduction to chapter 3 140
3.1 Decontamination of Spores on Model Stainless-Steel Surface by Using Foams Based on Alkyl Polyglucosides 141
3.1.1 Introduction 142
3.1.2 Results and Discussion 144
3.1.2.1 Model Surfaces, Spores, and Surfactant Solutions Characterization 144
3.1.2.2 Effect of Surfactants on Spore Detachment under Static Conditions 145
3.1.2.3 Effect of Foams on the Detachment of Spores 146
3.1.2.4 Foam Characterizations before and After Flowing Inside the Duct 148
3.1.2.5 Foam Destruction and Recycling of Surfactant Solutions by Filtration 151
3.1.3 Materials and Methods 155
3.1.3.1 Materials 155

3.1.3.2 Methods 157
3.1.4 Conclusions 163
3.1.5 References 164
Chapter 4: Water-in-water emulsion formulation as possible innovative cleaning method. . 169
Introduction to chapter 4 170
4.1 Mixture of fatty alcohols and alkyl polyglucosides stabilizing Water-in-water Emulsions 171
4.1.1 Introduction 172
4.1.2 Materials and Methods 175
4.1.2.1 Materials 175
4.1.2.2 Preparation of the stock solutions 175
4.1.2.3 Preparation of the stabilized W/W emulsions 176
4.1.2.4 Preparation of the foamulsion 177
4.1.2.5 Stability and partial phase diagram of the W/W emulsions 177
4.1.2.6 Structural characterization of W/W emulsions by Small Angle X-ray Scattering (SAXS) 178
4.1.2.7 Determination of the critical micellar concentration (CMC) via surface tension 178
4.1.2.8 Evaluation of the W/W stability by centrifugation 178
4.1.2.9 Statistical Analysis 178
4.1.3 Results and discussion 179
4.1.3.1 Phase diagram of the W/W emulsions 179
4.1.3.2 Long-term stability of W/W emulsions stabilized by LGNs 185
4.1.3.3 Structural characterization of W/W emulsions 187

4.1.3.4 Versatility of the W/W emulsion stabilized by mixture of fatty alcohols and APGs 189

4.1.4 Conclusion 192

4.1.5 References 194

Chapter 5: Conclusions and perspectives 205

5.1 Conclusions 206

5.2 Perspectives 210

5.3 References 211

List of figures

Figure 1.1.1: Scheme showing the different stages of biofilm formation. First some bacteria attach to the surface, and the cellular exopolymer matrix is formed, then more bacteria attach (potentially from other species) and finally, there is a dispersal of the bacteria to the environment. 28

Figure 1.1.2: Scheme of a spore of *Bacillus subtilis*. The presence of the coat is what makes them more resistant to heat and to chemicals, compared to vegetative cells. The figure was reproduced from (McKenney et al., 2013). 29

Figure 1.2.1: Illustration of the Sinner circle. The figure was reproduced from (Basso et al., 2017). 31

Figure 1.2.2: Scheme of a typical CIP system, which mainly consists of four tanks: a water recovery tank (recovers the water from the last rinse of the last cycle, which is then reused as pre-wash water in the next cycle), a tank for the alkaline solution, a tank for the acid solution and a tank for the final rinse water. The figure was reproduced from (Moerman et al., 2014). 34

Figure 1.3.1: Representation of the successive levels of organization of a foam stabilized by surfactants according to their spatial scales from the macroscopic scale to the nanoscale. 37

Figure 1.3.2: Different structures according to liquid fractions. (a) Dry foam. (b) Wet foam. (c) Bubbly liquid. 39

Figure 1.3.3: Foam production methods: (a) Bubbling the gas in a stationary liquid through a porous disc. The figure was repruced from (Denkov, 2004) (b) Double syringe technique. The image was reproduced from (Schad et al., 2021). (c) Gas entrainment and bubble break-up using a kitchen blender. The image was reproduced from (Politova et al., 2018). (d) Different ways to carry out the shaking technique: handshaking, automated shaking using a typical laboratory shaker, automated shaking machine employed for the Bartsch test (from left to right). The third image was reproduced from (Petkova et al., 2021). 43

Figure 1.3.4: Schematic showing the three main mechanisms of destabilization of foams. (a) Drainage. (b) Coalescence. (c) Coarsening. 44

Figure 1.4.1: (a) Surfactant structure. (b) Evolution of the surface tension with surfactant concentration. The CMC indicates the point at which the surface tension reaches the minimum value. 45

Figure 1.4.2: Classification of surfactants according to the charge of the polar head. 46

Figure 1.4.3: (a) Structure of sodium dodecyl sulfate (SDS) (Bruce et al., 2002) (b) Example of the typical structure of an alkyl polyglucoside (Drakontis and Amin, 2020). 47

Figure 1.4.4: Scheme of the values to be considered when calculating the packing parameter (p). 48

Figure 1.4.5: scheme of the different self-assembly that can be formed according to packing parameter (p). (a) Micelles. (b) Vesicles. (c) Bilayers. (d) Inverse micelles. 49

Figure 1.4.6 : Scheme of the scatered techniques. 50

Figure 1.5.1: Scheme of three mechanisms involve in foam cleaning in static condition, using foams with different liquid fractions and sunflower oil as model contaminant. The figure was reproduced from (Schad et al., 2021). 53

Figure 1.5.2: (a) microscopic image of a wafer after a static foam test, at ×5 magnification, showing distinct patterns in the sebum. (b) Scheme of the possible cleaning mechanism associated with a non-wetting and wetting situations. The figure was reproduced from (Jones et al., 2016). 54

Figure 1.5.3: Pictures showing the effect of foams on cleaning oil from glass surfaces. In the foams with a liquid fraction of 5% with and without PFH the imbibition mechanism is promoted, but in the foam without PFH (less stable) the wiping mechanism is also promoting resulting in a better cleaning efficiency. The figure was reproduced from (Schad et al., 2021). 56

Figure 1.5.4: Historical object (left) before cleaning, (center) during cleaning with foam, and (right) after cleaning The figure was reproduced from (Schad et al., 2022b). 57

Figure 1.5.5. Pictures of the pilot set up used for the study of foam flow for nuclear decontamination. The figure was adapted from (Gossard et al., 2022)..... 59

Figure 1.5.6: Schematic diagram of the system called “foam-chain circulation” developped by (Turchet et al., 2002) which consists of altering injections of foam and air at different times. The figure was adapted from (Gossard et al., 2022). 59

Figure 1.5.7: Diagram of the foam flow set up used in the works of Al Saabi et al. et Dallgi et al. (Al Saabi et al., 2021; Dallagi et al., 2022c, 2022b). The figure was adapted from (Dallagi et al., 2022a). 62

Figure 1.6.1 : Scheme of the general procedure to obtain a water-in-water emulsion..... 64

Figure 2.1.1. Surface tension of aqueous solutions of 10-HSA/MEA as a function of the concentration at T = 20 ± 1 °C. 81

Figure 2.1.2. (a) Phase contrast microscopy picture of 10-HSA at 25 °C. (b) SANS intensity profile of 10-HSA at 25 °C. The black line correspond to the best fit of the data described in the Supporting Information. (c) Oscillatory measurements of 10-HSA, elastic G’ (●) and viscous G’’ (○) moduli plotted as a function of the strain amplitude, □ at constant f = 1 Hz at 25 °C..... 83

Figure 2.1.3. (a) Phase contrast microscopy picture of 10-HSA at 65 °C. (b) Variations of elastic G’ (●) and viscous G’’ (○) moduli upon heating. The moduli were measured at □ = 0.1 % and f = 1 Hz. (c) SANS intensity profile of 10-HSA at 75 °C. The line correspond to the best fit of the spectrum de-scribed in the Supporting Information. 85

Figure 2.1.4. (a) Evolution of the foam volume (purple), and of the liquid volume in the foam (green) with time with time at 25 °C. (b) Evolution of the foam stability by measuring the evolution of foam volume with time at different temperatures: 25 °C when multilamellar tubes were present and at 65 °C when spherical micelles were present. 87

Figure 2.1.5. (a) Spores log reduction on the model surface after 30 min for water, 10-HSA disper-sion, hand-shaking (HS) foam, and double syringe (DS) foam. The small letters a-b indicate groups of statistical differences according to Tukey’s test ($p < 0.05$). (b)

Epifluorescence micros-copy pictures of the model surface contaminated by fluorescent spores before cleaning, and (c) af-ter 30 min of cleaning with DS foam. The scale bar represents 50 µm for all the pictures. 89

Figure 2.1.6. Epifluorescence microscopy pictures of the penetration of aqueous dispersion of spores into a double syringe foam with time. t = 0, corresponds to the image taken just after contact with the foam. The scale bar represents 1 mm for all the pictures. 90

Figure 2.1.7. Schematic showing the methodology for spores removal on stainless steel surfaces by using foam: (1) Five drops (1 µl) of the spore suspension were placed on the surface of the model plate with a micropipette; (2) the plates were dried in a oven for 1 h at 30 °C; (3) the soiled plates were then placed in the tubes containing the foams and they were kept in horizontally position for 30 min; (4) each plate was sampled with a dry cotton swab; (5) the swab was put in a tube with 5 mL of sterile Mill-Q water and vortexed for 1 min at 2400 rpm; (6) serial dilutions were made in sterile Milli-Q water for each tube and there were plated in Tryptic Soy Agar and incubated for 24 h at 30 °C; (7) the number of colony forming units (CFU) was counted manually. 96

Figure 2.2.1. Methodology for spores' removal on stainless steel surfaces by using static foam cleaning: (1) The foams were produced by the double syringe method; (2) the soiled plates were placed in petri dishes and the foam was placed on the top of each plate. They were kept in horizontally position for 30 minutes; (4) each plate was sampled with a dry cotton swab (5) the swab was put in a tube with 5mL of sterile Mill-Q water and vortexed for 1 minute at 2400 rpm (6) serial dilutions were made in sterile Milli-Q water for each tube and there were plated in Tryptic Soy Agar and incubated for 24 h at 30 ◦C (7) the number of colony forming units (CFU) was counted manually 115

Figure 2.2.2. Solutions of SCI at 1, 5 and 10 wt.%, from left to right (a) in the form of crystals (room temperature) below the Kraftt temperature (b) in the soluble micellar state leafing to limpid solution above the Krafft temperature 116

Figure 2.2.3. Evolution of the surface tension of aqueous solutions of SCI as a function of the concentration at T= 20 °C ± 1 °C. 117

Figure 2.2.4. SANS profiles for SCI at three concentrations at: (a) 20 °C and (b) 50 °C. The profiles are offset on the vertical scale for clarity. The line corresponds to the best fit described in the main text. 119

Figure 2.2.5. Evolution of the foam height for foams with different liquid fractions (13%, 22% and 27%)..... 120

Figure 2.2.6. Mean bubbles area of foams with different liquid fractions (13%, 22% and 27%) and their bubbles corresponding pictures: (a) at t=0 (b) at t=30 min. The small letters a–b indicate groups of statistical differences according to Tukey's test ($p < 0.05$). 121

Figure 2.2.7. Spore log reduction on the stainless-steel plates after 30 min of static foam cleaning with foams with different liquid fractions (13%, 22% and 27%). The small letters, a, indicate groups of statistical differences according to Tukey's test ($p < 0.05$). 124

Figure 2.2.8. Spore log reduction for different drying times of the Bs PY79 spore's suspension (hydrophilic spores) on the stainless-steel plates after 30 min of static foam cleaning with the foam of 27% liquid fraction. The small letters, a, indicate groups of statistical differences according to Tukey's test ($p < 0.05$). 126

Figure 2.2.9. Spore log reduction for different drying times of the Bs PY79 spsI spore's suspension (hydrophobic spores) on the stainless-steel plates after 30 min of static foam cleaning with the foam of 27% liquid fraction. The small letters, a, indicate groups of statistical differences according to Tukey's test ($p < 0.05$). 128

Figure 3.1.1. Spores log reduction on the plate under static dipping conditions as a function of the surfactant in comparison to water. The small letters a–b indicate groups of statistical differences according to Tukey's test ($p < 0.05$). 146

Figure 3.1.2. Spores log reduction on the plate in dynamic condition during foam flow cleaning after 1 and 30 min of foam flow as a function of the surfactant in comparison to water. The small let-ters a–d indicate groups of statistical differences according to Tukey's test ($p < 0.05$)

between the water and the surfactants for 1 min of foam flow cleaning and for 30 min of foam flow cleaning. 147

Figure 3.1.3. Epifluorescence microscopy pictures of a stainless-steel plate contaminated by spores and stained with acridine orange: (a) before cleaning by foam flow, (b) after one minute of foam flow cleaning based on DG, and (c) after 30 min of foam flow cleaning based on DG. The scale bar represents 1 mm for all the pictures. 148

Figure 3.1.4. Evolution of the foam height for SDS, DG, and LG: (a) before the foam passed through the duct containing the plate contaminated with spores and (b) after the foam passed through the duct. 150

Figure 3.1.5. Mean bubbles area of the foams produced with SDS, DG, and LG with the correspond-ing microscopic pictures: (a) before the foam passed through the duct containing the plate con-taminated with spores and (b) after the foam passed through the duct. The scale bar represents 1 mm for all the foam pictures. The small letters a–b indicate groups of statistical differences ac-cording to Tukey's test ($p < 0.05$). 151

Figure 3.1.6. Pictures of the foams produced from the surfactants solution (SDS, DG, and LG) before and after filtration to remove the spores, showing a similar foamability and foam stability around 5 min after producing the foam. The scale bar represents 2 cm for all the pictures. . 153

Figure 3.1.7. Environmental comparison between foam cleaning process with APG and foam clean-ing process with SDS (reference system) by impact category (ReCiPe midpoint H). . 154

Figure 3.1.8. Different steps of stainless-steel plate surface preparation methodology: (1) 15 cycles of immersion of the plate in milk at room temperature for 30 min and in sodium hydroxide at 70 °C for 30 min; (2) biofilm formation on the plate; (3) rubbing of the plate with commercial undiluted surfactant (RBS) followed by immersion of the plate in surfactant aqueous solution at 5 wt.% at 60 °C for 10 min; (4) the plate sterilization in a hot air oven at 180 °C for 1 h; (5) soiling of the plate with 5 drops of 1 µL of the spore suspension at a concentration of 108 CFU.mL−1. 156

Figure 3.1.9. The process flowchart for the foam cleaning process formulated with: (a) SDS and (b) APG..... 163

Figure 4.1.1. Partial phase diagram determined by visual observations by varying the decyl glucoside (DG) concentration as a function of the molar ratio between decanol and decyl glucoside showing the stable domain of W/W emulsion (dashed black line). Red crosses correspond to samples where macroscopic phase separation occurred after 24 hours. Orange circles correspond to samples where a slight macroscopic phase separation occurred after 24 hours. Green circles correspond to stable samples after 24 hours. On the right side, pictures of samples illustrate the three regimes. The samples are from left to right: unstable W/W emulsion for DG = 9 mM and R = 0:1, medium stability W/W emulsion for DG = 6 mM and R = 3:1, and high stability W/W emulsion for DG = 9 mM and R = 2:1. 180

Figure 4.1.2. Partial phase diagram determined by visual observations by varying the lauryl glucoside (LG) concentration as a function of the molar ratio between decanol and Lauryl glucoside showing the stable domain of W/W emulsion (dashed black line). Red crosses correspond to samples where macroscopic phase separation occurred after 24 hours. Orange circles correspond to samples where a slight macroscopic phase separation occurred after 24 hours. Green circles correspond to stable samples after 24 hours..... 182

Figure 4.1.3. Effect of both DG concentration and decanol:DG ratio (R) on W/W emulsions droplets size. Confocal microscopy images of the W/W emulsions taken at t=0 for two different DG concentrations: 6 mM (top) and 12 mM (bottom), and three different R: R = 3:1(left), R = 6:1 (middle) and R = 9:1 (right). Droplets are labeled with FITC-dextran dye. The scale bar represents 15 μm. 185

Figure 4.1.4. Effect of centrifugation on the stability of the W/W emulsions. Epifluorescence microscopy images of W/W emulsions stabilized with DG (top) or LG (bottom) at a concentration of 12 mM with a molar ratio of R = 3:1, taken before centrifugation (left) and after centrifugation (right). Droplets are labeled with FITC-dextran dye. The scale bar represents 60 μm. 186

Figure 4.1.5. (a) Confocal microscopy image of dextran-in-PEG emulsion stabilized with LG at a concentration of 9 mM and with a molar ratio of decanol:LG at 1:1, showing the presence of lamellar phases (some of them identified with white arrows) in the continuous phase of the emulsion. Nile red was used to label the surfactant and fatty alcohol. The scale bar represents 15 μm. (b) 1D SAXS diffractogram of a water-in-water emulsion stabilized by a mixture of LG and decanol with a LG concentration of 12 mM and a molar ratio of decanol:LG at 3:1. Only the third order Bragg peak (3Q0) is identified on the scattering pattern, labeled with a black arrow. Schematic showing the stabilization of the W/W emulsion by lamellar phase surrounding the dextran-rich droplets. 188

Figure 4.1.6. W/W emulsions stabilized with DG in combination with two different fatty alcohols: dodecanol and myristil alcohol. Epifluorescence microscopy images of W/W emulsions stabilized with DG at 12 mM and Dodecanol: DG ratio equal to 6:1 (left) and DG at 12 mM and myristyl alcohol: DG ratio equal to 6:1 (right), taken at t=0 (top) and at t=24h (bottom). Droplets are labeled with FITC-dextran dye. The scale bars represent 60 μm. 190

Figure 4.1.7. (a) Stability of the foamulsion. Pictures of the foam produced with the W/W emulsion (LG 12 mM, decanol: LG ratio 3:1) with the addition of SDS at 18mM and its evolution over time. (b) Epifluorescence microscopy image of the foamulsion at t=0. Droplets are labeled with FITC-dextran dye. The scale bar represents 30 μm. 192

Figure 5.1.1. (a) Escheria coli at the interface surrounding the droplets of a dextran-in-PEG emulsion. (b) Bacillus subtilis encapsulated inside the droplets of dextran-in-PEG emulsion. 209

Abstract

In the food industry, surfaces contaminated with microorganisms are a major cause of cross-contamination, resulting in foodborne illness and food waste. Despite thorough cleaning efforts, foodborne illness rates are rising, suggesting current practices are insufficient. Traditional cleaning methods also consume large amounts of water, energy, and chemicals, raising sustainability and environmental concerns. The industry is exploring more sustainable alternatives, such as dry-cleaning methods, eco-friendly products, and advanced control systems, to reduce resource consumption while maintaining hygiene standards. One promising alternative for cleaning closed surfaces is the use of foam, a method already used for open surfaces. Foam cleaning can potentiallyreduce water, energy, and chemical consumption. The aim of this thesis is to study the links between foam properties and removal of microorganisms from both open and closed surfaces, and explores innovative cleaning techniques to develop more sustainable and efficient methods for the food industry.

The first part is dedicated to the cleaning of open surfaces, i.e., static foam cleaning. Here we study the removal of hydrophilic and hydrophobic *Bacillus subtilis* spores from stainless steel surfaces by using foams. The model foams are formulated with bio-based surfactants (10-hydroxystearic acid and sodium cocoyl isethionate). The relationship between bubbles size and foam liquid fraction and the decontamination efficiency is investigated to determine the mechanisms of foam action. Foams themselves can decontaminate surface soiled with spores, most probably by wiping and imbibition mechanisms. Foams with smaller bubbles size have the highestdecontamination efficiency. Under the conditions studied, the liquid fraction is not the main parameter governing the decontamination efficiency.

The second part is dedicated to the cleaning of closed surfaces, i.e., foam flow cleaning. Here we study the efficiency of foam flow formulated with a model surfactant (Sodium dodecyl sulfate) in comparison with foam flow formulated with bio-based surfactants (alkyl polyglucosides) to remove hydrophilic spores from pipes. We demonstrate similar efficiency

for short cleaning times). In addition, through a life cycle assessment we demonstrate the reduction of several environmental impacts with the use of bio-based surfactant compared to the model surfactant.

The third part is dedicated to the stabilization of water-in-water emulsions and the production of a foamulsion based ont these emulsions. We study the stabilization of PEG-in-Dextran emulsions with lamellar gel networks based on alkyl polyglucosides and fatty alcohols. We show that highly stable emulsions are obtained over a long period of time for specific formulation conditions. We also demonstrate for the first time the production of a foamulsion based on water-in-water emulsions.

Résumé

Dans l'industrie alimentaire, les surfaces contaminées par des micro-organismes sont une cause majeure de contamination croisée, entraînant des maladies d'origine alimentaire et du gaspillage alimentaire. Malgré des efforts de nettoyage rigoureux, les taux de maladies d'origine alimentaire augmentent, ce qui suggère que les pratiques actuelles sont insuffisantes. Les méthodes de nettoyage traditionnelles consomment également de grandes quantités d'eau, d'énergie et de produits chimiques, soulevant des préoccupations en matière de durabilité et d'environnement. L'industrie explore des alternatives plus durables, telles que les méthodes de nettoyage à sec, les produits écologiques et les systèmes de contrôle avancés, pour réduire la consommation de ressources tout en maintenant les normes d'hygiène. Une alternative prometteuse pour le nettoyage des surfaces fermées est l'utilisation de la mousse, une méthode déjà utilisée pour les surfaces ouvertes. Le nettoyage avec de la mousse peut potentiellement réduire la consommation d'eau, d'énergie et de produits chimiques. L'objectif de cette thèse est d'étudier les liens entre les propriétés de la mousse et l'élimination de micro-organismes sur des surfaces ouvertes et fermées, et d'explorer des techniques de nettoyage innovantes afin de développer des méthodes plus durables et efficaces pour l'industrie alimentaire.

La première partie est consacrée au nettoyage des surfaces ouvertes, c'est-à-dire au nettoyage par de la mousse en condition statique. Nous étudions ici l'élimination des spores hydrophiles et hydrophobes de *Bacillus subtilis* des surfaces en acier inoxydable en utilisant des mousses. Les mousses modèles sont formulées avec des tensioactifs biosourcés (acide 10-hydroxystéarique et cocoyl iséthionate de sodium). La relation entre la taille des bulles et la fraction liquide de la mousse et l'efficacité de la décontamination est étudiée pour déterminer les mécanismes d'action de la mousse. Les mousses elles-mêmes peuvent décontaminer les surfaces souillées par des spores, très probablement par des mécanismes de frottement/balayage et d'imbibition. Les mousses avec des bulles plus petites ont la plus grande efficacité de

décontamination. Dans les conditions étudiées, la fraction liquide n'est pas le principal paramètre gouvernant l'efficacité de la décontamination.

La deuxième partie est consacrée au nettoyage des surfaces fermées, c'est-à-dire au nettoyage par écoulement de mousse. Nous étudions ici l'efficacité de l'écoulement de mousse formulée avec un tensioactif modèle (dodecyl sulfate de sodium) en comparaison avec l'écoulement de mousse formulée avec des tensioactifs biosourcés (alkyl polyglycosides) pour éliminer les spores hydrophiles des tuyaux. Nous démontrons une efficacité similaire pour des temps de nettoyage courts. De plus, grâce à une évaluation du cycle de vie, nous démontrons la réduction de plusieurs impacts environnementaux avec l'utilisation de surfactants biosourcés par rapport au surfactant modèle.

La troisième partie est consacrée à la stabilisation des émulsions eau-dans-eau et à la production d'une mousse basée sur ces émulsions. Nous étudions la stabilisation des émulsions PEG-dans-Dextran avec des réseaux de gel lamellaire basés sur des alkylpolyglycosides et des alcools gras. Nous montrons que des émulsions très stables sont obtenues sur une longue période pour des conditions de formulation spécifiques. Nous démontrons également pour la première fois la production d'une mousse basée sur des émulsions eau-dans-eau.

General Introduction

While systematic cleaning processes are typically implemented in agri-food industries, they may fall short of optimal effectiveness, leaving surfaces inadequately sanitized. Consequently, residual dirt can persist, providing an environment conducive to bacterial growth (Midelet et al., 2024). If these surfaces remain dirty and they get in contact with food, cross-contamination can occur, which in turn can lead to food-borne illness for the consumer. Foodborne diseases are of great concern, affecting 600 million people a year and causing 420,000 deaths worldwide (WHO, 2022). Bacteria constitute the most prevalent cause of food-borne illnesses existing in a diverse array of forms, e.g. in their vegetative cellular form, or by forming biofilms. In addition, some bacteria can produce spores, a resilient form that exhibits high resistance to heat, desiccation and disinfectants. Once these bacterial forms develop on surfaces, they adhere to them, making them more difficult to remove through cleaning processes.

On one hand, Cleaning in Place (CIP) stands out as the predominant method for cleaning enclosed surfaces such as pipes in food industries (Pant et al., 2023). CIP is an automated process that involves circulating chemical solutions at elevated temperatures. However, it incurs significant resource consumption, including water, chemicals, and energy. On the other hand, one of the most prevalent approaches for cleaning open surfaces such as equipment exteriors and walls in food industries is the use of foams (EHEDG, 2021). Foams serve as the vehicle for delivering active chemicals to these surfaces.

Foams are a dispersion of gas in the form of bubbles within a continuous phase which can be liquid, solid or semi-solid (Cantat et al., 2013). Foams have a particular behavior which is given by the combination of gas properties and continuous phase properties. They find applications in several fields, like, in foodstuffs, in construction materials, personal care products, etc. Foams are thermodynamically unstable systems. Therefore, at least one foam stabilizer is always included in the formulation (Malysa and Lunkenheimer, 2008). One of the most common foam stabilizers are surfactants, which are amphiphilic molecules, i.e. they have an

affinity for both phases (Cantat et al., 2013). In liquid foams, where the continuous phase is a liquid, the surfactants are solubilized in a liquid and then the foam is produced introducing gas to the system. Depending on the conditions of the solution (concentration, pH, temperature, tec.) the surfactants can adopt different self-assembled structures which can completely change the properties of the foams (Fameau and Salonen, 2014).

Despite the scientific consensus that foams play no role in cleaning procedures and that they are used mainly as carriers, Schad et al. conducted a study on static foam cleaning of oil contaminated surfaces and elucidated three different mechanisms demonstrating that foams have cleaning power (Jones et al., 2016; Schad et al., 2021). However, to our knowledge there is only one study that shows that static foam cleaning can remove bacteria and nothing is discussed about the mechanisms involved (Le Toquin, 2018). Moreover, it has recently been shown that foam flow can remove bacterial spores and biofilms from closed surfaces (pipes) (Dallagi, 2022). Foams present a promising eco-friendly cleaning solution for the food industry. Composed mainly of air, they offer a substantial reduction in the resources needed for cleaning. In fact, Dallagi et al. have shown that foam flow allows to reduce the environmental impacts compared to the traditional CIP (Dallagi et al., 2022c).

The general objective of this thesis is to use various liquid foams systems as an innovative eco-friendly cleaning method for the food industry, and to understand the foam properties governing the decontamination process.

This work was carried out at Institut National de Recherche pour l'Agriculture, l'Alimentation, et l'Environnement (INRAE) at Unité Matériaux et Transformations (UMET) within the group of Processus aux Interfaces et Hygiène des Matériaux (PIHM). The thesis was co-financed by INRAE and the region of Haut-de-France.

This thesis is structured into three main parts. The first one concerns the investigation of static foam cleaning, the second one explores foam flow cleaning, and the final one focuses on the design of possible new foam systems for cleaning applications.

The thesis is divided into 4 chapters:

- **Chapter 1:** corresponds to the literature survey on the importance of cross-contamination of food by contaminated surfaces. It comprehensively reviews the existing cleaning processes employed in the food industry, explores potential environmentally friendly alternatives, and elucidates the key properties of foams. Additionally, it investigates the diverse applications of foams in cleaning both open and closed surfaces.
- **Chapter 2:** gathers the results of this thesis regarding foam cleaning in static condition and is divided in two subchapters:
    - **Subchapter 2.1:** concerns the study of the self-assembly and foaming properties of 10-hydroxystearic acid (10-HSA) soap in an aqueous solution and the use of foams based on 10-HSA for foam cleaning in static condition of stainless-steel surfaces soiled with bacterial spores. We studied the influence of the bubble size and liquid fraction on cleaning efficiency. The results were published in *Molecules* journal (Dari et al., 2023a);
    - **Subchapter 2.2:** concerns the study of the self-assembly and foaming properties of Sodium Cocoyl Isethionate (SCI), and the use of foams based on SCI for foam cleaning in static condition of stainless-steel surfaces soiled with two different types of bacterial spores. We studied the influence of different liquid fractions, foams with and without drainage, as well as, different levels of attachment of the spores to the surface, in order to elucidate the static foam cleaning mechanisms. The results are gathered in one paper to be submitted to *Colloids and Surfaces A: Physicochemical and Engineering Aspects* journal.
- **Chapter 3:** gathers the results of this thesis regarding foam cleaning in dynamic condition (foam flow). Here we studied the foam flow cleaning of pipes contaminated with spores using foams based on alkyl polyglucosides and compared to foams bases on SDS as model surfactant. We also carried a Life Cycle Assessment (LCA) comparing

the foam flow cleaning using both surfactants and we evaluated the destruction of the foam and the reutilization of the surfactant solution. The results were published in *Molecules* journal (Dari et al., 2023b).

- **Chapter 4:** we chose to study 'water-in water' emulsions as a new possible soft material system for cleaning purposes. We studied the stabilization of emulsions based on dextran in poly(ethylene glycol) with Lamellar gel Network (LGNs) based on Alkyl polyglucosides (APGs) and fatty alcohol. Then, we tried for the first time to produce foams based on W/W emulsions. The results were published in *Frontiers in Soft Matter* journal (Dari et al., 2023c).

Thesis outputs

Publications:

- Dari C., Hamiot A., Lemy C., Le Coeur C., Benezech T., Fameau A-L. Static Foam Cleaning with Sodium Cocoyl Isethionate-Based Foams for Spore Removal from Solid Surfaces. *Colloids and Surfaces A: Physicochemical and Engineering Aspects* (under submission).
- Dallagi H., Dari C., Faille C., Fameau A-L., Aloui F., and Benezech T. Wet foam flow for cleaning food industry equipment: role of geometry in maintaining removal efficiency of Bacillus spores. *Journal of Food Engineering*, 376, (2024) 112064. https://doi.org/10.1016/j.jfoodeng.2024.112064
- Dari C., Si Y., Douliez J-P., Tahon J-F., Benezech T., Clegg PS and Fameau A.-L. Mixture of fatty alcohols and alkyl polyglucosides stabimizing water-in-water emulsions. *Frontiers in Soft Matter*, 3 (2023). https://doi.org/10.3389/frsfm.2023.1328195
- Dari C., Cousin F., Le Coeur C., Dubois T., Benezech T., Saint-Jalmes A., and Fameau A.-L. Ultrastable and Resposive Foams Based on 10-Hydroxystearic Acid Soap for Spore decontamination. *Molecules*, 28 (11), 4295 (2023). https://doi.org/10.3390/molecules28114295
- Dari C., Dallagi H., Faille C., Dubois T., Lemy C., Deleplace M., Abdallah M., Gruescu C., Beaucé J., Benezech T., and Fameau A.-L. Decontamination of Spores on Model Stainless- Steel Surface by Using Foams Based on Alkyl Polyglucosides. *Molecules*, 28 (3), 936 (2023). https://doi.org/10.3390/molecules28030936

Conferences: oral presentation:

- EUfoam 2024 (European foam congress), Dresde, Germany. (2024). Lamellar-gel-networks based stabilizing water-in-water emulsions.
- ESC 2024 (European Student Colloid Conference), Bordeaux, France. (2024). Lamellar-gel-networks based stabilizing water-in-water emulsions.
- ICEF14 (International congress on Engineering and Food), Nantes, France. (2023). Foams based on Alkyl polyglucosides and SDS for cleaning pipes contaminated with Bacillus subtilis spores.
- EUfoam 2022 (european congress on foams), Krakow, Poland. (2022). Foams based on alkyl polyglucosides for cleaning pipes contaminated with Bacillus subtilis spores.

Conferences: poster presentation:

- EUfoam 2024 (European foam congress), Dresde, Germany. (2024). Foams based on 10-hydroxystearic acid for spore decontamination.

Chapter 1: Review of literature

1.1 Cross-contamination of food by contaminated surfaces

As the global population continues to grow, the scale of food production expands in tandem, thereby amplifying the risk of foodborne illnesses (DeFlorio et al., 2021). Foodborne diseases can be infectious or toxic. They are caused by bacteria, viruses, parasites or chemicals transmitted through contaminated foods. According to the World Health Organization (WHO, 2022) there are 600 million cases of food-borne illnesses and 42,0000 deaths worldwide each year due to the consumption of contaminated food. In 2019 in Europe, there were 5175 foodborne outbreaks, with 49,463 cases of illnesses, 3859 hospitalizations and 60 deaths, which was higher than the previous year (Sarno et al., 2021). The main causes of these foodborne outbreaks were pathogenic bacteria such as: *Salmonella*, *Campylobacter*, *Escherichia coli* (*E. coli*) and *Listeria* (Sarno et al., 2021; WHO, 2022). The resulting effects on public health systems and the financial losses incurred by companies can be notably substantial. (DeFlorio et al., 2021; Midelet et al., 2024).

Food contamination can occur at any stage of food production chain between the farm and the consumer (Midelet et al., 2024). Cross-contamination is defined as the transfer of microorganisms from a contaminated source to a non-contaminated product (Pérez-Rodríguez et al., 2008). There are three types of cross contaminations: between different foods, between equipment surfaces and food, and between individuals and food (Midelet et al., 2024). In the food industry, food contact surfaces are considered to be one of the main sources of cross-contamination leading to foodborne illness (DeFlorio et al., 2021; Midelet et al., 2024).

As described above, bacteria constitute the most prevalent cause of food-borne illnesses existing in a diverse array of forms, e.g in their vegetative cellular form, or by forming biofilms. Biofilms are a community of bacteria that colonize a living or inert surface (**Figure 1.1.1**). They are usually embedded in a matrix of cellular exopolymers that make them resistant to adverse circumstances (Midelet et al., 2024). In food industries, bacterial biofilms are often formed by

pathogenic and non-pathogenic bacteria. Biofilms are of increasing concern in the food industry because they sometimes have the ability to persist despite cleaning and disinfection operations (Midelet et al., 2024). In addition, some bacteria have the ability to produce spores, a resilient form that exhibits high resistance to heat, desiccation and disinfectants (e.g. *Clostridium botulinum*, *Clostridium perfringens*, *Bacillus subtilis*, *Bacillus cereus*) and therefore they tend to adhere to the equipment and survive the cleaning process (**Figure 1.1.2**) (Lücking et al., 2013; Bintsis and Department of International Trade, TEI of West Macedonia, Kastoria, Greece, 2017)

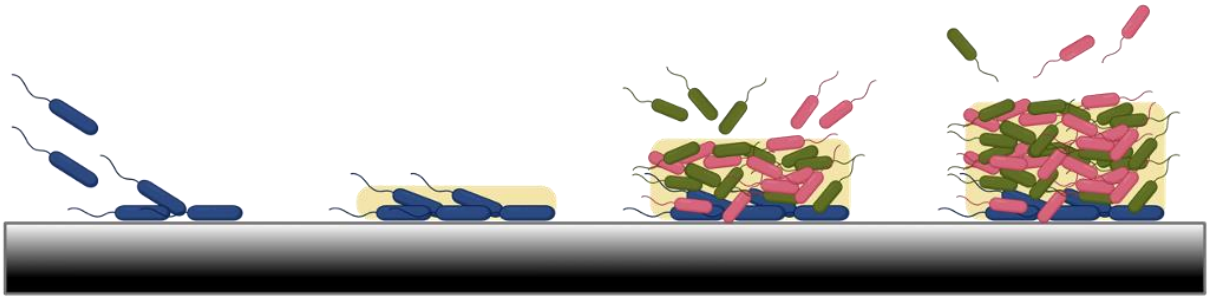

Figure 1.1.1: Scheme showing the different stages of biofilm formation. First some bacteria attach to the surface, and the cellular exopolymer matrix is formed, then more bacteria attach (potentially from other species) and finally, there is a dispersal of the bacteria to the environment.

In the dairy industry, numerous authors have documented the existence of pathogenic bacteria biofilms in milk processing lines and pasteurization tanks of different commercial dairy products (Sharma and Anand, 2002; Gunduz and Tuncel, 2006; D'Amico, 2008). Moreover, the presence of different bacteria such as *E. coli* and *Bacillus cereus* was identified on stainless-steel pipes of milk-processing lines (Cherif-Antar et al., 2016). Regarding spores, they pose significant concerns within the dairy industry, primarily because raw materials frequently serve as a major source of contamination. Spore-formers of *Bacillus* strain are the most common in the dairy industry. *Bacillus cereus* is therefore well known to cause foodborne illnesses due to

the production of toxins. Moreover, *Bacillus* strains can also be the cause of food spoilage (Lücking et al., 2013). Therefore, cleaning and disinfection operations are essential to control food contamination related to surfaces to eliminate: bacteria, biofilms and spores.

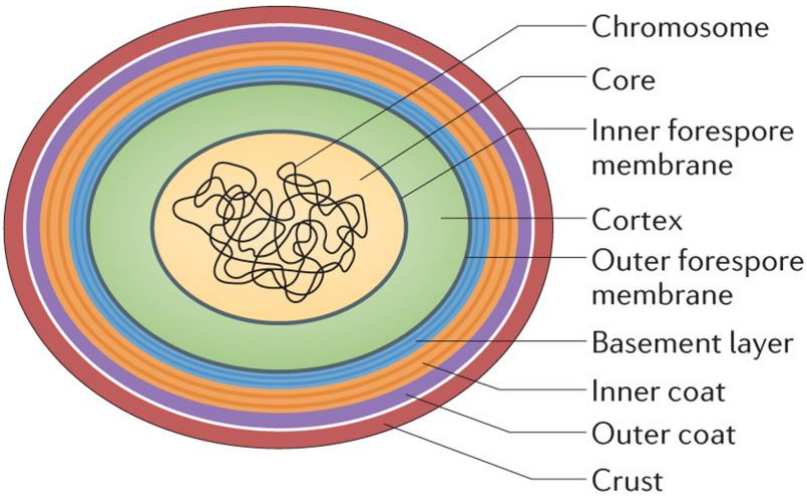

Figure 1.1.2: Scheme of a spore of *Bacillus subtilis*. The presence of the coat is what makes them more resistant to heat and to chemicals, compared to vegetative cells. The figure was reproduced from (McKenney et al., 2013).

1.2 Cleaning of surfaces in food industries

Cleaning is defined as a series of operations carried out to remove organic and inorganic dirt from surfaces by chemical and physical methods (Sansebastiano et al., 2007). It also should remove any unwanted material. Dirt on surfaces in the food industry generally includes residues of food, chemicals, micro-organisms, dust from the environment, etc. Cleaning is the previous step of disinfection, whose main objective is to eliminate and/or reduce the viability of microorganisms to a level that does not pose a significant risk (Lelieveld et al., 2003). In some cases, cleaning and disinfection are combined, when a cleaning solution with both detergent and sanitizer properties is used (Lelieveld et al., 2003). It should be noted that cleaning should also reduce the number of microorganisms, even if there might be a significant number of of

viable microorganisms remaining, therefore disinfection appeared to be mandatory to mitigate the risk of food cross contamination by pathogenic microorganisms.

Cleaning and disinfection protocols usually include several steps, where the first step is aimed at removing the gross dirt, then comes the actual cleaning step and finally the disinfection step (EHEDG, 2021). In most cases, the cleaning step involves a wet operation, where detergents are typically applied and then rinsed off with water (Wirtanen and Salo, 2003). When working with product lines featuring low humidity content, the cleaning step is executed using methods that involve minimal moisture or directly employing dry methods.

According to Sinner's circle, there are four parameters that can be tuned in cleaning and disinfection operations (**Figure 1.2.1**) (Basso et al., 2017):

- **Chemical action:** The chemicals used are chosen according to the reactions to be promoted in order to dissolve the different types of soiling.
- **Mechanical action:** the mechanical action is usually given by the manual cleaning or by the flow rate which allows to induce different shear forces in relation to the pressure variations.
- **Temperature:** it favors the interaction of the surfactant with the dirt and accelerates its removal. It is also involved in the performance of surfactants, since important surfactant parameters, such as surface tension and Krafft temperature are temperature-dependent (see section 4).
- **Time:** The duration must allow for the reactions to take place effectively, but it should not be excessively long, as this could result in the re-adherence of dirt. Moreover, exceeding the allotted time may lead to unnecessary consumption of resources.

According to the Sinner's circle, these four parameters can be tuned in a way that the reduction of one factor can be compensate by any of the other factors. Although this may not always be the case, it is really useful (Basso et al., 2017).

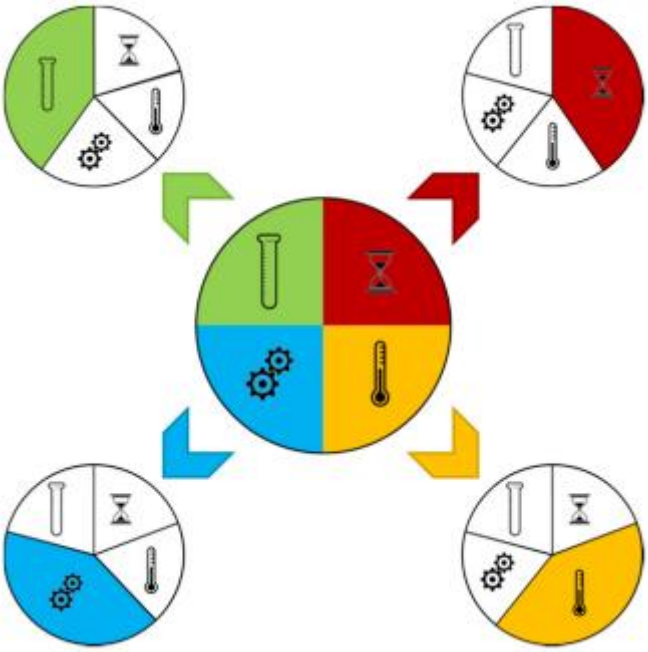

Figure 1.2.1: Illustration of the Sinner circle. The figure was reproduced from (Basso et al., 2017).

The choice of cleaning method will depend mainly on the type of contamination, e.g., food fouling, biological fouling, corrosion fouling, etc., and also on the type of surface, i.e., whether the surfaces are accessible for cleaning by an operator or not. Taking this last criterion into account, we will classify the cleaning processes in two categories: cleaning of open surfaces and cleaning of closed surfaces.

1.2.1 Cleaning of open surfaces

As mentioned above, cleaning is usually carried out mainly with chemicals that react to dissolve the type of dirt to be removed from the surfaces. On open surfaces, foams are the most commonly method used for applying the chemicals. Chemicals are often applied in the form of foam mainly because of their rheological properties they can adhere to surfaces, even vertical surfaces, allowing the chemicals to act for as long as necessary (Le Toquin, 2018). The cleaning efficiency occurs when the bubbles are broken and the drained solution with the chemical comes into contact with the surface (EHEDG, 2021).

To generate foam, various systems can be employed, including centralized pressure systems, decentralized foam stations, and mobile foam systems. These systems have in common that foam is generated by injecting a concentrated solution of detergent, water and air through a nozzle. Foam is generally applied at low to medium pressure, as this reduces the production of aerosols, avoids damage to sensitive equipment and ensures a safe working environment for operators (EHEDG, 2021). Foams with varying liquid fractions can be produced depending on the foaming device and foaming solution. Sometimes so-called “gel foams” are also used. From the four parameters important to take into account in a cleaning process as described above, in the case of foams, time and chemicals are the most important ones. The foam application time is generally 20 minutes, as shorter times may not be sufficient to remove the dirt, and longer times may reorganize and re-solidify the residues (EHEDG, 2021). The detergent formula may also be combined with other active compounds (acids, complexing agents, enzymes etc.) to improve the removal of soiling. Optimally, the cleaning foams should be stable, well visible, adhere strongly to the surfaces and not dry out during the application time (EHEDG, 2021). After the application time the foams are rinsed with water jets. It is important to mention that the use of chemicals can be combined with physical methods. for example, walls and floors are cleaned with scrubbers and formula containing detergents at the same time (Lelieveld et al., 2003).

When low water content methods are required, wet wipes or steam dry can be used. In cases where completely dry methods are required, the following methods can be used: scrapers, brushes, compressed air, vacuum cleaning, dry ice (Lelieveld et al., 2003; EHEDG, 2021).

1.2.2 Cleaning of closed surfaces

Cleaning in Place (CIP) is the most widely used method for cleaning closed surfaces in the food industry (**Figure 1.2.2**) (Pant et al., 2023). It consists of different steps involving the circulation of solutions with chemical agents and rinses with water. It's an automated process with the primary advantage of cleaning without the need for disassembling enclosed machinery and

pipes. This efficiency saves time and renders the process cost-effective (Moerman et al., 2014; Dallagi, 2022).

CIP usually involves five steps (Pant et al., 2023):

1. A pre-rinse with water
2. An alkaline wash
3. A post-rinse with water
4. An acidic wash
5. A post-rinse with water, this step may include a disinfectant solution.

Alkaline solutions are typically used to remove organic residues, whereas acid solutions are used to remove mineral deposits and remaining alkaline chemicals (Moerman et al., 2014). Since temperature increases the efficiency of cleaning, alkaline solutions are usually circulated at around 80 °C and acidic solutions at around 55 °C (Moerman et al., 2014). The flow conditions are generally turbulent, which ensures the mechanical action given by the shear forces (EHEDG, 2021).

The duration of CIPs is variable as each step can take between 5 to 60 minutes, depending mainly on the type of soiling, the type of cleaning solutions and the temperatures (Moerman et al., 2014). In general, longer durations result in higher efficiency.

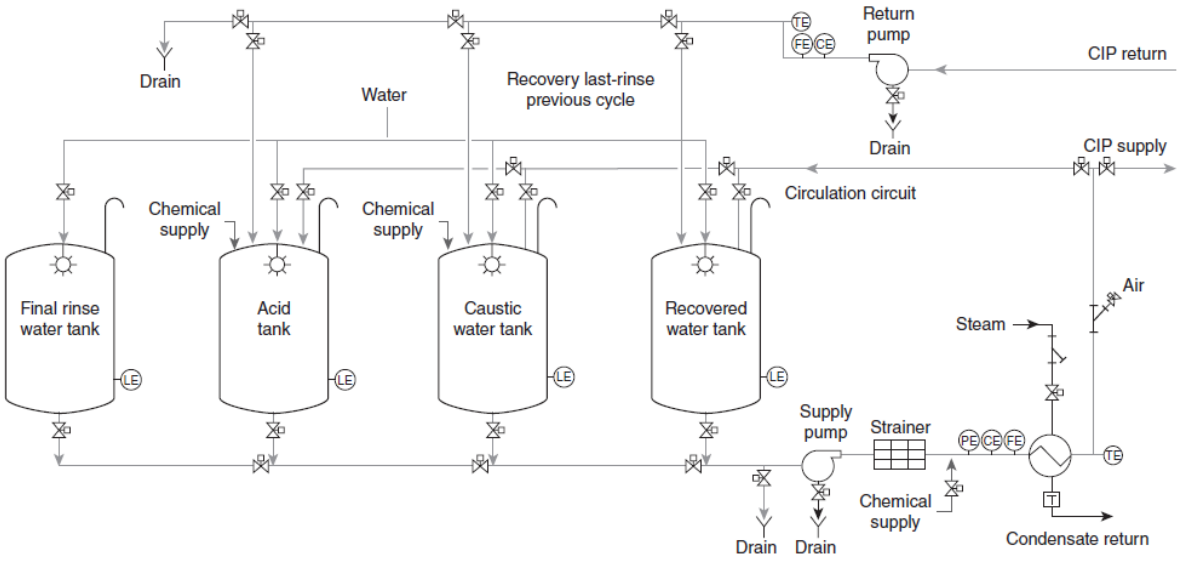

Figure 1.2.2: Scheme of a typical CIP system, which mainly consists of four tanks: a water recovery tank (recovers the water from the last rinse of the last cycle, which is then reused as pre-wash water in the next cycle), a tank for the alkaline solution, a tank for the acid solution and a tank for the final rinse water. The figure was reproduced from (Moerman et al., 2014).

Cleaning operations consume huge amounts of water, energy, chemicals and time (Tomas and Tiwari, 2013; Dallagi, 2022). In addition, it can negatively affect the environment due to the large quantities of polluted wastewater they generate (Tomas and Tiwari, 2013; Dallagi, 2022)

The amount of water consumed for cleaning in food industries can be up to 70 % of the total water consumed by the whole process (Dallagi, 2022). For example, the dairy industry consumes 25-40 % of the total water for sanitization processes; for the fishing industry, the amount can range from 10-50 % (Timmerman, 2022). These values may vary mainly according to the type of product and the level of automation of the process (Garnier et al., 2023).

One of the positive points of the CIP is that it is possible to recycle the water, as the wash water from the last cycle is generally used for pre-washing the next one (Garnier et al., 2023). This can reduce water consumption by up to 50%. Pingulini et al., (2017) conducted a study at a brewery where the highest amount of wastewater (42 %) was from cleaning (Pinguli et al.,

2017). They demonstrated that CIP modification with recirculation can reduce water, energy and chemical consumption by 35, 15 and 15 % respectively.

1.2.3 New eco-friendly cleaning methods in food industries

The environmental and economic impacts resulting from the extensive use of resources in cleaning processes, together with the production of wastewater, underline the imperative need to advance research and development of new cleaning methods. These methods are crucial not only to mitigate environmental pollution, but also to improve the efficiency of cleaning practices. Moreover, in line with UNESCO's ambitious 2030 target to reduce water consumption in industry by 20 %, the development of innovative cleaning technologies is even more pertinent (Garnier et al., 2023). In this regard, Dallagi et al (2023) have highlighted various methods that are currently implemented primarily on a pilot scale or to a limited extent in industrial operations for removing biocontamination in food industries (Dallagi et al., 2023). Some of these methods are mentioned below.

Ice pigging consists of pieces of ice suspended in a liquid containing a substance that lowers the freezing point. The cleaning is achieved through the mechanical action of the ice impacting the surfaces. This method has been mainly used to clean drinking water pipes lines and heat exchangers (Ainslie et al., 2009; Ramsay et al., 2018). Ice pigging proved to be more effective in removing biofilms than traditional hydraulic flushing (Fann et al., 2019). Although it lacks life cycle analysis (LCA) data, it is an environmentally friendly method, as it does not require a lot of resources (Dallagi et al., 2023). However, mechanical action of the ice may cause damage to the surfaces, and the melting time of ice at high temperatures must be taken into account.

Another method is the bubbles flow, which consists of the introduction of bubbles in liquid flow. This cleaning method relies on the mechanical action generated by the movement of bubbles and the properties of the interfaces between air and liquid. It has been mainly used for removing fouling from membranes with a better cleaning performance than traditional CIP (Lee

et al., 2016). An advantage of this method is its chemical free-nature. The main drawback of this method is to be able to control the size of the bubbles and scale up (Dallagi et al., 2023). Moreover, the laboratory results need to be verified at industrial scale.

Pulsed flow is the use of a fluid (water or air) in an oscillating form, which improves shear stresses imposed on a surface (Augustin et al., 2010; Dallagi et al., 2023). It has been used for cleaning pipes and tanks. Silva et al., (2021) have shown that the use of pulsed flow in the CIP for removing biofilms allows to save 67 % of energy compared to the traditional CIP where stationary flow is used (Silva et al., 2021). However, this method requires specific equipment for its application and there is still a lack of information on its use on closed surfaces in the presence of sensors.

Foam flow is the use of foam in dynamic condition to clean closed surfaces. Foam flow has demonstrated a higher cleaning efficiency in removing spores from pipes than traditional CIP (Dallagi et al., 2022b). In addition, foam flow allows to reduce the amounts of water and energy and the LCA has shown that it reduces the environmental impacts up to 80% (non-renewable energy and ionizing radiation) compared to the traditional CIP (Dallagi et al., 2022c). The primary limitations of this method include potential instability of the foam with complex geometries and the necessity of an additional step to destroy the foam at the end of the process and recycle the liquid (Dallagi et al., 2024).

1.3 Foams

As described previously, foams have shown both great interest for cleaning in food industries for close and open surfaces. In this section, we outline the key information necessary to understand the key parameters utilized in this thesis for adjusting foam properties based on the desired cleaning outcomes, whether in static (open surfaces) or dynamic conditions (closed surfaces).

1.3.1 Foam structure

Foam is a dispersion of gas within a liquid, where the liquid phase remains continuous, contrasting with the gaseous phase, which forms bubbles (Langevin, 2023). Foams are thermodynamically unstable, i.e., they tend to separate into the two phases over time (Malysa and Lunkenheimer, 2008). That is why its formulation includes the presence of foam stabilizers. The most common foam-stabilizers are surfactants, proteins, polymers and /or particles (Cantat et al., 2013; Langevin, 2023). Foams exhibit varying levels of organization across different scales (**Figure 1.3.1**). On a macroscopic level (10^{-2} – 1 m), foams behave as fluid-like substances with a solid appearance. At a smaller scale (10^{-4} – 10^{-2} m), we observe the arrangement of bubbles and the network of liquid channels that separates them (Lamolinairie, 2023). Zooming in further to the micrometer scale, we can identify Plateau borders, which are the liquid channels of the foams; and the films, which constitute the walls of the bubbles. Finally, at the nanoscale, the presence of foam stabilizer such as surfactant molecules at the water/air interface becomes discernible (Cantat et al., 2013; Fameau and Salonen, 2014).

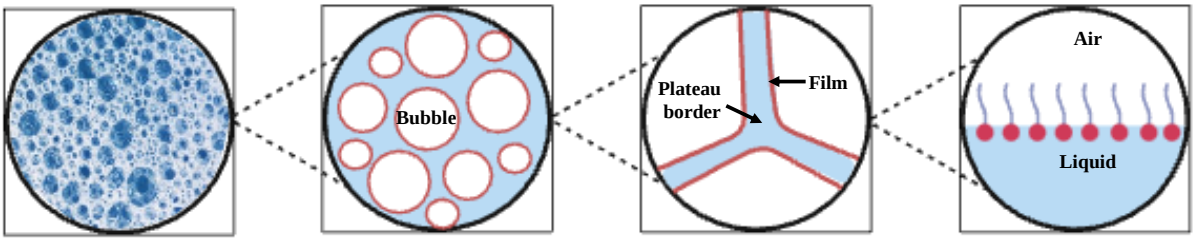

Figure 1.3.1: Representation of the successive levels of organization of a foam stabilized by surfactants according to their spatial scales from the macroscopic scale to the nanoscale.

One of the parameters that characterize foams is their liquid fraction Φ, which is calculated as follows:

Equation 1:

$$\Phi = \frac{V_{liq}}{V_{foam}}$$

where V_{liq}, corresponds to the volume of liquid in the foam, and V_{foam} corresponds to the total volume of the foam (Cantat et al., 2013).

Different types of structures can be found according to the liquid fraction (**Figure 1.3.2**):

- For $\Phi < 5$ % the bubbles are in contact with each other, and deform into polyhedrons, which faces are the thin films of liquid. The edges joining these films are the liquid channels, called Plateau borders, and the points where the Plateau borders meet are called vertices. This system is called a dry foam (**Figure 1.3.2**.**a**).

- For $5\% < \Phi < \Phi_c$ the shape of the bubbles is almost round, since they are deformed by being in contact with each other. The vertices touch, and the plateau borders occupy more volume. This system is called a wet foam (**Figure 1.3.2**.**b**).

- For $\Phi > \Phi_c$ the bubbles are no longer in contact with each other and are perfectly round. There are no more vertices or Plateau borders. This system is called bubbly liquid (**Figure 1.3.2**.**c**).

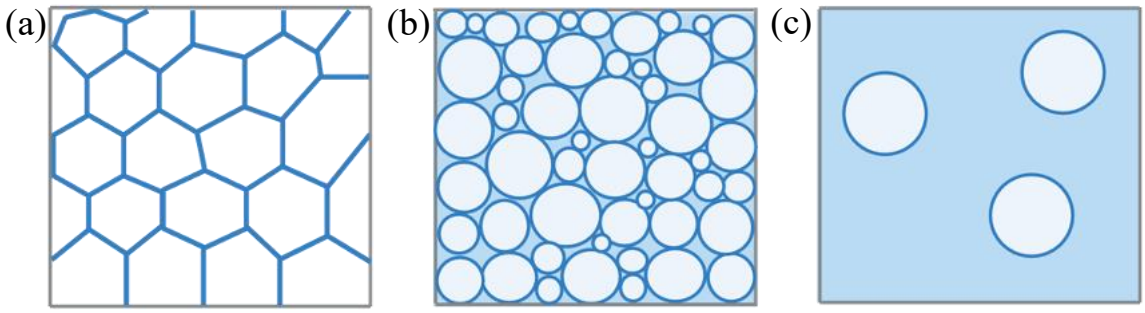

Figure 1.3.2: Different structures according to liquid fractions. (a) Dry foam. (b) Wet foam. (c) Bubbly liquid.

1.3.2 Foam production methods

The physical properties of the foam depend on its structure. The structure, i.e., liquid fraction and bubble size, can be controlled mainly by the foam production method. The choice of foaming method can be a difficult task, especially as each method allows working in a narrow range of liquid fractions and bubble sizes (Drenckhan and Saint-Jalmes, 2015).

Regardless of the method, foams can be produced in one step, when the foaming technique results in the final foam, or in two steps, when the foaming technique generates bubbles that in a second step must be compacted or divided to produce the final foam (Drenckhan and Saint-Jalmes, 2015).

Foam production methods may be physical, when mechanical force is used or phase transitions occur; they may be chemical, when gas is released in a chemical reaction; or they may be biological, when some micro-organism produces gas (Drenckhan and Saint-Jalmes, 2015). Here we will discuss only physical methods based on mechanical force.

Drenckhan and Saint-Jalmes (2015) describe the physics behind foam formation and then list different techniques to produce them (Drenckhan and Saint-Jalmes, 2015). A summary of these methods is given below:

Bubbling into a stationary liquid

This technique consists of bubbling the gas in a stationary liquid through an orifice, several orifices, a perforated plate or through a porous disc (**Figure 1.3.3.a**). Characteristic bubble sizes range from around 100 micrometers to 1 centimeter (Drenckhan and Saint-Jalmes, 2015). The foam may be monodispersed if similar orifices and good flow conditions are used, otherwise it is polydisperse (Drenckhan and Saint-Jalmes, 2015). With this technique, foams with very high liquid fractions are usually obtained, as the foam is produced in the liquid.

Foaming *via* co-injection of gas in and liquid:

This group includes all the techniques where the foam is produced by flowing both the gas and the foaming solution. This allows better control over the liquid fractions in the foam, as the bubbles are moved away from the bubbling site (Drenckhan and Saint-Jalmes, 2015).

One way to perform it is by making pass the two fluids through complex pore geometries. The resulting bubbles size will be of the order of the pore's sizes, i.e. micrometric (Drenckhan and Saint-Jalmes, 2015). On the same principle, but to increase the foam production rate, static mixers and mixers including a fine grid have been developed (Drenckhan and Saint-Jalmes, 2015). These devices allow high gas and liquid flow rates but still have good control over bubble formation (Drenckhan and Saint-Jalmes, 2015).

To reproduce this principle but in small quantities, one of the most used techniques is the double syringe. This technique consists of connecting two syringes, one of which contains the gas and the other the foaming solution; the syringes are then pushed together a couple of times to produce the foam (**Figure 1.3.3.b**) (Drenckhan and Saint-Jalmes, 2015). This technique produces foams with very small bubble size (around 10-20 μm) and controlled liquid fractions (Drenckhan and Saint-Jalmes, 2015; Gaillard et al., 2017). In addition, Gaillard et al, (2017) have studied this technique in detail and they highlighted that this is the only technique that allows to obtain foams with liquid fractions that are independent of the foam bubbles size (Gaillard et al., 2017).

It is also possible to produce foams by passing both fluids through a tube of millimetric dimensions. The length of the tube has to be larger than its diameter (Drenckhan and Saint-Jalmes, 2015). Foams with bubble sizes in the order of 10 μm and various ranges of liquid fractions can also be obtained (Drenckhan and Saint-Jalmes, 2015).

Gas entrainment at free surfaces and bubble break-up under shear:

This group includes the use of a kitchen blender, where the gas and the foaming solution are sheared (**Figure 1.3.3.c**). In this equipment, large bubbles are first formed by the entrainment of the gas into the liquid; these bubbles are then broken by the shear produced by the blender to obtain smaller bubbles (Drenckhan and Saint-Jalmes, 2015). This technique allows the liquid fraction and the size of the bubbles, which can range from 10 μm to a few millimeters, to decrease over time (Drenckhan and Saint-Jalmes, 2015).

Another way to implement this principle is by using rotor-stator mixers. These devices allow a more explicit determination of the amount of air incorporated (Drenckhan and Saint-Jalmes, 2015). The bubbles size obtained can be up to a few micrometers (Drenckhan and Saint-Jalmes, 2015).

Another device is based on the narrow annular gap unit (Drenckhan and Saint-Jalmes, 2015). In these devices, a pre-foam is first formed by mixing the gas and the liquid, usually using a porous plate, which is then injected into the impellers (Drenckhan and Saint-Jalmes, 2015). The bubble size is around 10 μm (Drenckhan and Saint-Jalmes, 2015). The main advantage of this equipment is that it requires lower rotational speeds.

In addition, there is a standardized method, called the Ross-Miles test, which is based on air entrainment and bubble break-up (Ross and Miles, 1941). This method consists of dropping a foaming solution from a certain height into a certain volume of the same foaming solution, and then measuring the foam height reached (Drenckhan and Saint-Jalmes, 2015). Monodisperse or polydisperse foams can be obtained by increasing the jet velocity (Drenckhan and Saint-Jalmes,

2015). The average size of the bubbles is usually in the order of a few hundred micrometers to a few millimeters; and the liquid fractions are usually high (Drenckhan and Saint-Jalmes, 2015).

This category also included the shaking foaming technique. This technique consists of shaking closed containers which are partially filled with the foaming solution (Drenckhan and Saint-Jalmes, 2015). This technique can be done by hand, or it can be done with a device in a more controlled manner (Drenckhan and Saint-Jalmes, 2015) (Figure 7d). The average bubble size depends on the amount of liquid (Drenckhan and Saint-Jalmes, 2015). A test, which is called the "Bartsch test", based on this technique is used as a quick method to measure the foamability of surfactant solutions (Petkova et al., 2021) (**Figure 1.3.3.d**).

Another technique based on air entrainment is the use of foam hoses. The air entrainment is achieved by passing the foaming solution through a nozzle or through venturi nozzle sections(Drenckhan and Saint-Jalmes, 2015). The size of the bubbles is usually in the order of a millimeter and liquid fractions are high (Drenckhan and Saint-Jalmes, 2015). If the liquid fraction is to be reduced, air can be injected (Drenckhan and Saint-Jalmes, 2015).

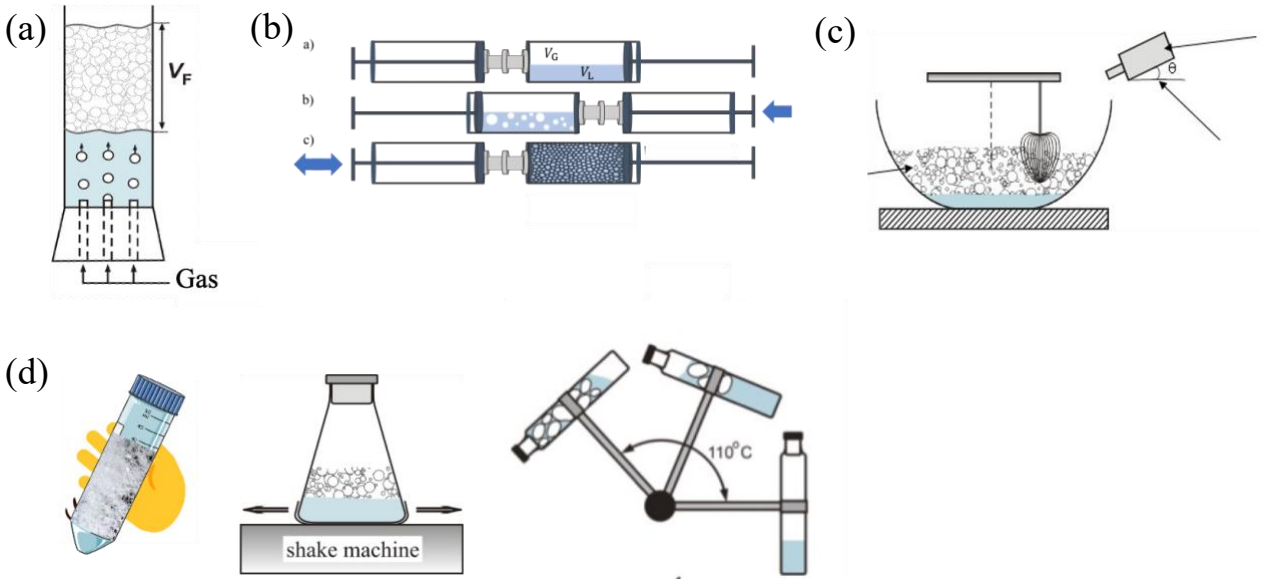

Figure 1.3.3: Foam production methods: (a) Bubbling the gas in a stationary liquid through a porous disc. The figure was repruced from (Denkov, 2004) (b) Double syringe technique. The image was reproduced from (Schad et al., 2021). (c) Gas entrainment and bubble break-up using a kitchen blender. The image was reproduced from (Politova et al., 2018). (d) Different ways to carry out the shaking technique: handshaking, automated shaking using a typical laboratory shaker, automated shaking machine employed for the Bartsch test (from left to right). The third image was reproduced from (Petkova et al., 2021).

1.3.3 Foam destabilization mechanisms

Foams are thermodynamically unstable systems, i.e. over time the two phases separate (Langevin, 2023). There are three different destabilization mechanisms that can occur in foams: drainage, coalescence and coarsening (**Figure 1.3.4**). Drainage is the flow of liquid through the foam due to the effect of gravity (**Figure 1.3.4.a**) (Cantat et al., 2013). The extent of drainage is given by the difference in density between the liquid and the gas (Cantat et al., 2013). Coalescence is the fusion of bubbles due to the collapse of liquid films between two or more bubbles (**Figure 1.3.4.b**) (Cantat et al., 2013). The more unstable the films are, the faster the coalescence occurs. In addition, the bubbles in contact with the outside are more fragile to

coalescence. Therefore, this mechanism is responsible for the collapse of the foam (Fameau and Salonen, 2014). Coarsening is the diffusion of gas from a small bubble into a bigger bubble due to the difference in the Laplace pressure (**Figure 1.3.4.c**) (Fameau and Salonen, 2014). The smaller bubbles withstand a higher pressure and then the gas diffuses into the neighboring bigger bubbles. Coalescence and coarsening lead to an increase in the mean bubbles size over time (Fameau and Salonen, 2014). The drainage causes the bubbles to be closer and thus accelerates coalescence and coarsening. The three mechanisms are connected, and one mechanism can accelerate another one.

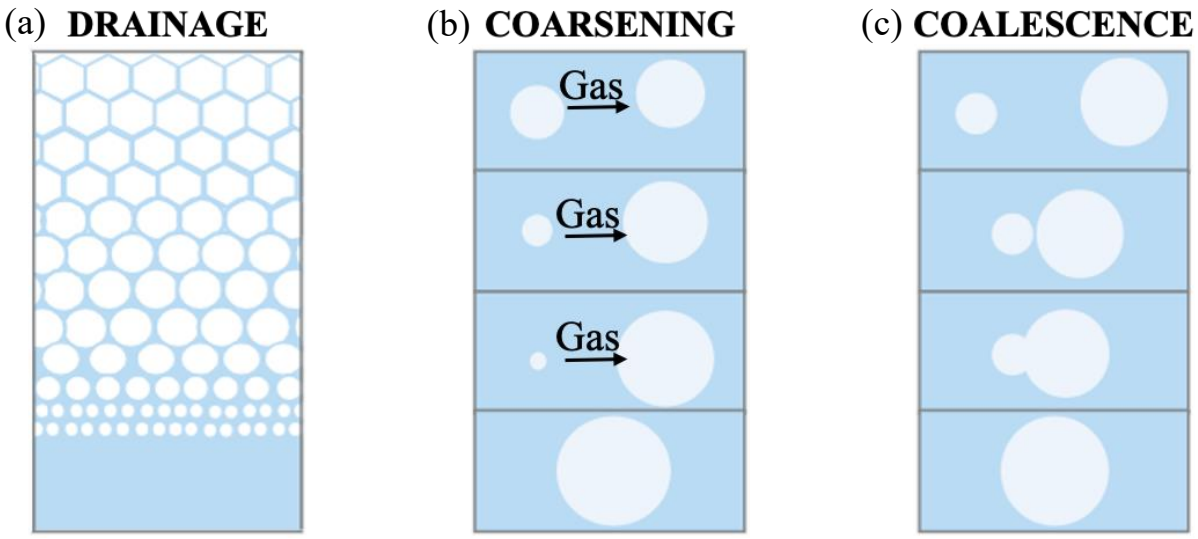

Figure 1.3.4: Schematic showing the three main mechanisms of destabilization of foams. (a) Drainage. (b) Coalescence. (c) Coarsening.

1.4 Surfactants as key foaming agent

1.4.1 Surfactant definition and classification

The energy needed to create an interface between two fluids is determined by the surface tension. Given the high surface tension of the air/water surface (72.7 $mN \cdot m^{-1}$ at 20 ºC), a bubble film formed exclusively with water is highly unstable (Cantat et al., 2013; Beattie et al., 2014). It is therefore necessary to introduce stabilizing agents, such as surfactants. Surfactants are

amphiphilic molecules composed of a hydrophilic head and of and hydrophobic tail (**Figure 1.4.1.a**). When dissolved in water, surfactants adsorb at the liquid-air interface, with their polar head oriented towards the liquid phase, and the non-polar tail oriented towards the gas phase. The addition of surfactants allows to reduce surface tension. As the surfactant concentration increases, the surface tension decreases, until the entire interface is saturated with the surfactant, and the surface tension remains constant (**Figure 1.4.1.b**). This specific concentration at which the surface tension reaches its minimum is referred to as the critical micellar concentration (CMC) (**Figure 1.4.1.b**) (Cantat et al., 2013). Once the interface is saturated in surfactant, if more surfactant molecules continue to be added, they self-assemble to form different structures, such as micelles (**Figure 1.4.1.b**).

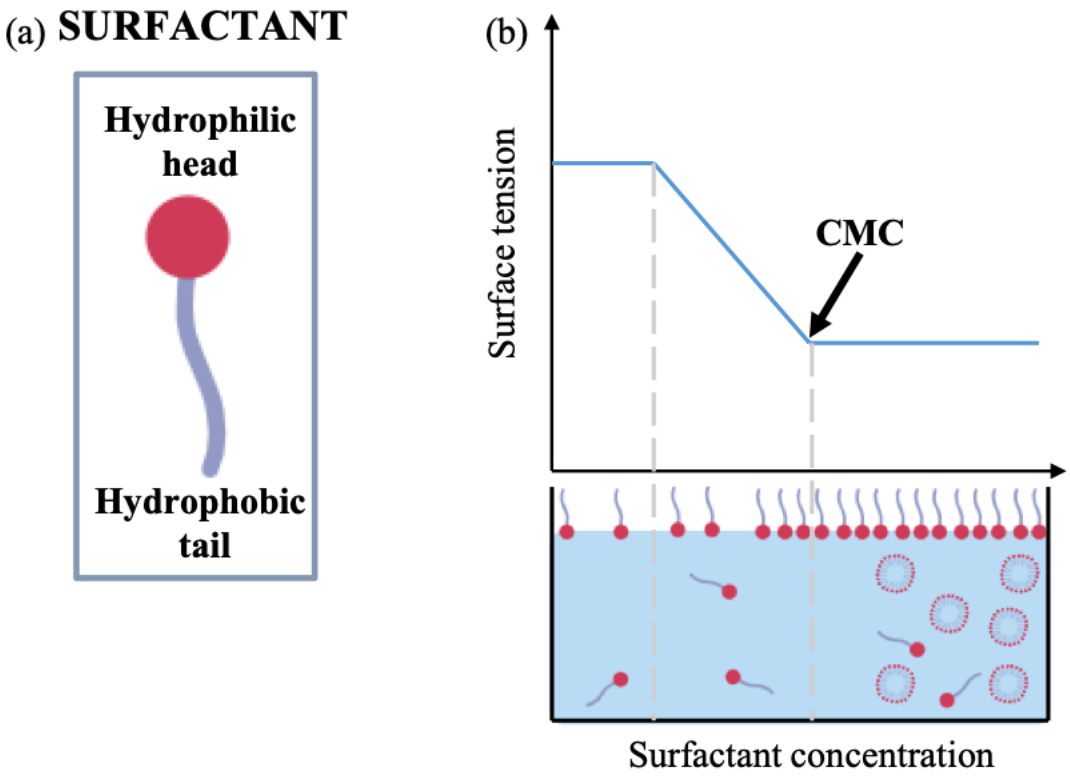

Figure 1.4.1: (a) Surfactant structure. (b) Evolution of the surface tension with surfactant concentration. The CMC indicates the point at which the surface tension reaches the minimum value.

The CMC is also related to the Krafft temperature, which is the minimum temperature at which surfactants change from the solid to the soluble state, allowing the formation of micelles (Arellano et al., 2023). Note that if the surface tension is measured at a temperature lower than the Krafft temperature, one can no longer speak of CMC, as micelle formation is not guaranteed, so CMC will be redefined as critical aggregation concentration (CAC).

According to the charge of the hydrophilic head, surfactant can be classified in non-ionic (with no charge), in anionic (negatively charged), in cationic (positively charged) or in amphoteric (positively or negatively charged depending on the pH) (**Figure 1.4.2**) (Cantat et al., 2013).

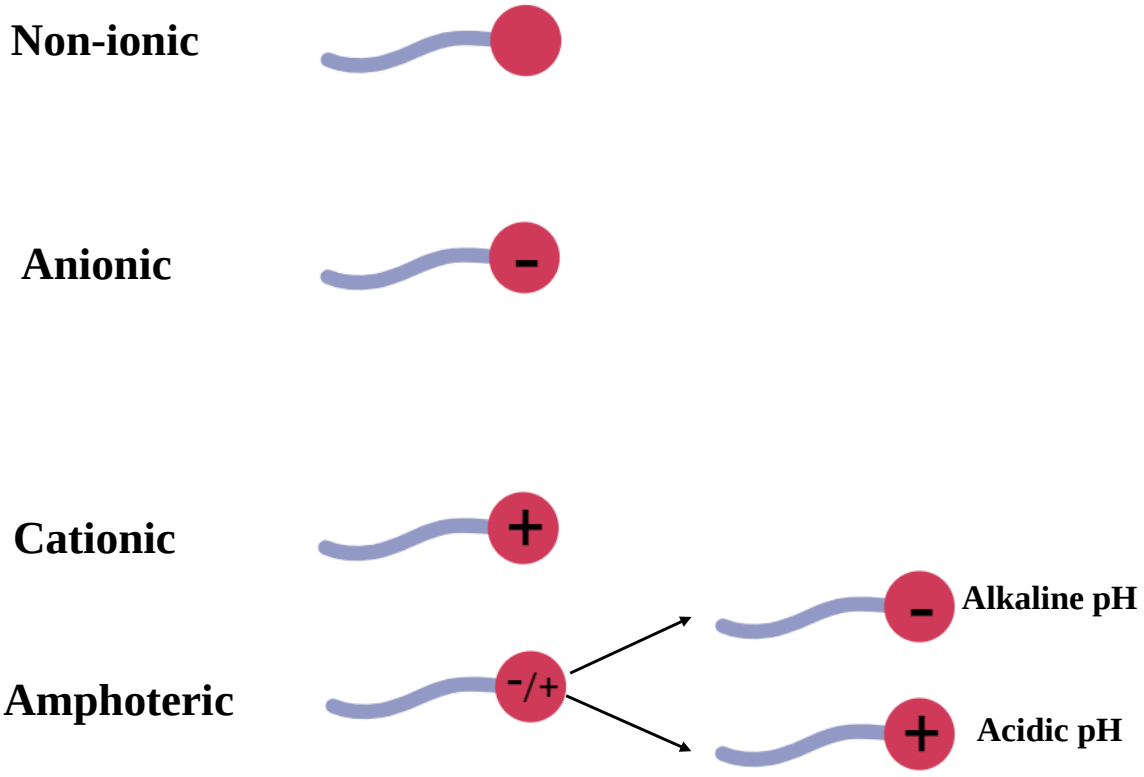

Figure 1.4.2: Classification of surfactants according to the charge of the polar head.

Most conventional surfactants are synthesized from petrochemical sources or combining renewable and petrochemical sources (Bhadani et al., 2020). For example, sodium dodecyl sulfate (SDS) is an anionic surfactant synthesized by sulfonation of petrochemical or oleo chemical based lauryl alcohols (Rebello et al., 2014) (**Figure 1.4.3.a**). However, growing concern for the environment is leading to the replacement of these surfactants for others

biobased surfactants. Among this group we can find chemically synthesized surfactants from renewable sources, such as alkyl polyglucosides (non-ionic) (**Figure 1.4.3.b**) or fatty acid soaps (anionic); or surfactants that come straightly from plants, like saponins, or from microorganisms, like glycolipids (Rebello et al., 2014; Farias et al., 2021). In the literature, the terminology used to refer to surfactants of biological origin is quite controversial. These surfactants are often categorized as either green surfactants or biosurfactants. Generally, the term green surfactants cover all those that come from renewable sources, no matter if they are chemically synthetized or not, and the term biosurfactants encompasses only those that are naturally produced by plants or, mostly, by microorganisms (Rebello et al., 2014; Farias et al., 2021).

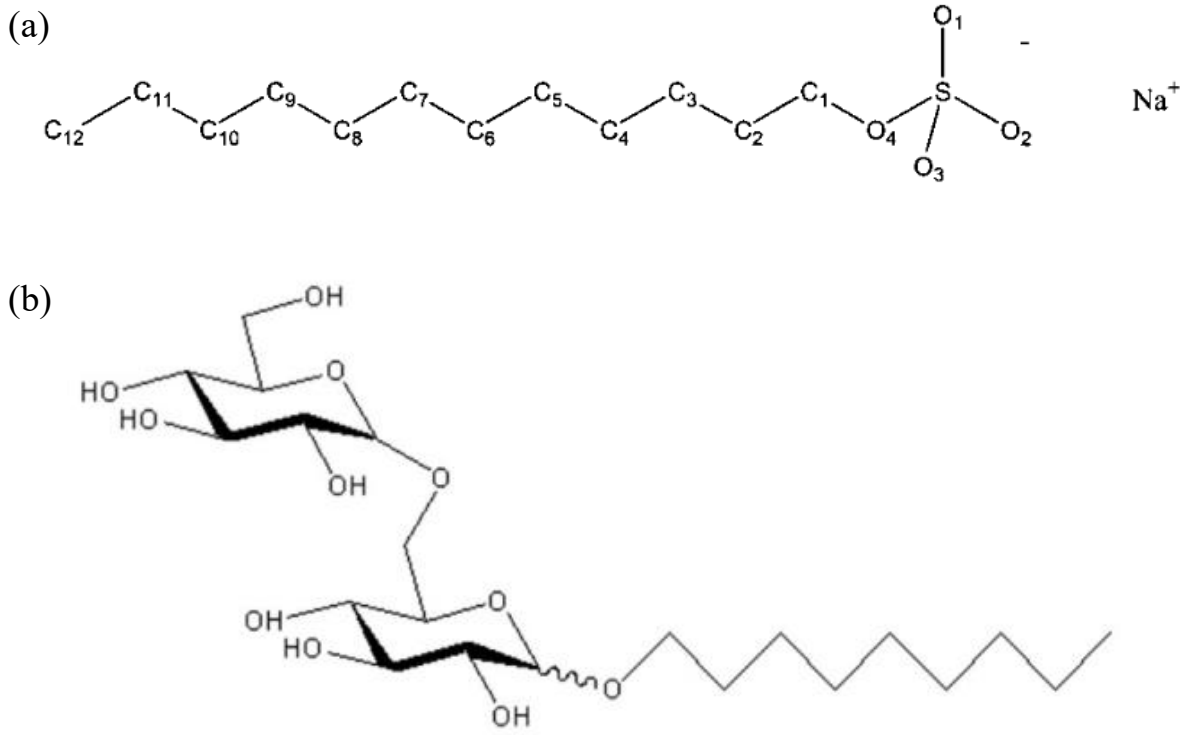

Figure 1.4.3: (a) Structure of sodium dodecyl sulfate (SDS) (Bruce et al., 2002) (b) Example of the typical structure of an alkyl polyglucoside (Drakontis and Amin, 2020).

1.4.2 Surfactant self-assembly

As mentioned previously, above the CMC, the surfactant molecules in solution assemble into different self-assembled structures. The type of self-assemblies can be predicted by the packing parameter (p), which is defined as:

Equation 2:

$$p = \frac{V}{a_0 * l_c}$$

where V is the volume occupied by the hydrophobic tail, a_0 is the area occupied by the hydrophilic head, and l_c is the length of the hydrophobic tail (**Figure 1.4.4**).

For $p < \frac{1}{3}$, the self-assemblies are micelles (**Figure 1.4.5.a**). For $\frac{1}{2} < p < \frac{1}{3}$ the self-assemblies are vesicles (**Figure 1.4.5.b**). For $p = 1$ the surfactant self- assembled into bilayers (**Figure 1.4.5.c**). For $p > 1$ the self-assembled structure are inverse micelles (**Figure 1.4.5.d**) (Mittal and Bothorel, 1986).

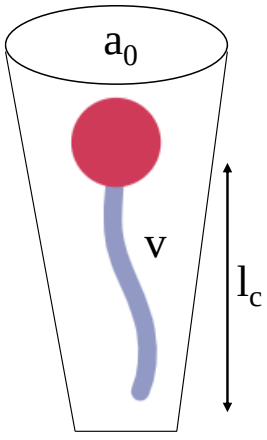

Figure 1.4.4: Scheme of the values to be considered when calculating the packing parameter (p).

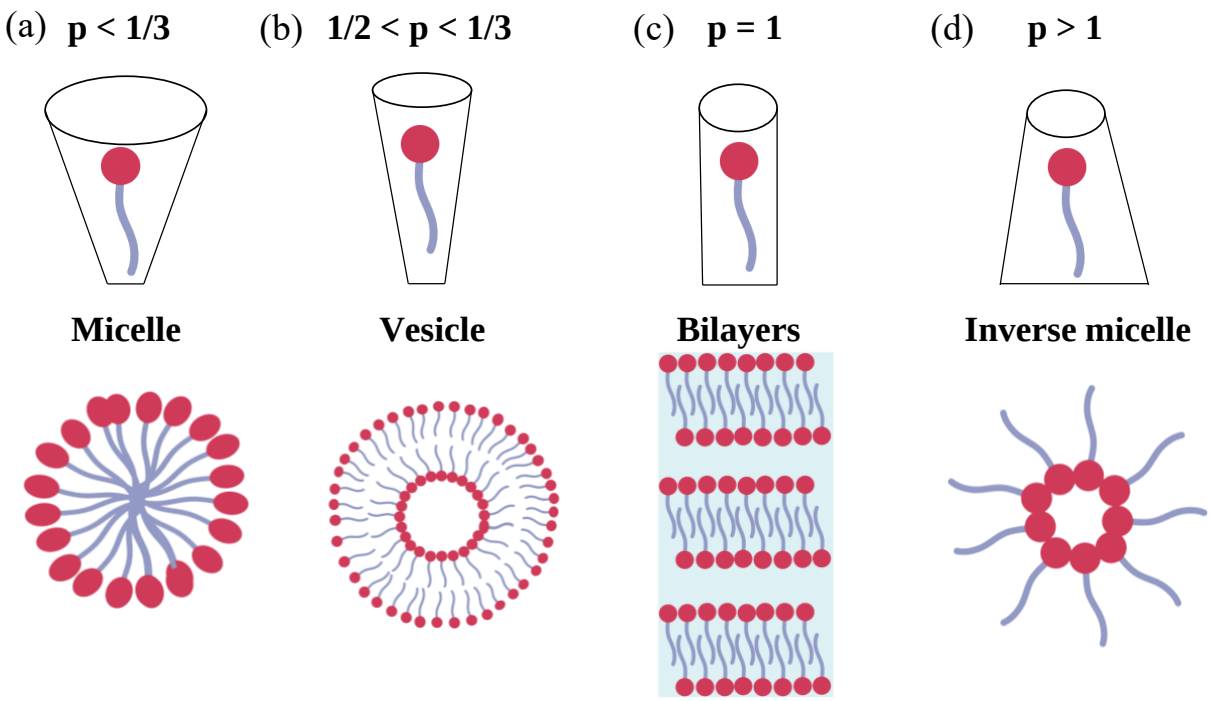

Figure 1.4.5: scheme of the different self-assembly that can be formed according to packing parameter (p). (a) Micelles. (b) Vesicles. (c) Bilayers. (d) Inverse micelles.

All these different self-assemblies depend not only on the molecular structure of the surfactants, but also on the medium conditions (pH, temperature, ionic strength, etc.) (Fameau and Salonen, 2014).

To determine the self-assembly structure of surfactants scattered techniques are used. Small-angle Neutron Scattering (SANS) and Small-angle X-ray Scattering provide information of the size, shaepe, distribution and interaction of particles at nanometre scale (Schnablegger and Singh, 2013). In these techniques, the neutron bean or the X-ray, depending on whether SANS or SAXS, are scattered by the sample, and the scattered intensity is tracked as a fuction of the wave vector Q, as illustrated in

Figure 1.4.6. If information is required at atomic or molecular scale, the scattered angle can be increased, to explore lowers Q, in this case the scattered technique is called Wide-ray Angle

Scatering (WAXS). On the contrary, to explore scales from a hundreds of nanometers to a few micrometers Ultra-Small-Angle X-ray Scattering (USAXS) can be used.

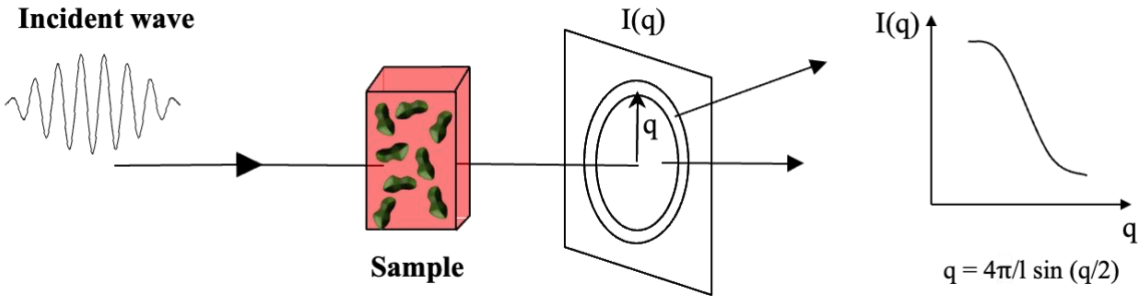

Figure 1.4.6 : Scheme of the scatered techniques.

1.4.3 Role of the surfactants on foam production and stability

Surfactants, in addition to lowering the surface tension and enabling the creation of the foam, play an important role in the stability of the foam. This role is related to their presence in the Plateau borders, in the thin films and at the air/water interface (Fameau and Salonen, 2014).

When foam is generated, the initial action of the surfactants is to adsorb at the interface, creating a monolayer. Specific surfactants (alone or in mixture) can form a monolayer with high compression rigidity and elasticity which might prevent coalescence and coarsening (Fameau and Salonen, 2014). However, in surfactant monolayers, an exchange of free monomers from the continuous phase and the interface can occur due to the affinity of the surfactant for both phases (Fameau and Salonen, 2014). This would lead to a layer less resistant to the foam destabilization processes.

The hydrophobic tail of the surfactant molecules allows other molecules to be solubilized in the solution that would otherwise be poorly soluble (Cantat et al., 2013). This is the case of the so-called co-surfactants, which can be added to the solution and intercalate with the surfactant molecules (Cantat et al., 2013). These molecules interact with the surfactants *via* electrostatic

or steric interactions. Their ability to enhance stability stems from their lower solubility, effectively inhibiting the exchange of molecules between the continuous phase and the interface (Cantat et al., 2013). Once the surfactants have covered the interface with their monolayer, they begin to self-assemble. The self-assembled structures can adsorb underneath the monolayer, forming a layer at the interface that confers high compression rigidity, slowing down coarsening and coalescence (Fameau and Salonen, 2014).

The various self-assembled structures in the Plateau borders of the foam increase the viscosity of the continuous phase slowing down or arresting drainage (Fameau and Salonen, 2014). In addition, these structures can be trapped in the foam films, pushing the bubbles away from each other by steric repulsion, preventing coalescence and coarsening (Fameau and Salonen, 2014).

1.5 Foam cleaning

In section 2.1 it was explained that foams are already used to clean open surfaces in the food industry. However, they are used as a means to apply chemicals, and not only for their cleaning power. The studies showing that foams have an effect on cleaning solid surfaces due to their physicochemical properties are fairly recent. Static foam cleaning is the process of cleaning a surface by simply putting in contact a foam with a surface for a certain amount of time (Schad et al., 2021, 2022a, 2022b; Guzmán García Lascurain et al., 2023). With this technique, foams have been used to clean lipids, oil and solid particles (dust) from solid surfaces, such as, wafers, glass plates and historical objects. Moreover, preliminary studies has recently been carried out to use foams for cleaning closed surfaces as a replacement for traditional CIP. Foam cleaning in closed surfaces refers to the foam flow inside of pipes for decontamination purposes (Fournel et al., 2003; Al Saabi et al., 2021; Dallagi et al., 2022b). It is a continuous process, in which foam is produced at the inlet of the pipe and circulated as long as the decontamination process requires.

The upcoming sections will explore in greater detail the current understanding regarding the utilization of foams in cleaning processes.

1.5.1 Mechanisms involve in foam cleaning

According to Schad et al., there are three mechanisms taking place when cleaning with foams in static conditions (**Figure 1.5.1**) (Schad et al., 2021):

- **Imbibition**: when a liquid is sucked up into the Plateau borders of the foam by capillary forces. This mechanism becomes stronger with small bubbles and small liquid fractions.
- **Wiping**: this mechanism occurs by re-arrangements of the bubbles, that leads to wiping motions between the foam and the surface. These wiping motions exert strong shear stress because of the movements of the thin wetting films and bubble meniscus along the surface. This mechanism is promoted in unstable foams where re-arrangements of the bubbles occur.
- **Drainage**: the liquid drained from a foam can flow under the soiled of the surface and lift the contaminant. When this happens, the contaminant is pushed together on the surface. This occurs in foams where the capillary forces are not enough to retain the liquid of the foam and so it drains.

These mechanisms are not isolated and usually occur more than one at a time. Imbibition and wiping are stronger with low liquid fractions. Wiping and drainage are stronger with unstable foams.

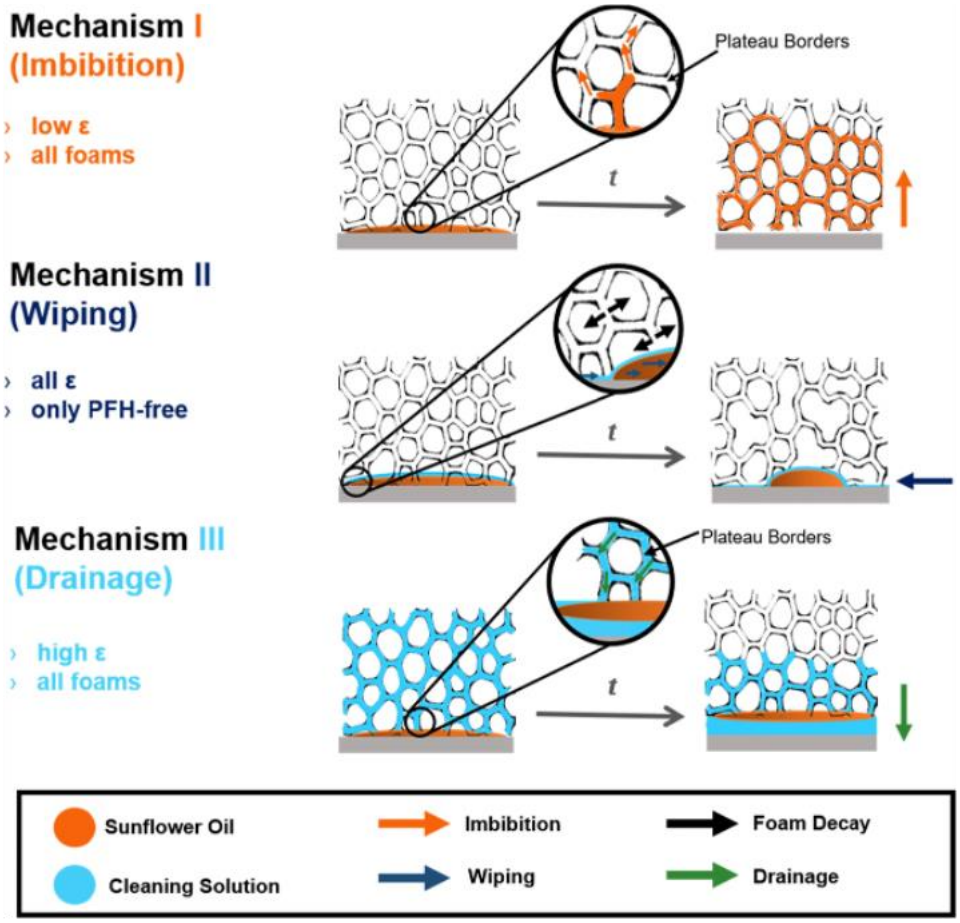

Figure 1.5.1: Scheme of three mechanisms involve in foam cleaning in static condition, using foams with different liquid fractions and sunflower oil as model contaminant. The figure was reproduced from (Schad et al., 2021).

In foam flow cleaning, the critical factor at play is the viscous stress within the foam. When a foam is subjected to a shear stress that exceeds the elastic limit of the foam, it flows (Denkov et al., 2009a). As the bubbles flow, they slide against each other and friction is generated within the foam, which causes energy dissipation, resulting in the appearance of foam viscous stress against the solid wall over which it is flowing (Denkov et al., 2009b). Thus, this mechanism hinges not only on the velocity of foam flow but also on the inherent characteristics of the foam, particularly regarding the composition of its films and interfaces. The friction within the foam significantly affects its interaction with the solid surface.

1.5.2 Wide range of applications of foams for cleaning purposes

1.5.2.1 Foam cleaning in open surfaces (static condition)

Despite the scientific consensus that foam generated in washing processes, such as for cleaning hair and skin (shampoo, shower gel, facial ceanser, etc.), has no effect on cleaning, Jones et al. carried out a study on the role of interfaces in the cleaning of silicon wafers coated with a mixture of model lipids, representing human sebum (Jones et al., 2020). The study primarily focused on surfactant solutions; however, as a final step, some initial investigations were conducted using foams. The static foam cleaning test was carried out by putting a foam in contact with the surface. As a result, they found some patterns in the foam that could suggest a role of foam in sebum removal (**Figure 1.5.2**). According to the authors, the role of foam can only occur if there is no liquid film between the surface and the foam. However, the authors are not sure whether a liquid film is present, so the role of foam and the mechanism of action are not clear.

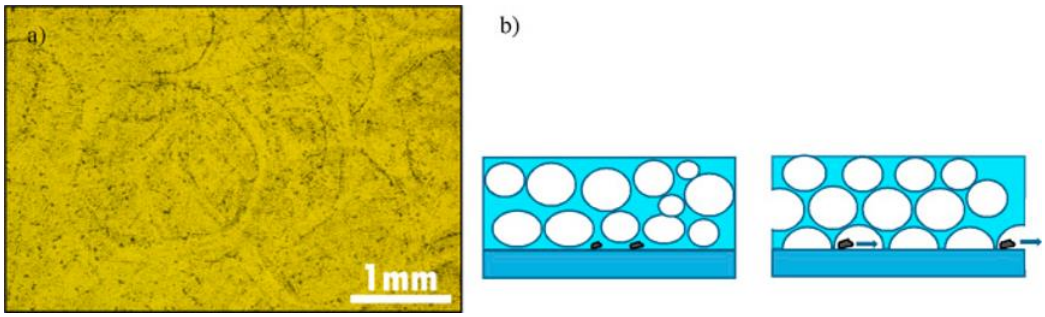

Figure 1.5.2: (a) microscopic image of a wafer after a static foam test, at ×5 magnification, showing distinct patterns in the sebum. (b) Scheme of the possible cleaning mechanism associated with a non-wetting and wetting situations. The figure was reproduced from (Jones et al., 2016).

Schad et al. have studied in detail the mechanisms involved in the cleaning of oil-soiled surfaces using the static foam cleaning technique (Schad et al., 2021). They produced foams based on alkyl polyglucosides (Glucopon 215 up) at a very high concentration (≈90 times the CMC)

using the double syringe technique to obtain small bubbles and tested different liquid fractions. In addition, they produced the same foams with the addition of perfluorohexane (PFH). The addition of PFH allows to obtain highly stable foams, as it has a very low solubility in water and so slows down coarsening. The cleaning efficiency was tested on glass plates, and the contact time with the foam was 15 min. The best cleaning result was obtained with the smaller liquid fraction and the foam without PFH (Figure 16). In this way, the authors demonstrated that the best way to clean oil from solid surfaces using static foam is promoting imbibition and wiping. The small bubbles size (radius ≈50-70 μm) obtained thanks to the double syringe technique and the smaller liquid fraction (≤ 5%) promoted the imbibition mechanism. Despite of this mechanism being promoted in both foams, with and without PFH, the foam without PFH cleaned better than the one with PFH, showing the importance of the wiping mechanism, since this mechanism is promoted in less stable foams (**Figure 1.5.3**). Schad et al. also showed that the same formulation can be used for cleaning glass surfaces soiled with oil containing soots (Schad et al., 2022a). In this case, the same cleaning mechanisms were involved. However, the authors also demonstrated that it is important that the liquid foam channels are big enough to let the particles pass through them. At the same time, it is important to note that it is thanks to the oil that particles can be sucked through the imbibition mechanism. In another study, Shad et al. demonstrated how static foam based on the formulation described previously can be used for cleaning historical objects (**Figure 1.5.4**) (Schad et al., 2022b). Once more, they attributed the effectiveness of the cleaning to the promotion of the mechanisms of imbibition and wiping; although attributing this effect to imbibition is not entirely correct as the soiling of historical objects was not related to liquid substances. It remains to be further discussed what cleaning mechanisms are involved in this case.

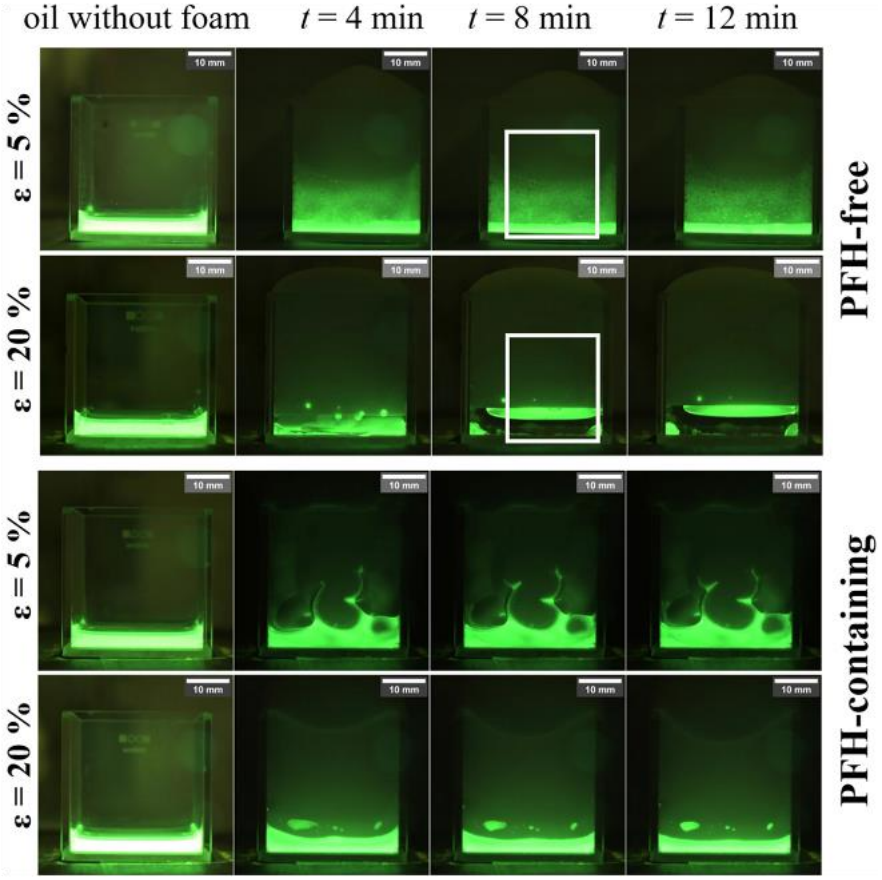

Figure 1.5.3: Pictures showing the effect of foams on cleaning oil from glass surfaces. In the foams with a liquid fraction of 5% with and without PFH the imbibition mechanism is promoted, but in the foam without PFH (less stable) the wiping mechanism is also promoting resulting in a better cleaning efficiency. The figure was reproduced from (Schad et al., 2021).

Figure 1.5.4: Historical object (left) before cleaning, (center) during cleaning with foam, and (right) after cleaning The figure was reproduced from (Schad et al., 2022b).

Notice that foams for cleaning purposes can also be applied in the form of a "gel-foam" i.e., foams whose continuous phase is a gel. Guzman Garcia Lascurain et al. studied the cleaning effect of agar foams on gypsum surfaces (Guzmán García Lascurain et al., 2023). However, such foams are mainly used because they allow a controlled release of water on the surface.

Le Toquin et al. worked with foams to decontaminate surfaces soiled with bacterial spores and biofilms(Le Toquin, 2018; Le Toquin et al., 2018). The study focused on foams containing bactericides and not on studying the effect of the foam itself. However, some tests were carried out with a a foam without bactericides and composed of alkyl polyglucosides (Glucopon 215) and xanthan gum (Le Toquin, 2018). The foam was produced in a tube containing glass beads by injecting the foaming solution and air (Figure 17). The liquid fraction of the foam was between 5 and 6 %. The foam was placed on the surface to clean in a horizontal position for 30 minutes. The cleaning efficiency was tested on different surfaces (aluminium, polystyrene, palience tile, glass, stainless steel and mortar), which were soiled with *Bacillus thuringiensis*

spores. Le Toquin showed that the foam itself reduced the percentage of spores on the surface by 15 to 33 % depending on the surface (28 % for stainless steel).

1.5.2.2 Foam cleaning in closed surfaces (dynamic condition)

To the best of our knowledge, foam flow cleaning on high scale level have only been used for nuclear decontamination. The use of foam flows in nuclear decontamination started to be used because it requires less chemicals and produces less radioactive waste than other processes, while obtaining the same cleaning efficiency (Gossard et al., 2022). At the French Alternative Energies and Atomic Energy Commission (CEA), the behavior of foam flow for nuclear decontamination at a pilot scale was studied (**Figure 1.5.5**) (Fournel et al., 2003). The foam was based on two surfactants: alkyl polyglucoside (non-ionic) and sulfobetaine (amphoteric). The liquid fraction was set at 10 wt.%. The formulation was designed so that other chemicals could be incorporated to allow the dissolution of the radioactive contaminants in the foam, taking advantage of the mechanism of destabilization by drainage. According to the authors, sulfobetaine adsorbs faster at the interface than APG, but does not produce a stable film; thus APG provides stability to the foam over time. In the meantime, liquid is released from the films, which upon contact with the surface, facilitates decontamination. The foam was produced with a static generator filled with glass spheres; at the end of the pipe, a vacuum pump maintained the depression. This system allows the decontamination of pipes up to 130 m in length. Another foam production system implemented by authors but developed by Turchet et al, allowed to increase the decontamination length to 130 m (Turchet et al., 2002). This system called “foam-chain circulation” consists of altering injections of foam and air at different times (**Figure 1.5.6**).

Figure 1.5.5. Pictures of the pilot set up used for the study of foam flow for nuclear decontamination. The figure was adapted from (Gossard et al., 2022).

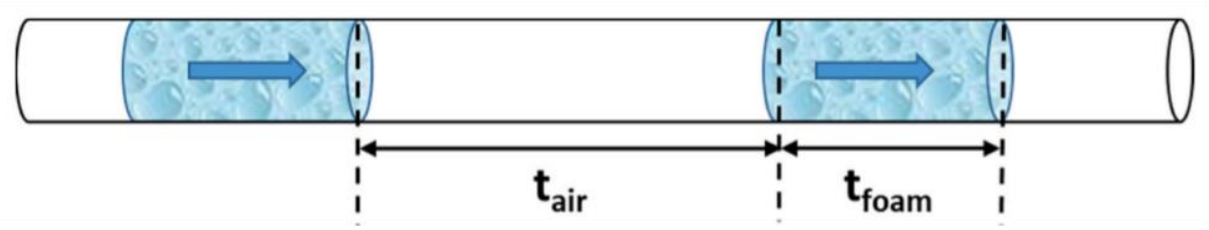

Figure 1.5.6: Schematic diagram of the system called "foam-chain circulation" developped by (Turchet et al., 2002) which consists of altering injections of foam and air at different times. The figure was adapted from (Gossard et al., 2022).

Al Saabi et al, conducted the first study on the removal of biocontamination in pipelines using foam flows (Al Saabi et al., 2021). The foam was based on SDS at a concentration slightly below to the CMC. The foam was produced by bubbling air through a porous disc into the surfactant solution, the foam continuously flowed through a square pipe (Figure 20). The authors tested three foam liquid fractions (0.5, 0.4 and 0.3) and three air and liquid flow rates for each liquid fraction, giving as result different foam flow velocities and different shear stress. First, they studied the kinetics removal of *B. subtilis* 98/7 spores (hydrophilic) from stainless steel surfaces (2B finish) at the bottom of the pipe. The cleaning efficiency was evaluated by

swabbing the surfaces and enumeration on tryptone soy agar of serial dilutions. They found two distinct removal phases for all conditions: one lasting less than 1 min and the other one lasting at least 20 min. The best cleaning efficiency was found with the foam with the liquid fraction of 0.5 with a mean velocity of 4 $cm.s^{-1}$ and a shear stress of 4.2 Pa. With these conditions the spores log reduction was 1.8 and 2 for 1 min and 20 of foam flow cleaning, respectively. In addition, the cleaning efficiency was 0.5 log higher than CIP at a shear stress of 5 Pa with much more water consumption for CIP (650 $l.h^{-1}$) than foam flow (9 $l.h^{-1}$). Then, the authors carried out experiments using *B. cereus* spores (hydrophobic), and they observed the same kinetics removal, although the cleaning efficiency was less for these spores.

Dallagi et al, continued working on the biodecontamination of pipelines by foam flow based on the work of Al Saabi et al (Al Saabi et al., 2021; Dallagi et al., 2022b). First, they studied the decontamination of pipes soiled with spores of two different strains, which differ only in their hydrophilicity/hydrophobicity properties: *Bacillus subtilis* PY79 (hydrophilic) and *Bacillus subtilis* PY79 spsA (hydrophobic). The foam was produced in the same set up as the works of Al Saabi et al, and was also based on SDS at the same concentration (below CMC) (Al Saabi et al., 2021) (

Figure 1.5.7). In this case, the authors worked at a fixed liquid fraction (0.5), which was the one that resulted in better cleaning efficiency in the previous work. In this work, they studied the effect of different foam flow velocities (1.5, 3, 4.5, 9 and 13.5 $cm.s^{-1}$) on spores detachment. The foams were characterized in terms of bubble size distribution, taking photos of the foam that passed through a transparent duct and using a software for image analysis. Moreover, the thin film thickness and the wall shear stress were measured by conductimetry and polarography respectively. The results showed that the cleaning efficiency was dependent on the foam flow velocity and on the spore hydrophobicity. The cleaning efficiency improved with increasing velocity, up to 9 $cm.s^{-1}$, but for the highest speed (13.5 $cm.s^{-1}$) the efficiency was lower than for 9 $cm.s^{-1}$. The authors explain this result by relating the variations in bubble size to the shear stress in the wall. The bubble size distribution decreased with increasing velocity up to 9 $cm.s^{-}$

[1]. However, when the velocity was increased further (13.5 $cm.s^{-1}$) a slight increase of the bubble size distribution was observed. At the same time, the wall shear stress increased with increasing velocity (for 1.5, 3 and 4.5 $cm.s^{-1}$) and the fluctuations in the wall shear stress decreased with increasing velocity. When extrapolating the results to the higher velocities (9 and 13.5 $cm.s^{-1}$), the authors found smaller fluctuations for 9 $cm.s^{-1}$ than for 13.5 $cm.s^{-1}$. According to the authors, this was related to the presence of smaller bubbles for the 9 $cm.s^{-1}$ velocity and this would explain its higher cleaning efficiency. The mean value of the film increased with increasing speed, which was 11, 12 and 13 μm for 1.5, 3 and 4.5 $cm.s^{-1}$ respectively; and the variations in film thickness were smaller with increasing speed. The foam flow cleaning kinetics followed the same tendency as for the work of Al Saabi. In addition, the spore removal was better for hydrophilic spores than for hydrophobic ones, reaching around 4 log of spore reduction and 2 log of spore reduction respectively, for 20 min of foam flow with the best condition.

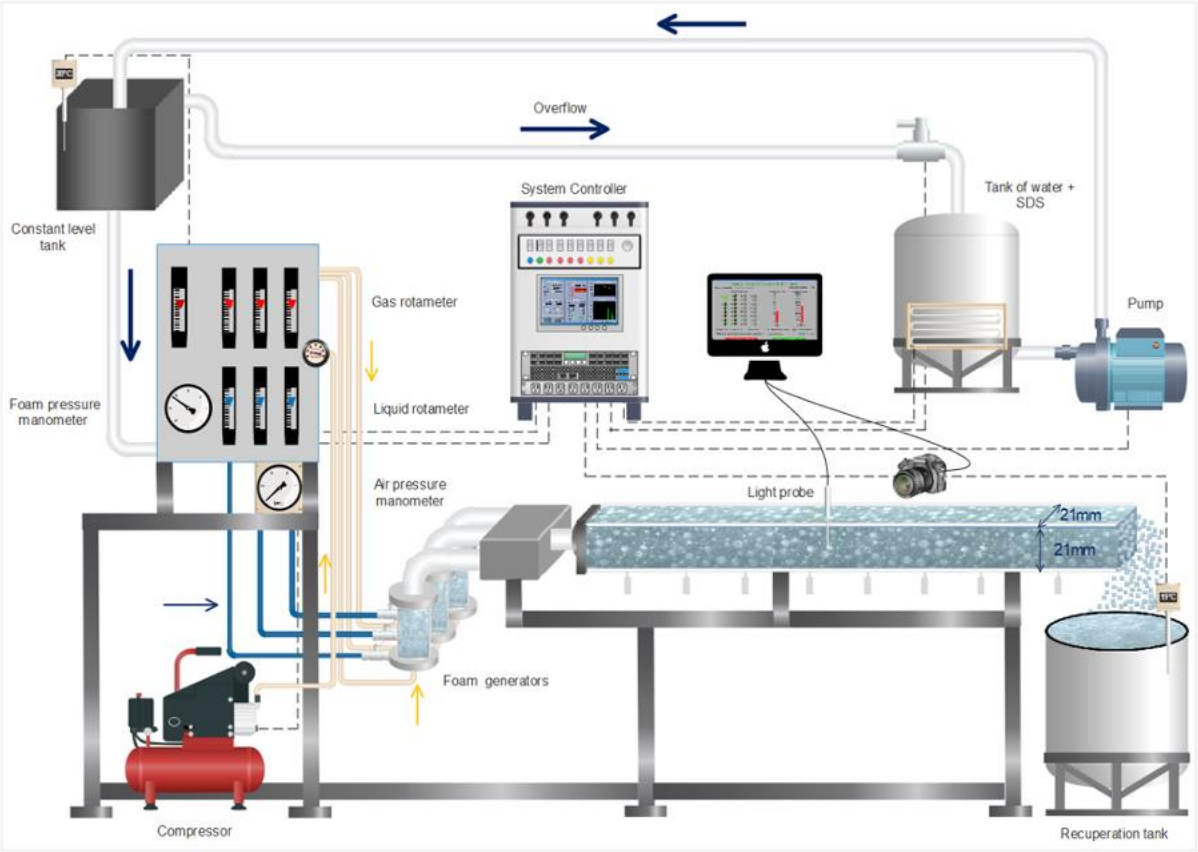

Figure 1.5.7: Diagram of the foam flow set up used in the works of Al Saabi et al. et Dallgi et al. (Al Saabi et al., 2021; Dallagi et al., 2022c, 2022b). The figure was adapted from (Dallagi et al., 2022a).

In a further step, Heni et al, investigated the effect of different foam flow velocities on the removal of biofilms of three different bacterial strains (*Escherichia coli* SS2, *Bacillus cereus* 98/4 and *Pseudomonas fluorescens* Pf1), meaning three different types of biofilms (Dallagi et al., 2022c). The *Escherichia coli* SS2 biofilm presented little resistance to foam flow, since a the lowest velocity (1.5 $cm.s^{-1}$) led to a strong removal (4-5 log reduction). As for the other two strains, the log reduction increased with the increasing in velocity (increasing in the shear stress). The highest log reduction was obtained with a velocity of 13.5 $cm.s^{-1}$, and it reached 2 log for *Bacillus cereus* 98/4 biofilm, and 1.4 log for *Pseudomonas fluorescens*, for 20 min of foam flow cleaning. In all cases the cleaning efficiency was better with foam flow in

comparison to CIP using SDS at the same concentration, and with a shear stress equal to the average of all those tested in the foam flow. Furthermore, the authors conducted a LCA comparing the impacts produced when cleaning with CIP using NaOH, CIP using SDS and foam flow cleaning (Dallagi et al., 2022c). The LCA showed that CIP with NaOH was the most harmful process, followed by the CIP with SDS. The main difference between these two-cleaning processes is the use of NaOH and the energy for heating the NaOH solution contributes to increase the impacts. The foam flow proved to be the least harmful process, as it significantly reduces the usage of chemicals (SDS) and water.

1.6 Generalities of Water-in-Water emulsions

Since the last chapter of this thesis focuses on the stabilisation of water-in-water (W/W) emulsions, with the aim of their subsequent use as an innovative cleaning method, an introduction to this topic is given in this section.

Aqueous Two-Phase Systems (ATPS) are aqueous mixtures that separate into two immiscible phases. Water-in-water emulsions can form in these systems and are therefore sometimes referred to as 'ATPS emulsions', although the more common term is 'water-in-water emulsions'.

Phase separation in aqueous systems can occur in two ways: by segregative phase separation or by associative phase separation. Here we will focus on the former. Segregative phase separation occurs when two hydrophilic polymers in solution above minimum concentrations separate into two immiscible phases in thermodynamic equilibrium (Esquena, 2016). Each phase is enriched in one of the polymers and saturated in the other (Esquena, 2016). By applying mechanical agitation to segregative phase separation systems, W/W emulsions can be produced (**Figure 1.6.1**).

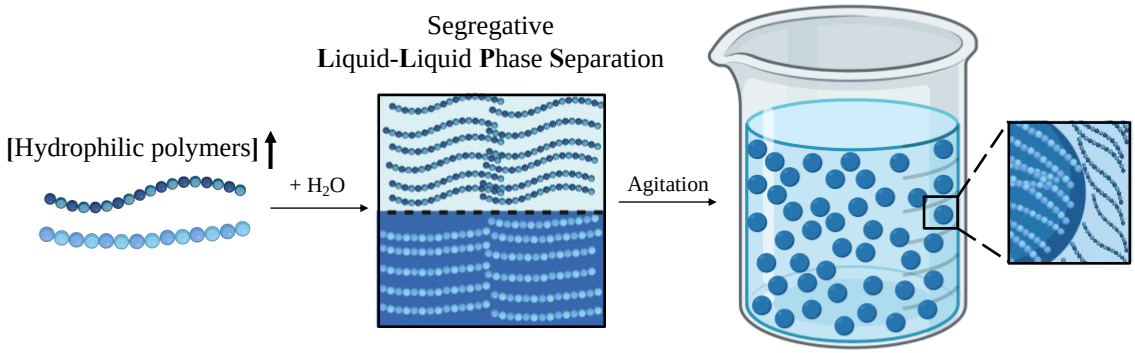

Figure 1.6.1 : Scheme of the general procedure to obtain a water-in-water emulsion.

In contrast to common oil-in-water emulsions, W/W emulsions are much more difficult to stabilize since the surface tension is very low (around 0.1-100 µN/m) and the interface thickness is large (10 to 100 nm) (Antonov et al., 2004; Esquena, 2016). For these physical reasons, W/W emulsions cannot be stabilized by the common surfactants (typical size ~1 nm) usually used for the stabilization of the oil-in-water or water-in-oil emulsions. Thus, the unstabilized W/W emulsion droplets coalesce with time, more or less quickly depending on the system investigated, resulting in macroscopic phase separation.

Given the fully aqueous composition, several potential applications of W/W emulsions have been reported, such as in foods, cosmetics, and biomedical applications (Esquena, 2016, 2023).

1.7 Conclusions and objective of the thesis project

As described in the state-of-art section, foams could be a promising eco-friendly cleaning method for the food industry as they reduce the consumption of water, energy and chemicals required for cleaning (Dallagi et al., 2022c). However, so far, they have only been used on an industrial scale for cleaning open surfaces and as a means of applying cleaning chemicals. Moreover, they are not yet used on an industrial scale for the cleaning of closed surfaces. It has already been shown that foams themselves can clean by different mechanisms (Schad et al.,

2021; Dallagi et al., 2022b). Static foam cleaning has proven effective in removing various types of contaminants (Jones et al., 2016; Schad et al., 2021, 2022a). However, as far as our understanding extends, only one study has investigated the static foam cleaning of surfaces contaminated with bio-contamination, yet it does not address the foam properties pertinent to the cleaning process. (Le Toquin, 2018). In addition, foam flow cleaning has successfully been used for removal of biocontamination from pipes at a pilot scale (Al Saabi et al., 2021; Dallagi et al., 2022c, 2022b). However, the surfactant used for this proof of concept was the SDS, which contributes to several environmental impacts and it was used at a concentration below to the CMC.

The general objective of this thesis is to use various liquid foams systems as an innovative eco-friendly cleaning method for the food industry, and to understand the foam properties governing the decontamination process.

This thesis is structured into three main parts: the first one concerns the investigation of static foam cleaning, the second one explores foam flow cleaning, and the final one focuses on the design of possible new foam systems for cleaning applications. The first part is divided in two chapters:

In the first chapter, we used the 10-hydroxystearic acid (10-HSA), a new hydroxylated fatty acid that can be easily obtained from oleic acid by using microorganisms to produce foams. We studied for the first time the self-assembly and the foaming properties of 10-HSA soap. Then, we used these foams for static foam cleaning of stainless-steel surfaces soiled with hydrophilic bacteria spores. Employing two distinct foam production methods, we generated foams to assess the influence of bubble size and liquid fraction on cleaning efficacy. Our findings revealed a difference in the power of cleaning depending on the size of the foam bubbles.

In the second chapter, we used a widely recognized commercial surfactant: Sodium Cocoyl Isethionate (SCI), a bio-derived surfactant extensively employed in the cosmetics industry. We studied for the first time in deep the bulk and the foaming properties of SCI. Then, we used the

foams produced with SCI for static foam cleaning of stainless-steel surfaces soiled with two types of bacteria spores, which differ in their hydrophobicity/ hydrophilicity character. We produced foams with the double-syringe technique to maintain the foam bubbles size but varying the liquid fraction. Different experimental conditions were carried out, such as different liquid fractions, foams with and without drainage, different levels of attachment of the spores to the surface. In this way the foam cleaning mechanisms were elucidated.

In the second part, we focused on the study of foam flow for the cleaning of bio-contamination in pipelines. The objective was to see what level of cleaning is achieved with micelle-stabilized foams with a model surfactant (SDS) and to compare it with micelle-stabilized foams with bio-based surfactants. For this purpose, we decide to choose alkyl polyglucosides to produce the foam, which are commercially available bio-based surfactants. Two different alkyl polyglucosides were used: decyl glucoside (DG) and lauryl glucoside (LG). We also carried a Life Cycle Analysis comparing both processes (with SDS and with alkyl polyglucosides). In addition, we evaluated the destruction of the foam by filtration and the reutilization of the surfactant solution. No effect on alkyl chain length between DG and LG was observed. We demonstrated that APGs are a good choice to replace SDS in foam flow cleaning, as they allow to further decrease the environmental impacts.

In the last part of this thesis, we aimed to identify and investigate a novel type of soft material system for cleaning purposes. We chose to study 'water-in-water emulsions' (W/W emulsions) where an aqueous solution forms droplets inside another aqueous solution (Esquena, 2016, 2023; Dickinson, 2019). One of the most interesting applications of W/W emulsions is their possible use for the design of novel encapsulation and delivery systems for labile molecules such as antibacterial agent but also for possible encapsulation and separation of spores/bacteria (Esquena, 2016). The lack of stability of W/W emulsions is the main drawback that limits their use for practical applications (Esquena, 2016). Here, we first study how W/W emulsions can be stabilized by mixture of surfactant (alkylpolyglucosides, APGs) and medium chain fatty alcohols. The mixture of surfactant and fatty alcohols are widely used in the field of cosmetic

and pharmaceutical industries to form Lamellar gel Network (LGNs) (Eccleston, 1997). Lamellar gel networks (LGNs), which are also termed "α-gels" in literature, are used to give creamy texture to the products (Eccleston, 1997; Iwata, 2017). Then, we tried for the first time to produce foams based on W/W emulsions.

1.8 References

Ainslie, E. A., Quarini, G. L., Ash, D. G., Deans, T. J., Herbert, M., and Rhys, T. D. L. (2009). HEAT EXCHANGER CLEANING USING ICE PIGGING.

Al Saabi, A., Dallagi, H., Aloui, F., Faille, C., Rauwel, G., Wauquier, L., et al. (2021). Removal of Bacillus spores from stainless steel pipes by flow foam: Effect of the foam quality and velocity. *Journal of Food Engineering* 289, 110273. doi: 10.1016/j.jfoodeng.2020.110273

Antonov, Y. A., Van Puyvelde, P., and Moldenaers, P. (2004). Interfacial tension of aqueous biopolymer mixtures close to the critical point. *International Journal of Biological Macromolecules* 34, 29–35. doi: 10.1016/j.ijbiomac.2004.01.001

Arellano, H., Nardello-Rataj, V., Szunerits, S., Boukherroub, R., and Fameau, A.-L. (2023). Saturated long chain fatty acids as possible natural alternative antibacterial agents: Opportunities and challenges. *Advances in Colloid and Interface Science* 318, 102952. doi: 10.1016/j.cis.2023.102952

Augustin, W., Fuchs, T., Föste, H., Schöler, M., Majschak, J.-P., and Scholl, S. (2010). Pulsed flow for enhanced cleaning in food processing. *Food and Bioproducts Processing* 88, 384–391. doi: 10.1016/j.fbp.2010.08.007

Basso, M., Simonato, M., Furlanetto, R., and De Nardo, L. (2017). Study of chemical environments for washing and descaling of food processing appliances: An insight in commercial cleaning products. *Journal of Industrial and Engineering Chemistry* 53, 23–36. doi: 10.1016/j.jiec.2017.03.041

Beattie, J. K., Djerdjev, A. M., Gray-Weale, A., Kallay, N., Lützenkirchen, J., Preočanin, T., et al. (2014). pH and the surface tension of water. *Journal of Colloid and Interface Science* 422, 54–57. doi: 10.1016/j.jcis.2014.02.003

Bhadani, A., Kafle, A., Ogura, T., Akamatsu, M., Sakai, K., Sakai, H., et al. (2020). Current perspective of sustainable surfactants based on renewable building blocks. *Current Opinion in Colloid & Interface Science* 45, 124–135. doi: 10.1016/j.cocis.2020.01.002

Bintsis, T. and Department of International Trade, TEI of West Macedonia, Kastoria, Greece (2017). Foodborne pathogens. *AIMS Microbiology* 3, 529–563. doi: 10.3934/microbiol.2017.3.529

Bruce, C. D., Berkowitz, M. L., Perera, L., and Forbes, M. D. E. (2002). Molecular Dynamics Simulation of Sodium Dodecyl Sulfate Micelle in Water: Micellar Structural Characteristics and Counterion Distribution. *J. Phys. Chem. B* 106, 3788–3793. doi: 10.1021/jp013616z

Cantat, I., Cohen-Addad, S., Elias, F., Graner, F., Hohler, R., Pitois, O., et al. (2013). Les mousses - Structure et dynamique.

Cherif-Antar, A., Moussa–Boudjemâa, B., Didouh, N., Medjahdi, K., Mayo, B., and Flórez, A. B. (2016). Diversity and biofilm-forming capability of bacteria recovered from stainless steel pipes of a milk-processing dairy plant. *Dairy Sci. & Technol.* 96, 27–38. doi: 10.1007/s13594-015-0235-4

Dallagi, H. (2022). Numerical and experimental investigations of the rheological behavior of foam flow: application to the cleaning of surfaces contaminated by microorganisms in the food industries.

Dallagi, H., Aloui, F., Bouvier, L., Wauquier, L., and Benezech, T. (2022a). Numerical and experimental investigations into the rheological behaviour of wet foam flowing under a fence. *Food and Bioproducts Processing* 132, 211–225. doi: https://doi.org/10.1016/j.fbp.2021.12.009

Dallagi, H., Dari, C., Anne-Laure, F., Aloui, F., Faille, C., and Benezech, T. (2024). Wet foam flow for cleaning food industry equipment: Role of geometry in maintaining removal efficiency of Bacillus spores. *Journal of Food Engineering* 376, 112064. doi: 10.1016/j.jfoodeng.2024.112064

Dallagi, H., Faille, C., Bouvier, L., Deleplace, M., Dubois, T., Aloui, F., et al. (2022b). Wet foam flow: A suitable method for improving surface hygiene in the food industry. *Journal of Food Engineering* 322, 110976. doi: 10.1016/j.jfoodeng.2022.110976

Dallagi, H., Faille, C., Gruescu, C., Aloui, F., and Benezech, T. (2022c). Foam flow cleaning, an effective and environmentally friendly method for controlling the hygiene of closed surfaces contaminated with biofilms. *Food and Bioproducts Processing* 136, 236–248. doi: 10.1016/j.fbp.2022.09.014

Dallagi, H., Jha, P. K., Faille, C., Le-Bail, A., Rawson, A., and Benezech, T. (2023). Removal of biocontamination in the food industry using physical methods; an overview. *Food Control* 148, 109645. doi: 10.1016/j.foodcont.2023.109645

D'Amico, D. (2008). Incidence, Ecology, and Fate of Target Foodborne Pathogens in the Cheesemaking Continuum. *Graduate College Dissertations and Theses*. Available at: https://scholarworks.uvm.edu/graddis/63

Dari, C., Cousin, F., Le Coeur, C., Dubois, T., Benezech, T., Saint-Jalmes, A., et al. (2023a). Ultrastable and Responsive Foams Based on 10-Hydroxystearic Acid Soap for Spore Decontamination. *Molecules* 28, 4295. doi: 10.3390/molecules28114295

Dari, C., Dallagi, H., Faille, C., Dubois, T., Lemy, C., Deleplace, M., et al. (2023b). Decontamination of Spores on Model Stainless-Steel Surface by Using Foams Based on Alkyl Polyglucosides. *Molecules* 28, 936. doi: 10.3390/molecules28030936

Dari, C., Si, Y., Douliez, J.-P., Tahon, J.-F., Benezech, T., Clegg, P. S., et al. (2023c). Mixture of fatty alcohols and alkyl polyglucosides stabilizing water-in-water emulsions. *Front. Soft Matter* 3. doi: 10.3389/frsfm.2023.1328195

DeFlorio, W., Liu, S., White, A. R., Taylor, T. M., Cisneros-Zevallos, L., Min, Y., et al. (2021). Recent developments in antimicrobial and antifouling coatings to reduce or prevent contamination and cross-contamination of food contact surfaces by bacteria. *Comp Rev Food Sci Food Safe* 20, 3093–3134. doi: 10.1111/1541-4337.12750

Denkov, N. D. (2004). Mechanisms of Foam Destruction by Oil-Based Antifoams. *ACS*

Publications. doi: 10.1021/la049676o

Denkov, N. D., Tcholakova, S., Golemanov, K., Ananthpadmanabhan, K. P., and Lips, A. (2009a). The role of surfactant type and bubble surface mobility in foam rheology. *Soft Matter* 5, 3389. doi: 10.1039/b903586a

Denkov, N. D., Tcholakova, S., Golemanov, K., Ananthpadmanabhan, K. P., and Lips, A. (2009b). The role of surfactant type and bubble surface mobility in foam rheology. *Soft Matter* 5, 3389–3408. doi: 10.1039/B903586A

Dickinson, E. (2019). Particle-based stabilization of water-in-water emulsions containing mixed biopolymers. *Trends in Food Science & Technology* 83, 31–40. doi: 10.1016/j.tifs.2018.11.004

Drakontis, C. E., and Amin, S. (2020). Biosurfactants: Formulations, properties, and applications. *Current Opinion in Colloid & Interface Science* 48, 77–90. doi: https://doi.org/10.1016/j.cocis.2020.03.013

Drenckhan, W., and Saint-Jalmes, A. (2015). The science of foaming. *Advances in Colloid and Interface Science* 222, 228–259. doi: 10.1016/j.cis.2015.04.001

Eccleston, G. M. (1997). Functions of mixed emulsifiers and emulsifying waxes in dermatological lotions and creams. *Colloids and Surfaces A: Physicochemical and Engineering Aspects* 123–124, 169–182. doi: 10.1016/S0927-7757(96)03846-0

EHEDG (2021). Doc. 52 Basic Principles of Cleaning and Disinfection in Food Manufacturing.
Esquena, J. (2016). Water-in-water (W/W) emulsions. *Current Opinion in Colloid & Interface Science* 25, 109–119. doi: 10.1016/j.cocis.2016.09.010

Esquena, J. (2023). Recent advances on water-in-water emulsions in segregative systems of two water-soluble polymers. *Current Opinion in Food Science* 51, 101010. doi: 10.1016/j.cofs.2023.101010

Fameau, A.-L., and Salonen, A. (2014). Effect of particles and aggregated structures on the foam stability and aging. *Comptes Rendus. Physique* 15, 748–760. doi: 10.1016/j.crhy.2014.09.009

Fann, S., Dawn, H., Treloar, P., and Mathews, A. (2019). Demonstration of Ice Pigging Technology to Remove Biofilms in Water Distribution Systems. Energy and Water Projects EW-201510. Naval Facilities Engineering and Expeditionary Warfare Center.

Farias, C. B. B., Almeida, F. C. G., Silva, I. A., Souza, T. C., Meira, H. M., Soares Da Silva, R. D. C. F., et al. (2021). Production of green surfactants: Market prospects. *Electronic Journal of Biotechnology* 51, 28–39. doi: 10.1016/j.ejbt.2021.02.002

Fournel, B., Faure, S., Pouvreau, J., Dame, C., and Poulain, S. (2003). Decontamination Using Foams: A Brief Review of 10 Years French Experience., in *9th ASME International Conference on Radioactive Waste Management and Environmental Remediation: Volumes 1, 2, and 3*, (Oxford, England: ASMEDC), 1483–1489. doi: 10.1115/ICEM2003-4526

Gaillard, T., Roché, M., Honorez, C., Jumeau, M., Balan, A., Jedrzejczyk, C., et al. (2017). Controlled foam generation using cyclic diphasic flows through a constriction. *International Journal of Multiphase Flow* 96, 173–187. doi: 10.1016/j.ijmultiphaseflow.2017.02.009

Garnier, C., Guiga, W., Lameloise, M.-L., and Fargues, C. (2023). Water reuse in the food processing industries: A review on pressure-driven membrane processes as reconditioning treatments. *Journal of Food Engineering* 344, 111397. doi: 10.1016/j.jfoodeng.2022.111397

Gossard, A., Lilin, A., and Faure, S. (2022). Gels, coatings and foams for radioactive surface decontamination: State of the art and challenges for the nuclear industry. *Progress in Nuclear Energy* 149, 104255. doi: 10.1016/j.pnucene.2022.104255

Gunduz, G. T., and Tuncel, G. (2006). Biofilm formation in an ice cream plant. *Antonie Van Leeuwenhoek* 89, 329–336. doi: 10.1007/s10482-005-9035-9

Guzmán García Lascurain, P., Goidanich, S., Briatico Vangosa, F., Anzani, M., Rabbolini, A., Sansonetti, A., et al. (2023). Agar Foam: Properties and Cleaning Effectiveness on Gypsum Surfaces. *Coatings* 13, 615. doi: 10.3390/coatings13030615

Iwata, T. (2017). "Lamellar Gel Network," in *Cosmetic Science and Technology*, (Elsevier), 415–447. doi: 10.1016/B978-0-12-802005-0.00025-2

Jones, L. D., Mana, T. S. C., Cadnum, J. L., Jencson, A. L., Silva, S. Y., Wilson, B. M., et al. (2020). Effectiveness of foam disinfectants in reducing sink-drain gram-negative bacterial colonization. *Infection Control & Hospital Epidemiology* 41, 280–285. doi: 10.1017/ice.2019.325

Jones, S., Rio, E., Cazeneuve, C., Nicolas-Morgantini, L., Restagno, F., and Luengo, G. S. (2016). Tribological influence of a liquid meniscus in human sebum cleaning. *Colloids and Surfaces A: Physicochemical and Engineering Aspects* 498, 268–275. doi: 10.1016/j.colsurfa.2016.03.047

Langevin, D. (2023). Recent Advances on Emulsion and Foam Stability. *Langmuir* 39, 3821–3828. doi: 10.1021/acs.langmuir.2c03423

Le Toquin, E. (2018). Mode d'action biocide de nouveaux procédés de décontamination sur deux formes de résistances bactériennes. Normandie. Available at: https://theses.fr/2018NORMR103 (Accessed April 12, 2024).

Le Toquin, E., Faure, S., Orange, N., and Gas, F. (2018). New Biocide Foam Containing Hydrogen Peroxide for the Decontamination of Vertical Surface Contaminated With Bacillus thuringiensis Spores. *Front. Microbiol.* 9, 2295. doi: 10.3389/fmicb.2018.02295

Lee, E.-J., Kim, Y.-H., Lee, C.-H., Kim, H.-S., and Kim, H.-S. (2016). Effect of different physical conditions on fouling control in in-situ chemical cleaning in place (CIP) for flat sheet membranes fouled by secondary effluents. *Chemical Engineering Journal* 302, 128–136. doi: 10.1016/j.cej.2016.05.039

Lelieveld, H. L. M., Mostert, M. A., Holah, B., and White, B. (2003). *Hygiene in Food Processing*. Cambridge, UK: Woodhead.

Lücking, G., Stoeckel, M., Atamer, Z., Hinrichs, J., and Ehling-Schulz, M. (2013). Characterization of aerobic spore-forming bacteria associated with industrial dairy processing environments and product spoilage. *International Journal of Food Microbiology* 166, 270–279. doi: 10.1016/j.ijfoodmicro.2013.07.004

Malysa, K., and Lunkenheimer, K. (2008). Foams under dynamic conditions. *Current Opinion in Colloid & Interface Science* 13, 150–162. doi: 10.1016/j.cocis.2007.11.008

McKenney, P. T., Driks, A., and Eichenberger, P. (2013). The Bacillus subtilis endospore: assembly and functions of the multilayered coat. *Nat Rev Microbiol* 11, 33–44. doi: 10.1038/nrmicro2921

Midelet, G., Brauge, T., and Faille, C. (2024). "Contamination croisée des aliments par des surfaces contaminées," in *Contrôle et Prévention des Risques Biologiques Associés à la Contamination des Aliments : Transformation, Distribution et Utilisation par le Consommateur*, (ISTE Editions). Available at: https://hal.univ-lille.fr/hal-04456514 (Accessed February 14, 2024).

Mittal, K. L., and Bothorel, P. eds. (1986). *Surfactants in Solution: Volume 4*. Boston, MA: Springer US. doi: 10.1007/978-1-4613-1831-6

Moerman, F., Rizoulières, P., and Majoor, F. A. (2014). "Cleaning in place (CIP) in food processing," in *Hygiene in Food Processing*, (Elsevier), 305–383. doi: 10.1533/9780857098634.3.305

Pant, K. J., Cotter, P. D., Wilkinson, M. G., and Sheehan, J. J. (2023). Towards sustainable Cleaning-in-Place (CIP) in dairy processing: Exploring enzyme-based approaches to cleaning in the Cheese industry. *Comp Rev Food Sci Food Safe* 22, 3602–3619. doi: 10.1111/1541-4337.13206

Pérez-Rodríguez, F., Valero, A., Carrasco, E., García, R. M., and Zurera, G. (2008). Understanding and modelling bacterial transfer to foods: a review. *Trends in Food Science & Technology* 19, 131–144. doi: 10.1016/j.tifs.2007.08.003

Petkova, B., Tcholakova, S., and Denkov, N. (2021). Foamability of surfactant solutions: Interplay between adsorption and hydrodynamic conditions. *Colloids and Surfaces A: Physicochemical and Engineering Aspects* 626, 127009. doi: 10.1016/j.colsurfa.2021.127009

Pinguli, L., Malollari, I., and Lici, L. (2017). OPTIMIZATION OF CLEANING PROCESS IN BREWERIES AN IMPORTANT TOOL IN EFFICIENT USE OF WATER AND MINIMIZATION OF DISCHARGES. 5.

Politova, N., Tcholakova, S., Valkova, Z., Golemanov, K., and Denkov, N. D. (2018). Self-regulation of foam volume and bubble size during foaming via shear mixing. *Colloids and Surfaces A: Physicochemical and Engineering Aspects* 539, 18–28. doi: 10.1016/j.colsurfa.2017.12.006

Ramsay, L. M., Lund, M. D., Baerentzen, R., Juhl, A. B., Pettit, P., and Andreasson, G. (2018). Effects of Ice Pigging on biofilm in non-chlorinated drinking water distribution systems in Denmark.

Rebello, S., Asok, A. K., Mundayoor, S., and Jisha, M. S. (2014). Surfactants: toxicity, remediation and green surfactants. *Environ Chem Lett* 12, 275–287. doi: 10.1007/s10311-014-0466-2

Ross, J., and Miles, G. D. (1941). An apparatus for comparison of foaming properties of soaps and detergents. *Oil Soap* 18, 99–102. doi: 10.1007/BF02545418

Sansebastiano, G., Zoni, R., and Bigliardi, L. (2007). "Cleaning and Disinfection Procedures in the Food Industry General Aspects and Practical Applications," in *Food Safety*, eds. A. McElhatton and R. J. Marshall (Boston, MA: Springer US), 253–280. doi: 10.1007/978-0-387-33957-3_13

Sarno, E., Pezzutto, D., Rossi, M., Liebana, E., and Rizzi, V. (2021). A Review of Significant European Foodborne Outbreaks in the Last Decade. *Journal of Food Protection* 84, 2059–2070. doi: 10.4315/JFP-21-096

Schad, T., Preisig, N., Blunk, D., Piening, H., Drenckhan, W., and Stubenrauch, C. (2021). Less is more: Unstable foams clean better than stable foams. *Journal of Colloid and Interface Science* 590, 311–320. doi: 10.1016/j.jcis.2021.01.048

Schad, T., Preisig, N., Drenckhan, W., and Stubenrauch, C. (2022a). Foam-based cleaning of surfaces contaminated with mixtures of oil and soot. *Journal of Surfactants and Detergents* 25, 377–385. doi: 10.1002/jsde.12580

Schad, T., Preisig, N., Piening, H., and Stubenrauch, C. (2022b). Innovative foam-based cleaning concepts for historical objects. *Tenside Surfactants Detergents* 59, 451–459. doi: 10.1515/tsd-2022-2478

Schnablegger, H., and Singh, Y. (2013). *The SAXS Guide*., 3rd edition. Austria: Anton Paar GmbH.

Sharma, M., and Anand, S. K. (2002). Characterization of constitutive microflora of biofilms in dairy processing lines. *Food Microbiology* 19, 627–636. doi: 10.1006/fmic.2002.0472

Silva, L. D., Filho, U. C., Naves, E. A. A., and Gedraite, R. (2021). Pulsed flow in clean-in-place sanitization to improve hygiene and energy savings in dairy industry. *J Food Process Engineering* 44, e13590. doi: 10.1111/jfpe.13590

Timmerman, H. (2022). Sustainability and cleaning: preparing for the future.
Tomas, N., and Tiwari, B. K. (2013). "Sustainable Cleaning and Sanitation in the Food Industry," in *Sustainable Food Processing*, eds. B. K. Tiwari, T. Norton, and N. M. Holden (Wiley), 363–376. doi: 10.1002/9781118634301.ch15

Turchet, J. P., Fournel, B., and Estienne, G. (2002). Pipe Decontamination Involving "String-Foam Circulation.", in *10th International Conference on Nuclear Engineering, Volume 1*, (Arlington, Virginia, USA: ASMEDC), 823–834. doi: 10.1115/ICONE10-22118
WHO (2022). Food Safety. Available at: https://www.who.int/news-room/fact-sheets/detail/food-safety

Wirtanen, G., and Salo, S. (2003). Disinfection in Food Processing – Efficacy Testing of Disinfectants. *Re/Views in Environmental Science and Bio/Technology* 2, 293–306. doi: 10.1023/B:RESB.0000040471.15700.03

Chapter 2: Foam cleaning in static condition

Introduction to chapter 2

As explained in the bibliography section, foams have long been employed to clean open surfaces in the food industry, primarily serving as a method for applying various chemicals. Traditionally, the scientific community believed that foams had no inherent cleaning properties. However, recent research has challenged this notion, demonstrating that foams can, in fact, provide superior cleaning efficacy compared to their non-foaming counterparts. The first objective of this thesis was to study the cleaning effect of foams on static conditions on model surfaces. In addition, we aimed to produce foams using bio-based surfactants to further minimize environmental impact of foam formulation and provide valuable insights to the scientific community on the properties of previously poorly studied or unstudied surfactants.

In our first work, we studied in depth the properties of 10-hydroxystearic acid (10-HSA) soap and conducted the first study on static foam cleaning to remove hydrophilic spores from stainless steel surfaces. The interest in using 10-HSA soap was based on the fact that 10-HSA can be easily obtained from oleic acid using microorganisms, and, to the best of our knowledge, there was no previous study on the surfactant properties of 10-HSA soap.

We showed that the cleaning efficiency of these foams depended on the size of the bubbles. Foams with bubble radius of around 100 µm demonstrated cleaning efficiency comparable to that of the non-foamed solution and water. However, foams with bubble radius of around 20 µm exhibited significantly better cleaning efficiency, achieving up to a 2 logs of spore reduction. In addition, we demonstrated that these foams are thermoresponsive, which could be an advantage for their industrial use, both for destruction and reutilisation, These results were gathered in one publication and were published in Molecules journal. However, with this foaming system it was difficult to tune and control the liquid fraction and keep in the same time a similar bubbles size. That is why, we studied in a second step another foaming system: sodium cocoyl isethionate (SCI), a bio-based surfactant widely employed in personal care products for its foaming and detergency properties.

Our focus was on the understanding of the influence of the liquid fraction on foam cleaning efficiency and elucidating the mechanisms behind spore decontamination. We chose SCI for two main reasons: despite its widespread use, there is limited data on its foaming properties, and it enabled us to create foams with varying liquid fractions while maintaining a consistent bubble size. To prevent the potential displacement of spores by draining liquid, we produced foams that exhibited no drainage during the cleaning process. We showed that when spores (hydrophilic or hydrophobic) are strongly attached to the surface, they can be removed by the foam, presumably by the wiping mechanism, with an efficiency of about 2 logs for hydrophilic spores and 1 log for hydrophobic spores. We showed that, in this condition the liquid fraction would have no influence on the cleaning efficiency. Then, we demonstrated that when the spores are suspended in a liquid the cleaning efficiency increased up to 4 logs of reduction for both types of spores presumably by the imbibition mechanism. These results were gathered in one publication to be submitted to Colloids and Surfaces A: Physicochemical and Engineering Aspects journal.

2.1 Ultrastable and responsive foams based on 10-hydroxystearic acid soap for spores' decontamination

Carolina Dari[1], Fabrice Cousin[2], Clemence Le Coeur[2,3], Thomas Dubois[1], Thierry Benezech[1], Arnaud Saint-Jalmes[4]*, and Anne-Laure Fameau[1]*

1 University Lille, CNRS, INRAE, Centrale Lille, UMET, 369 Rue Jules Guesde, F-59000 Lille, France;

2 Laboratoire Léon Brillouin, Université Paris-Saclay, CEA-CNRS UMR CEA Saclay,91191 Gif sur Yvette, France ; fabrice.cousin@cea.fr (F.C.);

3 Univ. Paris Est Creteil, CNRS, ICMPE, UMR 7182, 2 rue Henri Dunant, 94320 Thiais, France ; cle-mence.le-coeur@cnrs.fr(C.LC.);

4 Univ Rennes, CNRS, IPR (Institut de Physique de Rennes) - UMR 6251, F-35000 Rennes, France ; ar-naud.saint-jalmes@univ-rennes1.fr (A.SJ.)

* **Correspondence:** anne-laure.fameau@inrae.fr

* **Correspondence:** arnaud.saint-jalmes@univ-rennes1.fr

Abstract: Currently, there is a renewed interest for using fatty acid soaps as surfactants. Hydroxylated fatty acids are specific fatty acids with a hydroxyl group in the alkyl chain giving rise to chirality and specific surfactant properties. The most famous hydroxylated fatty acid is the 12-hydroxystearic acid (12-HSA), widely used in the industry and coming from castor oil. A very similar new hydroxylated fatty acid, the 10-hydroxystearic acid (10-HSA) can be easily obtained from oleic acid by using microorganisms. Here, we studied for the first time the self-assembly and foaming properties of R-10-HSA soap in aqueous solution. A multiscale approach was used by combining microscopy techniques, small angle neutron scattering, wide angle X-ray scattering, rheology experiments, and surface tension measurements as a function of the temperature. The behavior of R-10-HSA was systematically compared with those of 12-HSA

soap. Although multilamellar mi-cron-size tubes were observed for both R-10-HSA and 12-HSA, the structure of the self-assemblies at the nanoscale was different, which is probably due to the fact that 12-HSA solutions were racemic mixtures while 10-HSA solutions were obtained from a pure R enantiomer. We also demonstrated that stable foams based on R-10-HSA soap can be used for cleaning applications by studying spores removal on model surfaces in static conditions by foam imbibition.

Keywords: hydroxy fatty acid; self-assembly; foam; spore; cleaning; imbibition

2.1.1 Introduction

Surfactants are extensively used in a wide range of industrial applications due to their ability to adsorb at interfaces, and to reduce interfacial tensions. For example, they are used in food, agricultural, paint, cosmetic and pharmaceutical applications. Surfactants can be of synthetic or biological origin; however, most of the ones used in industries are of synthetic origin, and potentially bring out environmental and toxicology problems [1]. So, currently, the trend is to replace synthetic surfactants by more environmentally friendly surfactants of different types [1]. This search for so-called green surfactants gives rise to a renewed interest in using fatty acid soaps in industrial applications instead of petrochemical derived surfactants [2]. Fatty acid soaps can be considered as one of the oldest surfactants and perhaps most natural surfactants since they were discovered than as early as in 2800 BC [3]. The rise of the soap industry was at the beginning of the 19th century due to the work of Le Blanc and Chevreul, which led to the well-known sapon-ification process of oil or fat by appropriate caustic substances [4]. In the last century, due to the modern petrochemical industry and the progress in chemical processes, specific “synthetic” surfactants were developed to replace soaps in many areas. Currently, the renew interest in fatty acid soaps come from their advantages: low price, present excellent biodegradability under both anaerobic and aerobic conditions and low toxicity [2]. The most important advantage is that they are produced from renewable oils. Indeed, fatty acids are obtained by hydrolysis of oils from various oleochemical sources. Moreover, large amount of

fatty acids can be extracted and transformed in value-added-new ma-terials from by-products from agriculture and the food industry [5]. Fatty acids have an aliphatic hydrophobic tail, which is either saturated or unsaturated, and can have some additional groups such as hydroxyl groups [6]. One of the most famous hydroxylated fatty acids is the 12-hydroxystearic acid (12-HSA) [7]. The presence of the –OH group (chiral center) confers to the 12-HSA its unique properties, since it can self-assemble into fibers and tubular structures leading to both organogel and hydrogel, and it is widely used in industrial applications for its lubricating and thickening properties [7]. 12-HSA is pro-duced only from ricinoleic acid coming from castor oil [7].

Recently, a hydroxylated fatty acid with a very similar structure emerged in the literature: the 10-hydroxy stearic acid (10-HSA) that differs from the 12-HSA only by the position on the –OH group on the alkyl chain. 10-HSA is produced from oleic acid by using microorganisms producing enzyme (oleate hydratase) with high enantioselectivity leading to R-10-HSA [8–13]. Oleic acid is a very cheap starting material in comparison to ricinoleic acid as it is the most common and abundant mono-unsaturated fatty acids present in vegetable oils. Thus, it is much easier, cheaper and better for the environ-mental point of view to produce 10-HSA in comparison to 12-HSA. Many studies in the literature describe and compare the different ways to produce 10-HSA from microor-ganisms, but to the best of our knowledge there is no study on the surfactant properties of 10-HSA soap. Only few data are available on the morphology of the self-assembled structures and gelling properties in non-aqueous solvents [14].

Our aim here was to study the self-assembled properties of a model 10-HSA soap system in bulk aqueous solution, and the resulting foaming properties in order to compare with 12-HSA soap for which there exists a large corpus of knowledge in liter-ature. Therefore, to disperse the 10-HSA in water and to compare with 12-HSA, we used the same strategy based on the use of monoethanolamine (MEA), a model organic counter-ion, to produce the fatty acid soap with a stoichiometric molar ratio between 10-HSA and MEA [15–17]. We used a multiscale approach to determine the self-assembled and surface properties of 10-HSA by combining microscopy techniques, small angle neutron scattering (SANS), wide angle X-ray scattering (SAXS),

rheology experiments, and surface tension measurements as a function of the temperature. We compared the respective behaviors of 10-HSA and 12-HSA at the different length scales. We also demonstrated how foams produced by 10-HSA soap can be used for cleaning and de-contamination applications by taking advantages of their stability to remove model contaminants (spores) from model surfaces.

2.1.2 Results and Discussion

2.1.2.1 Critical Aggregation Concentration (CAC) of 10-HSA dispersion

First, we studied the CAC of 10-HSA dispersion. Surface tensions of the aqueous 10-HSA/MEA solutions were determined as a function of 10-HSA concentration at T = 20 ± 1 °C. The CAC was determined at around 10 mM (3.3 $mg.mL^{-1}$) associated to a plateau of surface tension at 45 N.m-1 ± 0.2 (**Figure 2.1.1**). The CAC was higher for 10-HSA than the values reported for 12-HSA [15,18]. Moreover, the surface tension reached above the CAC was much lower for 12-HSA than for 10-HSA. For example, at 10 $mg.mL^{-1}$, the surface tension value was around 23 mN.m-1 for 12-HSA [19]. We hypothesize that the difference in CAC and surface tension values between 12-HSA and 10-HSA may originate from either the position of the –OH group on the alkyl chain or/and the chirality, since the 12-HSA was studied in racemic mixture. The chirality of 12-HSA on the molecular scale is known to have a strong effect at much larger scales and controlled the self-assembled structures properties and interfacial properties [7]. Indeed, it was shown in the literature that the presence of a racemic mixture for 12-HSA has a stronger effect on the surface property than the difference of two carbons for the –OH position between 12-HSA and 10-HSA [20–22].

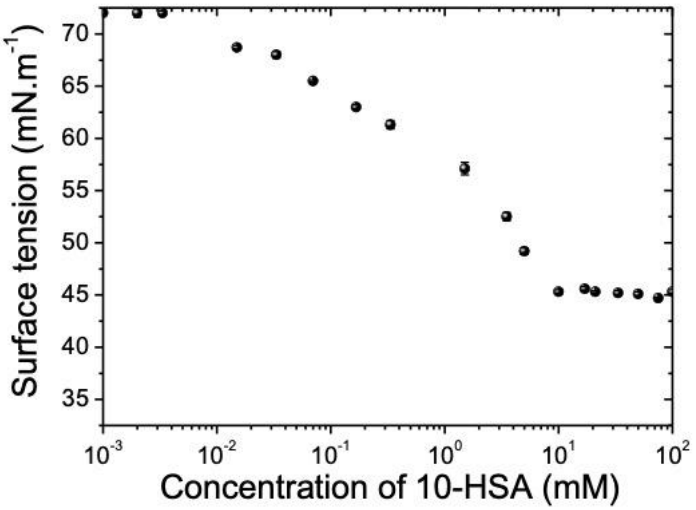

Figure 2.1.1. Surface tension of aqueous solutions of 10-HSA/MEA as a function of the concentration at T = 20 ± 1 °C.

2.1.2.2 Self-assembled structure and rheological properties at 25°C

The concentration of 10-HSA was fixed at 10 mg.mL^{-1} to be above the CAC (around 3 times the CAC) and to compare with previous studies done with 12-HSA at this concentration [16,19,23]. At room temperature, a homogenous turbid phase with birefringence was observed. By using phase contrast microscopy, the presence of micron-size rods was observed (**Figure 2.1.2.a**). These rods were very similar in shape and in length size to the ones obtained by using 12-HSA [17]. In order to gain insight into the local structure of these rods at the nanometric scale, SANS experiments were performed. This technique does not provide information on the total size of the tubes observed by microscopy, but it allows us to understand the self-association of fatty acids on a scale of up to a hundred nanometers. **Figure 2.1.2.b** displays the scattering profile. In the low Q region, four sharp peaks were observed. Their positions were in a ratio 1: 2: 3: 4 (Q0, 2Q0, 3Q0, 4Q0). The presence of a first strong correlation peak followed by its harmonics showed that the inner of rods were formed by periodically stacked bilayers separated by water layers. Above Q=0.02 Å^{-1}, the slope in Q^{-3} showed the presence of large objects observed previously: the rods. The 10-HSA bilayers arrange themselves as multilamellar tubes, as the 12-HSA bilayers do. The interlamellar spacing corresponding to one lipid bilayer plus

one water layer in the stack of bilayers was determined by using the position of the first correlation peak at 0.0237 $Å^{-1}$. It was equal to $2\pi/Q0$ = 263 Å. which was lower than for 12-HSA self-assemblies for which a value of around 320 Å was obtained in the same experimental conditions of ethano-lamine/fatty acids ratio and concentrations [16]. The swelling of the bilayer was lower for 10-HSA than for 12-HSA. From the SANS fitting (see Supporting information for details), we determined both the number of stacked bilayers and the Caillé parameter, accounting for the thermal fluctuations of the bilayers [24]. From the fit, we found that the Caillé parameter was around 0.06 with 5 bilayers. In the case of 12-HSA, the Caillé parameter was around 0.1 with 4 bilayers [15]. For the 10-HSA, the bilayers were more rigid than the 12-HSA, most probably coming from the fact that the molecules are more organized when they are not in a racemic mixture.

In the high Q region, the bilayer thickness was determined from the oscillation of the form factor (**Figure S1.a**) at around 20.5 Å. This thickness is lower than twice the 10-HSA molecule in its extended conformation suggesting (21 Å) that the bilayers could be either in Lβ gel state with its alkyl chain interdigitated or in a Lα fluid state [17]. To determine the 10-HSA alkyl chain state of crystallinity, we performed then wide-angle X-ray scat-tering experiment (WAXS). Four diffraction peaks were observed in the WAXS diffrac-togram (**Figure S1.b**) located respectively at 1.37, 1.47, 1.55 and 1.59 $Å^{-1}$. We deduce that 10-HSA were mostly in triclinic conformations, and that the alkyl chains were under gel state. This result was different from the 12-HSA in the same experimental conditions since the bilayer was under a gel state, but with a bilayer thickness around 42 Å, twice the length of the 12-HSA molecule and therefore not interdigitated, and with an orthorhombic conformation [6]. This difference between the two systems can again originate from the chirality, since the 12-HSA studied was a racemic mixture and not the 10-HSA (R-10-HSA). The chirality has already been shown to have a strong effect on alkyl chain packing in alkane system [25].

Oscillatory tests were performed to determine the rheological behaviors of the 10-HSA aqueous dispersion of multilamellar tubes at 25 °C. In **Figure 2.1.2.c**, results of amplitude sweeps (at a fixed frequency f = 1 Hz) is shown. The dispersion was viscoelastic, with the viscous and elastic moduli (G' and G'') depending on the applied amplitude. At low amplitude γ (below 3 %), G' was higher than G'', but at the highest amplitude G'' was higher than G'. At low γ, there was gel-like behavior of the multilamellar tubes. As the amplitude was increased, there was a yield point, and the dispersion started to flow above a typical yield strain of γ = 1% (values for which G' started to rapidly decrease). This behavior is fully reminiscent to the one of the 12-HSA dispersions, only the values of G' and G'' were slightly higher, and the yield strain was at 0.5 % [19]. We suppose that this difference could come from the length or/and or the diameter of the tubes [19].

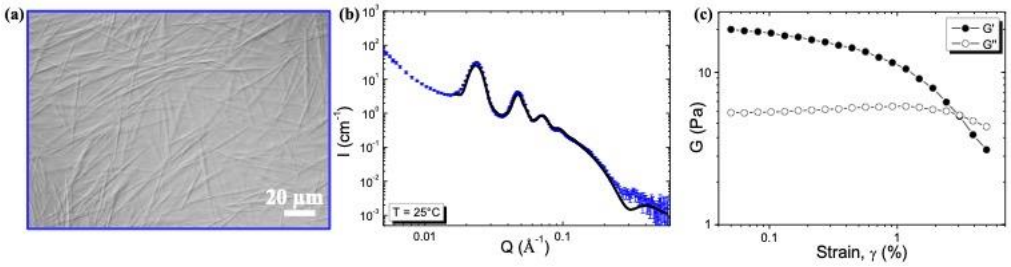

Figure 2.1.2. (a) Phase contrast microscopy picture of 10-HSA at 25 °C. (b) SANS intensity profile of 10-HSA at 25 °C. The black line corresponds to the best fit of the data described in the Supporting Information. (c) Oscillatory measurements of 10-HSA, elastic G' (●) and viscous G'' (○) moduli plotted as a function of the strain amplitude, γ at constant f = 1 Hz at 25 °C.

2.1.2.3 Evolution of the self-assembled structure and rheological properties by increasing temperature

By increasing the temperature, we observed that around 65 °C the turbid sample turned into a limpid sample. By phase contrast microscopy, no rods were any longer observed (**Figure 2.1.3.a**). In order to determine precisely the temperature transition threshold, we studied the

evolution of the elastic and viscous moduli, G' and G'', respectively, monitored as a function of the amplitude of deformation and at a fixed frequency for various temperatures (**Figure S2**). In **Figure 2.1.3.b**, the quantitative dependence on temperature for G' and G'' found in the low amplitude plateau below yielding (low amplitude of 0.1 % and frequency of 1 Hz) is represented. Below 60 °C, when multilamellar tubes were present in solution, we observed that both the viscous and elastic moduli, remained almost contant around 20-40 Pa for G', and around 6-10 Pa for G''. At 60 °C, a sharp decrease of both G' and G" was observed down to very low values at 65 °C even below the limit of resolution for G'. This strong variation of the moduli over only few degrees confirm that the temperature transition was at around 65 °C from rheological point of view. Due to the experimental limit of the rheometer, we did not observe the cross over between G' and G'' during the transition. The SANS spectrum was recorded above this transition at 75 °C (**Figure 2.1.3.c**). It does no longer shows the typical features of a lamellar phase but displays the characteritic features of spheres interacting through repulsive interactions. At large Q, the spectrum was fitted with a form factor of a sphere and a structure factor with a radius of 21 Å, that correponds to the length of the fatty chain (**Figure S1.c**). Therefore, spherical micelles were present inside the limpid solution. At low Q, in the SANS spectrum, a decrease in the scattered intensity was observed when going towards low Q. This decrease comes from the low isothermal compressibility of the system, since the 10-HSA micelles were mainly composed by the ionized 10-HSA molecules which were negatively charged. Therefore, the spherical micelles repelled each other due to electrostatic repulsions over large distances, which gave rise to the presence of a broad correlation peak. In the direct space, the position of the broad correlation peak corresponds to the average distance between spherical micelles. The position of the broad correlation peak at Q = 0.058 Å, corresponds to a mean distance between micelles of around 108 Å. The 10-HSA multilamellar tubes exhibits a transition into spherical micelles above 65 °C.

By decreasing the temperature from 70 °C to 25 °C, the rods appeared back by optical phase contrast microscopy showing that the self-assembled transition was reversible. The 10-HSA

multilamellar tubes transit into spherical micelles in the same way than for 12-HSA multilamellar tubes as depicted in reference [17], but at a lower temperature (65 °C for 10-HSA and 70 °C for 12-HSA). The size of the spherical micelles was similar, as well as the mean average distance given that the fatty acid concentration was the same. At high temperatures, the size of the self-assembled structures in solution are mainly linked to the size of the molecules wich is similar between 12-HSA and 10-HSA, and the presence of racemic mixture does not play anymore a role.

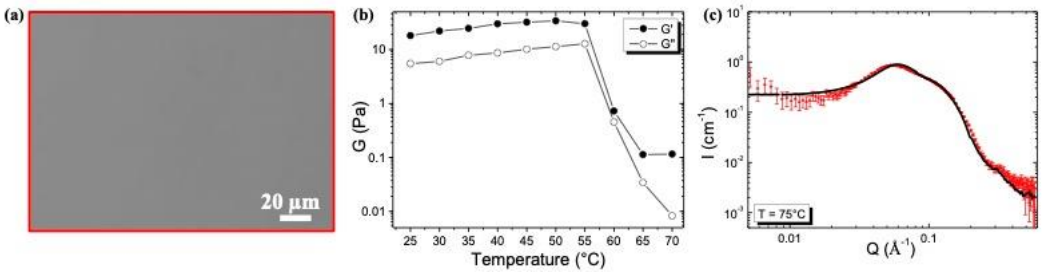

Figure 2.1.3. (a) Phase contrast microscopy picture of 10-HSA at 65 °C. (b) Variations of elastic G' (●) and viscous G'' (○) moduli upon heating. The moduli were measured at γ = 0.1 % and f = 1 Hz. (c) SANS intensity profile of 10-HSA at 75 °C. The line corresponds to the best fit of the spectrum de-scribed in the Supporting Information.

2.1.2.4 Foaming properties with time and temperature

The foaming properties of 10-HSA dispersion was evaluated for two different ways of producing foams: hand-shaking and gas bubbling through the tubes dispersion. A large volume of foam can be produced from the 10-HSA multilamellar tubes dispersion by hand-shaking, demonstrating the high foamability of the dispersion (**Figure S3**). This foam was shown to be very stable with time when kept at room temperature during one month (Figure S3). To quantify the foaming properties in terms of foamability, stability with temperature and evolution of liquid fraction, we produced foams by bubbling gas into the 10-HSA aqueous dispersion at 25 °C (**Figure 2.1.4**). The fixed foam volume to reach was 45 cm3 with a gas flow rate fixed at 35 mL.min-1. It was reached in around 75 s, showing that all the gas was incorporated inside the

foam. The foamability was thus optimal, and the gas bubbles were quickly and efficiently stabilized (**Figure 2.1.4.a**). Then, the foam volume remained constant with time during all the experiment confirming the ultrastable character of the foam. In terms of liquid fraction, at the end of bubbling, the average liquid fraction was around 24 %, corresponding to a so-called wet foam. The liquid drained quickly out of the foam in the first minutes, and then the liquid fraction stabilized at around 7.5 %. This foaming behaviour was very similar to the one obtained for 12-HSA multilamellar tubes dispersions [23]. Microscopically, we expect that the foams were first stabilized by the 10-HSA monomers released from the tubes at the gas-solution interfaces, and that these monomers protect the bubbles and provide some stability to the films separating the bubbles. In parallel, the crowding of the multilamellar tubes within the liquid foam channels stabilize this liquid skeleton and prevent further destabilization. At this stage, foams based on 10-HSA and 12-HSA appeared very similar in terms of foaming properties, since the foaming properties are mainly linked to the presence of tubes at the micron scale and to their quantity, which was similar.

Then, we studied the foam stability behaviour as a function of temperature below and above the temperature theshold transition between tubes and spherical micelles (Figure 4.b and Figure S4). At 25 °C, when multilamellar tubes were present within the foams, the foam volume remained stable with time (**Figure 2.1.4.b**). However, when the foam temperature was increased at 65 °C, the transition of tubes into micelles inside the foam liquid channels led to a rapid foam volume decrease from 40 cm3 to 25 cm3. By switching back the temperature quickly to 25 °C, the decrease of the the foam volume was stopped and such foam volume remained constant with time because the micelles transit back to tubes inside the foam (**Figure 2.1.4.b**). 10-HSA dispersion led to thermoresponsive foams in the same way than previously described fro 12-HSA dispersion [23]. Only the temperature at which the foam stability could be switched between stable to usntable state was different, since it was driven by the temperature transition threshold between multilamellar tubes and spherical micelles.

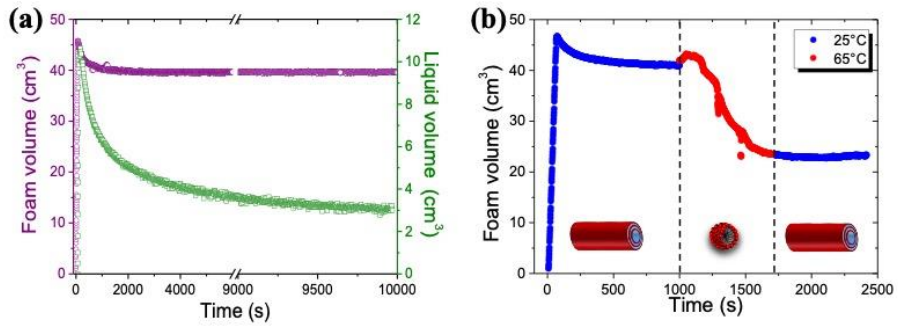

Figure 2.1.4. (a) Evolution of the foam volume (purple), and of the liquid volume in the foam (green) with time with time at 25 °C. (b) Evolution of the foam stability by measuring the evolution of foam volume with time at different temperatures: 25 °C when multilamellar tubes were present and at 65 °C when spherical micelles were present.

2.1.2.5 Cleaning of spores contamination on surface by foam imbibition

Then, we took advantages of the 10-HSA foam stability to study the potential of these foams to decontamination applications [26]. We used stainless-steel plates as model sur-faces and spores from Bacillus subtilis (size around 400-700 nm) as the model contaminant to study the absorption process due to imbibition inside the foam [27]. The model surfaces were kept in horizontal position, and the foams were put directly in contact with the contaminated surface (see section 2.1.3.2). To favor foam imbibition, to avoid the detachment of the spores from the surface induced by drainage and ensure that plates remain un-derneath the foam together with a lot of liquid, we decided to first let dry the foam during 10 min, and then to put the foam on the contaminated surfaces with spores. We produced foams with two different foaming techniques to vary the bubbles size and the liquid fraction, which are the main parameters governing the imbibition. Thus, we produced foams by the hand-shaking (HS) method and the double syringes (DS) method [28]. Before cleaning, the average bubbles radius was 103 ± 69 µm and 19 ± 8 µm for HS foam and DS foam, respectively. The remaining average liquid fraction of the foams after 10 min was around 10 ± 0.4 % and 19 ± 0.8 % for HS foam and DS

foam, respectively. It is important to note that the liquid fraction was most probably not uniform trough the foam, with drier foams at the top than at the bottom. The foams remained in contact with the contaminated surfaces in horizontal position during 30 min. First, we checked the bubbles size evo-lution after 30 min of cleaning. The bubbles size slightly increased to reach 129 ± 88 µm and 19 ± 8 µm for HS foam and DS foam, respectively. Multilamellar tubes were clearly observed inside the foam before and after cleaning (**Figure S5**). Then, the stainless-steel plates were removed, and the effect of the contact with a foam was quantified by measuring the spore log reduction after 30 min as shown **Figure 2.1.5.a.** The spores log reduction was around 1.13 ± 0.14 for the water, due to the hydrophilicity of the spores as already observed previously, which could be removed by water [29]. The spores log reduction for the pure 10-HSA dispersion was 0.92 ± 0.20, and thus similar to water. It is important to point out that the 10-HSA dispersion did not have an effect on spore's via-bility, it was similar between water and 10-HSA dispersion. The spores log reduction for the 10-HSA foams was 0.98 ± 0.10, and 2.40 ± 0.10, respectively, for HS and DS. The HS foam had a similar effect than just water or the 10-HSA dispersion on spore's removal. However, the spores' log reduction value was much higher for 10-HSA DS foam, showing that foam could efficiently remove spores' from the plate. The spores due to their small sizes compared to the foam liquid channels and Plateau borders could be efficiently remove by the foam. The effect of foam cleaning on spore's removal was also followed by epifluorescence microscopy before and after foam cleaning (**Figure 2.1.5.b**). Before foam cleaning, the fluorescent spores could be easily detected on the model surfaces. After foam cleaning with DS foam, almost no more spores could be observed confirming the results of spore log reduction quantification.

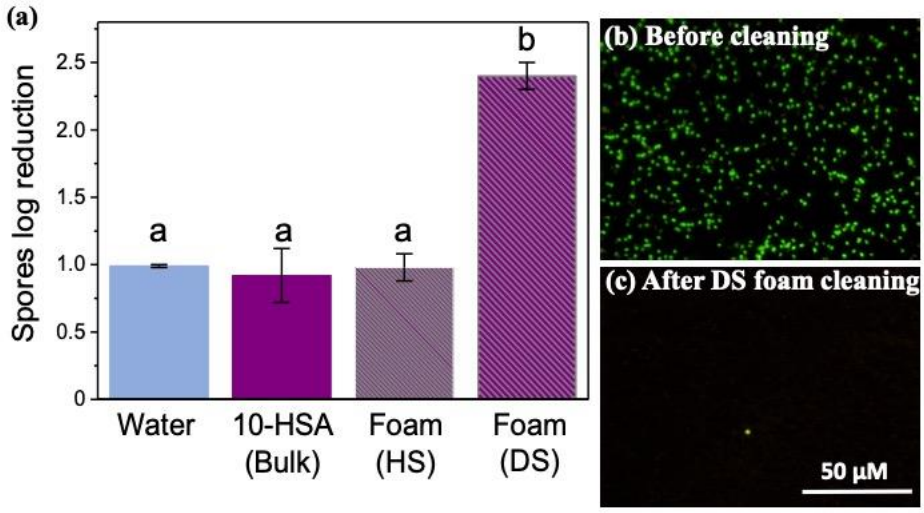

Figure 2.1.5. (a) Spores log reduction on the model surface after 30 min for water, 10-HSA disper-sion, hand-shaking (HS) foam, and double syringe (DS) foam. The small letters a-b indicate groups of statistical differences according to Tukey's test ($p < 0.05$). (b) Epifluorescence micros-copy pictures of the model surface contaminated by fluorescent spores before cleaning, and (c) af-ter 30 min of cleaning with DS foam. The scale bar represents 50 µm for all the pictures.

To visualize and to confirm how spores could be soaked up by the DS foam, we followed with fluorescence microscopy the spores' penetration dynamic into 10-HSA DS foam as already done in the literature for oil imbibition in foams (**Figure 2.1.6**) [30–32]. Immediately after the initial contact of spores' suspension with the foam, we observed the penetration of the fluorescent spores inside the foam without destroying the foam. Therefore, the high spores log reduction for DS foam came from the foam imbibition phenomenon resulting in a very quick detachment of the adhering spores and the penetration inside the foam. The difference between HS and DS foam could be explained by the bubbles size difference (factor of ten between HS and DS foam bubbles size), since it is known that the smaller the bubble size, the smaller the liquid channel section, the larger is the capillary pressure and the imbibition phenomenon [26,33]. In our case, we suppose that even if the average liquid fraction were different, they were still in the range of wet foams, and we suppose that only the bubbles size had an effect on

foam imbibition [32]. Moreover, by comparing the log reduction obtained for DS foam to the ones obtained for foam flow in dynamic conditions on the same spore's model and same surface, we observed that the values are similar, showing that foams in static conditions are very good to remove efficiently spores contamination thanks to the imbibition process [29].

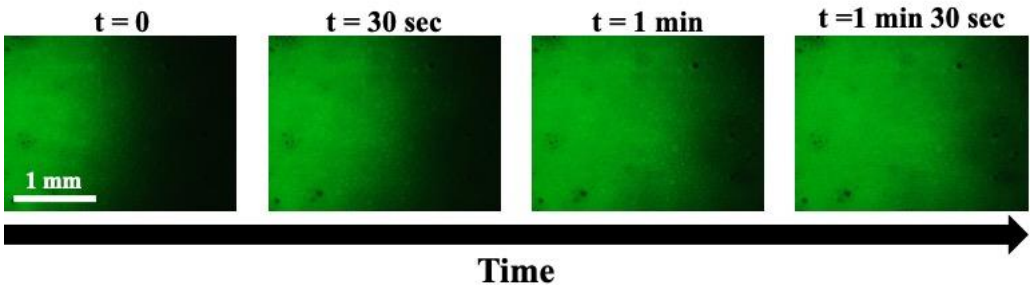

Figure 2.1.6. Epifluorescence microscopy pictures of the penetration of aqueous dispersion of spores into a double syringe foam with time. t = 0, corresponds to the image taken just after contact with the foam. The scale bar represents 1 mm for all the pictures.

2.1.3 Materials and Methods

2.1.3.1 Materials

2.1.3.1.1 Preparation of 10-hydroxystearic acid dispersion

Monoethanolamine was purchased from Sigma Aldrich and used as received. 10-HSA was obtained from the following method [34]. 10-HSA was weighted exactly in a tube and ultrapure water was added so that the concentration was 10 $mg.mL^{-1}$ (1 wt.% in water). Next, the desired volume of a 1 $mol.L^{-1}$ monoethalolamine solution prepared in MilliQ water was incorporated to reach the equivalence (molar ratio=nmonoethanolamine/n10-HSA=1, with n the molar concentration in $mol.L^{-1}$). The mixture was heated at 80°C during 15 minutes until all the 10-HSA powder was fully dispersed, and then vortexed. Samples were further stored at 4 °C and prior to be used, they were heated again around 80 °C during 5 minutes and cooled to room temperature.

2.1.3.1.2 Preparation of Solid Model Surfaces

All the cleaning experiments were carried out on rectangular (45 mm x 15 mm) AISI 316 stainless-steel plates (APERAM, Isbergues, France) with a 2R factory finish. In order to have similar surface properties to those found in the food industry, the surfaces were subjected to a conditioning process described previously [29]. In brief, the plates were immersed in milk at room temperature for 30 min and then they were rinsed under osmosis water for 5 min by overflow. The plates were immersed in a 0.5 wt.% sodium hydroxide solution at 70 °C for 30 min and then they were rinsed in osmosis water for 5 min. This cycle was repeated 15 times. Then, they were fouled with Escherichia coli strains previously shown to produce biofilms on stainless-steel surfaces. Afterward, the plates were submitted to cleaning and disinfection steps. 24 hours before each experiment, the plates were sterilized in a dry heat oven at 180 °C for 1 h.

2.1.3.1.3 Preparation of hydrophilic spore's Suspension

Bacillus subtilis PY79 is a laboratory strain known to produce hydrophilic spores. The Bacillus subtilis PY79 strain was tagged with green fluorescent proteins to make the spores fluorescent. The method to produce the spores was described previously [27].

2.1.3.2 Methods

2.1.3.2.1 Determination of the Critical Aggregation Concentration by Surface Tension Measurements

The measurements of the air-solution surface tension as a function of the concentration of 10-HSA/monoethanolamine dispersion were performed by using the automatized surface tension plate reader Kibron Delta-8 (Kibron, Finland). A volume of 50 µL of aqueous dispersion was placed on the 96-hole platform. Measurements were performed at 20 °C after a waiting time of 10 minutes to ensure equilibrium at the air-water interface. A calibration was performed by using ultrapure water at 20 °C. Measurements were per-formed three times for each concentration.

2.1.3.2.2 Microscopic Observation of 10-HSA dispersion

Phase contrast microcopy observations were performed at different temperatures (25°C-75°C) at 40x magnification using an optical microscope in the phase contrast mode (Nikon Eclipse E-400) equipped with a STC-CM202 USB color camera (Sentech).

2.1.3.2.3 Rheological measurements

An Anton Paar MCR301 rheometer was used to study the viscoelastic properties of the dispersions. Experiments were performed with a cone-plate cell setup. The walls of the tools in contact with the samples are rough to avoid wall slips. The rheometer was equipped with a Peltier system to control the temperature.

2.1.3.2.4 Small Angle Neutron Scattering (SANS) and Wide Angle X-ray Scattering (WAXS)

SANS experiments were performed at Laboratoire Léon Brillouin (Saclay, France). Samples were prepared with deuterated water and were held in flat quartz cells with a 2 mm optical path length for the sample with a concentration of 10 $mg.mL^{-1}$ (1 wt.%). The PAXY diffractometer was used for the SANS experiments. Four configurations were chosen to get a Q-range lying between 2.10-3 and 5.10-1 Å-1 (respectively λ = 5 Å, D = 1 m; λ = 5 Å, D = 3.5 m; λ = 8 Å, D = 5 m; λ = 15 Å, D = 7 m)) with a significant overlap between the three configurations. The temperature was controlled by a circulating fluid to within ± 0.2°C. The neutron wavelength was set to the desired value with a mechanical velocity selector ($\Delta\lambda/\lambda \approx 0.1$). The azimuthally averaged spectra were corrected for solvent, empty cell, as well as background noise, and were normalized to the incoherent H2O signal by using PASINET software package provided at the beamline. Fitting software used was SasView 5.0.4 (http://www.sasview.org/.). Fitting models are detailed in the supple-mentary information.

WAXS experiments were carried out with an Xeuss 2.0 instrument from Xenocs (Gre-noble, France) using a micro-focused sealed tube Cu K-alpha source with a wavelength of 1.54 Å. The temperature was fixed at 25°C. The dispersion was held in a 1.5 mm glass capillary.

2.1.3.2.5 Foam characterization with temperature and time

Foams were produced with the FoamScan apparatus (IT CONCEPT, Longessaigne, France). Foam was generated in a round glass column (21 mm in diameter) by sparging N2 gas through a fixed volume (12 mL) of the 10-HSA dispersion via a porous disk (pore size 10-14 µm) located at the bottom of the glass column. The flow rate was fixed at 35 mL.min-1. The FoamScan uses image analysis to monitor the foam formation and stability with a CCD camera (Sony Hexwave HAD). In all our measurements, a foam volume of 45 mL was generated. The temperature of the glass column was controlled by a water bath. The liquid volume in the foam was assessed by mean of conductivity measurements.

2.1.3.2.6 Production and characterization of foams for spore's detachment

The foams were produced at room temperature by two techniques to change the liquid fraction and the bubbles size: hand-shaking and double-syringe. For the hand-shaking foam method, we put 15 ml of the 10-HSA dispersion in a 50 ml cylindrical graduated plastic containers (falcon tube 50 mL, internal diameter 2.5 cm, 11.5 cm height). Then, the dispersion was agitated for 15 seconds to produce the foam and always produced by the same operator. For the double-syringe foam method, two 12-mL syringed were connected with a luer-lock connector. One syringe was filled with 3.6 ml of cleaning solution and 8.4 ml of air. The second one was kept with the piston in the fully closed position. The foam was then produced by pushing the plungers of the connected syringes by hand for 30 times. Then, the foam produced was placed in a 50 ml falcon tube. In order to have enough foam to cover the plates, it was necessary for the double-syringe technique to produce the foam with the double syringe technique more than once (three times), and mixed all together in the 50 mL tube. Once the foams were produced, we waited 10 minutes for the liquid of the foams to drain, and stabilized the liquid fraction. Then, we removed the drained liquid by drilling a small hole in the falcon tube with a thumbtack. The final liquid fraction was determined with Equation 1:

$$\emptyset = (V_{initial\ liquid} - V_{drained\ liquid}) / V_{foam} \quad (1)$$

With $V_{initial\ liquid}$ corresponding to the initial amount of liquid; $V_{drained\ liquid}$ corresponding to the amount of liquid drained after 10 min, and V_{foam} corresponding to the volume of foam after 10 min.

The bubbles size of the foams produced before and after the cleaning tests were deter-mined by optical microscopy (Zeiss Axioskop 2 Plus, Oberkochen, Germany) by fol-lowing the method introduce in Gaillard et al. by using ImageJ software [35]. We used the fluorescence mode of the same microscope to follow the imbibition of fluorescent spores in the foam. A volume of 100 µL of spore's suspension was carefully injected between the microscopic slides containing the foam. All experiments were carried out in triplicate.

2.1.3.3 Viability of spores

We carried out serial dilutions of the spore suspension in sterile Milli-Q water and in 10-HSA dispersion. The dilutions were then plated in Tryptic Soy Agar (TSA; Biokar Diagnostics, Allonne, France) and the plates were incubated for 24 h at 30 °C. The number of colonies forming units (CFU) was counted manually and the results were expressed as CFU.mL^{-1}.

2.1.3.3.1 Spores Detachment Analysis

The spores detachment analysis protocol was adapted from the literature and summarized in the Figure 7 [29,36]. The spore suspension was diluted in sterile Milli-Q water to obtain a concentration of 108 CFU.mL−1. In order to avoid the presence of spore aggregates, the spore suspension was sonicated for 2 min 30 s in an ultrasonic bath (Bransonic 2510E-MT, Branson Ultrasonics Corporation, Danbury, CT, USA) before use. Five drops of 1 µl of the spore suspension were placed on the surface of each plate with a micropipette (**Figure 2.1.7**). The plates were then dried in an oven for 1 h at 30 °C. The soiled plates were then placed in the tubes containing the foam (one plate per tube) or in 15 mL of the cleaning solution, or in 15 mL

of pure water, and they were kept in horizontally position for 30 minutes. A soiled plate was used as a control for the quantification of the initial spore concentration in each experiment.

To isolate the adhered spores, each plate was sampled with a dry cotton swab (Copan, Brescia, Italy), which was then placed in a tube containing 5 mL of sterile Milli-Q water. Each tube was vortexed for 1 minute at 2400 rpm and then the swabs were removed from the tubes. For the quantification of the spores, serial dilutions were made in sterile Milli-Q water for each tube and then were plated in Tryptic Soy Agar (TSA; Biokar Diagnostics, Allonne, France). The plates were incubated for 24 h at 30 °C and the number of colony forming units (CFU) was counted manually. The results were expressed as $CFU.plate^{-1}$. The foam cleaning efficiency was calculated by dividing the number of viable spores after the cleaning tests by the number of spores on plates used as a control for the initial spore concentration. The cleaning efficiency was expressed in terms of log reduction using Equation (2):

$$Log\ reduction = log\ (CFU.plate^{-1}{}_{t30min} - CFU.plate^{-1}{}_{t0})$$

with CFU.plate−1 t: the number of the colony-forming units per plate after cleaning (t = 30 min); CFU.plate−1t0: the initial number of the colony-forming units per plate. All the experiments were carried out in triplicate.

The spore drops placed on the plate surfaces were observed also before and after cleaning by using the same epifluorescence microscope as described previously. For each plate, 4 pictures were taken. The experiments were carried out in duplicate.

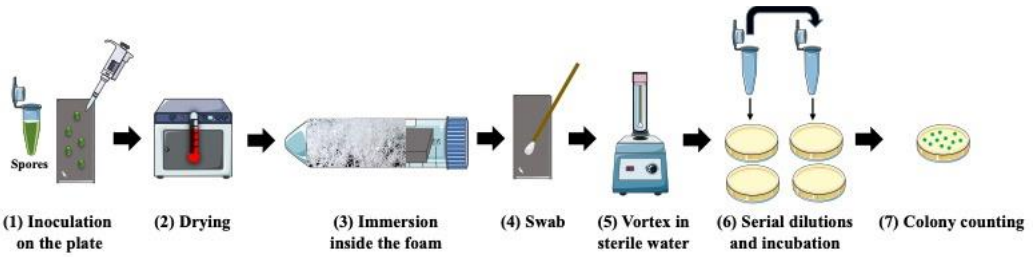

Figure 2.1.7. Schematic showing the methodology for spores removal on stainless steel surfaces by using foam: (1) Five drops (1 µl) of the spore suspension were placed on the surface of the model plate with a micropipette; (2) the plates were dried in a oven for 1 h at 30 °C; (3) the soiled plates were then placed in the tubes containing the foams and they were kept in horizontally position for 30 min; (4) each plate was sampled with a dry cotton swab; (5) the swab was put in a tube with 5 mL of sterile Mill-Q water and vortexed for 1 min at 2400 rpm; (6) serial dilutions were made in sterile Milli-Q water for each tube and there were plated in Tryptic Soy Agar and incubated for 24 h at 30 °C; (7) the number of colony forming units (CFU) was counted manually.

2.1.3.3.2 Statistical Analysis

All the experiments were carried out in triplicate and the results were expressed as the mean ± standard deviation. The results were compared by one-way analysis of variance and Tukey's test to analyze statistical differences ($p < 0.05$). The analysis was performed using SAS V8.0 software (SAS Institute, Gary, NC, USA).

2.1.4 Conclusions

We provide for the first time results concerning the behavior of 10-HSA as a soap in aqueous dispersion. Our study showed that 10-HSA in presence of monoethanolamine with a molar stochiometric ratio led to the formation of micron-size multilamellar tubes in aqueous dispersion, which transit into spherical micelles at high temperature above a temperature threshold. This behavior is similar to those of 12-HSA molecules solubilized in water in the same experimental conditions with the same protocol [15,16,23]. However, the structure at the

nanoscale, the thermal behavior, and the interfacial properties are different from 10-HSA to 12-HSA [19,37]. Such a difference likely comes from the use of a racemic mixture for 12-HSA in the previous studies whereas the 10-HSA molecules under scrutiny here was just based of the R-enantiomer [7,15]. Our results confirm thus the outmost importance of the chirality on the self-assembled structures and their thermal behavior, as already observed in case of 12-HSA organogels [7]. The position of the -OH group on the alkyl chain plays also a role. In the future, it would be interesting to compare R-12-HSA with the results obtained here with 10-HSA. Anyway, given that 10-HSA produced micron-size multilamellar tubes as 12-HSA do, their aqueous dispersions can be used to design ul-tra-stable foams with a threshold temperature of destabilization triggered by the tubes/micelles transition [23,38,39]. These stable foams are good candidates for cleaning or decontamination processes as shown here for spores removal. The efficiency of the de-contamination could be improved by decreasing further the bubbles size and the liquid fraction, or by adding a biocide agents inside [40]. We hope that our study will open the route for various applications where 10-HSA fatty acids could replace 12-HSA ones. In-deed, contrary to 12-HSA that it difficult to get as it comes only from the ricinoleic acid of the castor oil, 10-HSA can be easily obtained from oleic acid and commercially available baker's yeast, or from the action of fatty-acid hydratase found in many common probiotic microorganisms [7,11,41].

Funding: This research was funded by the region Hauts de France and INRAe TRANSFORM department. This work was also supported by the project Veg-I-Tec (programme Interreg V France476 Wallonia-Flanders GoToS3).

Acknowledgments: C. Dari would like to thank the region Hauts de France and INRAe TRANSFORM department for the allocation of her PhD grant. We would like to thank C. Lemy and Dr. C. Faille for their help during the microbiology experiments. This work benefited from the use of the SasView application, originally developed under NSF award DMR-0520547. SasView contains code developed with funding from the European Union's Horizon 2020 research and innovation programme under the SINE2020 project, grant agreement No 654000.

2.1.5 References

[1] C.E. Drakontis, S. Amin, Biosurfactants: Formulations, Properties, and Applications, Curr. Opin. Colloid Interface Sci. (2020).

[2] S. Wolfrum, J. Marcus, D. Touraud, W. Kunz, A renaissance of soaps?—How to make clear and stable solutions at neutral pH and room temperature, Adv. Colloid Interface Sci. 236 (2016) 28–42. https://doi.org/10.1016/j.cis.2016.07.002.

[3] J.S. Raut, V.M. Naik, S. Singhal, V.A. Juvekar, Soap: The polymorphic genie of hierarchically structured soft condensed-matter products, Ind. Eng. Chem. Res. 47 (2008) 6347–6353. https://doi.org/10.1021/ie0714753.

[4] M. Wilcox, Pouchers perfumes, cosmetics and soaps, Soap, 10th Ed., Butl. H., Ed. Ed. (1993) 453–465.

[5] A.-L. Fameau, C. Gaillard, D. Marion, B. Bakan, Interfacial properties of functionalized assemblies of hydroxy-fatty acid salts isolated from fruit tomato peels, Green Chem. 15 (2013) 341–346. https://doi.org/10.1039/c2gc36677k.

[6] A. Fameau, A.G. Marangoni, Back to the future: Fatty acids, the green genie to design smart soft materials, J. Am. Oil Chem. Soc. 99 (2022) 543–558.

[7] A.-L. Fameau, M.A. Rogers, The curious case of 12-hydroxystearic acid — the Dr. Jekyll & Mr. Hyde of molecular gelators, Curr. Opin. Colloid Interface Sci. 45 (2020) 68–82. https://doi.org/10.1016/j.cocis.2019.12.006.

[8] Y.-C. Joo, E.-S. Seo, Y.-S. Kim, K.-R. Kim, J.-B. Park, D.-K. Oh, Production of 10-hydroxystearic acid from oleic acid by whole cells of recombinant Escherichia coli containing oleate hydratase from Stenotrophomonas maltophilia, J. Biotechnol. 158 (2012) 17–23.

[9] E.-Y. Jeon, J.-H. Lee, K.-M. Yang, Y.-C. Joo, D.-K. Oh, J.-B. Park, Bioprocess engineering to produce 10-hydroxystearic acid from oleic acid by recombinant Escherichia coli expressing the oleate hydratase gene of Stenotrophomonas maltophilia, Process Biochem. 47 (2012) 941–947.

[10] Y.-X. Wu, J. Pan, H.-L. Yu, J.-H. Xu, Enzymatic synthesis of 10-oxostearic acid in high space-time yield via cascade reaction of a new oleate hydratase and an alcohol dehydrogenase, J. Biotechnol. 306 (2019) 100008.

[11] S. Serra, D. De Simeis, A. Castagna, M. Valentino, The fatty-acid hydratase activity of the most common probiotic microorganisms, Catalysts. 10 (2020) 154.

[12] S. Koritala, C.T. Hou, C.W. Hesseltine, M.O. Bagby, Microbial conversion of oleic acid to 10-hydroxystearic acid, Appl. Microbiol. Biotechnol. 32 (1989) 299–304.

[13] S. Serra, D. De Simeis, New insights on the baker's yeast-mediated hydration of oleic acid: the bacterial contaminants of yeast are responsible for the stereoselective formation of (R)-10-hydroxystearic acid, J. Appl. Microbiol. 124 (2018) 719–729. https://doi.org/10.1111/jam.13680.

[14] F. Asaro, C. Boga, R. De Zorzi, S. Geremia, L. Gigli, P. Nitti, S. Semeraro, (R)-10-Hydroxystearic Acid: Crystals vs. Organogel, Int. J. Mol. Sci. 21 (2020) 8124.

[15] J.-P. Douliez, C. Gaillard, L. Navailles, F. Nallet, Novel lipid system forming hollow microtubes at high yields and concentration, Langmuir. 22 (2006) 2942–2945.

[16] A.-L. Fameau, B. Houinsou-Houssou, B. Novales, L. Navailles, F. Nallet, J.-P. Douliez, 12-Hydroxystearic acid lipid tubes under various experimental conditions, J. Colloid Interface Sci. 341 (2010).

[17] A.-L. Fameau, F. Cousin, A. Saint-Jalmes, Morphological Transition in Fatty Acid Self-Assemblies: A Process Driven by the Interplay between the Chain-Melting and Surface-Melting Process of the Hydrogen Bonds, Langmuir. 33 (2017). https://doi.org/10.1021/acs.langmuir.7b02651.

[18] A.-L. Fameau, J. Ventureira, B. Novales, J.-P. Douliez, Foaming and emulsifying properties of fatty acids neutralized by tetrabutylammonium hydroxide, Colloids Surfaces A Physicochem. Eng. Asp. 403 (2012). https://doi.org/10.1016/j.colsurfa.2012.03.059.

[19] A.-L. Fameau, A. Saint-Jalmes, Yielding and flow of solutions of thermoresponsive surfactant tubes: Tuning macroscopic rheology by supramolecular assemblies, Soft Matter. 10 (2014) 3622–3632. https://doi.org/10.1039/C3SM53001A.

[20] K.S. Yim, B. Rahaii, G.G. Fuller, Surface rheological transitions in Langmuir monolayers of bi-competitive fatty acids, Langmuir. 18 (2002) 6597–6601.

[21] D. Vollhardt, S. Siegel, D.A. Cadenhead, Effect of hydroxyl group position and system parameters on the features of hydroxystearic acid monolayers, Langmuir. 20 (2004) 7670–7677.

[22] D. Vollhardt, S. Siegel, D.A. Cadenhead, Characteristic features of hydroxystearic acid monolayers at the air/water interface, J. Phys. Chem. B. 108 (2004) 17448–17456.

[23] A.-L. Fameau, A. Saint-Jalmes, F. Cousin, B. Houinsou Houssou, B. Novales, L. Navailles, F. Nallet, C. Gaillard, F. Boué, J.-P. Douliez, Smart foams: Switching reversibly

between ultrastable and unstable foams, Angew. Chemie - Int. Ed. 50 (2011) 8264–8269. https://doi.org/10.1002/anie.201102115.

[24] F. Nallet, R. Laversanne, D. Roux, Modelling X-ray or neutron scattering spectra of lyotropic lamellar phases: interplay between form and structure factors, J. Phys. II. 3 (1993) 487–502.

[25] C. Alonso, F. Artzner, B. Suchod, M. Berthault, O. Konovalov, J. Pecaut, D. Smilgies, A. Renault, Two-and three-dimensional stacking of chiral alcohols, J. Phys. Chem. B. 105 (2001) 12778–12785.

[26] T. Schad, N. Preisig, D. Blunk, H. Piening, W. Drenckhan, C. Stubenrauch, Less is more: Unstable foams clean better than stable foams, J. Colloid Interface Sci. 590 (2021) 311–320.

[27] T. Dubois, F. Krzewinski, N. Yamakawa, C. Lemy, A. Hamiot, L. Brunet, A.-S. Lacoste, Y. Knirel, Y. Guerardel, C. Faille, The sps genes encode an original legionaminic acid pathway required for crust assembly in Bacillus subtilis, MBio. 11 (2020) e01153-20.

[28] T. Gaillard, M. Roché, C. Honorez, M. Jumeau, A. Balan, C. Jedrzejczyk, W. Drenckhan, Controlled foam generation using cyclic diphasic flows through a constriction, Int. J. Multiph. Flow. 96 (2017) 173–187.

[29] C. Dari, H. Dallagi, C. Faille, T. Dubois, C. Lemy, M. Deleplace, M. Abdallah, C. Gruescu, J. Beaucé, T. Benezech, A.-L. Fameau, Decontamination of Spores on Model Stainless-Steel Surface by Using Foams Based on Alkyl Polyglucosides, Molecules. 28 (2023) 936.

[30] J. Sonoda, T. Sakai, Y. Inomata, Liquid oil that flows in spaces of aqueous foam without defoaming, J. Phys. Chem. B. 118 (2014) 9438–9444.

[31] A. Kusaka, J. Sonoda, H. Tajima, T. Sakai, Dynamics of liquid oil that flows inside aqueous wet foam, J. Phys. Chem. B. 122 (2018) 9786–9791.

[32] R. Mensire, E. Lorenceau, Stable oil-laden foams: Formation and evolution, Adv. Colloid Interface Sci. 247 (2017) 465–476.

[33] T. Schad, N. Preisig, W. Drenckhan, C. Stubenrauch, Foam-based cleaning of surfaces contaminated with mixtures of oil and soot, J. Surfactants Deterg. 25 (2022) 377–385.

[34] R. Schütz, A. V Rawlings, E. Wandeler, E. Jackson, S. Trevisan, J. Monneuse, I. Bendik, M. Massironi, D. Imfeld, Bio-derived hydroxystearic acid ameliorates skin age spots and conspicuous pores, Int. J. Cosmet. Sci. 41 (2019) 240–256.

[35] T. Gaillard, C. Honorez, M. Jumeau, F. Elias, W. Drenckhan, A simple technique for the automation of bubble size measurements, Colloids Surfaces A Physicochem. Eng. Asp. 473 (2015) 68–74.

[36] H. Dallagi, C. Faille, C. Gruescu, F. Aloui, T. Benezech, Foam flow cleaning, an effective and environmentally friendly method for controlling the hygiene of closed surfaces contaminated with biofilms, Food Bioprod. Process. (2022).

[37] A.-L. Fameau, J.-P. Douliez, F. Boué, F. Ott, F. Cousin, Adsorption of multilamellar tubes with a temperature tunable diameter at the air/water interface, J. Colloid Interface Sci. 362 (2011).

[38] A.-L. Fameau, S. Lam, O.D. Velev, Multi-stimuli responsive foams combining particles and self-assembling fatty acids, Chem. Sci. 4 (2013). https://doi.org/10.1039/C3SC51774H.

[39] A.-L. Fameau, F. Cousin, R. Derrien, A. Saint-Jalmes, Design of responsive foams with an adjustable temperature threshold of destabilization, Soft Matter. 14 (2018). https://doi.org/10.1039/C8SM00190A.

[40] E. Le Toquin, S. Faure, N. Orange, F. Gas, New biocide foam containing hydrogen peroxide for the decontamination of vertical surface contaminated with Bacillus thuringiensis spores, Front. Microbiol. 9 (2018) 2295.

[41] S. Serra, D. De Simeis, New insights on the baker's yeast-mediated hydration of oleic acid: the bacterial contaminants of yeast are responsible for the stereoselective formation of (R)-10-hydroxystearic acid, J. Appl. Microbiol. 124 (2018) 719–729.

Supporting Information: Ultrastable and responsive foams based on 10-hydroxystearic acid soap for spores' decontamination

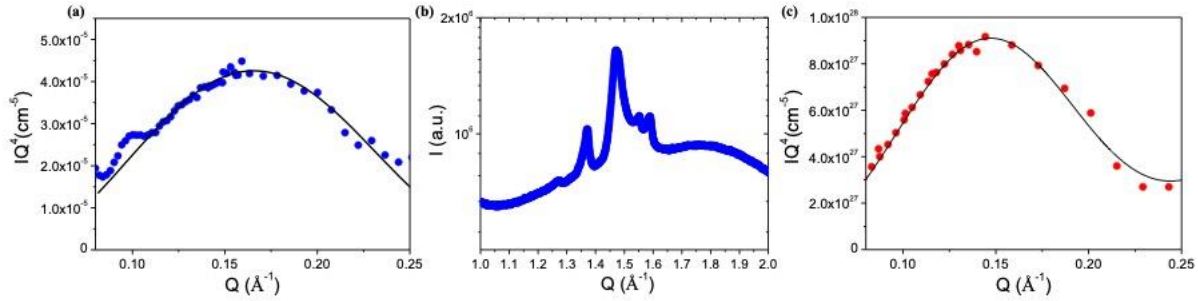

Figure S1. (a) SANS intensity profile of 10-HSA aqueous dispersion at 25 °C displayed in the Porod representation. The lines correspond to the best fit of the data using the model described in the literature [1]. (b) WAXS intensity spectrum of 10-HSA aqueous dispersion at 25 °C. (c) SANS intensity profile of 10-HSA aqueous dispersion at 75 °C displayed in the Porod representation. The lines correspond to the best fit of the data using the model described in the literature.

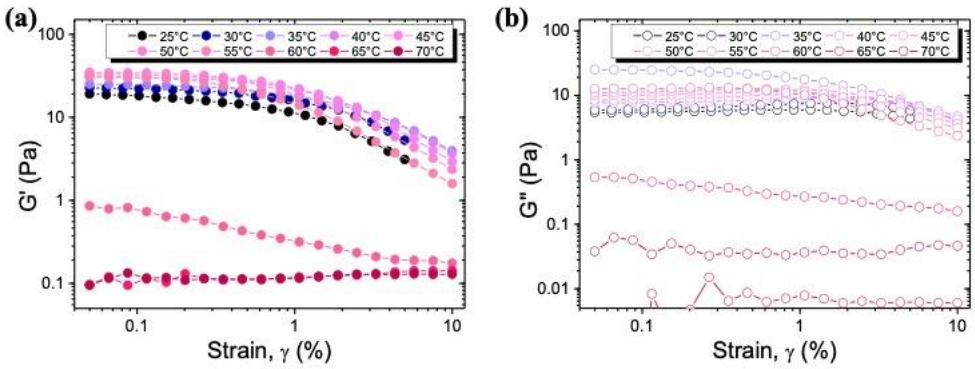

Figure S2. Oscillatory measurements of 10-HSA aqueous dispersion as a function of the strain amplitude, γ at constant f = 1 Hz at different temperatures: (a) elastic G' (●) and (b) viscous G'' moduli.

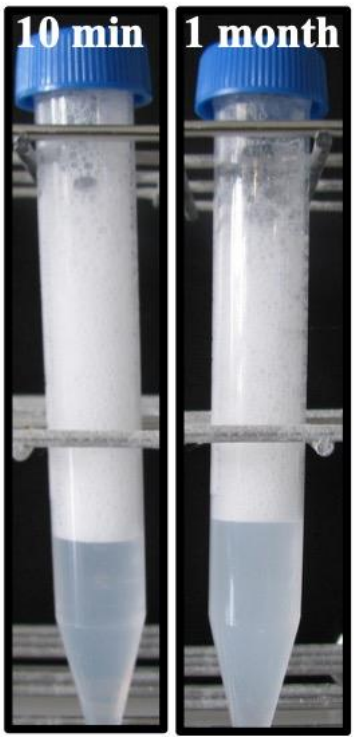

Figure S3. Pictures of 10-HSA foam produced by hand-shaking and kept at room temperature, just after foam formation (10 min) and after one month of conservation.

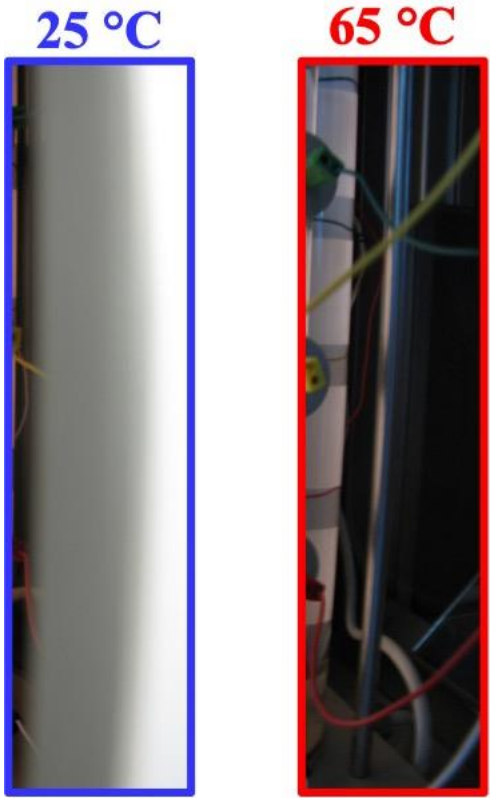

Figure S4. Pictures of the foam produced by bubbling gas using the Foamscan apparatus. Stable foam was obtained at 25°C, but by increasing the foam temperature at 65 °C, the foam was destroyed quickly in few minutes.

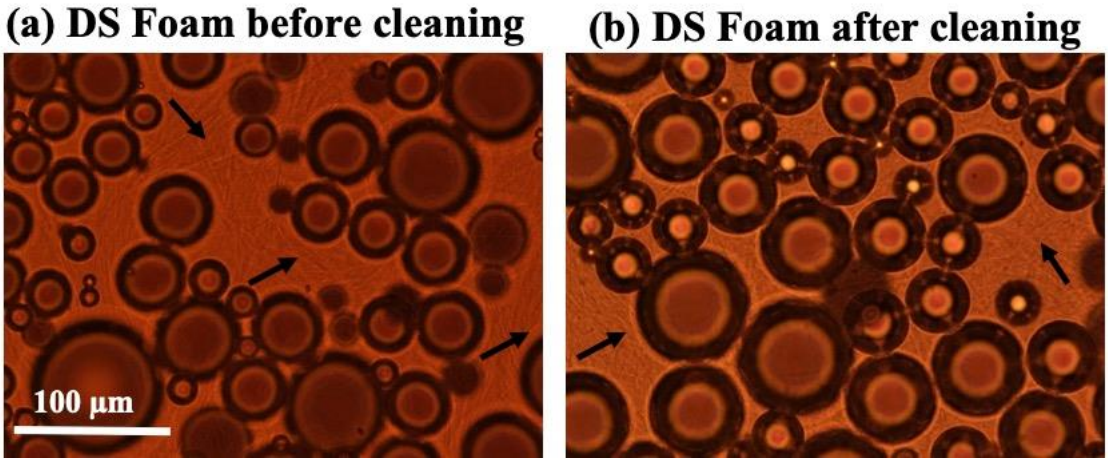

Figure S5. Pictures obtained by phase contrast microscopy of the double syringe (DS) foam: (a) before cleaning and (b) after cleaning. The arrows are pointing at some of the 10-HSA multilamellar tubes.

SANS data fitting:

The intensity scattered by objects in solution can be described as a product of structure factor S(Q), characteristic of the correlations between objects, by a form factor P(Q), that describes the shape of the objects. At large Q, the scattering curves scatters like Q-4 that is characteristic of a Porod behavior corresponding to the surface scattering of 3-D objects. The main equations used to fit the data of our system and consequently get further information on the objects in solution are those for lipids embedded in flat lamellar structures or micelles. For lamellar structure, the spectrum was fitted with a lamellar stack Caillé model used in SasView 5.0.4 (http://www.sasview.org/.), that is a random lamellar sheet with a Caillé structure factor. In this model of Caille S(Q) is used for the lamellar stacks. Through the form factor it is possible to describe some specific characteristics of the spectrum, namely the thickness of the membrane δ, with the function.

We fixed the scattering length density of the solvent and the membranes (i.e. the fatty acids) and the total concentration, the others parameters were fitted. The line in the main text corresponds to the best fit of the data [1].

The form factor of a completely filled spherical object of radius R like micelles is given by:

Psphere(Q)=9[(sin(QR)-QRcos(QR))/(QR)3]

For centrosymetrical objects like spheres, it is often considered that the structure factor S(Q) ~ 1 at large Q. Consequently, the radius of the micelle can be estimated from the form factor. The structure factor, S(q), which quantifies the intermicellar interactions/correlations, is included in our fitting process using the "Hayter-MSA-Structure" model displayed in the SASview software. This accounts for a repulsive screened Coulombic intermicellar interaction potential. The broad interaction peak observed in small angle neutron scattering spectra comes from the deprotonation of the COOH which introduces negative charges at the micellar/solvent interface. Six parameters are needed to compute the Hayter and Penfold structure factor: the dielectric constant, the volume fraction, the effective radius of interacting objects, the temperature, the surface charge of the micelle, and the salt concentration. We fixed the dielectric constant, the volume fraction, the temperature, the scattering length density of the solvent and the sphere (in our case we took only the scattering length density of the fatty acid and not the MEA: Nb = -0.28*10-6 $Å^{-2}$), and the salt concentration. Thus, the micelle charge is the only fitting parameter for the calculation of S(q), and we found a value of -251. In the main text, the line corresponds to the best fit of the data according to the form and structure factor model. We observed the presence of negatively charged spherical micelles for all systems.

References:

[1] A.-L. Fameau, F. Cousin, A. Saint-Jalmes, Morphological Transition in Fatty Acid Self-Assemblies: A Process Driven by the Interplay between the Chain-Melting and Surface-Melting Process of the Hydrogen Bonds, Langmuir. 33 (2017). https://doi.org/10.1021/acs.langmuir.7b02651.

2.2 Static Foam Cleaning with Sodium Cocoyl Isethionate-Based Foams for Spore Removal from Solid Surfaces

Carolina Dari[1], Audrey Hamiot[1], Christelle Lemy[1], Clemence Le Coeur[2,3], Thierry Benezech[1], Anne-Laure Fameau[1*]

1 INRAe, University Lille, CNRS, INRAe, Centrale Lille, UMET, 59000 Lille, France.

2 Laboratoire Léon Brillouin, University Paris-Saclay, CEA-CNRS UMR CEA Saclay, F-91191 Gif sur Yvette, France ;

3 CNRS, ICMPE, UMR 7182, University Paris Est Creteil, 2 rue Henri Dunant, F-94320 Thiais, France

* **Correspondence:**

Corresponding Author

Anne-laure.fameau@inrae.fr

Keywords: foam1; cleaning; spores; sodium cocoyl isethionate.

Abstract: Surface contamination with microorganisms is a significant concern in the food industry as it can lead to cross-contamination of food products. Foams are the most common method to clean open surfaces in the food industry. In this context, foams serve primarily as carriers for disinfectants rather than for their inherent cleaning properties. The formulation of cleaning foams involves the use of surfactants. Increasing concern for the environment is leading to the replacement of petrochemical surfactants by bio-based surfactants. Sodium cocoyl isethionate (SCI) is a bio-based surfactant widely used in personal care products. However, little is known about its foaming properties. Here, we studied the self-assembly, interfacial and foaming properties of SCI. A multiscale approach was used combing optical microscopy, small-angle neutron scattering and surface tension measurements. Then, we produced foams based on SCI to elucidate the cleaning mechanisms of of foams for cleaning

solid surfaces contaminated with spores in static conditions. We studied both the effect of different liquid fractions and different levels of contamination attachment to the surfaces on the foam cleaning efficiency. We showed that foams can remove spores from solid surfaces when whipping and imbibition mechanisms are promoted.

2.2.1 Introduction

Contamination of surfaces with micro-organisms is a major concern in the food industry as it can cause cross-contamination of foodstuffs, leading to two main problems: food spoilage and consumer illness (Lücking et al., 2013; DeFlorio et al., 2021; Midelet et al., 2024). Food spoilage is a major contributor to food waste and therefore has a negative effect on the environmental sustainability of the food industry (Snyder et al., 2024). According to World Health Organisation, every year in the world, there are 600 million cases of food-borne illnesses of which 420.000 result in death (WHO, 2022). This clearly brings with it a negative impact on public health as well as financial losses to the industries (DeFlorio et al., 2021; Midelet et al., 2024).

Cleaning and disinfection operations are essential to control food contamination related to surfaces to eliminate: bacteria, biofilms and spores. Foams are the most commonly used method for cleaning open surfaces, such as the exterior of equipment, floors and walls, in the food industries (EHEDG, 2021). In this context, foams are applied as carriers for disinfectants or other chemicals that will have an effect on cleaning. Note that foams are often considered to have no effect on cleaning, however, recent studies have shown otherwise (Jones et al., 2020; Schad et al., 2021, 2022b, 2022a). In fact, Schad et al., conducted a study on foam cleaning of solid surfaces soiled with oil, in which they proposed three main foam cleaning mechanisms (Schad et al., 2021):

- Imbibition: when a liquid is sucked up into the Plateau borders of the foam by capillary forces. This mechanism becomes stronger with small bubbles and small liquid fractions.

- Wiping: this mechanism occurs by re-arrangements of the bubbles, that leads to wiping motions between the foam and the surface. This mechanism is promoted in unstable foams where re-arrangements of the bubbles occur.

- Drainage: the liquid drained of a foam can flow under the soiled of the surface and lift the contaminant. This occurs in foams where the capillary forces are not enough to retain the liquid of the foam and so it drains.

In addition, we have recently demonstrated that foams based on 10-HSA soap can remove spores from stainless-steel surfaces. In this study we showed the influence of the bubbles size on the cleaning efficiency of foams (Dari et al., 2023a).

Foams for cleaning are based on surfactant as foam stabilizer. However, due to the increasing concern for the environment is causing petrochemical surfactants to be replaced by bio-based surfactants in order to obtain more sustainable cleaning formulations (Drakontis, 2020). Sodium cocoyl isethionate (SCI) is a bio-based surfactant composed of fatty acid derived from coconut oil and an ester of isethionic acid. SCI is used on an industrial scale in personal care products such as soap bars, shampoos and skin cleansers, mainly because of its low toxicity and good foaming properties (Petter, 1984; Burnett et al., 2017; Jeraal et al., 2018). Its utilization dates back more than 40 years, which makes it a cost-effective surfactant. Despite its widespread use, only few data are available regarding its self-assembly, interfacial and foaming properties (Petter, 1984; Jeraal et al., 2018; Ananthapadmanabhan, 2019).

The aim of this study was to use SCI as foaming agent to produce foams with controlled structure (liquid fraction and bubbles size) to determine the main parameters governing the removal of Bacillus subtilis spores from solid surfaces in static conditions. First, we studied the self-assembled properties of SCI in bulk aqueous solution, the air/water surface properties and the resulting foaming properties. We used a multiscale approach by combining microscopy techniques, small-angle neutron scattering (SANS), wide-angle X-ray scattering (SAXS), Differential Scanning Calorimetry and surface tension measurements. Then, we produced

foams with different liquid fractions but keeping similar bubbles size to understand the role of liquid fractions in foam cleaning for spores' removal. For this purpose, we carried out the cleaning tests of stainless-steel surfaces soiled with bacteria spores. We carried out tests with two types of different spores: hydrophilic and hydrophobic. We studied the influence of different levels of attachment of the spores to the surface by varying the drying time, in order to elucidate the static foam cleaning mechanisms.

2.2.2 Materials and methods

2.2.2.1 Materials

2.2.2.1.1 Preparation of the stock solutions

Sodium Cocoyl Isethionate (SCI) was provided by BASF (Ludwigshafen, Germany) and used as received. The required amount of SCI was weighed and MilliQ water was added to obtain solutions with 1, 5 and 10 wt.%. Then, the mixture was stirred magnetically at 80 °C until the surfactant was completely dissolved and the solutions were clear. The stock solutions were stored at around 4 °C in a fridge.

2.2.2.1.2 Methods

2.2.2.1.3 Determination of the Krafft temperature by Differential Scanning Calorimetry (DSC) and by optical microscopy

The Krafft temperature of the SCI solutions was determined by two different methods. First, the Krafft temperature of SCI solutions was determined for two different concentrations of SCI (5wt.% and 10 wt.%) using a Differential Scanning Calorimeter (Q100 TA Instrument, France). A mass of approximately 20 mg of the SCI solutions was placed in aluminum hermetic pans. To ensure the validity of the results samples underwent two successive cycles of heating and cooling from 5 °C to 75 °C at a rate of 2 °C/min with 2 min intervals at 80 °C. The thermodynamic equilibrium of the samples was assessed by the unchanged response between the first and second cycles.

To determine the Krafft temperature for a wider range of concentration, we used then optical microscopy. An aliquot of the SCI solution was placed on a slide and the slide was placed on a temperature-controlled plate (Linkam, model LTS120) connected to a water circulation pump. Observations of the sample were made using an optical microscope (Zeiss) at 40x magnification. The Krafft temperature was determined as the temperature at which the crystals began to melt. The measurements were carried out in triplicate for SCI solutions of different concentrations (0.5 wt.%, 1 wt.%, 2 wt.%, 3 wt.%, 4 wt.%, 5 wt.%, and 10 wt.%).

2.2.2.1.4 Determination of Critical Aggregation Concentration (CAC) via Surface Tension Measurements

The CAC value of the SCI was determined by measuring the air-solution surface tension as a function of the concentration of the SCI solutions using the Kibron Delta-8 automated surface tension plate reader (Kibron, Finland). The SCI solutions were first pre-heated at around 40°C. A volume of 50 µL of each solution was placed on the 96-hole platform. Measurements were performed at 20 °C ± 1 °C after a waiting time of 10 min to ensure equilibrium at the air-water interface. Measurements were performed in triplicate. Calibration was performed with MilliQ water at 20 °C ± 1 °C.

2.2.2.1.5 Small-angle neutron scattering (SANS)

SANS patterns were recorded at D22 beamline at the Institut Laue–Langevin – The European Neutron Source (ILL, Grenoble, France), with a wavelength λ of 0.60 nm (relative full width at half maximum 10%) and two 3He multi-PSD tube detectors, one at 1.4 m sample-to-detector distance and the second at 17.6 m, covering a total q-range of 0.023 to 6.4 nm^{-1}, where q is the magnitude of the wavevector ($Q= 4\pi\sin(\theta/2)/\lambda$, with θ the scattering angle). For this experiment the samples were prepared in D2O instead of ultrapure water to increase contrast and reduce background. Solutions were kept in quartz cuvettes of 1 mm pathway (type 110-QS, Hellma GmbH, Müllheim, Germany), placed on a sample-changer thermalized at 20 °C or 50 °C. Data reduction was performed with the program GRASP V.10.17i (DOI: 10.1107/S1600576723007379) to correct for flat field, parallax, transmission, scattering by the

empty cell, detector background as measured with an absorber (sintered 10B4C) at the sample position, using the monitor to normalize data, and with a measure of the direct beam attenuated with a calibrated chopper leading to corrected data in absolute units (cm-1), which were radially averaged and binned according to resolution. Data are available at DOI: 10.5291/ILL-DATA.9-11-2107. Contributions from solvent and incoherent scattering were then subtracted. All spectra were fitted by using SasView 5.0.4 (http://www.sasview.org/).

The intensity scattered by surfactant self-assembly in solution can be described as a product of structure factor S(Q), characteristic of the correlations between the self-assembled structure, by a form factor P(Q), that describes the shape of the self-assembly. At large Q, the scattering curves scatters like Q-4 that is characteristic of a Porod behavior corresponding to the surface scattering of 3-D objects. The form factor of a completely filled spherical object of radius R like micelles is given by:

Equation 1 :

$$P_{sphere}(Q)=9[(\sin(QR)-QR\cos(QR))/(QR)^3]$$

For centrosymetrical objects like spheres, it is often considered that the structure factor S(Q) ~ 1 at large Q. Consequently, the radius of the micelle can be estimated from the form factor. The structure factor, S(Q), which quantifies the intermicellar interactions/correlations, is included in our fitting process using the "Hayter-MSA-Structure" model displayed in the SASview software. This accounts for a repulsive screened Coulombic intermicellar interaction potential. The broad interaction peak observed in small angle neutron scattering spectra comes from the the negative charge of the SCI at the micellar/solvent interface. Six parameters are needed to compute the Hayter and Penfold structure factor: the dielectric constant, the volume fraction, the effective radius of interacting objects, the temperature, the surface charge of the micelle, and the salt concentration. We fixed the dielectric constant, the volume fraction, the temperature, the scattering length density of the solvent and the sphere (in our case we took the scattering length density of the SCI: Nb = -0.28*10-6 $Å^{-2}$), and the salt concentration. Thus, the

micelle charge is the only fitting parameter for the calculation of S(Q) and we found a value of -20. In the main text, the line corresponds to the best fit of the data according to the form and structure factor model.

2.2.2.1.6 Preparation of the solid model surfaces for spores' decontamination

To carry out the tests for spores' decontamination, we used rectangular AISI stainless-steel plates (45mm x 15mm) (APERAM, Isbergues, France) with a 2R factory finish. These surfaces were subjected to a conditioning process that was previously described (mention papaer 1) in order to have similar properties to the surfaces found in the dairy industry. In brief, the surfaces were immersed in milk at 30 degrees for 30 minutes, then washed with osmosis water for 5 minutes, and then immersed in sodium hydroxide (0.5 wt.%) at 70 °C for 15 minutes. This cycle was repeated 15 times. Afterward, the surfaces were soiled with an E. coli biofilm. Then, they were clean and disinfected with an alkaline detergent RBS T105 (Chemical products, Brussels, Belgium) following a protocol that was previously described (Dari et al., 2023b) 24 hours before each experiment the surfaces were sterilized in a dry-heat oven at 180 °C for 1h.

2.2.2.1.7 Preparation of the spores suspensions

Two Bacillus subtilis strains were used in study : *Bacillus subtilis* PY79 (subsequently named Bs PY79), a laboratory strain producing hydrophilic spores, and a recombinant strain Bs PY79 deletion in spsI (Dubois et al., 2020)(subsequently named Bs PY79 spsI), producing hydrophobic spores. Both Bacillus strains were tagged with green fluorescent proteins to make the spores fluoresce. Both spores' suspensions were produced with a methodology that was previously described (Faille et al., 2019; Dari et al., 2023b).

The concentration of the spore's suspension used for each experiment was around 108. Before each experiment the suspensions were sonicated for 2 min and 30 s in an ultrasonic bath (Bransonic 2510E-MT, Branson Ultrasonics Corporation, Danbury, CT, USA) to avoid the presence of spore aggregates.

2.2.6 Production of the foams for spores' decontamination

For the production of the foams, the 1 wt.% and 10 wt.% solutions were used. Before producing the foams, the solutions were heated to 80 °C until they were clear. The foams were then produced with the solutions at 40 °C. To produce the foams, we used the double-syringe method (Figure 1) (Gaillard et al., 2017). Two 50 mL syringes were connected with a luer-lock connector. In one syringe the necessary amount of liquid was added and then the piston was moved to the maximum capacity of the syringe, to have the necessary amount of air; the other syringe was left with the piston closed; then both syringes were connected and the pistons were moved 20 times to produce the foam. With the 10 wt.% solution, to produce foams with different liquid fractions, the volumes of liquid in the syringe were changed. The same was done with the 1 wt.% solution, but the foams were also left to stand for 15 minutes and the drained liquid was removed.

2.2.2.1.8 Characterization of the foams for spores' decontamination

The foams produced were characterized in terms of bubbles size, foam height, and liquid fraction. The liquid fraction was calculated with the following equation:

Equation 2 :

$$\emptyset = (V_{liquid\ initial} - V_{liquid\ drained}) / V_{foam}$$

With $V_{liquid\ initial}$ corresponding to the initial amount of liquid; $V_{liquid\ drained}$ corresponding to the amount of liquid drained after 15 min (only for foams produced with the 1 wt.% solution), and V_{foam} corresponding to the total volume of foam.

The foams bubbles size and the foam height were simultaneously measured using a dynamic foam analyzer-DFA100 (KRUSS, Hamburg, Germany) as previously described (Dari et al., 2023b). In brief, the foams were put in a glass column with a prism incorporated in the whole length of the column. The foams height was tracked for 1800 seconds, using an LED panel at the front- and a-line sensor at the back of the column, which detected changes in light

transmission. The foams bubbles size was monitored using a camera positioned in the column. The prism in the column facilitated the capture of 2D images of the foam structure, which were analyzed with KRUSS foam analysis software to record the average bubble area at each time step over the same 1800 second period. The experiments were carried out in triplicate.

2.2.2.1.9 Foam spores decontamination analysis

The methodology for evaluating the efficiency of foams to decontaminate surfaces contaminated with spores was adapted from the literature (Dari et al., 2023b, 2023a). The plates were soiled with 5 drops of 1µL of the spore suspension using a micropipette. Experiments were then carried out without drying the plates or drying them at two different times: 30 min and 60 min, in an oven at 30 °C. The plates were then placed in petri dishes and 20mL of foam or the solution without foaming were placed on the top of each plate (**Figure 2.2.1**). After 30 min, the foam was removed with osmosis water. Three soiled plates were used in each experiment, and an additional plate was used as a control for quantification of the initial spore concentration in each experiment.

To remove the adherent spores, each plate was swabbed with a dry cotton swab (Copan, Brescia, Italy) and placed in a tube containing 5 mL of sterile Milli-Q water. Each tube was vortexed for 1 min at 2400 rpm, and then each swab was removed from the tubes. The detached spores were serially diluted in MilliQ water and then plated on tryptic soy agar (TSA; Biokar Diagnostics, Allonne, France). After 24h of incubation at 30°C the colonies were counted manually and the number of forming units (CFU) was calculated for each plate. The foam decontamination efficiency was calculated in terms of log reduction with the equation previously described in the literature (Dari et al., 2023a). The experiments were carried out in duplicate.

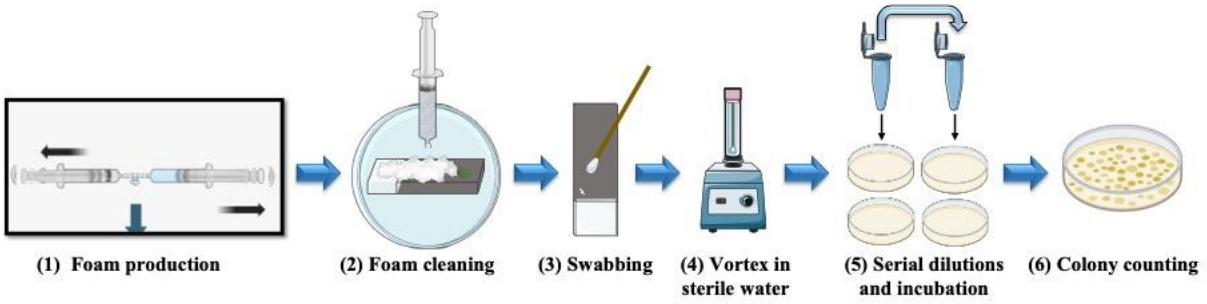

Figure 2.2.1. Methodology for spores' removal on stainless steel surfaces by using static foam cleaning: (1) The foams were produced by the double syringe method; (2) the soiled plates were placed in petri dishes and the foam was placed on the top of each plate. They were kept in horizontally position for 30 minutes; (4) each plate was sampled with a dry cotton swab (5) the swab was put in a tube with 5mL of sterile Mill-Q water and vortexed for 1 minute at 2400 rpm (6) serial dilutions were made in sterile Milli-Q water for each tube and there were plated in Tryptic Soy Agar and incubated for 24 h at 30 ◦C (7) the number of colony forming units (CFU) was counted manually

2.2.2.1.10 Statistical Analysis

The results were expressed as the mean ± standard deviation. The results were compared by one-way analysis of variance and Tukey's test to analyze statistical differences ($p < 0.05$). The analysis was performed using SAS V8.0 software (SAS Institute, Gary, NC, USA).

2.2.3 Results

2.2.3.1 Krafft temperature and Critical Aggregation Concentration of the SCI dispersion

First, we determined the Krafft temperature, i.e. the temperature of transition of the SCI from a crystal state to soluble state (**Figure 2.2.2**). The Kraft temperature was determined by two different methods: DSC and optical microscopy. The Kraft temperature determined by DSC was 28.1°C and 30.4°C for 5 wt.% and 10 wt.% SCI, respectively (**Figure S1**). The Kraft temperature determined by optical microscopy was 34.5 ± 1.2°C, 34.7 ± 1°C and 32.8 ± 1°C for SCI at 1 wt.%, 5 wt.% and 10 wt.%, respectively (**Figure S2**).

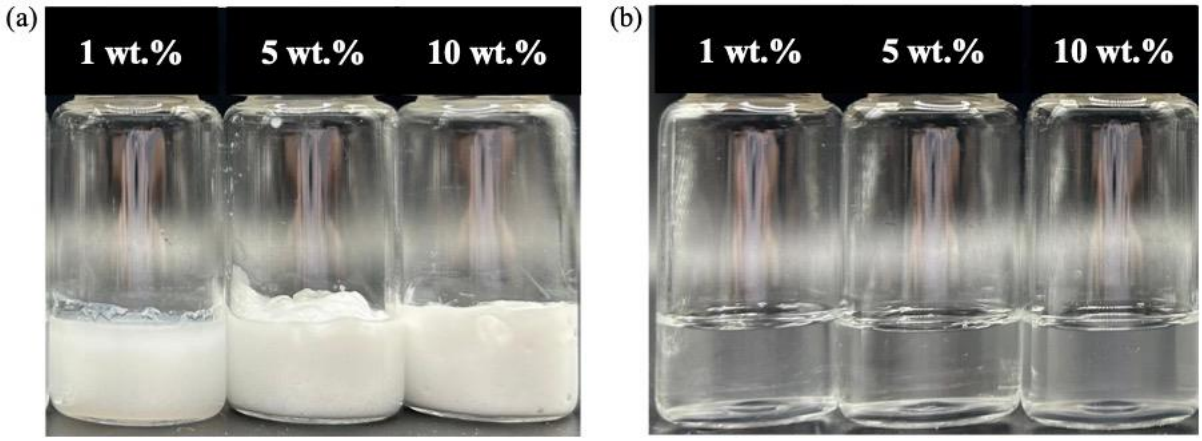

Figure 2.2.2. Solutions of SCI at 1, 5 and 10 wt.%, from left to right (a) in the form of crystals (room temperature) below the Kraftt temperature (b) in the soluble micellar state leaving to limpid solution above the Krafft temperature.

Then, we determined the CAC by tensiometry experiments. The SCI solutions were heated above its kraft temperature (~ 40 °C) and the surface tensions were determined as a function of the SCI concentration. The CAC was determined to be around 0.7 wt.%, associated with a plateau surface tension at 28.2 mN.m-1 ± 0.3 (**Figure 2.2.3**). In the literature, the surface tension of the SCI was reported to be 27 mN.m-1 for a concentration of 0.1 wt.% (Burnett et al., 2017). Although this surface tension is close to the one obtained in this study, in this case it was obtained for a higher concentration. The differences obtained may be due to differences in purity and it should also be noted that the method by which it was measured in that study is unknown (Jeraal et al., 2018). Furthermore, Jeraal et al, studied the CMC of Sodium Lauroyl Isethionate, which is one of the most abundant isethionates present in the SCI blend (Jeraal et al., 2018). They reported a CMC of 0.1 wt.% with a plateau surface tension of 37.9 $mN.m^{-1}$. The surface tension obtained in our study for the same concentration (34.3 ± 0.3 for 0.1 wt.%) is close to the one reported by Jeraal et al, (Jeraal et al., 2018). It should be noted that the surface tension was measured by another method (pendant drop). However, the differences may be due to the fact that in our case we used SCI, which contains a mixture of different chain lengths of

isethionates, unlike Jaraal et al, who used only sodium lauroyl isethionate, 12 carbons chain lengths (Jeraal et al., 2018).

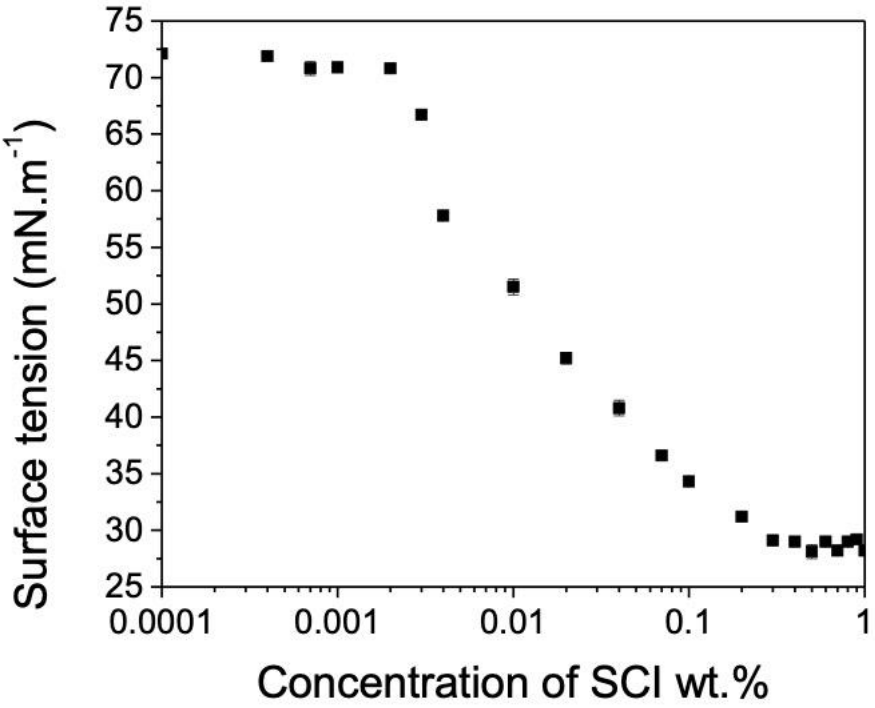

Figure 2.2.3. Evolution of the surface tension of aqueous solutions of SCI as a function of the concentration at T= 20 °C ± 1 °C.

2.2.3.2 Characterization of the self-assembled structure at 20 °C and at 50 °C by optical microscopy and SANS

The concentration of SCI was fixed above the CAC at 1, 5 and 10 wt.%. At 20 °C, a homogenous turbid phase with birefringence was observed for all the concentrations. By using phase contrast microscopy, we observed entangled fibrillar aggregates with no long-range ordering at 1 wt.% (**Figure S3**). The length of these fibers could not be probed by optical microscopy, as the fibers were longer, on average, than the field of view. The fiber morphology was a mixture of either straight or curved, indicative of flexible fibrillar aggregates. The same fibrillar aggregates were observed at 5 and 10 wt.% but in higher quantity. In order to gain insight into the structure of these fibrillar aggregates at the nanometric scale, SANS experiments

were performed. This technique does not provide information on the total size of the fibrillar aggregates observed by microscopy, but it allows us to determine the structure at the nanoscale.

Figure 3a displays the scattering profile for the three concentrations studied at 20 °C. SANS measurements revealed a lamellar mesophase evident from the emergence of the equally spaced Bragg peaks at Q= 0.138, and 0.275 Å−1, attributed to nα = 1 and 2 lamellar peak order, for the three concentrations (**Figure 2.2.4.a**). The Bragg peaks were more pronounced by increasing the concentration from 1 to 10 wt.%. The lamellar d-spacing calculated from the Bragg peak positions is d ~ 45.5 Å. SANS results indicate that lamellar stacks were the building units which bundle into fibrillar aggregates observed microscopically. At 50 °C, we observed the characteristic features of micellar phase for all concentrations (**Figure 2.2.4.b**). At large q, we fitted the scattering curve with a form factor of a sphere of radius 2.2 nm at 1 wt.%. The scattering intensity decreased when going toward medium-q, demonstrating that the micellar phase showed the presence of a structure factor, indicative of interactions between micellar aggregates in solution. Then, we fitted all the other scattering curves with the same model used for 1 wt.% by including the structure factor described in the materials and methods section and with a charge of - 20. In all concentrations, we observed negative charged spherical micelles with the same diameter. It is important to notice that we observed at low Q, a Q^{-2} decay. We suppose that it could come from the presence of a small amount of swollen bilayer structure present in mixture with micelles.

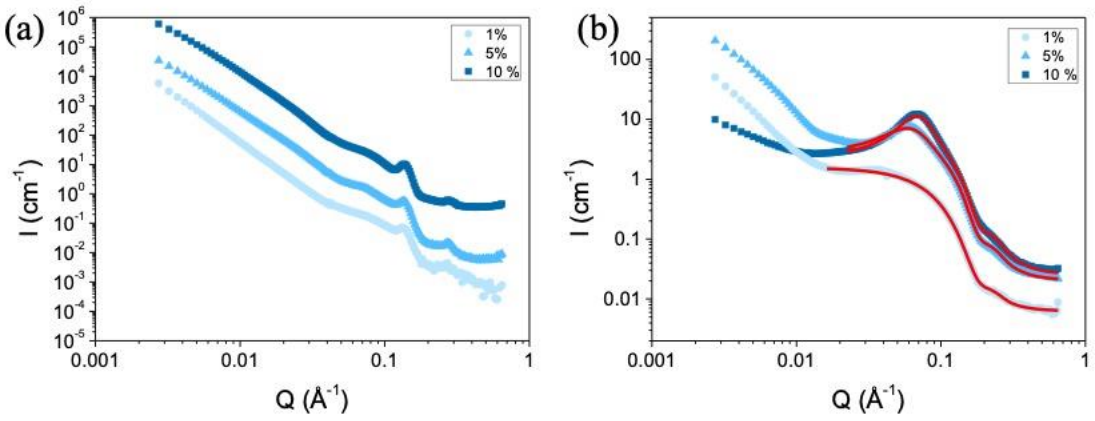

Figure 2.2.4. SANS profiles for SCI at three concentrations at: (a) 20 °C and (b) 50 °C. The profiles are offset on the vertical scale for clarity. The line corresponds to the best fit described in the main text.

2.2.3.3 Characterization of the foams for spores' decontamination

As the main objective of this work was to study the influence of liquid fractions on the foams cleaning efficiency, it was important to produce foams with different liquid fractions but similar bubble size. That is to say stable foams with no drainage. Our strategy was to produce the foam in the micellar state above the Krafft temperature to have high quantity of foam, and then the formation of crystals at room temperature inside the foam could stabilize the foam and limit the drainage as already demonstrated for foams stabilized by surfactant crystals (Zhang et al., 2015). First, it was important to study the properties of the foams. The foams were produced with the double syringe technique and then they were analyzed in vertical conditions using a glass column for the same time as the cleaning tests (30 min). The foams were characterized in terms of foam stability by measuring the drainage, the foam height and the mean bubbles radius.

The normalized foam height was followed as a function of time (**Figure 2.2.5**). The foam height after 30 min was 98% ± 2, 98% ± 1 and 95% ± 2 for the foams with a liquid fraction of 13%, 22% and 27% respectively, showing that very stable foams were obtained. In addition, we

followed the evolution of the liquid drained over time. No drainage was observed in any of the foams after 30 minutes, further confirming their stability.

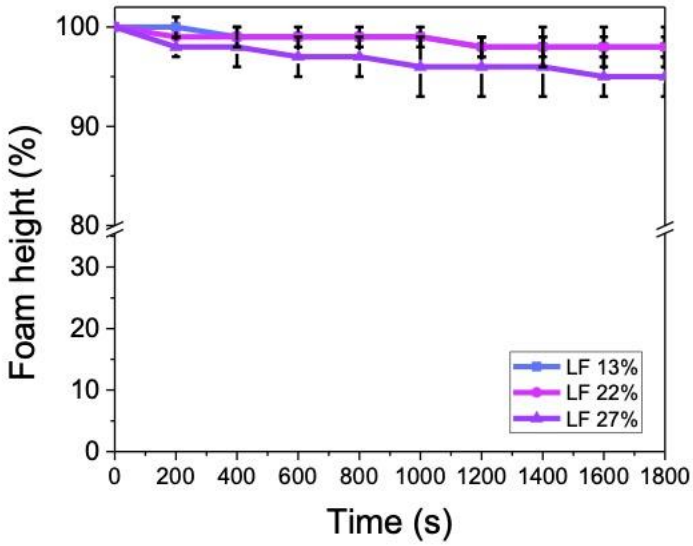

Figure 2.2.5. Evolution of the foam height for foams with different liquid fractions (13%, 22% and 27%).

Figure 2.2.6 shows the initial mean bubbles radius for the foams with the three different liquid fractions. The initial mean bubbles radius was 50 ± 5 µm, 39 ± 4 µm and 35 ± 1 µm for the foams with a liquid fraction of 13%, 22% and 27%, respectively. As shown also in the bubble's pictures of the **Figure 2.2.6.a**, the initial mean bubble size was similar for the foams with a liquid fraction of 22% and 27% and slightly higher for foam with a liquid fraction of 13%. After 30 min, the mean bubbles radius was 68 ± 16 µm, 76 ± 10 µm and 93 ± 3 µm for the foams with a liquid fraction of 13%, 22% and 27%, respectively (**Figure 2.2.6.b**). As we can also see in the bubble's pictures the mean bubbles size increased by approximately a factor of 2 for the three foams (**Figure 2.2.6.b**). This increase in the bubbles size is due to coalescence and coarsening (Schad et al., 2021). The mean bubble size trend after 30 minutes was similar to the initial time, i.e., the foams with liquid fractions of 22% and 27% had similar bubble sizes and the one with 13% presented a slightly larger bubble size. Note that in the bubble's pictures after

30 min the bubbles do not look perfectly round, this may be due to the presence of high amount of SCI crystals (**Figure 2.2.6.b**). In addition, the difficulty to see the bubbles at the initial time of the foams with liquid fractions of 22% and 27% may be due to the fact that they are so small that it is difficult for the camera to distinguish them from the turbid continuous phase.

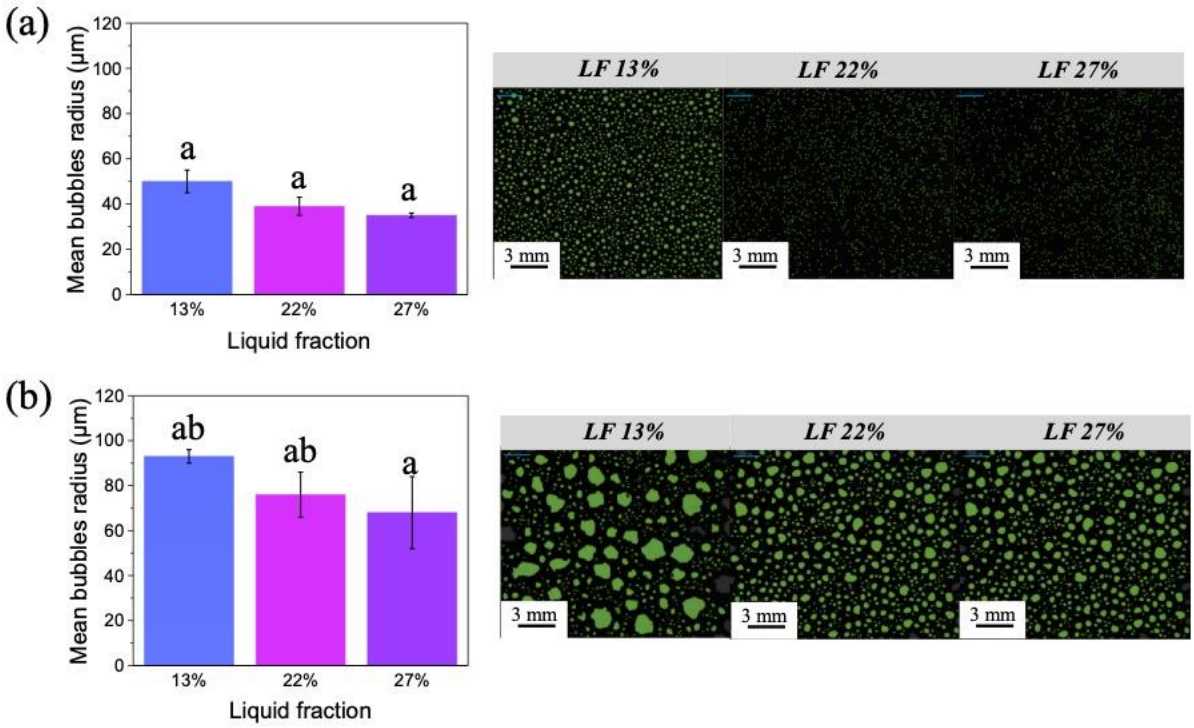

Figure 2.2.6. Mean bubbles area of foams with different liquid fractions (13%, 22% and 27%) and their bubbles corresponding pictures: (a) at t=0 (b) at t=30 min. The small letters a–b indicate groups of statistical differences according to Tukey's test ($p < 0.05$).

The surfactant solution (SCI 10 wt.%) used for these experiments and the foam production technique (double syringe) to produce the foams, allowed us to obtain foams with 3 different liquid fractions (13%, 22% and 27%) which are the ones presented here so far. Therefore, in order to test other liquid fractions, we decided to do experiments with a solution of SCI at 1wt.%. This solution allowed us to obtain two foams with two different liquid fractions: 7% and 16%. The foam height after 30 min was 93% ± 4 and 95% ± 3 for the foams with a liquid fraction of 7% and 16 %, respectively (**Figure S4**). These results were similar to those obtained with the other foams based on 10 wt.%. In addition, no drainage was observed after 30 min,

meaning that foams with similar stability were obtained. The initial mean bubbles size was 82 ± 5 µm and 48 ± 9 µm for the foams with a liquid fraction of 7% and 16% respectively (**Figure S5a**). The foam with a liquid fraction of 16% showed a similar bubble size to the previous foams based on 10 wt.% SCI, however this was not the case for the foam with 7% liquid fraction, whose initial bubble size was bigger than the other foams based on 10 wt.% SCI. After 30 min, the mean bubbles radius was 124 ± 18 µm and 77 ± 9 µm for the foams with a liquid fraction of 7% and 16%, respectively (**Figure S5b**). Both foams exhibited an increase of their bubbles size with time, meaning that coalescence and coarsening also occurred in these foams. The two foams with the liquid fractions of 7% and 16% after 30 min had a similar bubbles size, which was also similar to the bubbles size of the other foams based on 10 wt.% SCI. In the case of the foam with a liquid fraction of 7%, coalescence and coarsening occur faster; and that is why we observed bigger bubble size both at the beginning and after 30 minutes. This foam is the most dry (liquid fraction of 7 %), the bubbles are compressed and the films are thinner, which facilitates the transfer of gas and also the rupture of the films (Denkov et al., 2020). However, it should be noted that all foams are within a small bubble size range.

2.2.3.4 Foam spores decontamination analysis

Then, we took the advantage of the possibility of SCI surfactant to produce foams with different liquid fractions that were stable over time to carry out cleaning tests. We carried out two different types of cleaning tests. First, we evaluated the effect of liquid fractions on the foam cleaning efficiency. Then, we evaluated the ability of the foam to clean against different levels of soil attachment by varying the drying times of the soil on the solid surface.

To evaluate the effect of the liquid fraction, the tests were carried out on stainless-steel plates soiled with a suspension of spores from the strain Bs PY79, which is known to produce hydrophilic spores. The contaminated plates were left to dry for 1 hour at 30 °C. First, we found that the log reduction of spores for the pure SCI dispersion was 0.9 ± 0.6 , which was similar to the values reported for pure water and for other surfactants already studied (Dari et al., 2023a). Thus, pure SCI dispersion had no effect on spore removal compared to water. We produced

foams with different liquid fractions (13%, 22% and 27%) using the double-syringe technique. The contaminated plates were left in a horizontal position and then the foams were placed in direct contact with them and left to act for 30 minutes. **Figure 2.2.7** shows the spore log reduction as a function of the different foam liquid fractions. The spores log reduction was 1.8 ± 0.3, 1.8 ± 0.4 and 1.9 ± 0.6 for SCI foams with a liquid fraction of 13%, 22% and 27% respectively. These results show that there is an effect of foams under static conditions on spore removal: spores were removed by the presence of the foam only, since SCI had no effect on the spore's removal. Statistical analysis indicates that no differences were observed between the foams with different liquid fractions in cleaning efficiency. Furthermore, these results are similar to those previously reported on similar surfaces soiled with the same type of spores but using a foam based on 10-HSA soap with a liquid fraction of 19% (Dari et al., 2023a). In addition, foams based on alkyl polyglucosides (Glucopon 215 UP) and xanthan gum with foams having a liquid fraction of 5 % have already been used to clean stainless-steel surfaces in horizontal position contaminated with spores of Bacillus thuringiensis (Le Toquin, 2018). In this work, the authors reported that the initial contamination was 108 and that the percentage of spores recovered by the foam was 27%, meaning that the spores log reduction was around 2.2, which is also similar to the results presented here.

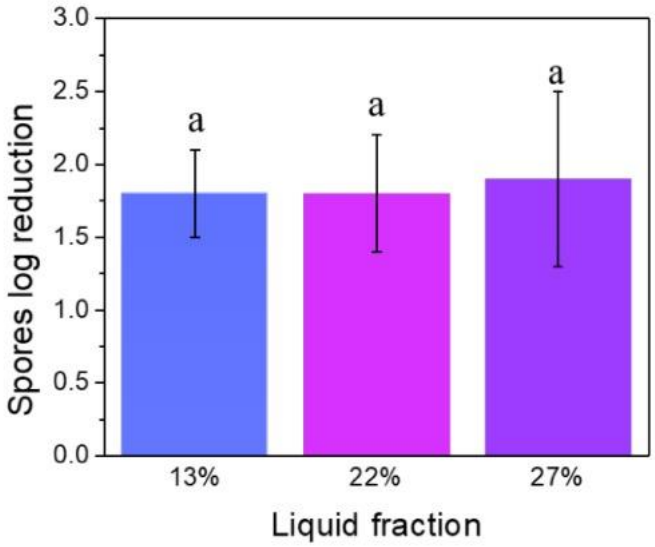

Figure 2.2.7. Spore log reduction on the stainless-steel plates after 30 min of static foam cleaning with foams with different liquid fractions (13%, 22% and 27%). The small letters, a, indicate groups of statistical differences according to Tukey's test ($p < 0.05$).

As explained in the section 2.2.3.3, in order to produce foams with other liquid fractions, we used a solution of the same surfactant (SCI) but a different concentration (1 wt. %). With this solution we are able to obtain foams with two different liquid fractions: 7% and 16%. We carried out same cleaning test with these two foams in order to further study the influence of the liquid fraction on foam cleaning efficiency. The spores log reduction was 1.1 ± 0.3 and 1.7 ± 0.4 for the foams with a liquid fraction of 7% and 16% respectively (**Figure S6**). The spore log reduction for the foam with a liquid fraction of 16% was similar to the value obtained with the other foams. However, the spores log reduction for the foam with liquid fraction of 7% was lower and similar to that of the pure solution without foaming, i.e., there was no effect of the foam in this case. We explain these results in relation to the properties of the foams. In fact, when characterizing the foams (section 2.2.3.3), the foams with liquid fractions of 13%, 22%, 27% and 16% all presented similar initial bubble sizes and also similar foam stability. In

contrast, the foam with a liquid fraction of 7% exhibited bigger bubbles than the previous ones and also a higher decay of the foam height in the first 200 seconds. In addition, in our previous work on 10-HSA foams, we showed that a foam with an initial bubble size of approximately 103 µm had the same cleaning effect as the pure surfactant solution, and with no effect of the foam (Dari et al., 2023a). We believe that in the foam with a 7% of liquid fraction, the bubbles are too big to achieve effective decontamination. For all the foams studied here, we suppose that the cleaning mechanism that took place was wiping; as this mechanism occurs with the rearrangement of the bubbles, and we previously demonstrated a change in bubble size over time (section 2.2.3.3). In addition, imbibition could not occur, as the soiled surfaces were previously dried, and therefore there was no liquid to support this mechanism. Furthermore, as mentioned in 2.2.3.3, no drainage was observed in the foams, so this mechanism was not promoted either (Schad et al., 2021).

Then, we evaluate the cleaning efficiency of the foam against different levels of fouling adhesion. For this purpose, we used the same stainless-steel plates as before, which were soiled with the same hydrophilic spores. To obtain different levels of adhesion of the spores to the surfaces, the surfaces soiled with the spore suspension were dried for different times: 0, 30 and 60 min. The foam used to carry out the test was the one with a liquid fraction of 27 %. **Figure 2.2.8** shows the spores log reduction for different drying times of the spore's suspension on the stainless-steel plates. The spores log reduction was 3.9 ± 0.3, 3.7 ± 0.5, and 1.8 ± 0.6 for 0 min, 30 min and 60 min of drying time respectively. The spores log reduction using the SCI solution (without foaming) was 0.6 ± 0.6 for 0 min of spores drying (data no shown). This confirms the cleaning effect of the foam. Comparing the cleaning efficiency with respect to drying time, it is observed that longer drying times (60 minutes) make it more difficult to remove the spores. In contrast, a shorter drying time (0 or 30 minutes) results in higher cleaning efficiency. This can be explained by the fact that the shorter the drying time, the more liquid remains on the surface and therefore an additional cleaning mechanism of foams can be promoted: the imbibition mechanism (Stubenrauch and Drenckhan, 2024). Indeed, Schad et al, in their study

showed a similar effect, where soot particles could be sucked up by the foam, thanks to being suspended in a liquid, which in their case was oil (Schad et al., 2022a). When comparing 30 minutes of drying with 0 minutes of drying, no significant differences were observed. In this case, it appears that the liquid remaining after 30 minutes of drying is already sufficient to promote the imbibition mechanism, resulting in the same outcome as with 0 minutes of drying. Note that we unequivocally demonstrated that this foam exhibited the imbibition mechanism by adding a water soluble colorant on liquid below the foam (**Figure S7**).

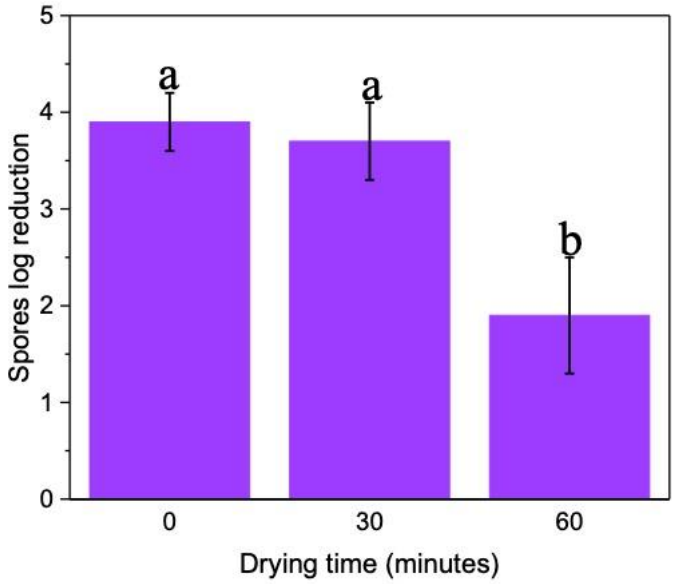

Figure 2.2.8. Spore log reduction for different drying times of the Bs PY79 spore's suspension (hydrophilic spores) on the stainless-steel plates after 30 min of static foam cleaning with the foam of 27% liquid fraction. The small letters, a, indicate groups of statistical differences according to Tukey's test ($p < 0.05$).

Finally, we studied the cleaning efficiency of this foam based on SCI by changing the properties of the spores used as model contaminant. For these experiments, we used spores from the strain Bs PY79 spsI. This strain is known to produce hydrophobic spores in contrast to the previously used strain which produces hydrophilic spores, which are more adherent to the surface. The model surfaces were soiled with the hydrophobic spore suspension and, as in the previous

experiment, different drying times of the suspension were used: 0, 30 and 60 min. The foam used to test the cleaning efficiency was the same than previously with a liquid fraction of 27%. **Figure 2.2.9** shows the spores log reduction for different drying times of the spore suspension Bs PY79 spsI on the stainless-steel plates. The spores log reduction was 3.1 ± 0,6, 1.9 ± 0.3, and 0.8 ± 0.1 for 0 min, 30 min and 60 min of drying time respectively. The spores log reduction for Bs PY79 spsI using the SCI solution (without foaming) was 1.1 ± 0.2 and 0.1 ± 0.1 for 0 min and 60 min of spores drying respectively (data no shown). These results show that the foam can also remove hydrophobic spores from solid surfaces. Furthermore, both hydrophilic and hydrophobic spores exhibit improved cleaning efficiency when suspended in liquid due to the imbibition mechanism. The cleaning efficiency at 0 min drying was similar for the hydrophilic and for the hydrophobic spores. Nevertheless, for the other drying times (0 min and 30 min) the efficiency achieved was lower with hydrophobic spores than with hydrophilic spores. This difference between hydrophobic and hydrophilic spores can be explained mainly by the formation of clusters and aggregates in hydrophobic spores (Deleplace et al., 2022). When a drop of the spore suspension is deposited on a surface, in the case of hydrophilic spores, they migrate easily to the surface of the drop; in contrast, the formation of clusters makes it more difficult for hydrophobic spores to migrate to the surface of the drop and makes it easier for them to interact with the material (Deleplace et al., 2022). In addition, in the case of hydrophilic spores, the fact that the spores migrate to the surface of the droplet means that, once the droplet is dry, a ring of spores forms on the surface which is then easier to remove than the removal of isolated or grouped spores on the surface (in the case of hydrophobic spores) (Deleplace et al., 2022). Note, that in other studies evaluating the efficiency of cleaning processes to remove spores with different hydrophilicity/hydrophobicity, they achieved a better cleaning efficiency with hydrophilic spores than with hydrophobic spores (Faille et al., 2002; Dallagi et al., 2022; Deleplace et al., 2022).

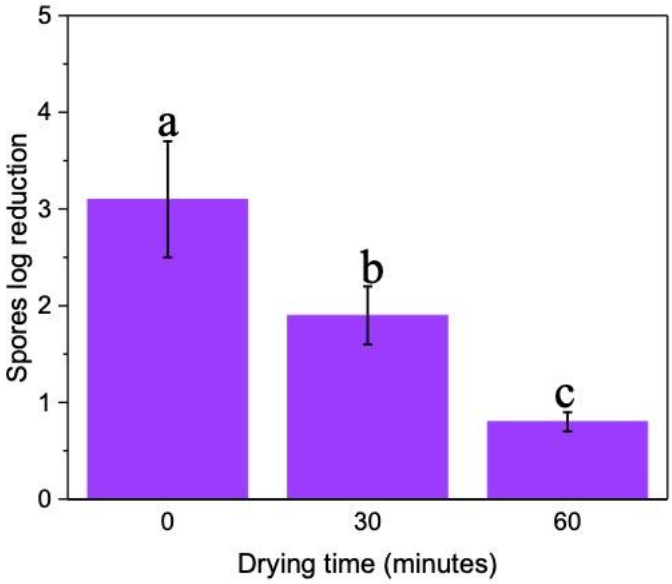

Figure 2.2.9. Spore log reduction for different drying times of the Bs PY79 spsI spore's suspension (hydrophobic spores) on the stainless-steel plates after 30 min of static foam cleaning with the foam of 27% liquid fraction. The small letters, a, indicate groups of statistical differences according to Tukey's test ($p < 0.05$).

To show the robustness of our results we decided to carried out the experiment with different levels of fouling adhesion with another foam. For this purpose, we used the foam with 16% of liquid fraction produced with the solution of 1 wt.% SCI. Experiments were carried out in the same way as for the other foam (27% liquid fraction produced with the solution of 10 wt%). We did one experiment with hydrophilic spores and another with hydrophobic spores. The results show the same tendency; that is, the efficiency of foam cleaning increases as the drying time of the foam on the surface decreases. (**Figure S8 and S9**). This confirms that when the imbibition mechanism is promoted, the cleaning efficiency is improved.

2.2.4 Conclusions

In this study, we conducted different experiments to elucidate the role of foams in the cleaning of solid surfaces contaminated with spores. First, we characterized the physical-chemistry properties of SCI, the surfactant used to produce the foams. SCI below the Krafft temperature

formed fibrillar crystals, and above the Krafft temperature negatively charged spherical micelles.

We demonstrate that SCI foams are capable of removing both hydrophilic and hydrophobic spores when these are strongly attached to solid surfaces, likely through the wiping mechanism. The cleaning efficiency is higher for hydrophilic spores, consistent with findings from other studies using different cleaning methods (Faille et al., 2002; Dallagi et al., 2022; Deleplace et al., 2022). Under these conditions, the liquid fraction does not affect cleaning efficiency. The most critical property of the foam appears to be bubble size, with smaller bubbles (between 20 and 50 µm) achieving higher cleaning efficiency. Additionally, we show that cleaning efficiency can be improved if the spores are suspended in a liquid and less attached to the surface, promoting the imbibition mechanism of the foam. Under these conditions, similar cleaning efficiency can be achieved for both hydrophilic and hydrophobic spores.

Future studies could investigate cleaning efficiency on surfaces with varying roughness and hydrophobicity compared to stainless steel, such as glass or polypropylene (Deleplace et al., 2022). Additionally, further research should examine the efficacy of cleaning different types of microbial contamination, including biofilms.

This study focused on static foam cleaning on horizontal surfaces. Future research could explore the effectiveness of cleaning on vertical surfaces, where foam behavior might differ, potentially impacting cleaning efficiency (Le Toquin, 2018). In our experiments, we used foams without drainage to eliminate this variable. However, other studies have demonstrated that drainage affects cleaning performance. Therefore, future experiments could include foams with varying drainage rates to study the impact of drained liquid on the removal of spores and biofilms.

2.2.5 References:

Ananthapadmanabhan, K. P. (2019). Amino-Acid Surfactants in Personal Cleansing (Review). Tenside Surfactants Detergents 56, 378–386. doi: 10.3139/113.110641

Burnett, C. L., Heldreth, B., Bergfeld, W. F., Belsito, D. V., Hill, R. A., Klaassen, C. D., et al. (2017). Amended Safety Assessment of Isethionate Salts as Used in Cosmetics. Int J Toxicol 36, 5S-16S. doi: 10.1177/1091581816685552

Dallagi, H., Faille, C., Bouvier, L., Deleplace, M., Dubois, T., Aloui, F., et al. (2022). Wet foam flow: A suitable method for improving surface hygiene in the food industry. Journal of Food Engineering 322, 110976. doi: 10.1016/j.jfoodeng.2022.110976

Dari, C., Cousin, F., Le Coeur, C., Dubois, T., Benezech, T., Saint-Jalmes, A., et al. (2023a). Ultrastable and Responsive Foams Based on 10-Hydroxystearic Acid Soap for Spore Decontamination. Molecules 28, 4295. doi: 10.3390/molecules28114295

Dari, C., Dallagi, H., Faille, C., Dubois, T., Lemy, C., Deleplace, M., et al. (2023b). Decontamination of Spores on Model Stainless-Steel Surface by Using Foams Based on Alkyl Polyglucosides. Molecules 28, 936. doi: 10.3390/molecules28030936

DeFlorio, W., Liu, S., White, A. R., Taylor, T. M., Cisneros-Zevallos, L., Min, Y., et al. (2021). Recent developments in antimicrobial and antifouling coatings to reduce or prevent contamination and cross-contamination of food contact surfaces by bacteria. Comp Rev Food Sci Food Safe 20, 3093–3134. doi: 10.1111/1541-4337.12750

Deleplace, M., Dallagi, H., Dubois, T., Richard, E., Ipatova, A., Bénézech, T., et al. (2022). Structure of deposits formed by drying of droplets contaminated with Bacillus spores determines their resistance to rinsing and cleaning. Journal of Food Engineering 318, 110873. doi: 10.1016/j.jfoodeng.2021.110873

Denkov, N., Tcholakova, S., and Politova-Brinkova, N. (2020). Physicochemical control of foam properties. Current Opinion in Colloid & Interface Science 50, 101376. doi: 10.1016/j.cocis.2020.08.001

Drakontis, C. E. (2020). Biosurfactants: Formulations, properties, and applications. Interface Science, 14.

Dubois, T., Krzewinski, F., Yamakawa, N., Lemy, C., Hamiot, A., Brunet, L., et al. (2020). The sps Genes Encode an Original Legionaminic Acid Pathway Required for Crust Assembly in Bacillus subtilis. mBio 11, e01153-20. doi: 10.1128/mBio.01153-20

EHEDG (2021). Doc. 52 Basic Principles of Cleaning and Disinfection in Food Manufacturing.

Faille, C., Jullien, C., Fontaine, F., Bellon-Fontaine, M.-N., Slomianny, C., and Benezech, T. (2002). Adhesion of Bacillus spores and Escherichia coli cells to inert surfaces: role of surface hydrophobicity. Can. J. Microbiol. 48, 728–738. doi: 10.1139/w02-063

Faille, C., Lemy, C., Allion-Maurer, A., and Zoueshtiagh, F. (2019). Evaluation of the hydrophobic properties of latex microspheres and Bacillus spores. Influence of the particle size on the data obtained by the MATH method (microbial adhesion to hydrocarbons). Colloids and Surfaces B: Biointerfaces 182, 110398. doi: 10.1016/j.colsurfb.2019.110398

Gaillard, T., Roché, M., Honorez, C., Jumeau, M., Balan, A., Jedrzejczyk, C., et al. (2017). Controlled foam generation using cyclic diphasic flows through a constriction. International Journal of Multiphase Flow 96, 173–187. doi: 10.1016/j.ijmultiphaseflow.2017.02.009

Jeraal, M. I., Roberts, K. J., McRobbie, I., and Harbottle, D. (2018). Process-Focused Synthesis, Crystallization, and Physicochemical Characterization of Sodium Lauroyl Isethionate. ACS Sustainable Chem. Eng. 6, 2667–2675. doi: 10.1021/acssuschemeng.7b04237

Jones, L. D., Mana, T. S. C., Cadnum, J. L., Jencson, A. L., Silva, S. Y., Wilson, B. M., et al. (2020). Effectiveness of foam disinfectants in reducing sink-drain gram-negative bacterial colonization. Infection Control & Hospital Epidemiology 41, 280–285. doi: 10.1017/ice.2019.325

Le Toquin, E. (2018). Mode d'action biocide de nouveaux procédés de décontamination sur deux formes de résistances bactériennes. Normandie. Available at: https://theses.fr/2018NORMR103 (Accessed April 12, 2024).

Lücking, G., Stoeckel, M., Atamer, Z., Hinrichs, J., and Ehling-Schulz, M. (2013). Characterization of aerobic spore-forming bacteria associated with industrial dairy processing environments and product spoilage. International Journal of Food Microbiology 166, 270–279. doi: 10.1016/j.ijfoodmicro.2013.07.004

Midelet, G., Brauge, T., and Faille, C. (2024). "Contamination croisée des aliments par des surfaces contaminées," in Contrôle et Prévention des Risques Biologiques Associés à la Contamination des Aliments : Transformation, Distribution et Utilisation par le Consommateur, (ISTE Editions). Available at: https://hal.univ-lille.fr/hal-04456514 (Accessed February 14, 2024).

Petter, P. J. (1984). Fatty acid sulphoalkyl amides and esters as cosmetic surfactants. International Journal of Cosmetic Science 6, 249–260. doi: 10.1111/j.1467-2494.1984.tb00382.x

Schad, T., Preisig, N., Blunk, D., Piening, H., Drenckhan, W., and Stubenrauch, C. (2021). Less is more: Unstable foams clean better than stable foams. Journal of Colloid and Interface Science 590, 311–320. doi: 10.1016/j.jcis.2021.01.048

Schad, T., Preisig, N., Drenckhan, W., and Stubenrauch, C. (2022a). Foam-based cleaning of surfaces contaminated with mixtures of oil and soot. Journal of Surfactants and Detergents 25, 377–385. doi: 10.1002/jsde.12580

Schad, T., Preisig, N., Piening, H., and Stubenrauch, C. (2022b). Innovative foam-based cleaning concepts for historical objects. Tenside Surfactants Detergents 59, 451–459. doi: 10.1515/tsd-2022-2478

Snyder, A. B., Martin, N., and Wiedmann, M. (2024). Microbial food spoilage: impact, causative agents and control strategies. Nat Rev Microbiol, 1–15. doi: 10.1038/s41579-024-01037-x

Stubenrauch, C., and Drenckhan, W. (2024). Cleaning solid surfaces with liquid interfaces and foams: from theory to applications. Current Opinion in Colloid & Interface Science, 101818. doi: 10.1016/j.cocis.2024.101818

WHO (2022). Food Safety. Available at: https://www.who.int/news-room/fact-sheets/detail/food-safety

Zhang, L., Mikhailovskaya, A., Yazhgur, P., Muller, F., Cousin, F., Langevin, D., et al. (2015). Precipitating Sodium Dodecyl Sulfate to Create Ultrastable and Stimulable Foams. Angew. Chem. 127, 9669–9672. doi: 10.1002/ange.201503236

Supporting Information: Static foam cleaning with foams based on Sodium Cocoyl Isethionate for the removal of spores from solid surfaces

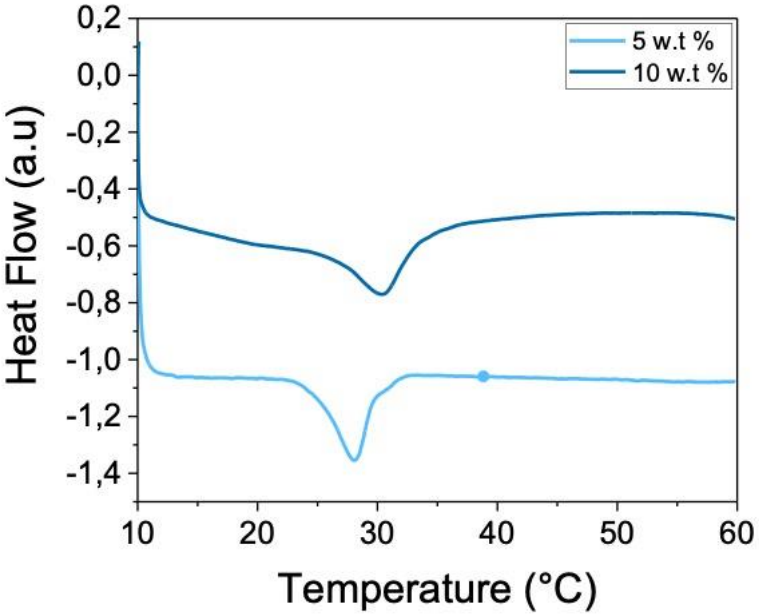

Figure S1 : Heat flux curves as a function of SCI concentration. After heating, a single endothermic peak, typical of a melting process, was observed.

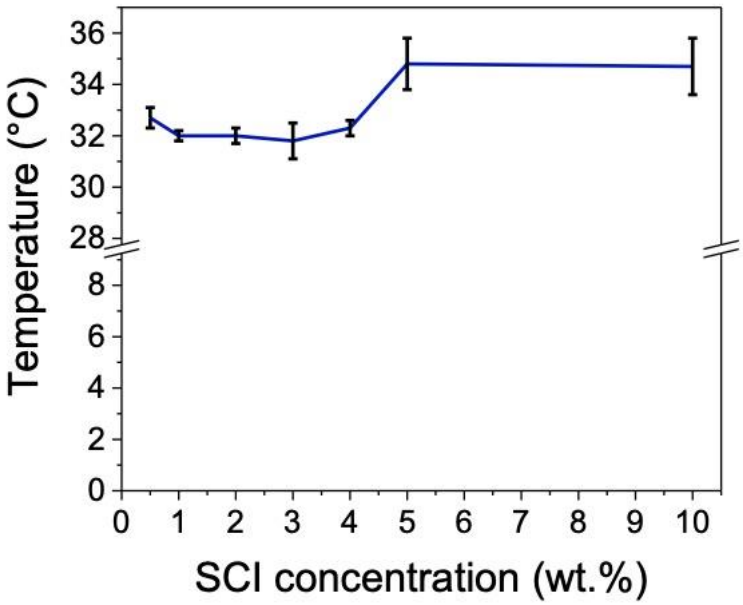

Figure S2 : The Kraft temperatures of the aqueous solutions of SCI as a function of the concentration, determined by optical microscopy. The temperature corresponds to the point at which the crystals began to melt.

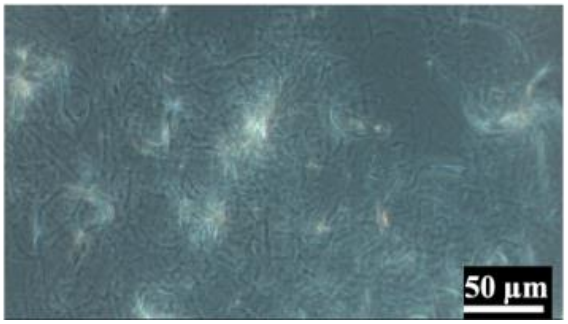

Figure S3 : Phase contrast microscopy image of SCI suspension at 1wt.% at room temperature.

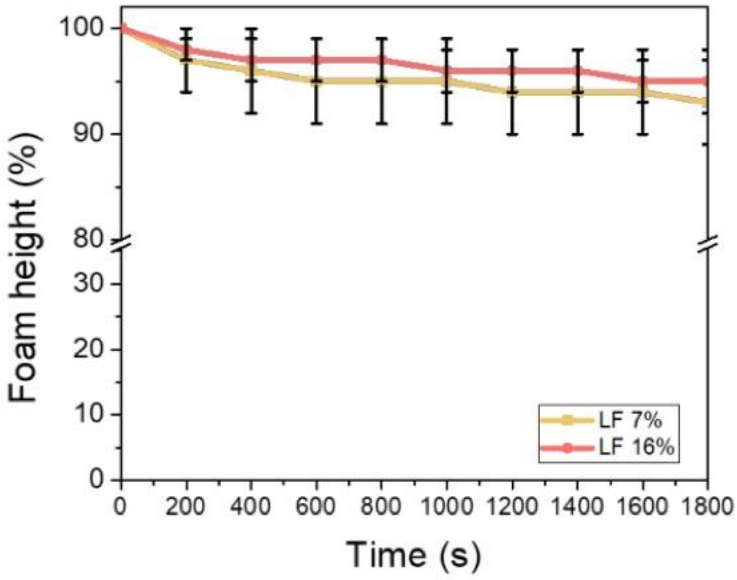

Figure S4 : Evolution of the foam height for the foams with a liquid fraction of 7%, and 16% produced with SCI at 1 wt.%.

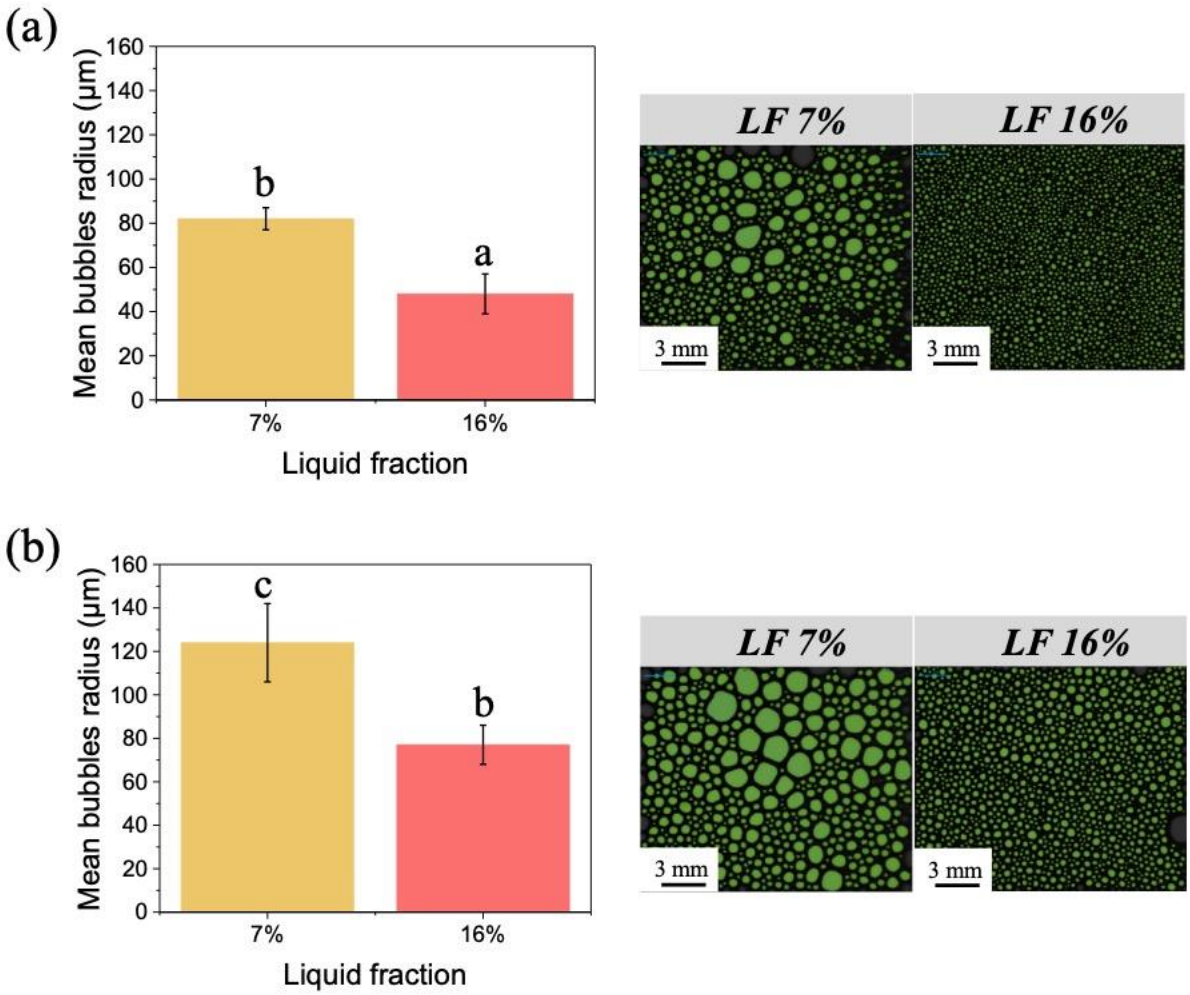

Figure S5 : Mean bubbles area of foams with different liquid fractions (7% and 16%) and their bubbles corresponding pictures: (a) at t=0 (b) at t=30 min. The small letters a–b indicate groups of statistical differences according to Tukey's test ($p < 0.05$).

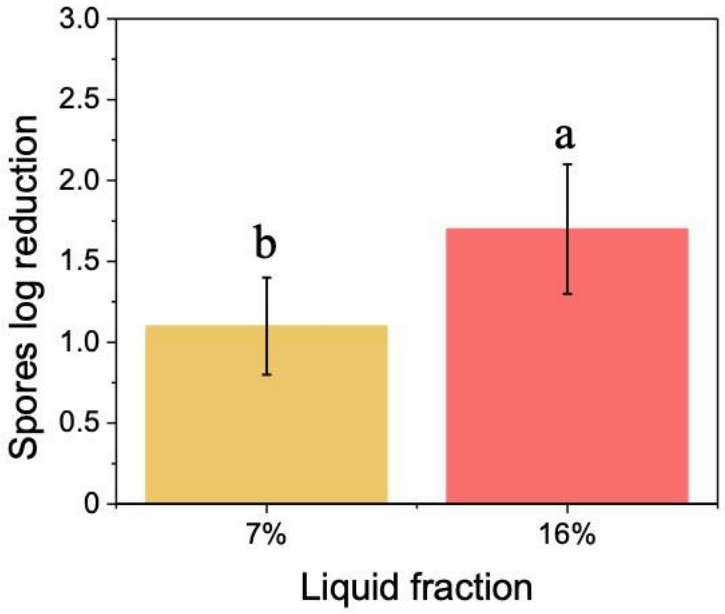

Figure S6: Spore log reduction on the stainless-steel plates after 30 min of static foam cleaning with foams with different liquid fractions (7% and 16%). The small letters, a, indicate groups of statistical differences according to Tukey's test ($p < 0.05$).

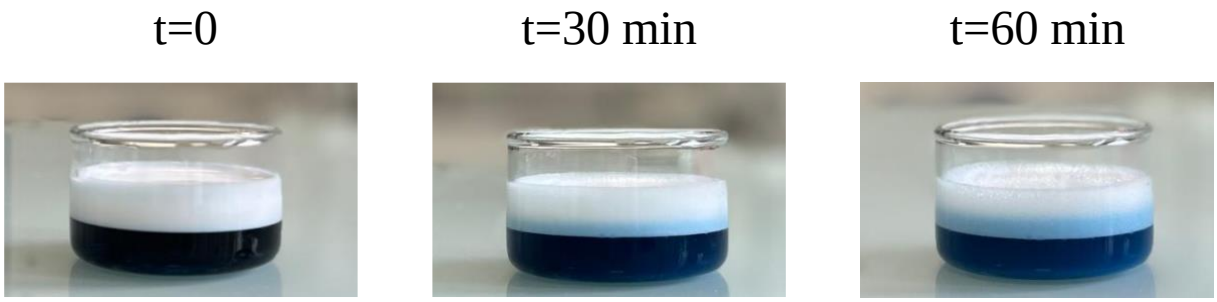

Figure S7: Photographs of the imbibition test at different times. The aqueous phase containing a blue dye is entering inside the foam with time showing the imbibition process of the foam. The foam corresponds to the one of 27% of liquid fraction.

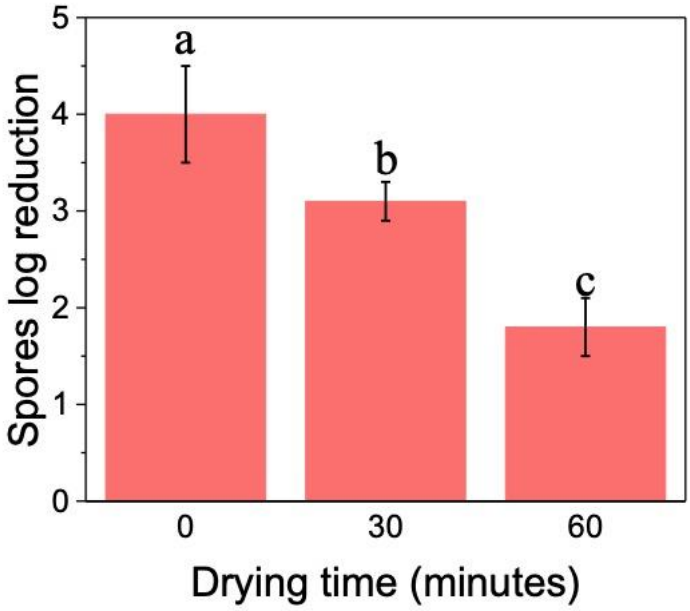

Figure S8: Spore log reduction for different drying times of the *Bs* PY79 spore's suspension (hydrophilic spores) on the stainless-steel plates after 30 min of static foam cleaning with the foam of 16% liquid fraction. The small letters, a, indicate groups of statistical differences according to Tukey's test ($p < 0.05$).

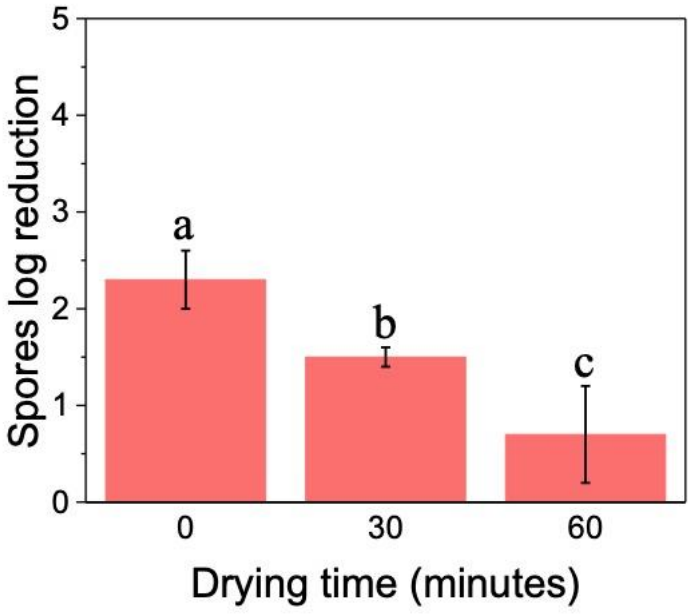

Figure S9: Spore log reduction for different drying times of the Bs PY79 spsI spore's suspension (hydrophobic spores) on the stainless-steel plates after 30 min of static foam cleaning with the foam of 16% liquid fraction. The small letters, a, indicate groups of statistical differences according to Tukey's test ($p < 0.05$).

Chapter 3: Foam cleaning in dynamic condition

Introduction to chapter 3

As detailed in the first chapter of the thesis, which covers the literature review, CIP is the most commonly used method for cleaning closed surfaces in the food industry. However, CIP consumes significant amounts of water, energy, and chemicals, leading to negative environmental impacts. Consequently, research is being conducted to explore alternative methods that are more environmentally friendly while maintaining effective cleaning efficiency. Recent studies have shown that foam flow can efficiently remove bacterial spores and biofilms from pipes. Furthermore, in one of these studies, through a life cycle analysis, it was shown that foam flow allows the reduction of several environmental impacts. However, in these studies, the foam was generated using SDS, a surfactant typically derived from petroleum. Additionally, the concentration of SDS used was below its critical micellar concentration (CMC). Thus, the quantity of surfactants was not enough to stabilize the foam during the foam flow. That is why the second objective of this thesis was to investigate the cleaning efficacy of foam flow formulated with SDS, but also two different APGs, commercially available bio-based surfactants at their respective CMCs. We evaluated and compared their efficiency in removing hydrophilic spores from stainless steel pipes. We demonstrated the same cleaning efficiency between APGS based foams and SDS based foams for short cleaning times (1 min). However, at longer cleaning times (30 min) the efficiency of the SDS-based foam improved. The APG-based foams were more stable, which could be an advantage for cleaning more complex installations. Furthermore, through a life cycle analysis, we demonstrated how the use of APGs allows the reduction of several environmental impacts with respect to the use of SDS.

In addition, with the aim of further improving environmental printing, in this work we demonstrate how, once the foam has been destroyed, the surfactant solution contaminated with spores can be filtered to remove spores below the limits of detection. This filtered solution can then be reused to generate new foam flows. These results were gathered in one publication and were published in Molecules journal.

3.1 Decontamination of Spores on Model Stainless-Steel Surface by Using Foams Based on Alkyl Polyglucosides

Carolina Dari, Heni Dallagi, Christine Faille, Thomas Dubois, Christelle Lemy, Maureen Deleplace, Marwan Abdallah, Cosmin Gruescu, Julie Beaucé, Thierry Benezech and Anne-Laure Fameau *

University Lille, CNRS, INRAE, Centrale Lille, UMET, 369 Rue Jules Guesde, F-59000 Lille, France;

* **Correspondence:** anne-laure.fameau@inrae.fr

Abstract: In the food industry, the surfaces of processing equipment are considered to be major factors in the risk of food contamination. The cleaning process of solid surfaces is essential, but it requires a significant amount of water and chemicals. Herein, we report the use of foam flows based on alkyl polyglucosides (APGs) to remove spores of Bacillus subtilis on stainless-steel sur-faces as the model-contaminated surface. Sodium dodecyl sulfate (SDS) was also studied as an anionic surfactant. Foams were characterized during flows by measuring the foam stability and the bubble size. The efficiency of spores' removal was assessed by enumerations. We showed that foams based on APGs could remove efficiently the spores from the surfaces, but slightly less than foams based on SDS due to an effect of SDS itself on spores removal. The destabilization of the foams at the end of the process and the recovery of surfactant solutions were also evaluated by using filtration. Following a life cycle assessment (LCA) approach, we evaluated the impact of the foam flow on the global environmental footprint of the process. We showed significant environ-mental impact benefits with a reduction in water and energy consumption for foam cleaning. APGs are a good choice as surfactants as they decrease further the environmental impacts.

Keywords: foam; spore; cleaning; surface hygiene; life cycle analysis

3.1.1 Introduction

Reducing food waste is one of the prominent goals set by the United Nations to achieve a more sustainable world by 2030. Indeed, food waste is responsible for un-necessary greenhouse emissions and waste of resources [1]. Therefore, limiting food waste is of major interest to limit climate change and ensure sustainability. An important contributor to food waste is microbial spoilage. Nearly one-third of all food produced worldwide is estimated to be lost mostly due to microbial spoilage after postharvest [1]. In the food industry, it is well known that surfaces in processing equipment can be con-taminated by microorganisms despite cleaning and disinfection procedures [2]. Once present, a large portion of these bacteria persists on surfaces depending on the envi-ronmental conditions and often produces biofilms. Thus, food contact surfaces in pro-cessing equipment are considered a major risk factor for food cross-contamination. The formation of bacterial biofilms on food-processing equipment and food-contact surfaces can act as a persistent source of contamination of food, threatening the safety of food products, which can result in foodborne diseases, financial losses, and a loss of credibility for the company [3]. In addition, bacteria spores are of major concern to the food industry because a number of species are pathogenic, whereas others are associated with spoilage. Spores also have the capacity to adhere to materials of importance in the processing industries, such as stainless steel widely used in food equipment manufacturing [4]. The cleaning phase is the most important stage for minimizing microbial colonization and removing attached micro-organisms. For example, the efficiency of cleaning and sanitation of milk contact surfaces are widely influenced by many factors such as the nature of contamination, the mi-crotopography of surfaces, the design of the equipment, and the cleaning conditions [5]. Cleaning-in-place (CIP) is the ubiquitous process used to maintain the hygienic state of the processing lines by cleaning their interior surfaces (pipelines and equipment) without dismantling the facilities. In the CIP process, cleaning solutions used include various types of detergents. CIP usually involves the circulation of cleaning solutions at high temper-atures through the plant under conditions of increased turbulence and flow speed. Therefore, the

effectiveness of cleaning is preconditioned by four main factors: chemical agent, mechanical power, temperature, and time of the procedure, which together form the Sinner circle [6]. However, the environmental impact of the CIP process is significant, as frequent cleaning is required and water is used intensively along with chemicals. For example, in the dairy industry, most of the water consumption is directly linked to a CIP between 0.6 and 6 L of water per liter of treated milk [2]. In addition, CIP generates large quantities of wastewater, with an additional economic burden on the industry, and an environmental burden on the community [7]. Hence, the food industry is currently looking for new cleaning processes to decrease the environmental impact.

Almost twenty years ago, foam circulation through pipes was described in the lit-erature to be very efficient for radioactive surface decontamination of solid surfaces, because the amounts of chemicals involved and the volume of radioactive waste produced were much lower than with other processes [8]. Thus, one strategy described recently in the literature is the use of foam flows for cleaning in the food industry [9–11]. Due to foam wall friction and specific foam rheology properties in terms of viscous stress, foam bubbles could remove efficiently spores and biofilms [12–14]. In addition, foams enable the drastic reduction in the amount of water used because foams are mainly composed of air bubbles [15]. Therefore, the use of foams could have a direct positive impact on the environmental footprint of the cleaning process [9–11]. These first studies were based on the use of sodium dodecyl sulfate (SDS) as a surfactant at a concentration well below the CMC, leading to unstable foam [9–11]. The aim of this study was to show that a decrease in the envi-ronmental footprint of foam flow cleaning was possible through the use of alkyl poly-glucosides surfactants (APGs). Indeed, APGs are biosurfactants produced from vegetable oils and starch (plant-derived feedstock chemicals) suitable for cleaning applications in food industries, but also already widely used for various applications in personal care products. Moreover, APG foams have been shown to be very efficient for spores de-contamination under static conditions on vertical surfaces [16]. We studied two different APGs known to be good cleansing and foaming agents: decyl glucoside (DG) and

lauryl glucoside (LG) [17,18]. Foams were characterized in terms of foamability, liquid fraction, and bubbles size. The efficiency of spores' removal by foam flows was studied on stainless-steel surfaces and assessed by enumeration. The impact of the foam flow process on the global environmental footprint was determined by the life cycle assessment (LCA) approach, and we compared foams based on APGs with foam based on SDS. We also evaluated the destabilization of the foams by ultrasound and the removal of spores and the recovery of clean surfactant solution in order to regenerate the foam at the end of the process and to limit the waste water.

3.1.2 Results and Discussion

3.1.2.1 Model Surfaces, Spores, and Surfactant Solutions Characterization

In this study, we used stainless-steel plates as model surfaces and spores from Bacillus subtilis as the model contaminant to study the cleaning process by the foam flow. To mimic the surfaces encountered in the dairy industry, we followed a protocol described and shown in section 3.1.2 to prepare the surfaces with different steps of soiling and cleaning [9]. The water contact angle was 45.1 ± 1.5, showing that the surfaces were hydrophilic. We also determined the hydrophobic/hydrophilic characteristic of the spores used by the MATH procedure. The aqueous affinity for the spores used in this study was higher than 90%, so they were considered as highly hydrophilic as it was also shown before [19]. To produce the foam, we used three different surfactants. Two alkyl poly-glucosides: decyl glucoside (DG) and lauryl glucoside (LG), were used to study the effect of the alkyl chain length on the foam flow cleaning efficiency. The SDS was used as a reference as it was the surfactant used for the first study on spores' decontamination by the foam flow [9]. The CMC of the three surfactants was determined in order to produce foam at a concentration close to the CMC. The CMC was estimated at 0.03 wt.% for DG, 0.03 wt.% for LG, and 0.23 wt.% SDS. These values are in accordance with the literature [17,20].

3.1.2.2 Effect of Surfactants on Spore Detachment under Static Conditions

Before studying the effect of foam flow cleaning, it was necessary first to study the effect of each surfactant solution on spore detachment under static conditions, that is to say, the chemical action. In this aim, the stainless-steel plates contaminated by the spores were directly dipped in the surfactant solution or in osmosis water for 30 min. Then, the re-maining spores on the plates were enumerated (**Figure 3.1.1**.). The spore log reduction was around 1.13 ± 0.14 for water, showing that dipping the contaminated plates in water results in more than one log removal of spores. This result suggested that some of the hydrophilic spores deposited on the surface of the plates were not strongly adherent [4]. For the two APGs, the spores log reduction was similar with a spores log reduction of 1.33 ± 0.01 and 1.37 ± 0.05 for DG and LG, respectively. These values were slightly higher than those for water alone, showing a slight effect on APGs on the spores' removal under static conditions. For SDS, the highest value was obtained, with a spores log reduction of 1.57 ± 0.10. Thus, SDS had the strongest effect on spores' removal under static conditions. We suppose that a chemical action of SDS is possible due to its anionic nature in comparison to APGs, which are non-ionic surfactants. In the literature, SDS is known to denature pro-teins even at room temperature and at sub-CMC concentrations [21]. Therefore, it is possible that in our experimental conditions, SDS could denature the spore surface pro-teins, thus facilitating the spores' detachment from surfaces.

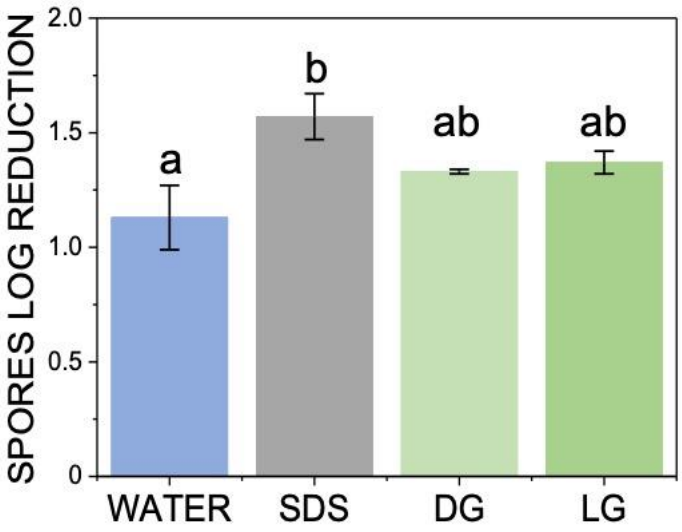

Figure 3.1.1. Spores log reduction on the plate under static dipping conditions as a function of the surfactant in comparison to water. The small letters a–b indicate groups of statistical differences according to Tukey's test ($p < 0.05$).

3.1.2.3 Effect of Foams on the Detachment of Spores

The effect of foam flow cleaning on spores' removal from the stainless-steel plate was investigated by introducing the plate in a duct. Then, the effect of the foam flow was quantified by measuring the spore log reduction after one minute and 30 min of foam flow (**Figure 3.1.2**). After one minute of foam flow, the spore log reduction was around 0.41 ± 0.09 for the water, due to the hydrophilicity of the spores. The spore log reduction was 1.92 ± 0.16, 2.15 ± 0.15, and 2.24 ± 0.15, respectively, for DG, LG, and SDS after 1 min of foam flow. These values were much higher than for water alone, showing that foam flows efficiently removed spores from the plate. The foam flow resulted in a very quick de-tachment of the adhering spores, due to a mechanical effect. In addition, there was no effect of the surfactant used. After 30 min of water flow, the spores log reduction increased to 0.95 ± 0.09, confirming the effect of water on the spores' removal as already shown under static conditions after 30 min of dipping in water. The two APGs had similar values of 2.11 ± 0.09 and 2.36 ± 0.06, for DG and LG, respectively,

after 30 min. These values show that for APGs, the foam flow cleaning was efficient in the first minute, and it could not be improved by increasing the time of cleaning. For SDS, the spore log reduction slightly increased with the increase in time and reached 2.87 ± 0.17 after 30 min of foam flow. Thus, after 30 min of cleaning, the foam based on SDS was the most efficient to spores removal. Based on the effect shown of SDS on spore removal under static conditions, we suppose that the effect of the SDS foam flow could be a combination of foam flow and/or SDS chemical action on spore surface proteins. It is important to point out also that in our previous studies, the foams based on SDS always had a stronger effect on the spores' removal than the surfactant solution whatever the foam properties in terms of bubbles size and foam flow velocity [9–11].

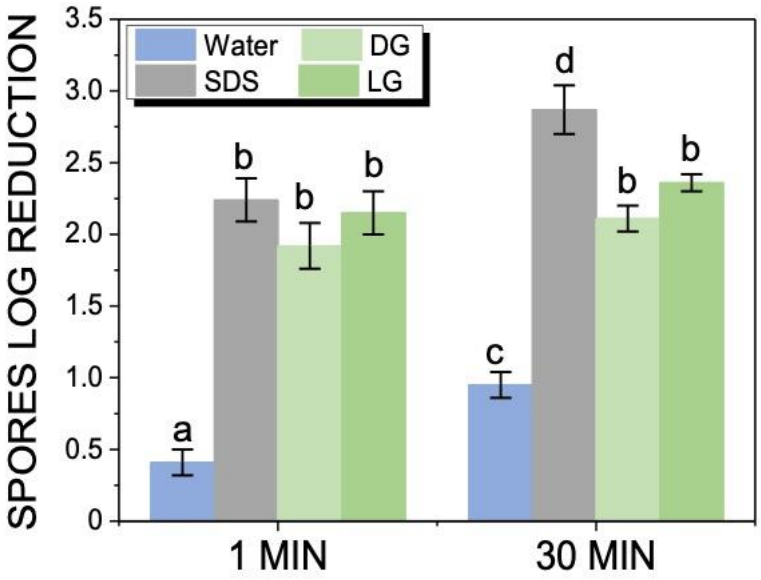

Figure 3.1.2. Spores log reduction on the plate in dynamic condition during foam flow cleaning after 1 and 30 min of foam flow as a function of the surfactant in comparison to water. The small let-ters a–d indicate groups of statistical differences according to Tukey's test ($p < 0.05$) between the water and the surfactants for 1 min of foam flow cleaning and for 30 min of foam flow cleaning.

The effect of foam flow cleaning on spore removal was also followed by epifluo-rescence microscopy before and after foam flow cleaning using the three surfactants. For all the foams, an efficient removal of spores was observed just after one minute of flow (**Figure 3.1.3**.). No differences could be observed between the three surfactant foams, confirming the results of spore log reduction quantification. Moreover, in all cases, there was no visible difference between the pictures after 1 or 30 min of foam flow.

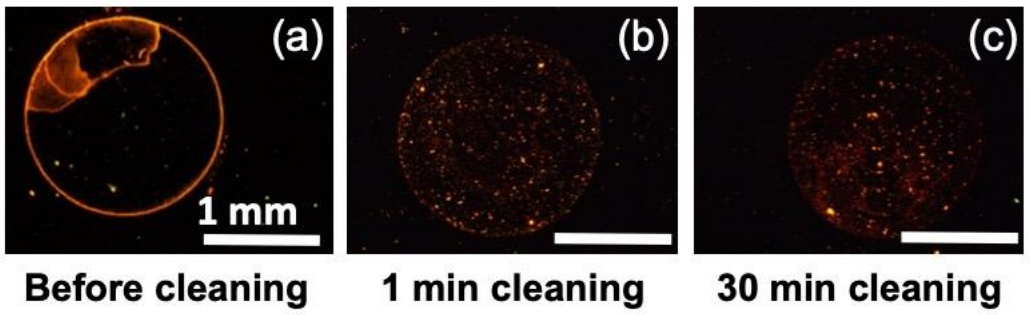

Figure 3.1.3. Epifluorescence microscopy pictures of a stainless-steel plate contaminated by spores and stained with acridine orange: (a) before cleaning by foam flow, (b) after one minute of foam flow cleaning based on DG, and (c) after 30 min of foam flow cleaning based on DG. The scale bar represents 1 mm for all the pictures.

3.1.2.4 Foam Characterizations before and After Flowing Inside the Duct

The characterization of foams during the flow inside the duct was very difficult to achieve in situ. That is why the foams based on SDS, DG, and LG were characterized in terms of foam stability under vertical conditions by measuring the drainage, the foam height, the mean bubbles area, and the bubbles size before and after the foam passed through the cleaning duct. Thus, we compared the foam before and after passing through the duct to obtain information on what happened to the foam during the flow in terms of foam stability (change in bubbles size and liquid fraction). It was important to determine if the foam properties changed during the flow and if it could explain the differences between the surfactants. The foams were sampled and immediately analyzed in vertical conditions using a glass column. The evolution of the

normalized foam height was fol-lowed as a function of time to obtain insight into the foam stability (**Figure 3.1.4**.). For the three surfactants before the foam flowed through the duct, a fast decrease in the foam height until 200–400 s was observed with around a decrease of 10% of the initial foam height (**Figure 3.1.4.a**). Then, the foam height was stabilized around 1800 s and was 86.9% ± 3.1, 93.6% ± 2.8, and 84.0% ± 2.2 for SDS, DG, and LG, respectively. After the foam flowed through the duct, SDS and LG showed the same evolution for the normalized foam height (**Figure 3.1.4.b**). However, the foam based on DG was slightly more stable. The foam height was stabilized around 1800 s and was 90.3% ± 3.3, 96.1% ± 0.5, and 88.8% ± 2.2 for SDS, DG, and LG, respectively. Before and after the duct, a relatively similar evolution was observed for the normalized foam height for the three surfactants. Before and after the duct, a very fast drainage was also observed until 200–300 s, for all the surfactants. The liquid fraction was measured directly for the three surfactants by sampling the foam before and after the duct, and in all cases, the three foams were considered wet foams with a liquid fraction above 5%.

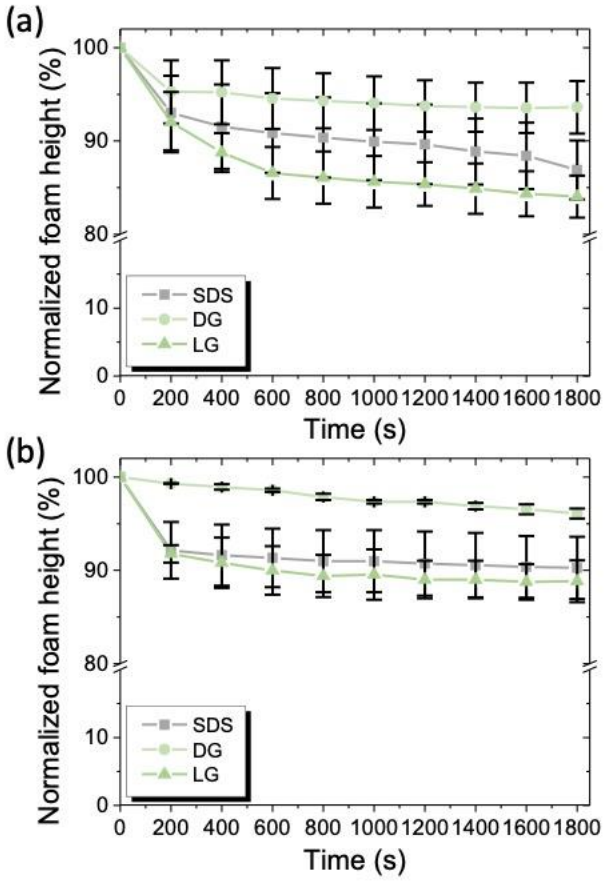

Figure 3.1.4. Evolution of the foam height for SDS, DG, and LG: (a) before the foam passed through the duct containing the plate contaminated with spores and (b) after the foam passed through the duct.

We compared the mean bubble area after 600 s for the three surfactants when the decrease in the foam height was almost stopped (**Figure 3.1.5**.). Before the duct, the mean bubble area was 0.19 mm2 ± 0.08, 0.06 mm2 ± 0.01, and 0.08 mm2 ± 0.01 for SDS, DG, and LG, respectively (**Figure 3.1.5.a**). As shown also in the bubble pictures in **Figure 3.1.5.a**, the bubble size was bigger for SDS than for DG and LG, which both showed similar bubble sizes. After the duct, the mean bubble area was 0.42 mm2 ± 0.07, 0.12 mm2 ± 0.04, and 0.10 mm2 ± 0.01 for SDS, DG, and LG, respectively (**Figure 3.1.5**.**b**). The bubbles size was bigger for SDS than for DG and LG, which both showed similar bubble sizes (Figure 5b). The statistical analysis showed that there was a difference in the mean bubble area before and after the foams passed through the duct for the SDS but not for the APGs. Foams based on APGs were much more stable during the flow than foams with SDS. Based on previous results described in the literature on the foam wall friction, for the three surfactants, the foams were similar in terms of foam-wall friction as they were wet foams with quite similar air volume fraction. Moreover, the three surfactants used are known to produce mobile surfaces at the air/water surface [12–14]. Therefore, our results show that the efficiency of the SDS foams in spore removal from the flow in comparison to APGs foams came from the chemical action of SDS as demonstrated under static conditions (Section 2.2).

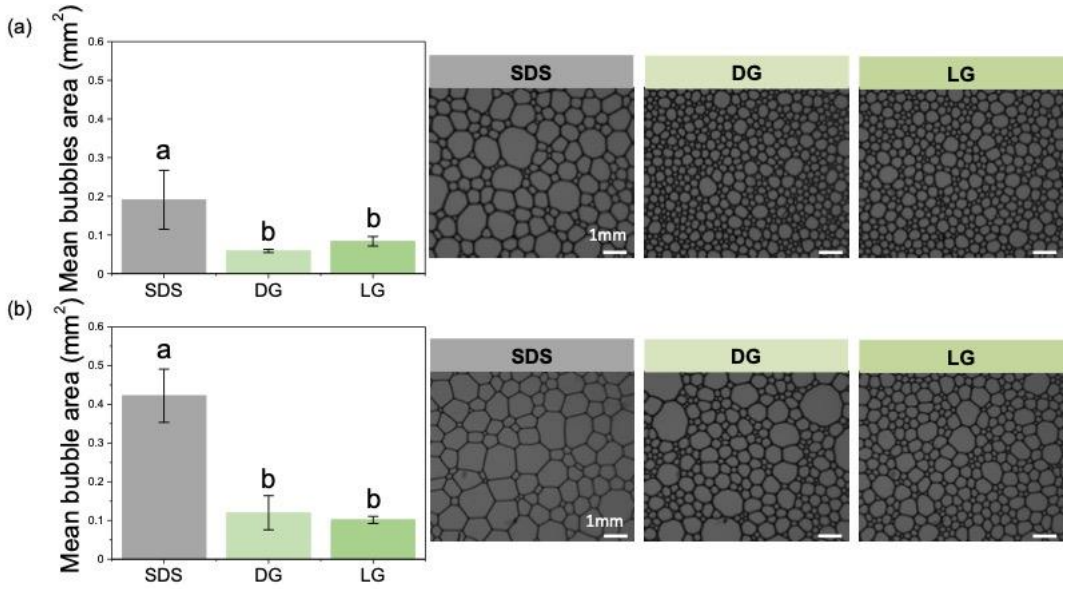

Figure 3.1.5. Mean bubbles area of the foams produced with SDS, DG, and LG with the correspond-ing microscopic pictures: (a) before the foam passed through the duct containing the plate con-taminated with spores and (b) after the foam passed through the duct. The scale bar represents 1 mm for all the foam pictures. The small letters a–b indicate groups of statistical differences ac-cording to Tukey's test ($p < 0.05$).

3.1.2.5 Foam Destruction and Recycling of Surfactant Solutions by Filtration

As already described for foams circulating through pipes for radioactive decon-tamination, the foam destruction at the end of the cleaning process and its regeneration is crucial [8]. Indeed, the aim of our foam cleaning process for the food industry is to generate foam, which then circulates through the ducts until the level of suitable cleaning is achieved. In order to efficiently destroy the foam on demand at the end of the process, the ultrasound technique seemed to be well adapted [22]. The ultrasound could be used at the end of the ducts as already described in the nuclear decontamination [8]. To regenerate the foam based on the same surfactant solution, perfect control of the decontamination of spores present inside the water was required. For this step, a filtration technique was used to illustrate how the spores could be removed. Filtration is widely used in the food in-dustry and for the treatment of effluents and wastewater [23]. It has competitive ad-vantages over other separation processes because it is easy to implement, flexible, compact, and automatic [24]. To determine the efficiency of the filtration step to

decon-taminate the spores from the surfactant solution, we quantified the number of spores present before and after the filtration. The results showed that for all surfactants solutions, the spore removal by filtration was very efficient as the number of spores after filtration was zero (below detection limit). Then, we compared the foaming properties of the surfactant solution before and after filtration by producing again the foam (**Figure 3.1.6**). As shown in **Figure 3.1.6**, the foam volume, stability, and appearance were the same for the three surfactants before and after filtration, showing that the filtration step was a good method to recycle the foaming surfactant solution without altering surfactant concentration and foaming ability. Thus, it would be possible after recovering the foam to destroy it by ultrasound, and the spores present inside the surfactants solution could be efficiently removed by filtration. The foam could then be regenerated based on the same surfactant solution during many filtration cycles (at least 10 cycles). In principle, the surfactant solution could be recyclable many times until the concentration of the surfactant solution would be too low due to the loss of surfactant during the cleaning and filtration steps.

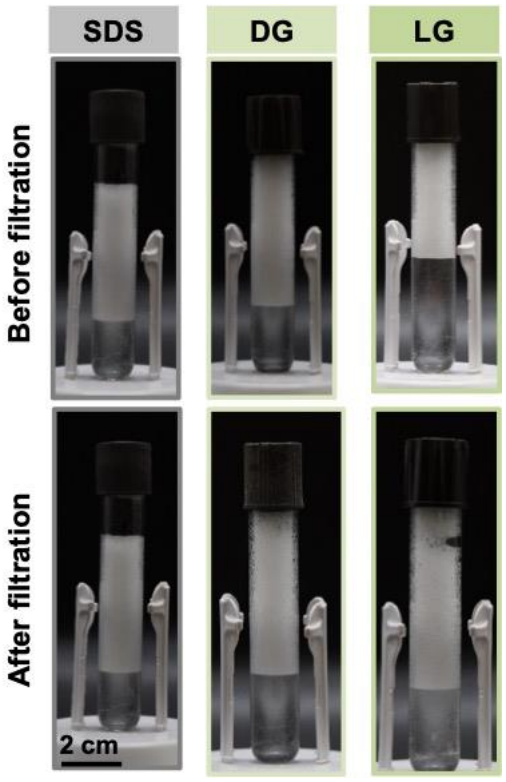

Figure 3.1.6. Pictures of the foams produced from the surfactants solution (SDS, DG, and LG) before and after filtration to remove the spores, showing a similar foamability and foam stability around 5 min after producing the foam. The scale bar represents 2 cm for all the pictures.

2.6. Life Cycle Assessment of the Foam Flow Process: Comparison between SDS and APGs

The results of the LCA modeling obtained by the ReCiPe method are shown in **Figure 3.1.7** and in Table S1 (in supplementary file). We compared the foams studied pre-viously with SDS (reference system) with foams produced with APGs [9,11]. It is important to notice that for the LCA analysis, we chose the fatty alcohol sulfate from renewable resources and not from petrochemical sources to reduce the possible impact of SDS [25]. In this study, for foams produced by both surfactants (SDS and APG), the contribution of the process parameters (water consumption for surfactant solution preparation, pump energy consumption, and compressed air consumption) contributed mainly to the impact of the process in the same way. The pump energy consumption seemed to be the major con-tributor to most of the impacts studied. By comparing the processes of cleaning with foam formulated with SDS and with APG, we observed that the most important impact of using APG instead of SDS was for natural land transformation (15% of reduction). For terrestrial ecotoxicity, the use of APG reduced the impact by around 9%. The negative impact of SDS for these two parameters came from the fatty alcohol sulfate used to produce SDS. This result was not surprising, as the fatty alcohol sulfate was reported to be a harmful con-tributor to most environmental impact indicators in previous LCA studies comparing different surfactants formulations for cleaning [25]. For marine ecotoxicity, human toxicity, fossil depletion, and climate change, the use of APG reduced them by around 11, 10, 8, and 5%, respectively. For these parameters, the fatty alcohol sulfate was the second most important contributor, after the pump energy consumption (present in both surfactant foam processes). For water depletion, the impact of using APG instead of SDS was very low, around 2%. For this parameter, the fatty alcohol sulfate was the third most important factor, after the pump energy consumption and the water consumption, which were

present in both foam processes. For marine eutrophication, the use of APG increased the impact in a negative way in comparison to SDS (around 6% of increase). Although the main contributor to marine eutrophication was the energy consumption of the pump, which was found in both processes, the potato starch used to produce the APG had a negative impact. We can conclude that the most harmful process was the one formulated with SDS, as it had a major contribution to all impacts except marine eutrophication. From the LCA study, the foams based on APGs helped to further decrease the environmental impacts of the cleaning process in comparison to the foams based on SDS used in the previous studies, even when SDS synthesis is not entirely coming from petrochemical resources [9,11].

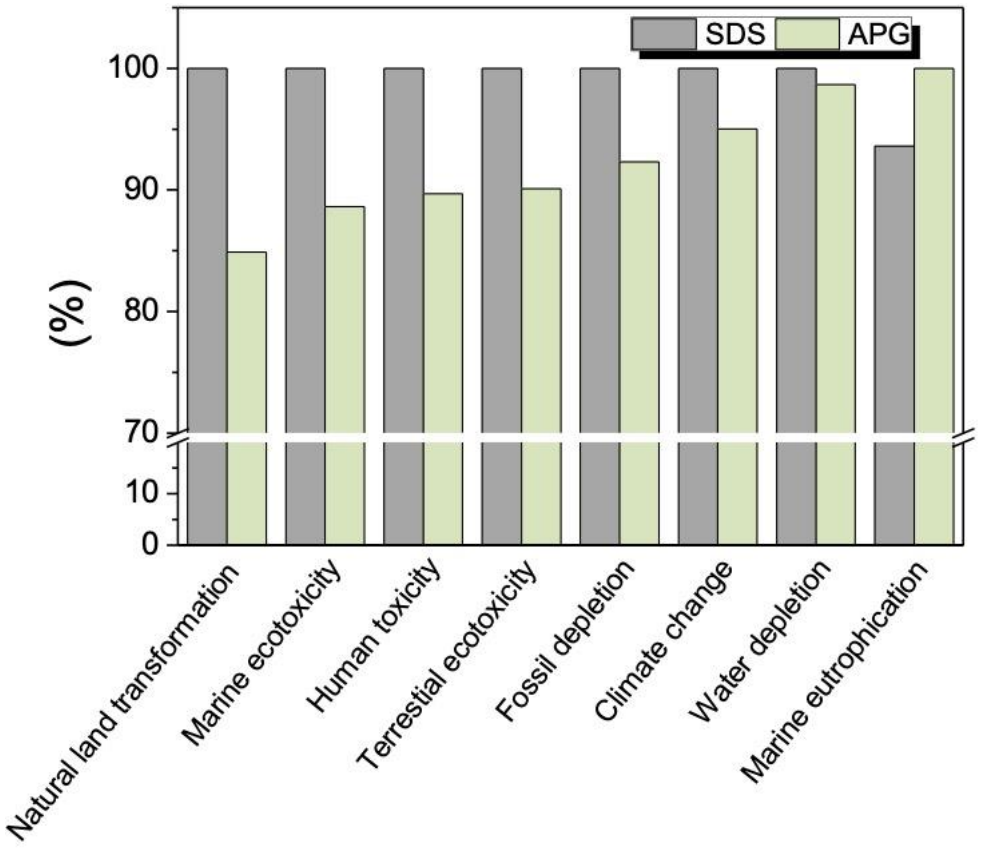

Figure 3.1.7. Environmental comparison between foam cleaning process with APG and foam clean-ing process with SDS (reference system) by impact category (ReCiPe midpoint H).

3.1.3 Materials and Methods

3.1.3.1 Materials

3.1.3.1.1 Preparation of Surfactant Solution

Lauryl glucoside (Plantacare 1200) with 51.3 wt.% of active matter and decyl glu-coside (Plantacare 2000) with 53.0 wt.% of active matter were provided by Ludwigshafen, BASF, Germany. Lauryl glucoside and decyl glucoside were used at a concentration of 0.1 wt.% of the active matter. Sodium Dodecyl Sulfate with 98.5% purity was purchased from Sigma Aldrich, Saint Quentin Fallavier , France. SDS was used at a concentration of 0.23 wt.%.

3.1.3.1.2 Preparation of Solid Model Surfaces

All the cleaning experiments were carried out on rectangular (45 mm x 15 mm) AISI 316 stainless-steel plates (APERAM, Isbergues, France) with a 2R factory finish. In order to have similar surface properties to those found in the food industry, the surfaces were subjected to a conditioning process shown in **Figure 3.1.8** [9]. The plates were immersed in milk at room temperature for 30 min and then they were rinsed under osmosis water for 5 min by overflow. The plates were immersed in a 0.5 wt.% sodium hydroxide solution at 70 °C for 30 min and then they were rinsed in osmosis water for 5 min. This cycle was repeated 15 times. Then, they were fouled with Escherichia coli strains previously shown to produce biofilms on stainless-steel surfaces [11]. For the biofilm formation, the plates were placed in a petri dish, and covered with 50 mL of a bacterial suspension consisting of 1/10 Tryptone Soy Broth (TSB, Biokar Diagnostics, Allonne, France) inoculated with 24 h of culture of Escherichia coli (final concentration around 107 CFU.mL−1), and they were incubated at 30 °C for 24 h. Afterward, the plates were submitted to cleaning and dis-infection steps. They were cleaned by rubbing the surfaces with an alkaline detergent RBS T105 (Chemical products, Brussels, Belgium) used usually for cleaning in the food industry [9]. They were immersed in a 5 wt.% RBS T105 solution at 60 °C for 10 min, followed by a rinse under running tap water for 5 min and then under osmosis water for 5 min. A period of 24 h before each experiment, the surfaces were sterilized in a dry heat oven at 180 °C for 1 h.

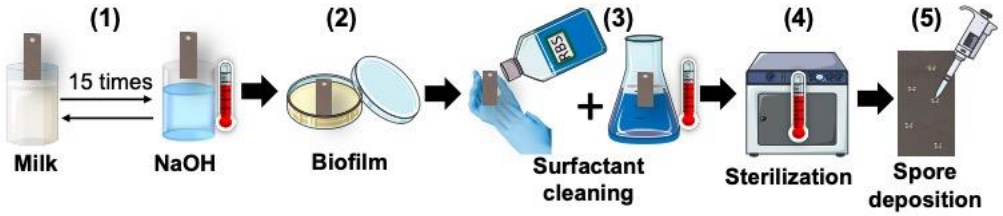

Figure 3.1.8. Different steps of stainless-steel plate surface preparation methodology: (1) 15 cycles of immersion of the plate in milk at room temperature for 30 min and in sodium hydroxide at 70 °C for 30 min; (2) biofilm formation on the plate; (3) rubbing of the plate with commercial undiluted surfactant (RBS) followed by immersion of the plate in surfactant aqueous solution at 5 wt.% at 60 °C for 10 min; (4) the plate sterilization in a hot air oven at 180 °C for 1 h; (5) soiling of the plate with 5 drops of 1 µL of the spore suspension at a concentration of 108 CFU.mL−1.

3.1.3.1.3 Preparation of Spore's Suspension

Bacillus subtilis PY79 is a laboratory strain known to produce hydrophilic spores. The Bacillus subtilis PY79 strain was tagged with green fluorescent proteins to make the spores fluorescent [19]. Frozen Bs PY79 was plated on nutrient broth agar (nutrient broth 13 g.L−1; agar 15 g.L−1) with an antibiotic (5 g.mL−1 of chloramphenicol) to promote the production of the green fluorescent protein, and incubated at 30 °C for 24 h. After 24 h, another plating was performed in the same conditions. The following day, some colonies were picked with a loop and inoculated in 50 mL of nutrient broth (Biokar Diagnostics, Beauvais, France) at 30 °C with continuous agitation for about 5 h until the absorbance at 600 nm was 1.2. Then, the suspension was centrifugated at 20 °C for 15 min at 1500× g. The amount of supernatant necessary was drained in order to leave a volume slightly greater than 200 µL per Petri dish to be seeded. The cell pellet was resuspended by shaking with a vortex and immediately used to inoculate the sporulation medium. The suspension was spread on Spo8-agar [26] and incubated at 30 °C for 10 days, when sporulation reached at least 95%. The spores were harvested by scraping the surface from the plates using sterile milli-Q water and washed five times in sterile milli-Q water by centrifugation (4 °C for 15 min at 3500× g) and resuspension.

To determine the spores' hydrophilic character, we used the microbial adhesion to hydrocarbons method (MATH), which is based on the affinity of the spores for hexadecane [26]. The hydrophilic characteristic corresponds to a high percentage of affinity for the aqueous phase, while a high percentage of affinity for the hexadecane corresponds to a hydrophobic characteristic. The spore suspension (108–109 spores.mL−1) was re-suspended in 8.5 g. L−1 of NaCl aqueous solution to obtain an absorbance value of 0.5 to 0.6 at 600 nm (A0). Three milliliters of the spore suspension were put in glass tubes with 500 µL of hexadecane each and the tubes were vortexed at 2400 rpm for times ranging from 5 to 900 s. Then, each tube was left to settle for 30 min and then the absorbance of the aqueous phase of each tube was measured at 600 nm (At). The percentage of affinity for the aqueous phase was calculated as follows (At /A0) × 100 for each vortex time [26].

3.1.3.1.4 Soiling of Surfaces with the Spores Suspension

The concentration of the spore suspension to soil the plates was set at 108 CFU.mL−1. In order to avoid the presence of spore aggregates, the spore suspension was sonicated in an ultrasonic bath (Bransonic 2510E-MT, Branson Ultrasonics Corporation, Danbury, CT, USA) before each experiment for 2 min and 30 s. A total of 5 drops of 1 µL of the spore suspension were placed in each plate. Then, the plates were dried for 1 h at 30 °C.

3.1.3.2 Methods

3.1.3.2.1 Determination of the Critical Micelle Concentration by Surface Tension Measurements

The critical micelle concentration (CMC) of APGs and SDS was estimated by surface tension measurements performed with a DSA100S drop shape analyzer (KRUSS, Hamburg, Germany) using the pendant drop method. The measurements were carried out at room temperature (23 °C ± 1.3 °C) with a stainless-steel needle 1 mm in diameter.

3.2.2. Contact Angle Measurements of the Model Surface

The surface wettability was determined by measuring the contact angle of a water droplet (1 µL) deposited directly into the surface with the DSA100S Drop shape analyzer (KRÜSS, Hamburg, Germany). The temperature during the analysis was 20 ± 2 °C. All measurements were performed in triplicate and for two different plates.

3.1.3.2.2 Spores Detachment Analysis

For the quantification of the adhered spores, each plate was sampled with a dry cotton swab (Copan, Brescia, Italy), which was then put in a tube containing 5 mL of sterile Milli-Q water. Each tube was vortexed for 1 min at 2400 rpm. Then, the swabs were removed from the tubes. Serial dilutions of the suspensions in the tubes were performed in sterile Milli-Q water and 100 µL of each dilution were plated in Tryptic Soy Agar (TSA; Biokar Diagnostics, Allonne, France). The plates were incubated for 24 h at 30 °C. The number of bacterial colonies was counted, and the results were expressed as the mean of the colony forming units plate−1 (CFU.plate−1). The cleaning efficiency was calculated by dividing the number of viable spores after the cleaning tests (whether static conditions or foam cleaning) by the number of spores on plates used as a control for the initial spore concentration. The cleaning efficiency was expressed in terms of log reduction using Equation (1):

$$Log\ reduction = log\ (CFU.plate^{-1}{}_{t} - CFU.plate^{-1}{}_{t0})$$

where CFU.plate−1 t: the mean number of the colony-forming units per plate after cleaning (t = 1 min or 30 min); CFU.plate−1t0 : the mean initial number of the colony-forming units per plate.

3.1.3.2.3 Spores Detachment under Static Conditions

Three soiled plates were dipped vertically in 1 L of each surfactant solution or only in osmosis water for 30 min at room temperature. Three soiled plates were used as a control for the enumeration of the initial spore concentration. The experiments were carried out in triplicate.

3.1.3.2.4 Production of Foams

The foam production device used in this study was the same as those used in previous works [9,10]. In brief, first, the surfactants were dissolved in osmotic water in the inlet tank of the foam production device. Before they were used for foam production, they were recirculated using a pump for five minutes, to ensure proper mixing. The surfactant solution was pumped into a tank, which was located at a 3 m height to ensure a constant flow due to gravity. The surfactant solution flowed at a flow rate of 4.5 L.h−1 into the foam generator, where the foam was produced by bubbling compressed air at a flow rate of 4.5 L.h−1 into the surfactant solution through a porous disc (pore size: 1–1.6 μm, DURAN, France). Then, the foam flowed through a horizontally placed square duct (1.5 cm high × 1.1 cm width × 23 cm in length) where the cleaning process was carried out.

The mean velocity of the foam (v) was around 1.5 cm.s−1 and it was calculated according to Equation (2):

$$v = (Qs + Qa)/S \quad (1)$$

where Qs : the surfactant solution flow rate in L.h−1; Qa: the air flow rate in L.h−1; S: the duct cross-section in cm.

The foam production parameters were chosen based on our previous studies on SDS foams in order to have an efficient spore's removal effect by producing foams with an adequate bubbles size and foam flow velocity [9–11].

3.1.3.2.5 Effect of Foams on the Detachment of Spores

The foam flow cleaning efficiency was evaluated after 1 and 30 min of foam flow. For each time, four soiled plates (one for microscopy and three for the spore quantification) were introduced in a rectangular stainless-steel duct, which was then connected to the foam flow cleaning setup. Three extra soiled plates were used as a control of the initial spore concentration.

3.1.3.2.6 Microscopic Observation of the Detachment of Spores

The microstructure of the spore drops placed on the plate surfaces was observed before and after cleaning. The spores deposited on the plates were stained with orange acridine at 0.01 wt.% and left for 15 min under dark conditions. Then, they were softly rinsed with osmosis water. Once they were dried, they were observed using an epifluorescence microscope at 50× magnification (Zeiss Axioskop 2 Plus, Oberkochen , Germany).

3.1.3.2.7 Foams Characterization

The foams produced in the foam flow cleaning setup were characterized in terms of bubble size, foam height, and drainage. For the liquid fraction, we took a known volume of foam after the foam passed through the cleaning duct. Then, we measured the volume of liquid remaining when the foam was destroyed after a few hours. From the volume of liquid and the liquid of foam, we calculated the liquid fraction corresponding to the ratio between the two values. The height of the foams and the bubble size over time were measured using a dynamic foam analyzer-DFA100 (KRUSS, Hamburg, Germany). The foams samples were collected directly in the glass column (40 mm inner diameter) with a prism incorporated in the whole length of the column. For each foam, a sample was taken before and after the foam passed through the cleaning duct. The foams' height and the bubbles' size were simultaneously measured. The foams' height was measured by using an LED panel and a line sensor located at the front and the back of the column, respectively. The foam height was monitored continuously for 1800 s by detecting the differences in light transmission through the glass column. For measuring the bubble size, a camera with a scanning area of 10.5 × 7.5 mm was positioned at a column height of 110 mm. The prism in the column allowed for obtaining images of the 2D foam structure. The resulting images were analyzed by the KRUSS Foam Analysis Software and the mean bubble area was recorded at every time step for 1800 s. The foams were characterized in triplicates.

3.1.3.2.8 Surfactant Solution Cleaning by Filtration

After the foam cleaning process, the cleaning of the foaming surfactant solution was evaluated by the filtration technique. An amount of 50 mL of each surfactant solution was placed in sterile glass containers with lids. Each of the surfactant solutions was inoculated with 50 microliters of spore suspension at a concentration of 108 CFU.mL−1 to mimic the contamination of the liquid phase of the foam after cleaning. Three samples of 5 mL from each surfactant solution were taken using a plastic syringe (Terumo, Leuven, Belgium) and they were filtered through a syringe filter (pore size: 0.2 µm, Sartorius, Goettingen, Germany). In order to control the spore concentration in the surfactant solutions, three samples of 100 µL each were taken from each of the surfactant solutions and serial dilu-tions were made in sterile Milli-Q water. Amounts of 100 µL of the filtered solutions and 100 µL of the serial dilutions were plated in Tryptic Soy Agar (TSA; Biokar Diagnostics, Allonne, France) and then incubated for 24 h at 30 °C. The number of bacterial colonies was counted, and the results were expressed as colony-forming units.mL−1 (CFU.mL−1).

3.1.3.2.9 Life Cycle Assessment

The environmental impacts of the foam cleaning process using SDS and APGs were compared based on Life cycle assessment (LCA). The LCA methodology is standardized by ISO 14040 (2006) [27] and ISO 14044 (2006)[28]. The LCA consists of four phases:

- The objective and scope definition;
- The inventory analysis;
- The environmental impact assessment;
- The interpretation of the results.

The modeling of the LCA was performed using the Ecoinvent v3.0 database.

- The objective and scope definition

The objective of the LCA was to compare the environmental impacts of the foam cleaning process using SDS and the foam cleaning process using APGs. The functional unit (FU) is a unit of reference that allows for comparing different systems. In this study, the FU was defined as a cleaning of 0.05 m2 of the stainless-steel surface with at least 2 log CFU/cm2 of spores removal after 30 min of cleaning.

- The life cycle inventory

The process flowchart for foam cleaning with SDS and with APG is given in **Figure 3.1.9**. In both processes, the water consumption for foam production was 6 L.h−1 as the flow rate was 4.5 L.h−1, but an extra consumption was considered until the foam flow was stabilized. The consumption of compressed air to produce the foam was 6 L.h−1, and also an extra consumption was considered until the foam flow was stabilized. The electricity consumed by the pump to transport the surfactant solutions was 0.31 kW.h−1. The electricity con-sumption to compress the air was already taken into account in the compressed air data supplied by the Ecoinvent v3.0 database. Given the lack of data (in Ecoinvent) concerning the SDS and the APG, these substances were modeled (created) by using 40% sodium carbonate and 60% fatty alcohol sulfate for the SDS [11,25], and 59.7% potato starch and 40.3% fatty alcohol for the APG [29]. This study did not take into account transportation and electricity consumption for surfactant production.

- The impact assessment

In this study, the ReCiPe (v1.09) method was chosen for the impact assessment as it includes categories of relevance that are not included in other methods [30]. We chose the hierarchical perspective (H), as it considers the impacts in a more balanced way with respect to the temporal framework [31]. In order to focus on relevant data, a selection of environmental impacts was performed, based on their importance in other LCA studies that involve CIP in the food industry [11,30]. Eight environmental impacts were selected: climate change (kg.CO2 eq), marine eutrophication (kg.Neq), human toxicity (kg.1,4-DB eq), terrestrial ecotoxicity (kg 1,4-DB),

marine ecotoxicity (kg.1,4-DB eq), natural land transformation (m2), water depletion (m3), and fossil resource depletion (kg.oil eq).

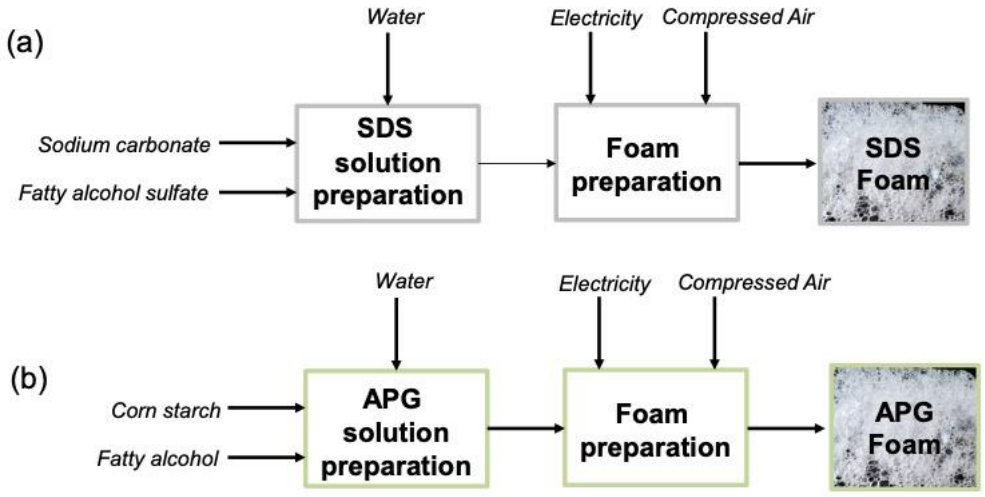

Figure 3.1.9. The process flowchart for the foam cleaning process formulated with: (a) SDS and (b) APG.

3.1.3.2.10 Statistical Analysis

All the experiments were carried out in triplicate and the results were expressed as the mean ± standard deviation. The results were compared by one-way analysis of variance and Tukey's test to analyze statistical differences ($p < 0.05$). The analysis was performed using SAS V8.0 software (SAS Institute, Gary, NC, USA).

3.1.4 Conclusions

This study showed that foams based on SDS and APGs could remove the spores deposited on model stainless-steel surfaces due to the foam wall friction mechanism. No effect on the APGs alkyl chain length between decyl glucoside and lauryl glucoside was observed. The foam properties were similar given the same effect on the foam flow removal of spores. After the foam cleaning process, the foams could be destabilized by ultrasound, and the spores be removed from the surfactant solutions by filtration, leading to a regeneration of the foam based on the same surfactant solutions. The LCA has shown that foam cleaning had significant environmental impact benefits with a reduction in water and energy consumption. The use of

APGs helped to further decrease the envi-ronmental impacts in comparison to SDS in terms of natural land transformation, ter-restrial ecotoxicity, marine ecotoxicity, human toxicity, fossil depletion, and climate change. Foams based on APGs were also more stable during the foam flow in comparison to foams based on SDS, which is an advantage to clean long ducts in the industry. In the future, it would be interesting to improve the foam stability by adding co-surfactants or polymers as already studied for foam flows in nuclear decontamination to try to improve further the spores' removal action of the foam by increasing the foam friction mechanism and higher foam viscous stress [32]. Moreover, foams are already used to decontaminate static vertical surfaces from spores by using disinfecting formulations [16]. The next step in this study would be in the same way to combine the mechanical action of the foam flows with a chemical action to clean and decontaminate in the same time.

Funding: This research was funded by the region Hauts de France and INRAe TRANSFORM department. This work was also supported by the project Veg-I-Tec (programme Interreg V France476 Wallonia-Flanders GoToS3).

Acknowledgments: C. Dari would like to thank the region Hauts de France and INRAe TRANSFORM department for the allocation of her PhD grant.

3.1.5 References

1. Xue, L.; Liu, G.; Parfitt, J.; Liu, X.; Van Herpen, E.; Stenmarck, Å.; O'Connor, C.; Östergren, K.; Cheng, S. Missing Food, Missing Data? A Critical Review of Global Food Losses and Food Waste Data. Environ. Sci. Technol. 2017, 51, 6618–6633.

2. Faille, C.; Cunault, C.; Dubois, T.; Benezech, T. Hygienic Design of Food Processing Lines to Mitigate the Risk of Bacterial Food Contamination with Respect to Environmental Concerns. Innov. Food Sci. Emerg. Technol. 2018, 46, 65–73.

3. González-Rivas, F.; Ripolles-Avila, C.; Fontecha-Umaña, F.; Ríos-Castillo, A.G.; Rodríguez-Jerez, J.J. Biofilms in the Spotlight: Detection, Quantification, and Removal Methods: Biofilms DQR in the Food Industry…. Compr. Rev. Food Sci. Food Saf. 2018, 17, 1261–1276, doi:10.1111/1541-4337.12378.

4. Deleplace, M.; Dallagi, H.; Dubois, T.; Richard, E.; Ipatova, A.; Bénézech, T.; Faille, C. Structure of Deposits Formed by Drying of Droplets Contaminated with Bacillus Spores Determines Their Resistance to Rinsing and Cleaning. J. Food Eng. 2022, 318, 110873, doi:10.1016/j.jfoodeng.2021.110873.

5. Tsai, J.-H.; Huang, J.-Y.; Wilson, D.I. Life Cycle Assessment of Cleaning-in-Place Operations in Egg Yolk Powder Production. J. Clean. Prod. 2021, 278, 123936, doi:10.1016/j.jclepro.2020.123936.

6. Wirtanen, G.; Salo, S. Disinfection in Food Processing–Efficacy Testing of Disinfectants. Rev. Environ. Sci. Biotechnol. 2003, 2, 293–306.

7. Lyndgaard, C.B.; Rasmussen, M.A.; Engelsen, S.B.; Thaysen, D.; van den Berg, F. Moving from Recipe-Driven to Measure-ment-Based Cleaning Procedures: Monitoring the Cleaning-In-Place Process of Whey Filtration Units by Ultraviolet Spec-troscopy and Chemometrics. J. Food Eng. 2014, 126, 82–88, doi:10.1016/j.jfoodeng.2013.10.037.

8. Gossard, A.; Lilin, A.; Faure, S. Gels, Coatings and Foams for Radioactive Surface Decontamination: State of the Art and

9. Dallagi, H.; Faille, C.; Bouvier, L.; Deleplace, M.; Dubois, T.; Aloui, F.; Benezech, T. Wet Foam Flow: A Suitable Method for Improving Surface Hygiene in the Food Industry. J. Food Eng. 2022, 322, 110976.

10. Al Saabi, A.; Dallagi, H.; Aloui, F.; Faille, C.; Rauwel, G.; Wauquier, L.; Bouvier, L.; Bénézech, T. Removal of Bacillus Spores from Stainless Steel Pipes by Flow Foam: Effect of the Foam Quality and Velocity. J. Food Eng. 2021, 289, 110273.

11. Dallagi, H.; Faille, C.; Gruescu, C.; Aloui, F.; Benezech, T. Foam Flow Cleaning, an Effective and Environmentally Friendly Method for Controlling the Hygiene of Closed Surfaces Contaminated with Biofilms. Food Bioprod. Process. 2022, 136, 236–248.

12. Denkov, N.D.; Subramanian, V.; Gurovich, D.; Lips, A. Wall Slip and Viscous Dissipation in Sheared Foams: Effect of Surface Mobility. Colloids Surf. Physicochem. Eng. Asp. 2005, 263, 129–145, doi:10.1016/j.colsurfa.2005.02.038.

13. Denkov, N.D.; Tcholakova, S.; Golemanov, K.; Subramanian, V.; Lips, A. Foam–Wall Friction: Effect of Air Volume Fraction for Tangentially Immobile Bubble Surface. Colloids Surf. Physicochem. Eng. Asp. 2006, 282–283, 329–347, doi:10.1016/j.colsurfa.2006.04.028.

14. Denkov, N.D.; Tcholakova, S.; Golemanov, K.; Ananthpadmanabhan, K.P.; Lips, A. The Role of Surfactant Type and Bubble Surface Mobility in Foam Rheology. Soft Matter 2009, 5, 3389, doi:10.1039/b903586a.

15. Drenckhan, W.; Saint-Jalmes, A. The Science of Foaming. Adv. Colloid Interface Sci. 2015, 222, 228–259.

16. Le Toquin, E.; Faure, S.; Orange, N.; Gas, F. New Biocide Foam Containing Hydrogen Peroxide for the Decontamination of Vertical Surface Contaminated With Bacillus Thuringiensis Spores. Front. Microbiol. 2018, 9, 2295, doi:10.3389/fmicb.2018.02295.

17. Ranieri, D.; Preisig, N.; Stubenrauch, C. On the Influence of Intersurfactant H-Bonds on Foam Stability: A Study with Techni-cal Grade Surfactants. Tenside Surfactants Deterg. 2018, 55, 6–16.

18. Nickel, D.; Rybinski, W. Von; Kutschmann, E.; Stubenrauch, C.; Findenegg, G.H. The Importance of the Emulsifying and Dis-persing Capacity of Alkyl Polyglycosides for Applications in Detergent and Cleaning Agents. Lipid/Fett 1996, 98, 363–369.

19. Dubois, T.; Krzewinski, F.; Yamakawa, N.; Lemy, C.; Hamiot, A.; Brunet, L.; Lacoste, A.-S.; Knirel, Y.; Guerardel, Y.; Faille, C. The Sps Genes Encode an Original Legionaminic Acid Pathway Required for Crust Assembly in Bacillus Subtilis. mBio 2020, 11, e01153-20, doi:10.1128/mBio.01153-20.

20. Fang, J.P.; Joos, P. The Dynamic Surface Tension of SDS— Dodecanol Mixtures. Colloids Surf. 1992, 65, 113–120, doi:10.1016/0166-6622(92)80266-5.

21. Bhuyan, A.K. On the Mechanism of SDS-Induced Protein Denaturation. Biopolymers 2010, 93, 186–199, doi:10.1002/bip.21318.

22. Fameau, A.-L.; Lam, S.; Velev, O.D. Multi-Stimuli Responsive Foams Combining Particles and Self-Assembling Fatty Acids. Chem. Sci. 2013, 4, 3874, doi:10.1039/c3sc51774h.

23. Daufin, G.; Escudier, J.-P.; Carrère, H.; Bérot, S.; Fillaudeau, L.; Decloux, M. Recent and Emerging Applications of Membrane Processes in the Food and Dairy Industry. Food Bioprod. Process. 2001, 79, 89–102, doi:10.1205/096030801750286131.

24. Arnould, A.; Cousin, F.; Salonen, A.; Saint-Jalmes, A.; Perez, A.; Fameau, A.-L. Controlling Foam Stability with the Ratio of Myristic Acid to Choline Hydroxide. Langmuir 2018, 34, 11076–11085, doi:10.1021/acs.langmuir.8b02261.

25. Van Lieshout, K.G.; Bayley, C.; Akinlabi, S.O.; von Rabenau, L.; Dornfeld, D. Leveraging Life Cycle Assessment to Evaluate Environmental Impacts of Green Cleaning Products. Procedia CIRP 2015, 29, 372–377, doi:10.1016/j.procir.2015.02.063.

26. Faille, C.; Lemy, C.; Allion-Maurer, A.; Zoueshtiagh, F. Evaluation of the Hydrophobic Properties of Latex Microspheres and Bacillus Spores. Influence of the Particle Size on the Data Obtained by the MATH Method (Microbial Adhesion to Hydro-carbons). Colloids Surf. B Biointerfaces 2019, 182, 110398, doi:10.1016/j.colsurfb.2019.110398.

27. ISO 14040 (2006) Environmental Management—Life Cycle Assessment—Principle and Framework. Available online: https://www.iso.org/standard/37456.html (accessed on 24 November 2022).

28. ISO 14044 (2006) Environmental Management—Life Cycle Assessment—Requirements and Guidelines. Available online: https://www.iso.org/standard/38498.html (accessed on 24 November 2022).

29. Brière, R.; Loubet, P.; Glogic, E.; Estrine, B.; Marinkovic, S.; Jérôme, F.; Sonnemann, G. Life Cycle Assessment of the Production of Surface-Active Alkyl Polyglycosides from Acid-Assisted Ball-Milled Wheat Straw Compared to the Conventional Pro-duction Based on Corn-Starch. Green Chem. 2018, 20, 2135–2141, doi:10.1039/C7GC03189K.

30. Gésan-Guiziou, G.; Sobańtka, A.P.; Omont, S.; Froelich, D.; Rabiller-Baudry, M.; Thueux, F.; Beudon, D.; Tregret, L.; Buson, C.; Auffret, D. Life Cycle Assessment of a Milk Protein Fractionation Process: Contribution of the Production and the Cleaning Stages at Unit Process Level. Sep. Purif. Technol. 2019, 224, 591–610, doi:10.1016/j.seppur.2019.05.008.

31. Goedkoop, M.; Heijungs, R.; Huijbregts, M.; De Schryver, A.; Struijs, J.; Van Zelm, R. ReCiPe 2008. Life Cycle Impact Assess. Method Which Comprises Harmon. Categ. Indic. Midpoint Endpoint Level; Ministerie van Volkshuisvesting: Amsterdam, The Netherlands, 2009, 1, 1–126.

32. Dame, C.; Fritz, C.; Pitois, O.; Faure, S. Relations between Physicochemical Properties and Instability of Decontamination Foams. Colloids Surf. Physicochem. Eng. Asp. 2005, 263, 210–218, doi:10.1016/j.colsurfa.2004.12.053.

Supporting Information: Decontamination of Spores on Model Stainless-Steel Surface by Using Foams Based on Alkyl Polyglucosides

Table S1: Contribution of the foam cleaning process with APG and the foam cleaning process with SDS to the environmental impact categories selected according to the ReCiPe midpoint (H) impact assessment method.

Impact category	Unit	Foam Cleaning process with APG	Foam Cleaning process with SDS
Natural land transformation	m^2	1,30E-03	1,53E-03
Terrestrial ecotoxicity	Kg.1,4-DB eq	1,46E-03	1,62E-03
Climate change	kg CO_2 eq	2,58E+00	2,72E+14
Marine ecotoxicity	kg 1,4-DB eq	1,31E-02	1,48E-02
Human toxicity	kg 1,4-DB eq	5,59E-01	6,23E-01
Fossil depletion	kg oil eq	8,59E-01	9,31E-01
Water depletion	m^3	2,24E+01	2,27E+01
Marine eutrophication	kg N eq	7,25E-04	6,79E-04

Chapter 4: Water-in-water emulsion formulation as possible innovative cleaning method.

Introduction to chapter 4

As mentioned in the general introduction, the objective of this thesis is not only to use foams as a cleaning method but also to explore innovative soft materials for cleaning purposes. To this end, we chose to work with water-in-water (W/W) emulsions, where one aqueous phase is dispersed within another aqueous phase. One of the most interesting applications of W/W emulsions is their potential use in designing innovative encapsulation and delivery systems for labile molecules, such as antibacterial agents. Additionally, they offer possibilities for the encapsulation and separation of bacteria.

However, a significant drawback of W/W emulsions is their difficulty in stabilization due to their very low surface tensions (around 0.1-100 µN/m) and large interface thickness (10 to 100 nm). For these physical reasons, W/W emulsions cannot be stabilized by the common surfactants and are generally stabilized by particles. A recent study has shown that it is possible to stabilize W/W emulsion with sodium oleate (anionic surfactant) in combination with decanol. The combination of surfactant with fatty alcohols is well-known in the literature and industries to lead to the formation of lamellar gel networks (LGNs), which are also already used for stabilizing oil-in-water emulsions. The objective of this chapter was to develop a new method to stabilize W/W emulsions based on LGNs and to give rise to a novel soft material based on a combination of foams and W/W emulsions.

In this chapter, we demonstrated that W/W emulsions can be effectively stabilized using lamellar gel networks (LGNs) composed of alkyl polyglucosides (APGs) and fatty alcohols. Moreover, we established the robustness of this system by showing that various types of APGs and fatty alcohols can be employed to create these LGNs. To our knowledge, this is the first example where a non-ionic surfactant has been utilized to stabilize W/W emulsions. Depending on the properties of the APGs, we achieved the production of emulsions with high stability over an extended period. Furthermore, we successfully developed a foamulsion based on W/W emulsions.

4.1 Mixture of fatty alcohols and alkyl polyglucosides stabilizing Water-in-water Emulsions

Carolina Dari[1], Yuchen Si[2], Jean-Paul Douliez[3], Jean-François Tahon[4], Thierry Benezech[1], Paul S. Clegg[2], and Anne-Laure Fameau[1*]

1 INRAe, University Lille, CNRS, INRAe, Centrale Lille, UMET, 59000 Lille, France.

2 School of Physics and Astronomy, University of Edinburgh, Peter Guthrie Tait Road, Edinburgh, EH9 3FD, UK.

3 Biologie du Fruit et Pathologie, UMR 1332, INRAE, Université De Bordeaux, Villenave d'Ornon, F-33140, France.

4 Unité Matériaux Et Transformations (UMET), UMR CNRS 8207, Université de Lille Nord de France, USTL-ENSCL, Bat C7, BP 90108, 59652, Villeneuve D'Ascq, France.

*** Correspondence:**

Corresponding Author

Anne-laure.fameau@inrae.fr

Keywords: emulsion1; lamellar phase2; fatty alcohol3; alkylpolyglucoside4.

Abstract

The combination of surfactants and fatty alcohols leads to the formation of lamellar gel network (LGNs) which are widely used in cosmetic and pharmaceutical industries. Alkyl polyglucosides (APGs) are known to stabilize oil-in-water emulsions and here, we report their use in combination with fatty alcohol for the stabilization of all-aqueous Water-in-water (W/W) emulsions based on dextran-in-poly(ethylene glycol). Two different APGs were used: decyl glucoside and lauryl glucoside. We systematically studied the influence of the concentrations of APGs, and the molar ratio between the APGs and decanol as model fatty alcohol on the size and stability of the aqueous emulsion droplets with time. The self-assembled structure formed

by decanol/APGs was characterized by using Small Angle X-ray Scattering and confocal microscopy, and shown to be lamellar in the bulk phase and probably also at the surface of dextran-rich droplets.

We also demonstrated that the stabilization of W/W emulsions can be extended to other APG and to other fatty alcohols. In addition, we reported the production of a foam using such W/W emulsions as the continuous phase. Our results show that it is possible to stabilized W/W emulsions using LGNs based on different APGs and fatty alcohols, which will undoubtedly expand the use of W/W emulsions for various fields.

4.1.1 Introduction

Emulsions, which are commonly used in a wide range of applications, are made up of two thermodynamically incompatible solutions or solvents (Leal-Calderon et al., 2007). The most conventional ones are oil-in-water or water-in-oil emulsions. However, a more unusual emulsion system is based on an aqueous solution that forms droplets into another aqueous solution, the so-called 'Water-in-water emulsions' (W/W emulsions) (Esquena, 2016, 2023; Dickinson, 2019) . The formation of W/W emulsions occurs when a moderately concentrated solution of incompatible polymers exhibits thermodynamic phase separation (Dickinson, 2019). In contrast to oil-in-water emulsions, W/W emulsions are much more difficult to stabilize since the surface tension is very low (around 0.1-100 µN. m-1) and the interface thickness is large (at least, few tens of nanometers) (Antonov et al., 2004; Esquena, 2016). For these physical reasons, W/W emulsions cannot be stabilized by the common surfactants usually used for the stabilization of the oil-in-water or water-in-oil emulsions. Thus, when formed upon mixing, droplets coalesce with time more or less quickly, depending on the system investigated and then, macroscopic phase separation occurs. The lack of stability of W/W emulsions is the main drawback that limits their use for practical applications (Esquena, 2016). Several applications of W/W emulsions have been reported in various fields: food, biomedical, drug delivery, etc. (Esquena, 2016, 2023). For example, they can be used to encapsulate active components and

labile molecules, and then be used as delivery systems. They can also be used as microreactors for the synthesis of high value-added products (Esquena, 2016, 2023). The field of water-in-water emulsions is experiencing growth, driven by the discovery of new methods to improve their stability. Therefore, finding new methods to effectively stabilize W/W emulsions is a major challenge for scientists to expand their use.

Despite the difficulties in stabilizing them, W/W emulsions have been shown to be efficiently stabilized by using a wide variety of chemicals and particles as reviewed by several authors (Nicolai and Murray, 2017; Dickinson, 2019; Chao and Shum, 2020). For example, W/W emulsions can be stabilized by polymer particles (Poortinga, 2008; Douliez et al., 2018, 2019), microgels (Merland et al., 2022; You et al., 2023), cellulose nanocrystals (Ben Ayed et al., 2018; Xie et al., 2023), protein particles (Nguyen et al., 2013), etc. Other stabilization methods based on the use of amphiphiles are also described in the literature such as: block copolymers, self-assembly of fatty acids and phospholipids, oligonucleotides, liposomes, etc.(Dewey et al., 2014; Chao and Shum, 2020). These chemicals or particles are positioned at the interface of the droplets, which prevents their coalescence and, subsequently, macroscopic phase separation. The mechanisms by which this occurs remain unclear in most cases and is probably due to an equal affinity of the particles or chemicals for the droplet-forming polymer and the continuous aqueous phase enriched in the other polymer.

Recently, stable W/W emulsions have been designed by using sodium oleate (surfactant) and decanol (fatty alcohol) with a simple addition process of the components to the two aqueous phase system (Coudon et al., 2022). The mixture of surfactant and fatty alcohols are widely used forming Lamellar gel Network (LGNs) that are of strong interest in the field of cosmetic and pharmaceutical industries (Eccleston, 1997). Lamellar gel networks (LGNs), which are also called “α-gel” in the literature, are used to give creamy texture to the products (Eccleston, 1997; Iwata, 2017). LGNs are based on the mixture of long-chain fatty alcohols with surfactants in aqueous solution (Iwata, 2017; Colafemmina et al., 2020; de Oliveira et al., 2020). By using appropriate concentrations and molar ratio of these two components, the formation of LGNs

occurs. It can be described as a multi-phase colloidal structure mainly composed of lamellar phase and bulk water. When oil droplets are present in the formulation, they are entrapped and stabilized by the LGNs both present in the bulk aqueous phase and surrounding them (Junginger, 1984; Eccleston, 1997; Nakarapanich et al., 2001). The study of Coudon et al. was the first one showing the use of LGNs to stabilize water-in-water (W/W) emulsions (Coudon et al., 2022).

In the current context of growing concern for the environment, natural-based surfactants became popular as an alternative to the synthetic ones to produce LGNs and are widely used for cosmetic and pharmaceutical applications (Savic et al., 2005; Terescenco et al., 2018a, 2018b). Alkylpolyglucoside (APG) is one of the well-known families of natural surfactants, derived from natural glucose and a fatty alcohol. It is considered as non-toxic, mild and environmentally friendly emulsifier (Dari et al., 2023). Our aim here was to study the stabilization of W/W emulsions by using LGNs based on various APGs. Interestingly, these surfactants (APGs) are non-ionic surfactant whereas most of the chemical components and particles that have been used in the literature for stabilizing W/W emulsions are either charged or at least, zwitterionic (Esquena, 2023). This could be an advantage when the systems require changes in pH or ionic strength that may alter the stability of the emulsion, as is the case when W/W emulsions are used for bacterial culture (Xie et al., 2023; Zhang et al., 2024).

Here, we used two different APGs: decyl glucoside (DG) and lauryl glucoside (LG). DG and LG differ in their alkyl chain length composition. DG comprises a mixture of alkyl chains ranging from 8 to 16 carbon atoms, while LG consists of a mixture ranging from 12 to 16 carbon atoms (Keck et al., 2014; Wu et al., 2017). In addition, they differ in their degree of glycosidation: DG has a value of 1.5 and LG, 1.4. These APGs were combined with decanol as model fatty alcohol. The model W/W emulsions system was based on dextran-in-poly(ethylene glycol) (PEG) droplets. We systematically investigated the influence of the concentrations of APG, and the molar ratio between this surfactant and the fatty alcohol on the size and stability with time of the aqueous emulsion droplets. Then, we gained insight into the structure by

combining confocal microscopy and Small Angle X-ray Scattering (SAXS). We also demonstrated the versatility of these surfactants mixtures by extending the approach to another APG (coco-glucoside, CG) and other fatty alcohols (dodecanol and myristyl alcohol). Furthermore, we show that a foamulsion could be produced from such stabilized W/W emulsion. Our results show that it is possible to use the combination of fatty alcohols and APGs for the formulation of different type of W/W emulsions, which will surely broaden the use of W/W emulsions for various fields such as cosmetics and pharmaceuticals.

4.1.2 Materials and Methods

4.1.2.1 Materials

The following chemicals were purchased from Sigma-Aldrich (Saint Quentin Fallavier, France) and used as received: dextran 450-650 kg/mol, poly(ethylene glycol) 20 kg/mol (PEG), Nile red, fluorescein isothiocyanate-dextran 500 kg/mol (FITC-dextran), 1-decanol, 1-dodecanol, ethanol, and sodium dodecyl sulfate (SDS) with 98.5% purity. Lauryl glucoside (plantacare 1200 up) (LG) with 51.3 wt.% of active matter, decyl glucoside (plantacare 2000 up) (DG) with 53.0 wt.% of active matter, coco glucoside (plantacare 818 up) with 51.4 wt.% of active matter and myristyl alcohol (lanette 14) were provided by BASF (Ludwigshafen, Germany) and used as received. Milli-Q water was used for all experiments.

4.1.2.2 Preparation of the stock solutions

To prepare the all-aqueous emulsion, both the polymers PEG and Dextran were weighed in a flask and Milli-Q water was added so that the PEG concentration was 7 wt. % and the dextran concentration was 3.25 wt. %. Then, the mixture was stirred magnetically at 60 °C until polymers were completely dissolved. It formed a slightly turbid dispersion formed by polydisperse droplets enriched in Dextran in the continuous PEG phase, which coalesced with time until macroscopic phase separation occurs as expected for such aqueous emulsion (not shown).

A solution of APG (DG, LG or CG) was prepared by weighing into a flask the APG and adding Milli-Q water so that the final concentration of the APG active matter was 5 wt. %, followed by stirring magnetically at 60°C until the APG was completely dissolved. Nile red was dissolved in ethanol to obtain a final concentration of 5 mg·mL−1, then an aliquot of this solution was added to each of the APGs solutions to obtain a final concentration of 0.1 mg·mL−1. A solution of FITC-dextran was prepared by weighing the dye and adding Milli-Q water so that the concentration was 20 mg·mL−1. All these stock solutions were stored at around 4 °C in a fridge.

4.1.2.3 Preparation of the stabilized W/W emulsions

Different protocols were used to prepare W/W emulsions depending on the fatty alcohols used and its melting point. To produce Dextran-in-PEG W/W emulsion, 5 ml of the PEG-dextran mixture was taken and placed in a 15 mL tube (Falcon) while stirring the mixture. 50 µL of the FITC-dextran stock solution were added to the tube and all was mixed by vortexing; followed by the addition of a given volume of the stock solution of APG (DG, LG or CG) doped with nile red. Then the emulsion was vortexed for another 30 seconds. The same protocol was used to prepare the inverse W/W emulsion (PEG-in-dextran emulsions) but starting with the preparation of PEG at 2 wt. % and Dextran at 14 wt. %.

To prepare the dextran-in-PEG emulsions in the presence of APG and dodecanol, 5 ml of the PEG-dextran mixture was taken and placed in a 15mL tube (Falcon) while stirring the mixture at 40°C. Then, 50 µL of the FITC-dextran stock solution was added to the tube and all were mixed by vortexing. A given volume of 1-dodecanol at 40 °C was added to the previous mixture and mixed thoroughly by vortexing, followed by the addition of a given volume of the stock solution of LG or DG doped with Nile red, then the emulsion was vortexed for another 30 seconds.

To prepare dextran-in-PEG emulsions in the presence of APG and myristyl alcohol, the myristyl alcohol was first heated to 90°C, until it was completely melted, and then the required amount

was weighed in a beaker. 5 ml of the PEG-dextran mixture was taken and placed in the same baker while stirring the mixture, 50 µL of the FITC-dextran stock solution was added, and all were mixed together under magnetic stirring at 60 °C until the myristyl alcohol was completely dissolved. The resulting mixture was placed in a 15mL tube (Falcon) and a given volume of LG or DG doped with Nile red was added while vortexing. Then, the emulsion was vortexed for another 30 seconds.

4.1.2.4 Preparation of the foamulsion

A dextran-in-PEG emulsion (10 wt.% of dextran and 10 wt.% of PEG) stabilized with LG and decanol was prepared as previously described. A given volume of the emulsion was transferred to a beaker and a given volume of surfactant was added. The mixture was slowly mixed with magnetic stirring for 30 seconds. To prepare the foamulsion, the double-syringe foaming technique was used (Gaillard et al., 2017). Two 10-mL syringes were connected with a Luer-lock connector. One syringe was filled with 3.5 mL of the mixture and 6.5 mL of air. The second syringe was maintained with the piston in the fully closed position. The foam was then produced by pushing the plungers of the connected syringes 30 times by hand. The stability of the resulting foams was followed by measuring both the evolution of the foam and the volume of drained liquid over time with the naked eye.

4.1.2.5 Stability and partial phase diagram of the W/W emulsions

The bulk stability of the W/W emulsions with different molar ratio (R) of decanol:APG was followed with the naked eye (phase separation), and also by confocal fluorescence microscopy observations. Experiments were performed immediately after the production of W/W emulsions (t=0) and after 24 hours (t=24h) of conservation at room temperature. Pictures of the tubes containing the samples were taken with an iPhone mini 13 (Apple). Microscopy images were acquired using a fluorescence confocal microscope (LSM 700, Zeiss) with ×63 oil immersion objective. Dyes were excited by using the following excitation (λex): FITC-dextran, λex = 488 nm; Nile Red, λex = 555 nm. The microscopy images were processed using ImageJ software, following the method introduced by Gaillard et al., (Gaillard et al., 2015) in order to obtain the

area of 50 droplets for each sample. Long-term evolution of the W/W was also done through microscopy observations of the samples using an epifluorescence microscope (Zeiss Axioskop 2 Plus, Oberkochen, Germany) with ×40 objective.

4.1.2.6 Structural characterization of W/W emulsions by Small Angle X-ray Scattering (SAXS)

SAXS experiments were performed on a XEUSS 2.0 device (XENOCS, Grenoble, France) operating under vacuum with a GeniX3D microsource (λ = 1.54 Å) at 0.6 mA and 50 kV and a 2D Pilatus 3 R 200 K detector. The sample was loaded in thin quartz capillaries (optical path 1.5 mm, WJM-Glas/Müller GmbH, Germany) and the signal collected for 3h. The detector was placed perpendicularly to the direct beam at distance of 2.3m, calibrated in both cases with a Silver Behenate standard. Peak fit® software was used for diffractogram deconvolution by using combination of Gaussian and Lorentzian functions.

4.1.2.7 Determination of the critical micellar concentration (CMC) via surface tension

The CMC values of the surfactants were obtained by using the automatized surface tension plate reader Kibron Delta-8 (Kibron, Finland). A volume of 50 µL of aqueous dispersion was placed on the 96-hole platform. Measurements were performed in duplicate at 28 ± 1 °C after a waiting time of 10 minutes to ensure equilibrium at the air-water interface. A calibration was performed by using ultrapure water at 28 ± 1 °C.

4.1.2.8 Evaluation of the W/W stability by centrifugation

The samples were centrifuged in a centrifuge (Sigma 6K15, Thermo Fisher Scientific, Strasbourg, France) at 1500 × g for 10 minutes. Microscopy images of the samples were taken before and after centrifugation using an epifluorescence microscope (Zeiss Axioskop 2 Plus, Oberkochen, Germany) with ×40 objective.

4.1.2.9 Statistical Analysis

The radius of 50 droplets was calculated for each sample and the average and standard deviation were determined. The results were compared by one-way analysis of variance and Tukey's test to analyze statistical differences ($p < 0.05$). The analysis was performed using SAS V8.0

software (SAS Institute, Gary, NC, USA).

4.1.3 Results and discussion

4.1.3.1 Phase diagram of the W/W emulsions

Dextran-in-PEG emulsions were prepared at 3.25 wt.% (W/W) dextran (450-650 kg/mol) and at 7 wt.% (W/W) PEG (20 kg/mol), since at this composition the polymers were fully phase-separated as determined previously in the literature (Diamond and Hsu, 1989). In these experimental conditions, dextran enriched droplets formed in the continuous enriched PEG phase. Droplets of ca. 10-50 µm formed upon shaking when observed immediately after preparation but coalesced with time yielding macroscopic phase separation as already described in the literature (Coudon et al., 2022).

Then, we added different quantities of decyl glucoside (DG) and decanol varying from 1 to 12 mM as described in the Materials and Methods Section. The concentration of the APGs varied from 2 to 20 times the CMC (**Supplementary Figure.1** and **Supplementary Figure.2**). The molar ratio (R) corresponds to the moles number between decanol and DG, and it varied from 1:0 to 0:1. The stability of the W/W emulsions were determined after 24 hours at room temperature with the naked eye to eventually determine the presence of a phase separation or a supernatant (**Figure 4.1.1**). When phase separation occurred, we defined this W/W emulsion as unstable. When a small supernatant was observed, we classified this emulsion as medium stability, and when no macroscopic change was observed, we defined these emulsions as stable (**Figure 4.1.1**).

The addition of the pure components, either DG or decanol, whatever the concentrations led to complete phase separation of the aqueous emulsion within 3 hours. Then, the pure components did not have a significant effect on the behavior of the polymer's mixtures, and they could not stabilize dextran-rich droplets. However, the addition of the two components (DG and decanol) led to stabilization of emulsions for a relatively large domain of concentrations and molar ratios.

A minimal concentration of DG (6 mM) and a minimal fraction of decanol (R= 0.5:1) were required to produce emulsions with medium stability. At the same DG concentration (6 mM), and with higher decanol fractions (R= 1:1 and R=2:1) emulsions with high stability were observed. However, when the decanol fraction was further increased (R ≥ 3:1), a supernatant was observed after 24 h leading to an emulsion with medium stability. When the concentration of DG was increased to 9 mM, an emulsion with medium stability was only observed for low R (R = 0.5:1). Then, emulsions with no supernatant were observed after 24 hours for all the other R studied (1:1 > R ≥ 9:1). At a DG concentration of 12 mM, emulsions with high stability were obtained both at low decanol fraction and at high decanol fractions (from R = 0.5:1 to R = 9:1).

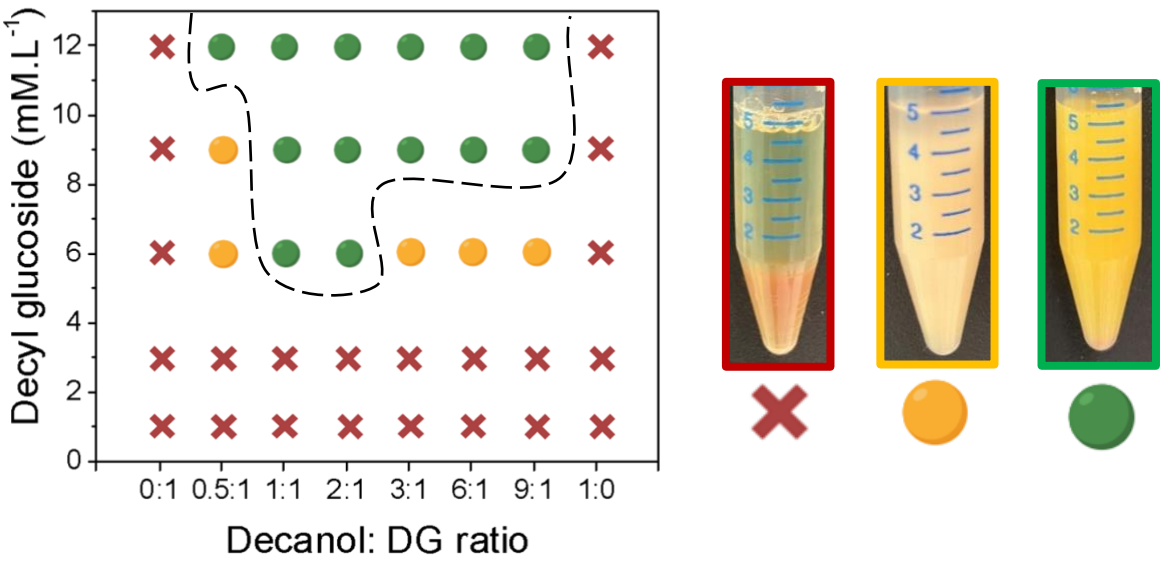

Figure 4.1.1. Partial phase diagram determined by visual observations by varying the decyl glucoside (DG) concentration as a function of the molar ratio between decanol and decyl glucoside showing the stable domain of W/W emulsion (dashed black line). Red crosses correspond to samples where macroscopic phase separation occurred after 24 hours. Orange circles correspond to samples where a slight macroscopic phase separation occurred after 24 hours. Green circles correspond to stable samples after 24 hours. On the right side, pictures of samples illustrate the three regimes. The samples are from left to right: unstable W/W emulsion

for DG = 9 mM and R = 0:1, medium stability W/W emulsion for DG = 6 mM and R = 3:1, and high stability W/W emulsion for DG = 9 mM and R = 2:1.

We then decided to test the substitution of the DG by another APG with a longer alkyl chain: lauryl glucoside (LG). Dextran-in-PEG emulsions were then prepared with different concentrations of LG from 1 to 12 mM and with a molar ratio (R) between decanol and LG, R varying from 1:0 to 0:1. The stability of the W/W emulsions were determined in the same way as for the emulsions stabilized with DG described previously (**Figure 4.1.2** and **Supplementary table 1.b**). The addition of pure LG whatever the concentration led to complete phase separation within 3 hours, as previously described for pure DG or pure decanol. The addition of decanol in combination with LG was necessary to stabilize the emulsions. A minimal concentration of LG (6 mM) and a minimal fraction of decanol ($R \geq 0.5:1$) were required to produce emulsions with medium stability. This result was similar to the one obtained for DG. When the molar ratio was increased ($R \geq 1:1$), emulsions with high stability were obtained for all the concentrations (6, 9 and 12 mM). The increase of the concentration of LG to 12 mM led to emulsions with high stability even at a minimal fraction of decanol (R = 0.5:1). Stable emulsions with LG were produced for a wider range of R in comparison to DG (**Figure 4.1.1** and **Figure 4.1.2**).

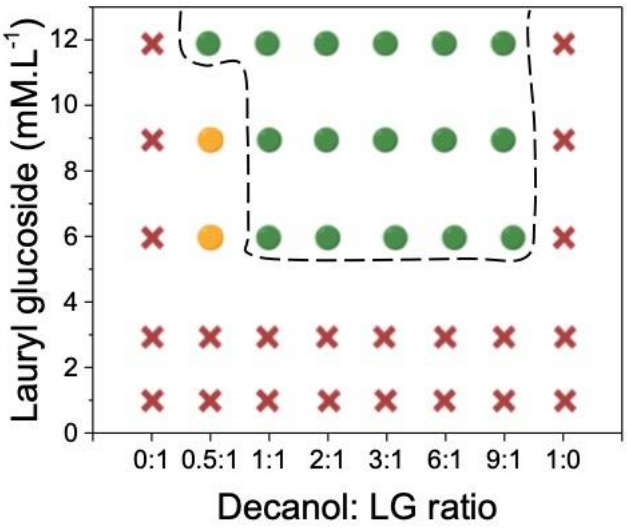

Figure 4.1.2. Partial phase diagram determined by visual observations by varying the lauryl glucoside (LG) concentration as a function of the molar ratio between decanol and Lauryl glucoside showing the stable domain of W/W emulsion (dashed black line). Red crosses correspond to samples where macroscopic phase separation occurred after 24 hours. Orange circles correspond to samples where a slight macroscopic phase separation occurred after 24 hours. Green circles correspond to stable samples after 24 hours.

Then, we also determined the droplets size evolution between the initial size (t=0, that stands for observations done immediately after mixing all components) and after 24 hours with statistical analysis by confocal fluorescence microscopy of the samples doped with FITC-dextran and Nile red (**Figure 4.1.3**, **Supplementary Figure 3** and **Supplementary Table 1.a-b**). First, we compared the initial droplets size between DG and LG for all the R and concentrations to determine the main parameters leading to the smallest droplets size. For DG with R = 0.5:1, by varying the concentration from 6 mM to 12 mM, we observed a decrease of the average radius from 7.3 ± 3.6 µm to 2.1 ± 1 µm. The same trend was observed for all the concentrations and all the R showing that the initial droplet sizes decreased by increasing the DG concentration (**Figure 4.1.3**). For LG with R = 0.5:1, by varying the concentration from 6

mM to 12 mM, we observed a decrease of the average radius from 5.9 ± 3.1 μm to 3 ± 1.1 μm, respectively for 6 mM and 9 mM. However, there was no statistical differences from 9 mM to 12 mM, with an average radius of 3 ± 1.1 μm and of 2 ± 0.5 μm for example for R = 0.5:1. The concentration of the APG was a key parameter for controlling the initial droplet size. We hypothesize that by increasing APGs concentration leading also to a concomitant increase of decanol in the formulation, an increase of viscosity of the bulk phase could occur leading to a decrease of the droplets size. However, it is important to keep in mind that other parameters could also explain this phenomenon: quantity and structure of the self-assembly formed, interaction between APGs and polymers, etc.

Between the two APGs, we observed also statistical differences between the initial droplet sizes, with bigger droplets for DG than for LG when the concentration was set at 6 mM and 9 mM. However, the initial droplet size was the same at 12 mM for both APGs. The difference between DG and LG could be explained by the fact that APGs have different CMC values (**Supplementary Figure 1**), with LG having a lower CMC than DG. Here, all the samples were produced above the CMC. However, at the same concentration, LG with a longer alkyl chains and lower CMC than DG produce more easily rod-like micelles (Platz et al., 1995). Thus, it is easier to transit from rod-like micelles to lamellar phases by adding a small amount of fatty alcohol than from spherical micelles. Moreover, the presence of an excess of lauryl glucoside under rod-like micelles leading to a more viscous bulk continuous phase than for DG under spherical micelles could also explain the difference of stability at the lowest concentration (6 mM) (Stradner et al., 2000; Chu et al., 2013) . We believe that the presence of rod-like micelles helps with the formation of the lamellar phases that stabilize the droplets. Then, we studied the effect of the molar ratio (R) between decanol and the APGs (DG or LG) on the initial droplets size (**Supplementary table 1.a-b**). For DG at the three concentrations, we observed that for R = 0.5:1 the initial droplet size was always higher than for all the others R. The same trend was observed for LG. For R = 0.5:1, there was an excess of APGs in comparison to the decanol which could lead to the formation of a low quantity of lamellar structures in a mixture with

APGs micelles and mixed micelles containing decanol (Möller et al., 1998). The quantity of lamellar strcutures could be not sufficient to stabilize small droplets during the production of the W/W emulsion. Then, we observed for both LG and DG that for R with high amount of decanol in comparison to the APG (R = 6:1 and R = 9:1), the droplet size was statistically lower than for R = 0.5:1 with an excess of APGs, but always higher than for intermediate R: R = 3:1, R =2:1 and R =1:1 (**Figure 4.1.3** and **Supplementary Figure 3**). The best R to have high stability with small droplet size were R = 3:1, R =2:1 and R =1:1. These three R lead to the smallest droplet size. Therefore, R is also a key parameter to take into account to reach small droplet size. A large excess of APG (R = 0.5:1) or decanol (R ≥ 6:1) is not appropriate for small droplet size. We compared also the droplet size evolution after 24 hours for all the stable samples detected by visual observations (**Figure 4.1.1** and **Figure 4.1.2**). No statistical difference was observed showing that in all cases the droplet size was stable after 24 hours (**Figure 3.1.3**, **Supplementary Figure 3** and **Supplementary Table 1.a-b**). Again, the composition (concentration and molar ratio) had been shown to influence the diameter of droplets in a similar system (Coudon et al., 2022).

Our results confirm that stabilization of the interface between hydrophilic polymers is not possible using amphiphilic molecules alone (Esquena, 2016). Instead, changing the self-assembly of these molecules by adding fatty alcohol proves to be an effective method to produce stable all-aqueous droplets (Coudon et al., 2022; Esquena, 2023). In addition, our results highlight that to obtain stable emulsions based on mixture of fatty alcohol and APGs, whatever the type of oil-in-water or water-in-water emulsion, a minimum molar ratio of 1:1 fatty alcohol:surfactant is required (Terescenco et al., 2018b). As described in the literature for LGNs formation based on mixture of fatty alcohols and surfactants, a minimum amount of fatty alcohol is required, and it is reported to be close to a weight ratio 1:1 as found in this study (Eccleston, 1997). Moreover, comparing our results to those obtained for LGNs based on sodium oleate and decanol, we observe that whatever the nature of the surfactants (anionic or

non-ionic surfactants) with fatty alcohol, stable W/W emulsions are only possible for a molar ratio higher than 1:1 (Coudon et al., 2022).

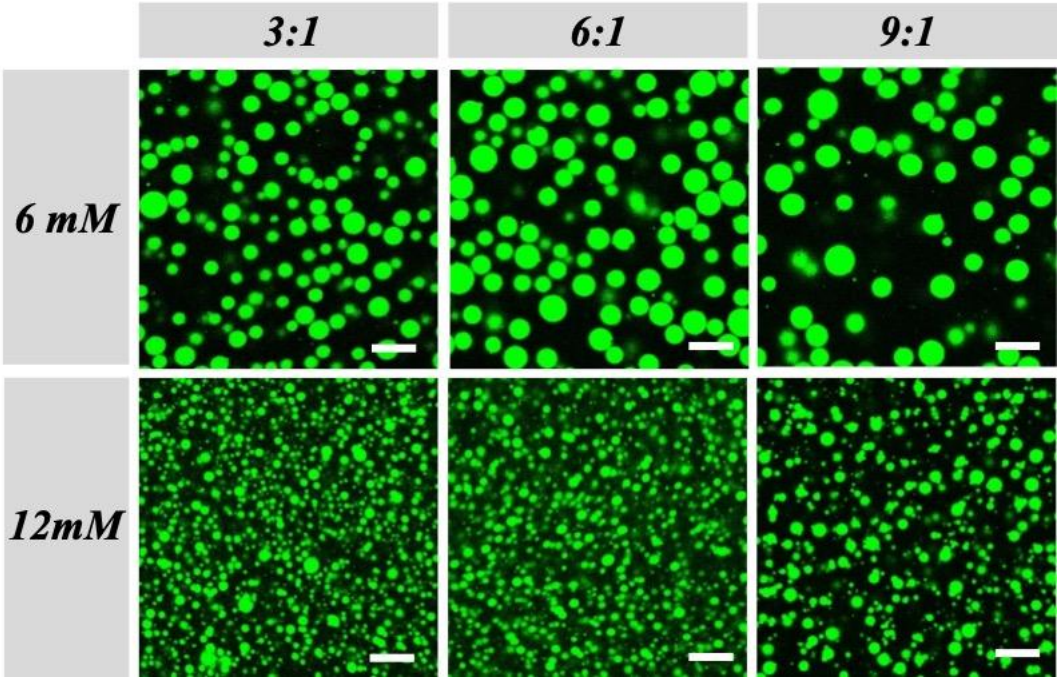

Figure 4.1.3. Effect of both DG concentration and decanol:DG ratio (R) on W/W emulsions droplets size. Confocal microscopy images of the W/W emulsions taken at t=0 for two different DG concentrations: 6 mM (top) and 12 mM (bottom), and three different R: R = 3:1(left), R = 6:1 (middle) and R = 9:1 (right). Droplets are labeled with FITC-dextran dye. The scale bar represents 15 μm.

4.1.3.2 Long-term stability of W/W emulsions stabilized by LGNs

The long-term stability of the emulsions was studied by microscopy observations during 42 days. Fluorescence microscopy observations of the emulsions stabilized with DG at a concentration of 12 mM and with R =3:1 showed the presence of uniform droplets that did not change significantly in size after 7 days compared to t=0 (average radius = 1.4 ± 0.4 μm) (**Supplementary Figure 4.a**). However, after 7 days a macroscopic phase separation was observed with the naked eye. Microscopy observations of the emulsions stabilized with LG at a concentration of 12 mM and with R = 3:1 showed the presence of uniform droplets that did not change significantly in size after 42 days compared to t=0 (average radius = 1.6 ± 0.6 μm)

(**Supplementary Figure 4.b**). In addition, we tested the robustness of the emulsions with centrifugation. After centrifugation at 1500 × g for 10 minutes, we observed neither phase separation nor supernatant showing that the self-assembled structure formed by decanol and APGs form a robust layer protecting the droplets against mechanical stress. We also checked the effect of the centrifugation directly on the droplets by measuring the droplets size before and after the centrifugation (**Figure 4.1.4**). The results show that both emulsions could be centrifuged without significant change in the droplet radius (average radius before centrifugation: 2.1 ± 0.7 μm and 1.7 ± 0.5 μm, respectively for DG and LG; average radius after centrifugation= 2.0 ± 0.6 μm for DG, and 1.8 ± 0.4 μm for LG) confirming that the self-assembled strcutures formed by APGs and decanol both in bulk and at the interface led to strong protection of the emulsion against destabilization.

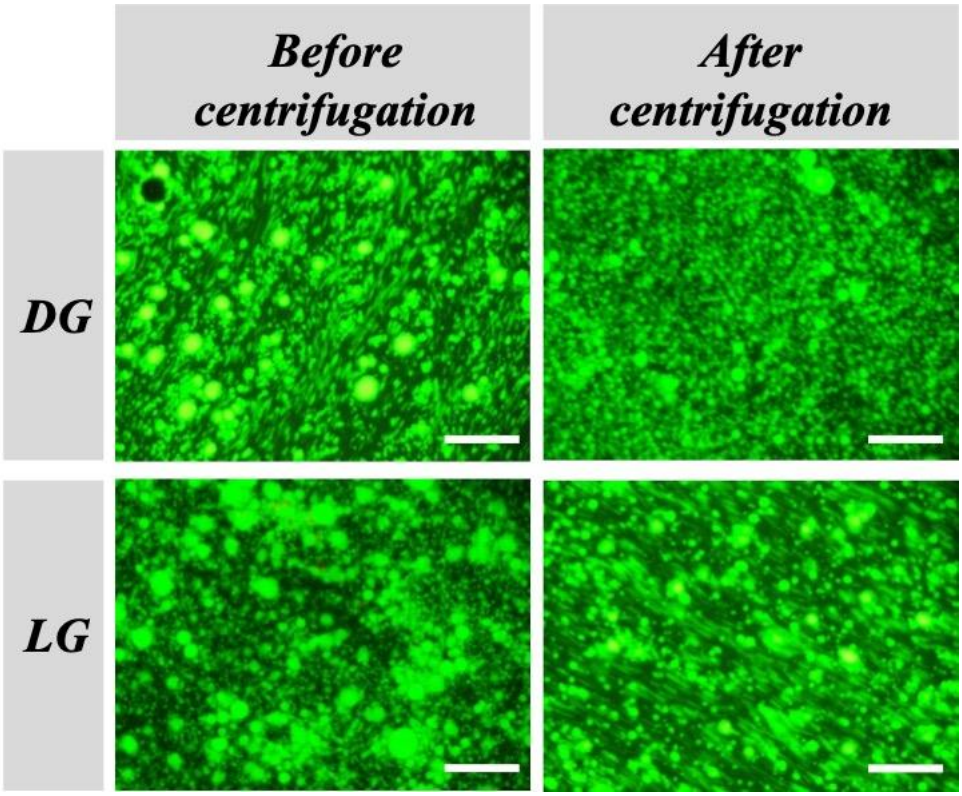

Figure 4.1.4. Effect of centrifugation on the stability of the W/W emulsions. Epifluorescence microscopy images of W/W emulsions stabilized with DG (top) or LG (bottom) at a concentration of 12 mM with a molar ratio of R = 3:1, taken before centrifugation (left) and after centrifugation (right). Droplets are labeled with FITC-dextran dye. The scale bar represents 60 μm.

4.1.3.3 Structural characterization of W/W emulsions

After establishing the phase diagrams of the W/W emulsions stabilized by the mixture of decanol and APGs, we tried to characterize the structure formed by the decanol:APGs in bulk and at the interface leading to the long-term stabilization of the droplets for specific ratios. By using confocal fluorescence microscopy with Nile red staining, the fatty alcohol, it was possible to highlight the presence of surfactant assemblies in the bulk phase surrounding the droplets (**Figure 4.1.5.a**). We observed the presence of lamellar structures in the bulk phase surrounding the droplets forming the so-called LGN.

However, with this microscopy technique it is impossible to study the interfacial structure and the eventual formation of LNGs around the droplets, since only a red layer is observed by confocal microscopy surrounding the droplets (**Figure 4.1.5.a**). That is why we used SAXS to get information at the interface scale. The stable emulsion formulated with LG at 12 mM and with R = 3:1 was chosen for SAXS analysis due to the long-term stability and high concentration to optimize the SAXS signal. On the SAXS scattering pattern, only one main peak could be distinguished at Q = 0.035 $Å^{-1}$ (**Figure 4.1.5.b**). By comparing with the literature and the SAXS results obtained by Coudon et al. (Coudon et al., 2022) on similar water-in-water emulsion system stabilized by a mixture of fatty alcohol and sodium oleate, we hypothesize that the peak at 0.035 $Å^{-1}$ is the third order peak of a lamellar phase surrounding the dextran-rich droplets. The lamellar phase would have a lamellar interspacing (d) of around 52 nm ($d= 2\pi/Q0$). Indeed, in the study from Coudon et al., they determined a lamellar spacing of around 78 nm, corresponding to a third order peak around 0.024 $Å^{-1}$ close to the peak determined here (Coudon et al., 2022). In our system, the lamellar spacing was lower than in the case of the lamellar phase made of sodium oleate and decanol system, which can be explained by the fact that we are working with non-ionic surfactant and lamellar phases are stabilized by steric repulsion and not electrostatic repulsion such as in the case of sodium oleate/decanol system. It is known that steric repulsion produced in lamellar gel network based on fatty alcohol leads to lower interlamellar spacing than LGNs produced by anionic surfactants (Iwata, 2017).

Therefore, the long-term stabilization and the resistance to centrifugation of the W/W emulsions could come from the LGNs formed by APGs and decanol both in bulk and at the interface leading to strong protection of the emulsion against destabilization. However, to confirm the interfacial structures, further investigations need to perform. For example, the use of freeze-Fracture transmission electron microscopy could help to better characterize the self-assembled structures formed at the interface as already demonstrated by Coudon et al. (Coudon et al., 2022). It is important also to notice that we do not know the quantity of each chemical components inside the self-assembled structures, and the concentration could be different from the initial weight ratios used to produce the W/W emulsion. Most probably lamellar phases are in coexistence with APGs micelles.

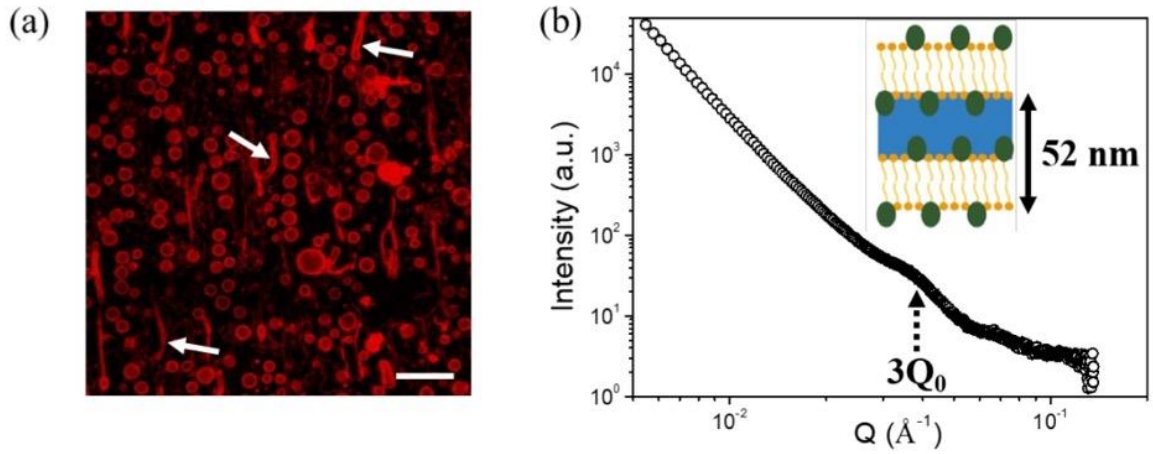

Figure 4.1.5. (a) Confocal microscopy image of dextran-in-PEG emulsion stabilized with LG at a concentration of 9 mM and with a molar ratio of decanol:LG at 1:1, showing the presence of lamellar phases (some of them identified with white arrows) in the continuous phase of the emulsion. Nile red was used to label the surfactant and fatty alcohol. The scale bar represents 15 μm. (b) 1D SAXS diffractogram of a water-in-water emulsion stabilized by a mixture of LG and decanol with a LG concentration of 12 mM and a molar ratio of decanol:LG at 3:1. Only the third order Bragg peak (3Q0) is identified on the scattering pattern, labeled with a black arrow. Schematic showing the stabilization of the W/W emulsion by lamellar phase surrounding the dextran-rich droplets.

4.1.3.4 Versatility of the W/W emulsion stabilized by mixture of fatty alcohols and APGs

Here, we varied the experimental conditions, either the concentration of polymers or the nature of LGNs but investigated only few different concentrations of each to demonstrate the versatility of the systems. First, we studied the effect of LGNs on the stabilization of the inverse W/W emulsion, that is, when polymer concentrations are adjusted so that PEG-rich droplets formed in a continuous dextran-rich phase (**Supplementary Figure 5**). Stable W/W emulsion were produced from both DG and LG at 12 mM with R = 3:1, since no change in the droplets size was observed after 24h. This result shows a general mechanism based on APG and fatty alcohol for stabilizing PEG and dextran interfaces regardless the nature of the droplets, which is in accordance with the observations of Coudon et al. on the stabilization W/W emulsion with decanol and sodium oleate (Coudon et al., 2022).

In a second step, we extended the production of W/W emulsions to another well-known and widely used APG: coco-glucoside (CG), composed of a mixture of alkyl groups with carbon chain lengths ranging from 8 to 16 atoms and with a higher proportion of longer alkyl chains in comparison to DG and LG (Aguirre et al., 2014). Self-assembled structures (lamellar phases and/or micelles) produced with CG 12 mM at different decanol: CG molar ratios, from R=1:1 to R=6:1, effectively stabilized dextran-in-PEG emulsions, since microscopy images showed that no significant differences in the droplet size were observed after 24h compared to the initial size (**Supplementary Figure 6**).

Finally, we extended our approach of stabilizing W/W emulsions produced from DG and LG to other fatty alcohols with longer alkyl chain length (dodecanol and myristyl alcohol) (**Figure 4.1.6** and **Supplementary Figure 7**). Microscopy images showed that dextran-in-PEG emulsions with high stability can be produced with DG at a concentration of 12 mM in combination with dodecanol (dodecanol:DG molar ratio R = 6:1), since no significant differences in the droplet size were shown after 24h compared to the initial size (average radius 4 ± 1.2 µm). The same observations were performed for emulsions stabilized with LG at a concentration of 12 mM (dodecanol:LG molar ratio R = 6:1) but the droplet size was slightly

smaller (average radius 2.2 ± 0.7 µm at t=0). The stabilization of dextran-in-PEG emulsion with APG and myristyl alcohol was also possible. Emulsions stabilized with DG at a concentration of 12 mM and myristyl alcohol (R = 6:1), showed high stability without significant changes in droplet size after 24h compared to the initial size (average radius = 3.2 ± 0.7 µm). The same emulsion stabilized with LG at a concentration of 12 mM (R = 6:1) led to a decrease in droplet size (average radius 1.6 ± 0.3 µm at t=0), with no significant change in size after 24h. These results show that it is possible to formulate W/W emulsions using APGs and different fatty alcohols. Thus, W/W emulsion stabilization is possible by using APGs and fatty alcohol when suitable concentration and ratios are used to obtain self-assembled structures such as lamellar phases.

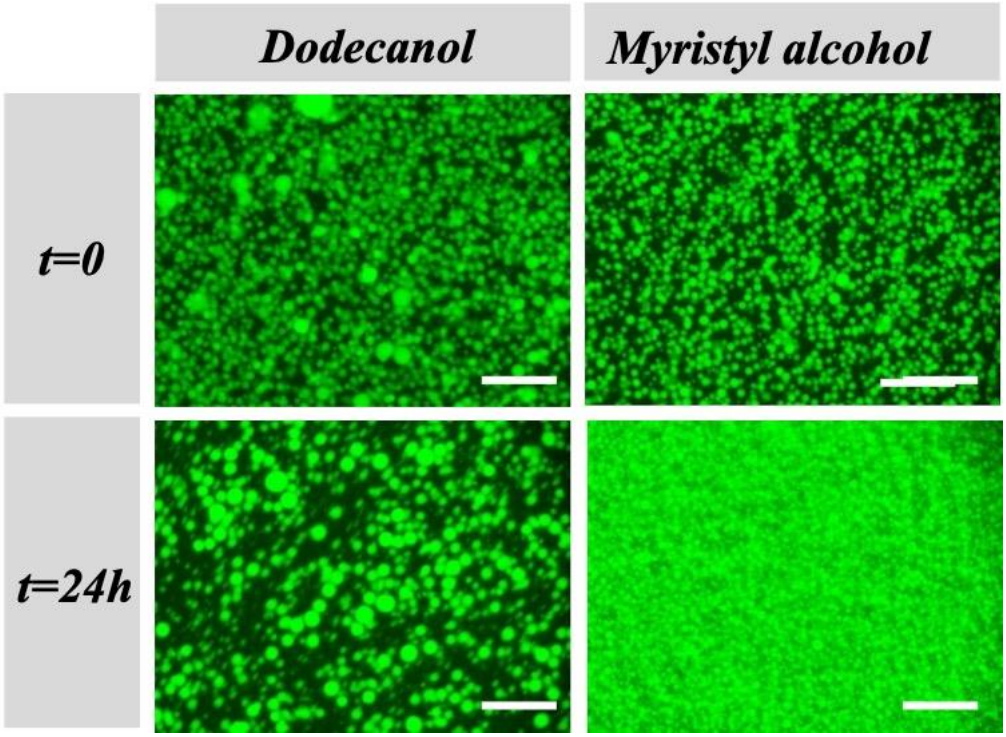

Figure 4.1.6. W/W emulsions stabilized with DG in combination with two different fatty alcohols: dodecanol and myristil alcohol. Epifluorescence microscopy images of W/W emulsions stabilized with DG at 12 mM and Dodecanol: DG ratio equal to 6:1 (left) and DG at 12 mM and myristyl alcohol: DG ratio equal to 6:1 (right), taken at t=0 (top) and at t=24h (bottom). Droplets are labeled with FITC-dextran dye. The scale bars represent 60 µm.

For certain applications, bubbles are added into emulsions to change their mechanical properties and/or sensorial performances (Salonen, 2020). It is the case, for example, for ice creams, whipped creams and pharmaceutical or cosmetic applications (Parsa et al., 2019; Murray, 2020; Luengo et al., 2021). These three phase systems are called foamulsions or "foamed emulsions", where the gas bubbles are surrounded by a continuous phase, traditionally composed of oil and water (Salonen, 2020; Zheng et al., 2022). The continuous phase is generally present in the form of oil-in-water emulsions, although it can also be in the form of water-in-oil emulsions (Salonen, 2020). However, to the best of our knowledge, a foamulsion where the continuous phase is composed of W/W emulsions has never been reported. We took the advantage of the high stability of the W/W emulsions developed here to study the possibility of producing a foamulsion by using dextran-in-PEG emulsion as the continuous phase of the foam. First, we prepared a dextran-in-PEG emulsion (10 wt.% of dextran and 10 wt.% of PEG) stabilized with LG at a concentration of 12 mM and with a molar ratio of decanol: LG equal to 3:1. Then, the double-syringe technique was used to produce the foams (Gaillard et al., 2017). First, we measured the foamability, that is to say the quantity of foam produced at the end of the foaming process. Then, the stability of the foams was followed by measuring both the evolution of the foam volume and the volume of drained liquid over time with the naked eye (**Supplementary Figure 8**).

Production of foam from the W/W emulsion stabilized by lamellar structures formed by APGs and fatty alcohols without the addition of additional surfactants was not possible (**Supplementary Figure 8.a**). Then, we tested the addition of surfactant inside the W/W emulsion and we studied the resulting foaming properties. With the addition of DG at a concentration of 18 mM, no foam was produced (**Supplementary Figure 8.b**). However, in the presence of SDS at a concentration of 18 mM, a high quantity of foam which was relatively stable with time was obtained (**Figure 4.1.7.a**). By fluorescence microscopy, the presence of droplets surrounding the air bubbles were clearly distinguished similar to the ones observed for foamulsion based on oil-in-water emulsion (**Figure 4.1.7.b**) (Salonen, 2020). The initial foam

volume was around 10.5 mL showing the good foamability of the foamulsion. Then, the foam volume decreased slightly in the first 4 hours to reach a foam volume around 7 mL associated with drainage (liquid volume inside the foam around 1 mL after 4 hours). After 24 hours, no more foam was present only few bubbles remained (**Figure 4.1.7.a** and **Supplementary Figure 9**). We performed control experiments by producing foams with only dextran and SDS or only PEG and SDS at the same concentration (18 mM). The foamulsion stabilized by mixture of fatty alcohols and APGs with 18 mM of SDS was observed to be much more stable than the foams produced with only dextran or only PEG since these controlled foams disappeared after 2-3 hours (**Supplementary Figure 10.a-b**). In the same way, no more foam was present after 3 hours when foam was produced directly from the pure W/W emulsion not stabilized by fatty alcohols and APGs and with only SDS (**Supplementary Figure 10.c**).

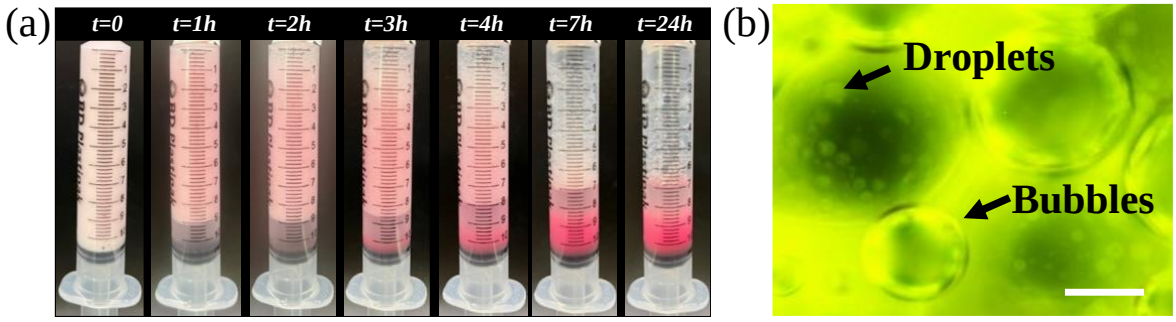

Figure 4.1.7. (a) Stability of the foamulsion. Pictures of the foam produced with the W/W emulsion (LG 12 mM, decanol: LG ratio 3:1) with the addition of SDS at 18mM and its evolution over time. (b) Epifluorescence microscopy image of the foamulsion at t=0. Droplets are labeled with FITC-dextran dye. The scale bar represents 30 μm.

4.1.4 Conclusion

In this study, we demonstrated that W/W emulsions can be efficiently stabilized by mixtures of APGs and fatty alcohol. The stability of the W/W emulsions is linked to the APGs concentration and the molar ratio between the APG and the fatty alcohol. We demonstrated the robustness of this system by using various APGs: decyl glucoside, lauryl glucoside and coco-glucoside, and

also by using fatty alcohols with different alkyl chain lengths (decanol, dodecanol and myristyl alcohol). An effect of the APGs alkyl chain length between DG and LG was observed, since the use of LG made it possible to produce emulsions with the same droplet size as with DG but at a lower concentration. In addition, emulsions prepared with LG were more stable in the long-term than emulsions prepared with DG. The molar ratio between the fatty alcohol and the APG is also a key parameter governing the stability. We hypothesized that the mixture of fatty alcohols and APGs led to the formation of LGNs stabilizing the W/W emulsions due to their presence both in the bulk phase and surrounding the droplets. The structure of the LGNs seems to depend on the molar ratio and APG concentration in the same way already described in aqueous solution (Terescenco et al., 2018a, 2018b).

Altogether, this confirms that stabilization of such aqueous droplets occurs when the chemicals (and eventually their assemblies) used for this task have an equivalent affinity for both the polymer within droplets and the polymer in the continuous phase. We believe that adjusting the concentrations and molar ratio control this affinity and affords chemicals to come and stay at the droplet interface, further preventing droplet coalescence. Further investigations using freeze-Fracture transmission electron microscopy and small angle neutron scattering are planned to better characterize the self-assembled structures formed both in the bulk and at the interface, and to confirm the formation of LGNs.

With preliminary results, we showed for the first time that the production of a foam based on W/W emulsion is possible; and that its stability is better than the foam produced with the polymers alone or with polymers in mixture without being stabilized by self-assembled structures formed by APGs and fatty alcohols. The inclusion of a third phase to emulsions could be a promising strategy to expand the use of W/W emulsions in various fields (Luengo et al., 2021; Zhili, 2022). Our results offer the possibility to formulate W/W emulsions based on chemical components widely used at industrial scale and at low cost associated with an easy and simple formulation process. Our approach could be extended to more complicated systems such as multiple water-in-water emulsion systems, and they could be used for encapsulation,

drug delivery, as micro reactors, etc. (Solans et al., 2003; Singh et al., 2018; Michaux et al., 2021).

Funding

This research was funded by the Region Hauts de France and the INRAe TRANSFORM department. This study was also supported by the French government through the Program "Investissements d'avenir" (I-SITE ULNE / ANR-16-IDEX-0004 ULNE) managed by the National Research Agency.

Acknowledgments

We acknowledge financial support from INRAe, TRANSFORM department, and region Hauts de France for the PhD grant of C. Dari. C. Dari would like to thank " l'École internationale de recherche d'Agreenium (EIR-A)" and the graduate program "Science for a Changing Planet" for the allocation of her travel grant to University of Edingburgh. Chevreul Institute (FR 2638), Ministère de l'Enseignement Supérieur, de la Recherche et de l'Innovation, Région Hauts de France and FEDER are acknowledged for SAXS facilities.

4.1.5 References

Aguirre, T. A. S., Rosa, M., Guterres, S. S., Pohlmann, A. R., Coulter, I., and Brayden, D. J. (2014). Investigation of coco-glucoside as a novel intestinal permeation enhancer in rat models. European Journal of Pharmaceutics and Biopharmaceutics 88, 856–865. doi: 10.1016/j.ejpb.2014.10.013.

Antonov, Y. A., Van Puyvelde, P., and Moldenaers, P. (2004). Interfacial tension of aqueous biopolymer mixtures close to the critical point. International Journal of Biological Macromolecules 34, 29–35. doi: 10.1016/j.ijbiomac.2004.01.001.

Ben Ayed, E., Cochereau, R., Dechancé, C., Capron, I., Nicolai, T., and Benyahia, L. (2018). Water-In-Water Emulsion Gels Stabilized by Cellulose Nanocrystals. Langmuir 34, 6887–6893. doi: 10.1021/acs.langmuir.8b01239.

Chao, Y., and Shum, H. C. (2020). Emerging aqueous two-phase systems: from fundamentals of interfaces to biomedical applications. Chem. Soc. Rev. 49, 114–142. doi: 10.1039/C9CS00466A.

Chu, Z., Dreiss, C. A., and Feng, Y. (2013). Smart wormlike micelles. Chem. Soc. Rev. 42, 7174–7203. doi: 10.1039/C3CS35490C.

Colafemmina, G., Palazzo, G., Mateos, H., Amin, S., Fameau, A.-L., Olsson, U., et al. (2020). The cooling process effect on the bilayer phase state of the CTAC/cetearyl alcohol/water surfactant gel. Colloids and Surfaces A: Physicochemical and Engineering Aspects 597, 124821. doi: 10.1016/j.colsurfa.2020.124821.

Coudon, N., Navailles, L., Nallet, F., Ly, I., Bentaleb, A., Chapel, J.-P., et al. (2022). Stabilization of all-aqueous droplets by interfacial self-assembly of fatty acids bilayers. Journal of Colloid and Interface Science 617, 257–266. doi: 10.1016/j.jcis.2022.02.138.

Dari, C., Dallagi, H., Faille, C., Dubois, T., Lemy, C., Deleplace, M., et al. (2023). Decontamination of Spores on Model Stainless-Steel Surface by Using Foams Based on Alkyl Polyglucosides. Molecules 28, 936. doi: 10.3390/molecules28030936.

de Oliveira, T. E., Leonforte, F., Nicolas-Morgantini, L., Fameau, A.-L., Querleux, B., Thalmann, F., et al. (2020). Fluid bilayer phase in aqueous mixtures of fatty alcohol and cationic surfactant. Phys. Rev. Res. 2, 013075. doi: 10.1103/PhysRevResearch.2.013075.

Dewey, D. C., Strulson, C. A., Cacace, D. N., Bevilacqua, P. C., and Keating, C. D. (2014). Bioreactor droplets from liposome-stabilized all-aqueous emulsions. Nat Commun 5, 4670. doi: 10.1038/ncomms5670.

Diamond, A. D., and Hsu, J. T. (1989). Phase diagrams for dextran-PEG aqueous two-phase systems at 22°C. Biotechnol Tech 3, 119–124. doi: 10.1007/BF01875564.

Dickinson, E. (2019). Particle-based stabilization of water-in-water emulsions containing mixed biopolymers. Trends in Food Science & Technology 83, 31–40. doi: 10.1016/j.tifs.2018.11.004.

Douliez, J.-P., Martin, N., Beneyton, T., Eloi, J.-C., Chapel, J.-P., Navailles, L., et al. (2018). Preparation of Swellable Hydrogel-Containing Colloidosomes from Aqueous Two-Phase Pickering Emulsion Droplets. Angew Chem Int Ed Engl 57, 7780–7784. doi: 10.1002/anie.201802929.

Douliez, J.-P., Perro, A., and Béven, L. (2019). Stabilization of All-in-Water Emulsions To Form Capsules as Artificial Cells. Chembiochem 20, 2546–2552. doi: 10.1002/cbic.201900196.

Eccleston, G. M. (1997). Functions of mixed emulsifiers and emulsifying waxes in dermatological lotions and creams. Colloids and Surfaces A: Physicochemical and Engineering Aspects 123–124, 169–182. doi: 10.1016/S0927-7757(96)03846-0.

Esquena, J. (2016). Water-in-water (W/W) emulsions. Current Opinion in Colloid & Interface Science 25, 109–119. doi: 10.1016/j.cocis.2016.09.010.

Esquena, J. (2023). Recent advances on water-in-water emulsions in segregative systems of two water-soluble polymers. Current Opinion in Food Science 51, 101010. doi: 10.1016/j.cofs.2023.101010.

Gaillard, T., Honorez, C., Jumeau, M., Elias, F., and Drenckhan, W. (2015). A simple technique for the automation of bubble size measurements. Colloids and Surfaces A: Physicochemical and Engineering Aspects 473, 68–74. doi: 10.1016/j.colsurfa.2015.01.089.

Gaillard, T., Roché, M., Honorez, C., Jumeau, M., Balan, A., Jedrzejczyk, C., et al. (2017). Controlled foam generation using cyclic diphasic flows through a constriction. International Journal of Multiphase Flow 96, 173–187. doi: 10.1016/j.ijmultiphaseflow.2017.02.009.

Iwata, T. (2017). “Lamellar Gel Network,” in Cosmetic Science and Technology (Elsevier), 415–447. doi: 10.1016/B978-0-12-802005-0.00025-2.

Junginger, H. E. (1984). Colloidal structures of O/W creams. Pharmaceutisch Weekblad Scientific Edition 6, 141–149. doi: 10.1007/BF01954041.

Keck, C. M., Kovačević, A., Müller, R. H., Savić, S., Vuleta, G., and Milić, J. (2014). Formulation of solid lipid nanoparticles (SLN): The value of different alkyl polyglucoside surfactants. International Journal of Pharmaceutics 474, 33–41. doi: 10.1016/j.ijpharm.2014.08.008.

Leal-Calderon, F., Bibette, J., and Schmitt, V. (2007). Emulsion Science: Basic Principles. New York, NY: Springer New York doi: 10.1007/978-0-387-39683-5.

Luengo, G. S., Fameau, A.-L., Léonforte, F., and Greaves, A. J. (2021). Surface science of cosmetic substrates, cleansing actives and formulations. Adv Colloid Interface Sci 290, 102383. doi: 10.1016/j.cis.2021.102383.

Merland, T., Waldmann, L., Guignard, O., Tatry, M.-C., Wirotius, A.-L., Lapeyre, V., et al. (2022). Thermo-induced inversion of water-in-water emulsion stability by bis-hydrophilic microgels. Journal of Colloid and Interface Science 608, 1191–1201. doi: 10.1016/j.jcis.2021.10.074.

Michaux, M., Salinas, N., Miras, J., Vílchez, S., González-Azón, C., and Esquena, J. (2021). Encapsulation of BSA/alginate water–in–water emulsions by polyelectrolyte complexation. Food Hydrocolloids 113, 106406. doi: 10.1016/j.foodhyd.2020.106406.

Möller, A., Lang, P., Findenegg, G. H., and Keiderling, U. (1998). Location of Butanol in Mixed Micelles with Alkyl Glucosides Studied by SANS. J. Phys. Chem. B 102, 8958–8964. doi: 10.1021/jp981819q.

Murray, B. S. (2020). Recent developments in food foams. Current Opinion in Colloid & Interface Science 50, 101394. doi: 10.1016/j.cocis.2020.101394.

Nakarapanich, J., Barameesangpet, T., Suksamranchit, S., Sirivat, A., and Jamieson, A. M. (2001). Rheological properties and structures of cationic surfactants and fatty alcohol emulsions: effect of surfactant chain length and concentration. Colloid Polym Sci 279, 671–677. doi: 10.1007/s003960000470.

Nguyen, B. T., Nicolai, T., and Benyahia, L. (2013). Stabilization of Water-in-Water Emulsions by Addition of Protein Particles. Langmuir 29, 10658–10664. doi: 10.1021/la402131e.

Nicolai, T., and Murray, B. (2017). Particle stabilized water in water emulsions. Food Hydrocolloids 68, 157–163. doi: 10.1016/j.foodhyd.2016.08.036.

Parsa, M., Trybala, A., Malik, D. J., and Starov, V. (2019). Foam in pharmaceutical and medical applications. Current Opinion in Colloid and Interface Science 44, 153–167. doi: 10.1016/j.cocis.2019.10.007.

Platz, G., Poelike, J., Thunig, C., Hofmann, R., Nickel, D., and Rybinski, W. von (1995). Phase Behavior, Lyotropic Phases, and Flow Properties of Alkyl Glycosides in Aqueous Solution. Langmuir 11, 4250.

Poortinga, A. T. (2008). Microcapsules from self-assembled colloidal particles using aqueous phase-separated polymer solutions. Langmuir 24, 1644–1647. doi: 10.1021/la703441e.

Salonen, A. (2020). Mixing bubbles and drops to make foamed emulsions. Current Opinion in Colloid & Interface Science 50, 101381. doi: 10.1016/j.cocis.2020.08.006.

Savic, S., Vuleta, G., Daniels, R., and Muller-Goymann, C. C. (2005). Colloidal microstructure of binary systems and model creams stabilized with an alkylpolyglucoside non-ionic emulsifier. Colloid Polym Sci 283, 439–451. doi: 10.1007/s00396-004-1174-4.

Singh, P., Medronho, B., Miguel, M. G., and Esquena, J. (2018). On the encapsulation and viability of probiotic bacteria in edible carboxymethyl cellulose-gelatin water-in-water emulsions. Food Hydrocolloids 75, 41–50. doi: 10.1016/j.foodhyd.2017.09.014.

Solans, C., Esquena, J., and Azemar, N. (2003). Highly concentrated (gel) emulsions, versatile reaction media. Current Opinion in Colloid & Interface Science 8, 156–163. doi: 10.1016/S1359-0294(03)00021-9.

Stradner, A., Glatter, O., and Schurtenberger, P. (2000). A Hexanol-Induced Sphere-to-Flexible Cylinder Transition in Aqueous Alkyl Polyglucoside Solutions. Langmuir 16, 5354–5364. doi: 10.1021/la991679r.

Terescenco, D., Picard, C., Clemenceau, F., Grisel, M., and Savary, G. (2018a). Influence of the emollient structure on the properties of cosmetic emulsion containing lamellar liquid crystals. Colloids and Surfaces A: Physicochemical and Engineering Aspects 536, 10–19. doi: 10.1016/j.colsurfa.2017.08.017.

Terescenco, D., Savary, G., Clemenceau, F., Merat, E., Duchemin, B., Grisel, M., et al. (2018b). The alkyl polyglucoside/fatty alcohol ratio effect on the formation of liquid crystal phases in binary systems. Journal of Molecular Liquids 253, 45–52. doi: 10.1016/j.molliq.2017.12.149.

Wu, P.-S., Lin, C.-H., Kuo, Y.-C., and Lin, C.-C. (2017). Formulation and Characterization of Hydroquinone Nanostructured Lipid Carriers by Homogenization Emulsification Method. Journal of Nanomaterials 2017, 1–7. doi: 10.1155/2017/3282693.

Xie, Y., Ruan, M., Zhang, J., Kibtia, M., Li, Y., Li, B., et al. (2023). Water-in-water Pickering emulsion stabilized by cellulose nanocrystals as space-confined encapsulating systems: From establishment to stability. Food Hydrocolloids 141, 108719. doi: 10.1016/j.foodhyd.2023.108719.

You, K.-M., Murray, B. S., and Sarkar, A. (2023). Tribology and rheology of water-in-water emulsions stabilized by whey protein microgels. Food Hydrocolloids 134, 108009. doi: 10.1016/j.foodhyd.2022.108009.

Zhang, J., Xie, Y., Liu, C., Cao, H., Li, Y., Li, B., et al. (2024). Water-in-water Pickering emulsion: A fascinating microculture apparatus for embedding and cultivation of Lactobacillus helveticus. Food Hydrocolloids 147, 109398. doi: 10.1016/j.foodhyd.2023.109398.

Zheng, R., Hu, X., Su, C., Jiang, J., Cui, Z., and Binks, B. P. (2022). Edible oil-water foamulsions stabilized by vesicle network of sucrose ester. Journal of Molecular Liquids 371. doi: 10.1016/j.molliq.2022.121066.

Zhili, W. (2022). Editorial overview: Moving towards designing new food colloids for healthy and sustainable foods. Current Opinion in Food Science 46, 100844. doi: 10.1016/j.cofs.2022.100844.

Supplementary Material: Mixture of fatty alcohols and alkylpolyglucosides stabilizing Water-in-water Emulsions

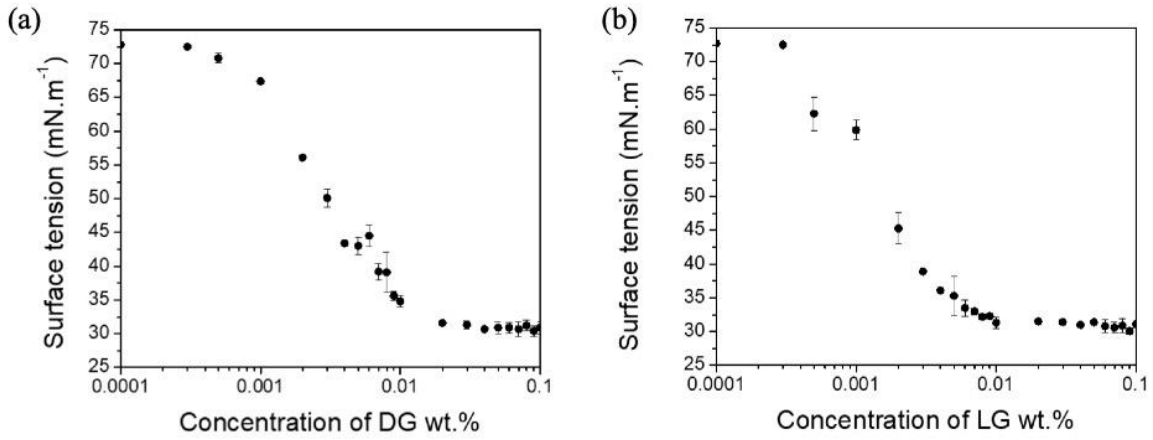

Supplementary Figure 1. Surface tension of aqueous solutions of (a) DG and (b) LG as a function of the concentration at T = 28 ± 1°C. The CMC were 0.6 mM for DG and 0.3mM for LG.

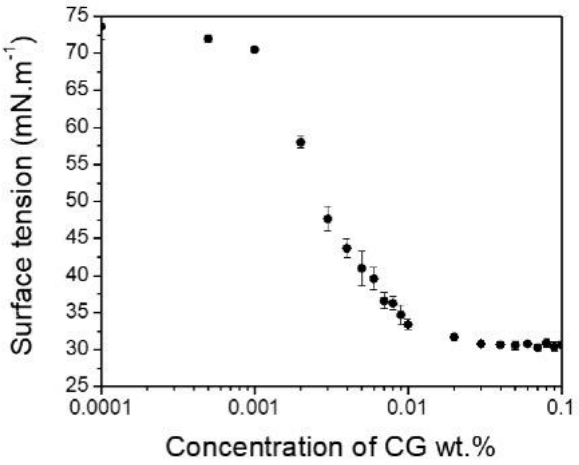

Supplementary Figure 2. Surface tension of aqueous solutions of CG as a function of the concentration at T = 23.1 ± 0.9°C. The CMC was 0.9 mM.

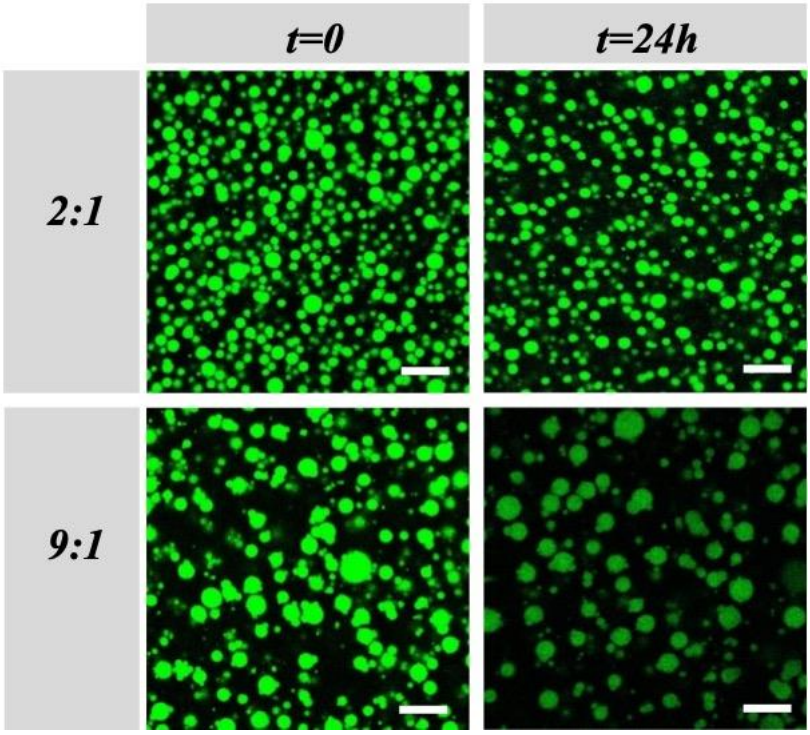

Supplementary Figure 3. Effect of the decanol:LG molar ratio on W/W emulsions droplets size evolution with time. Confocal microscopy images of the W/W emulsions taken at t=0 (left) and at t=24h (right) for two different decanol: LG molar ratios: R = 2:1 and R = 9:1, at the same LG concentration (12 mM). Droplets are labeled with FITC-dextran dye. The scale bar represents 15 μm.

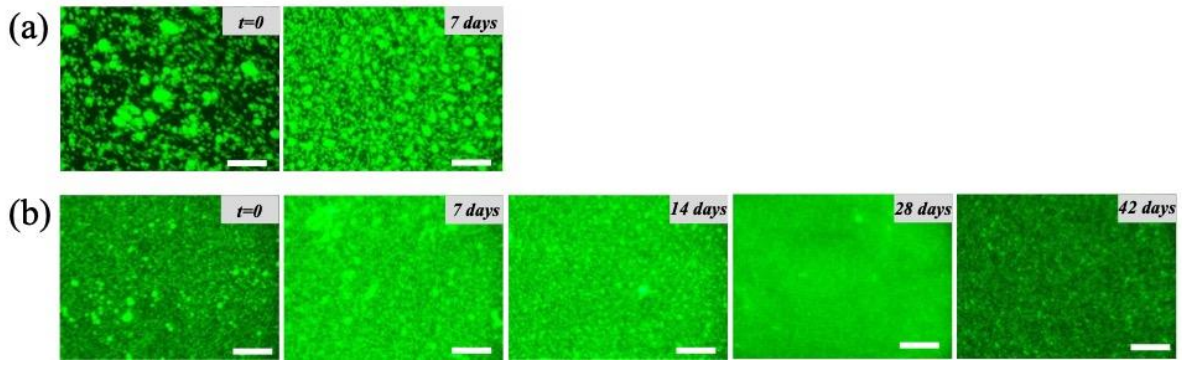

Supplementary Figure 4. Long-term stability of W/W emulsions. (a) Epifluorescence microscopy images of dextran-in-PEG emulsions stabilized by DG at 12 mM and with a ratio equal to 3:1 (top) showing that small droplets were observed during 7 days. (b) Epifluorescence microscopy images of dextran-in-PEG emulsions stabilized by LG at 12 mM and with a ratio equal to 3:1 (bottom) showing that small droplets were observed during 42 days. Droplets are labeled with FITC-dextran dye. The scale bar represents 60 μm.

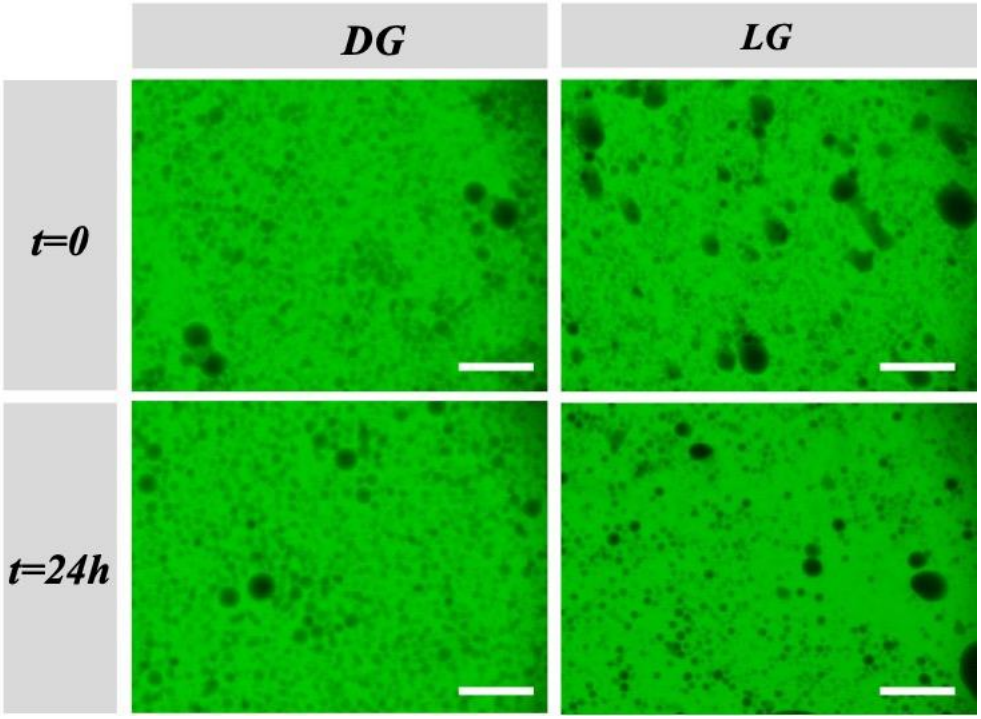

Supplementary Figure 5. Epifluorescence microscopy images of the inverse emulsion PEG-in-dextran stabilized with DG at 12mM and with a molar ratio equal to 3:1 (left) and LG at 12 mM and with a molar ratio equal to 3:1 (right), taken at t=0 (top) and at t=24h (bottom). The continuous phase is labeled with FITC-dextran dye. The scale bar represents 60 µm.

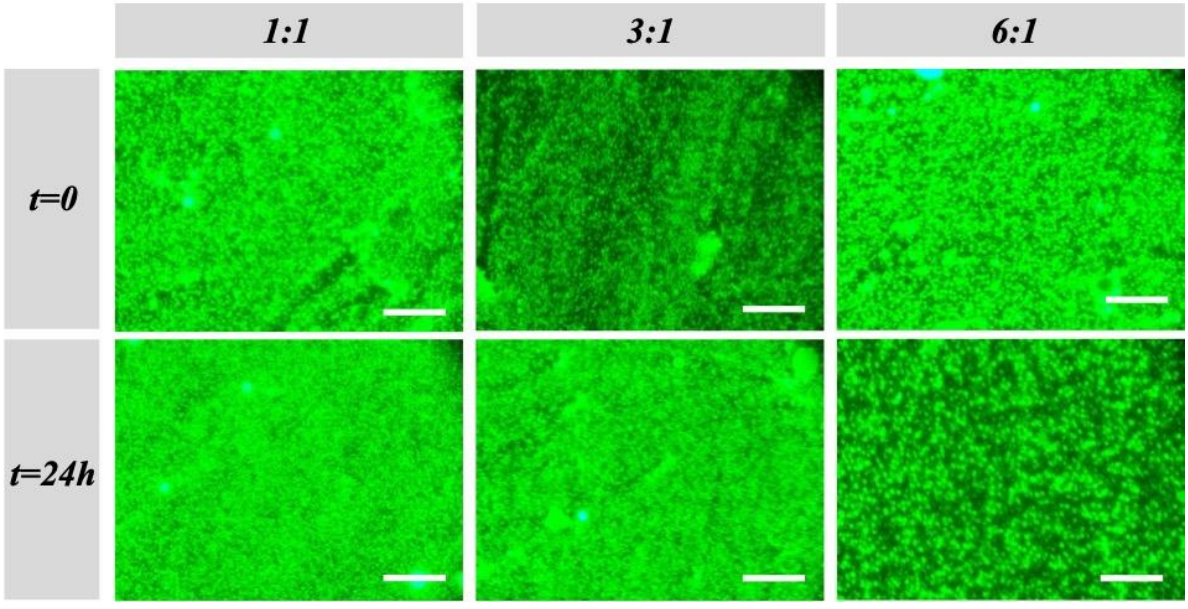

Supplementary Figure 6. Epifluorescence microscopy images of dextran-in-PEG emulsions stabilized with CG at 12 mM and decanol, at different decanol: CG molar ratios (R) (R=1:1, R=3:1 and R= 6:1, from left to right). Droplets are labeled with FITC-dextran dye. The scale bar represents 60 µm.

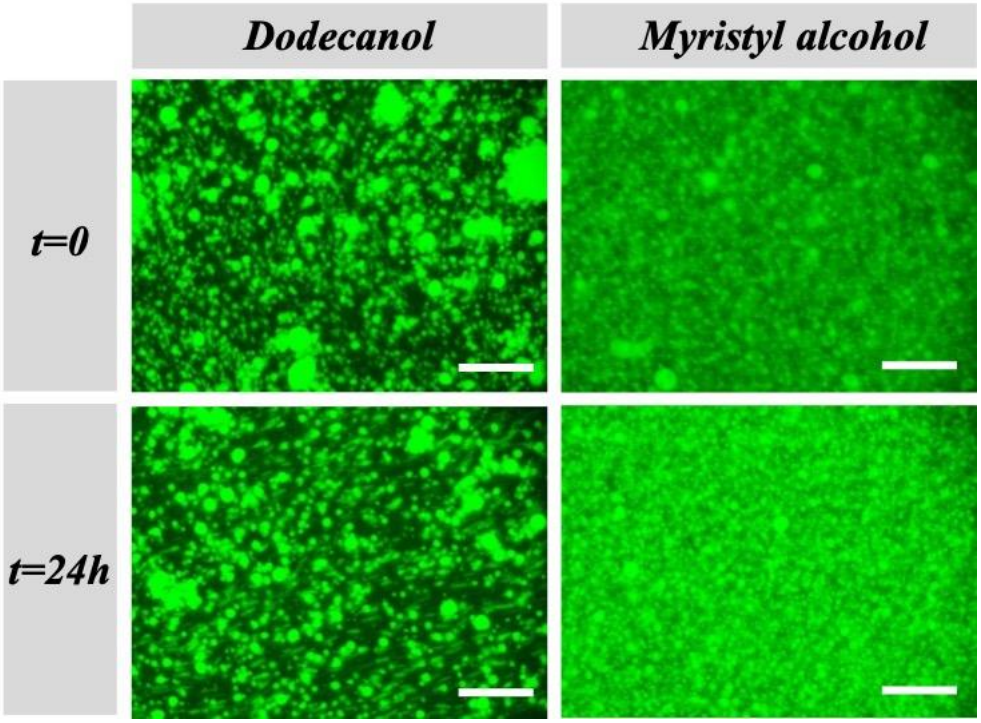

Supplementary Figure 7. W/W emulsions stabilized with LG in combination with two different fatty alcohols: dodecanol and myristyl alcohol. Epifluorescence microscopy images of W/W emulsions stabilized with LG at 12 mM and dodecanol: LG molar ratio equal to 6:1 (left) and LG at12 mM and myristyl alcohol: LG ratio equal to 6:1 (right), taken at t=0 (top) and at t=24h (bottom). Droplets are labeled with FITC-dextran dye. The scale bar represents 60 µm.

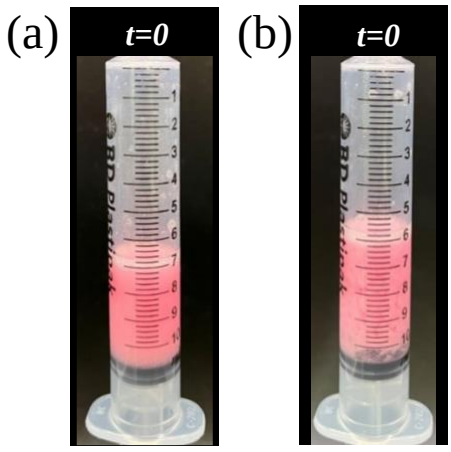

Supplementary Figure 8. Foam production: (a) without the addition of surfactant and (b) with addition of DG at 18 mM. The composition of the W/W emulsion used in both samples correspond to a dextran-in-PEG emulsion (10 wt.% dextran and 10 wt.% PEG) stabilized with LG at 12 mM and decanol:LG molar ratio equal to 3:1.

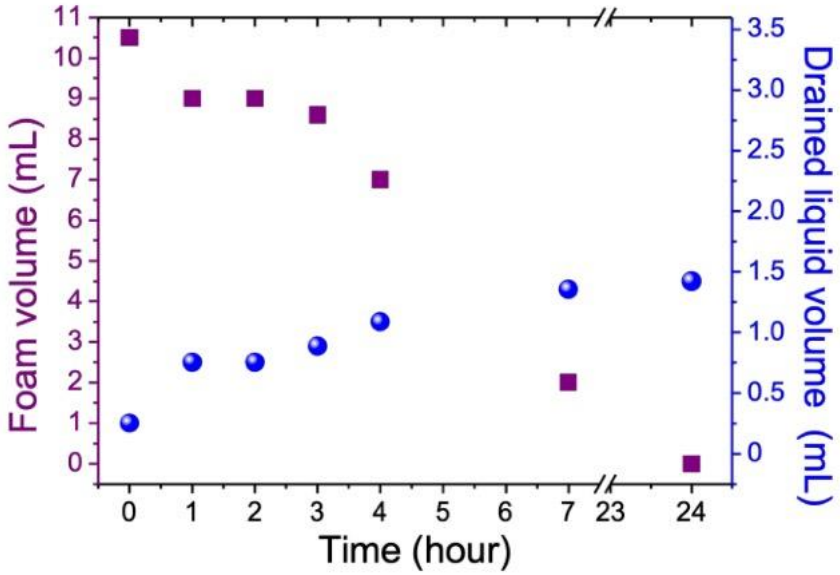

Supplementary Figure 9. Evolution of the foam volume and the liquid drained over time of the foamulsion (dextran 10 wt.%, PEG 10 wt.%, LG at 12 mM, decanol:LG molar ratio equal to 3:1 and SDS at 18 mM).

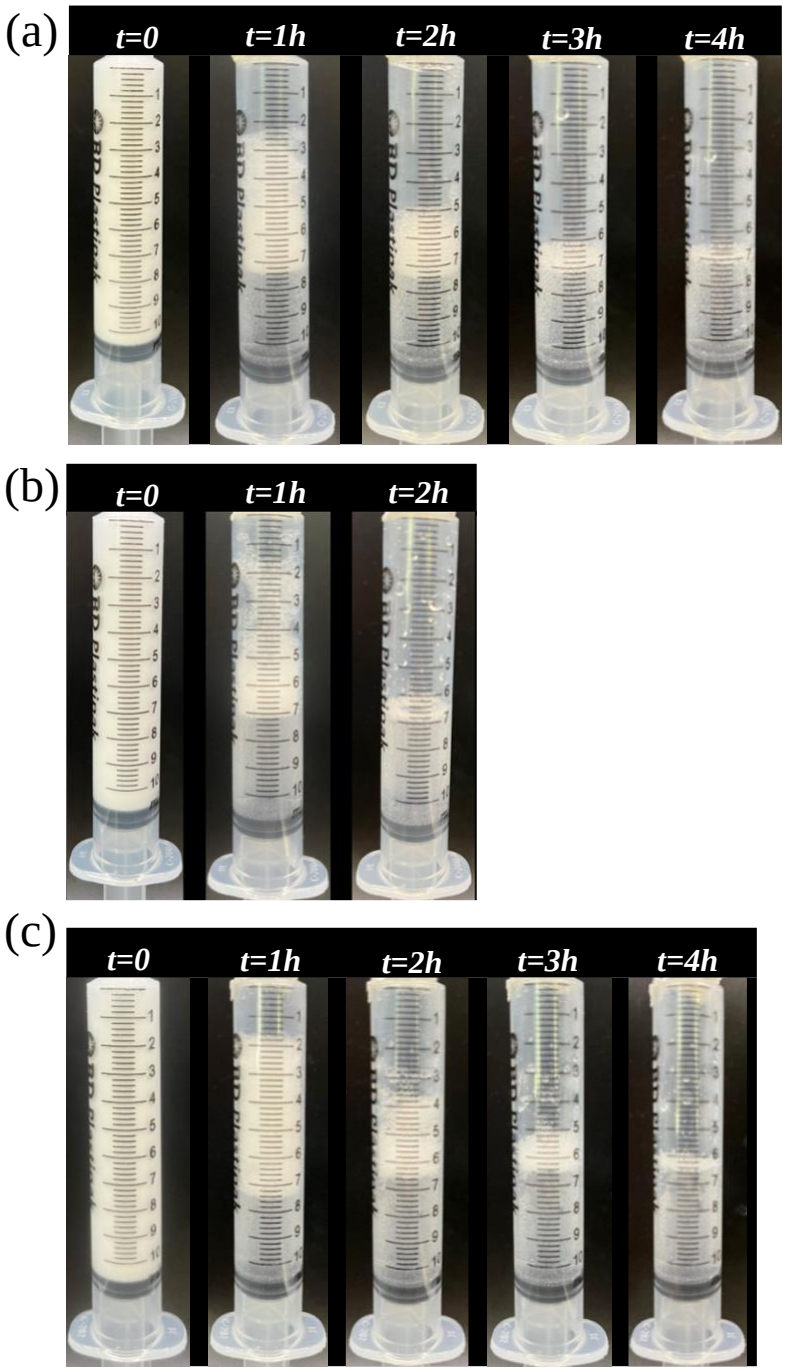

Supplementary Figure 10. (a) Image of the foam produced with Dextran (10 wt. %) and SDS at 18 mM, and its evolution over time. (b) Image of the foam produced with PEG (10 wt. %) and SDS at 18 mM, and its evolution over time. (c) Image of the foam produced with the W/W emulsion (Dextran at 10 wt.% with PEG at (10 wt. %) and SDS at 18 mM without LGNs, and its evolution over time.

Chapter 5: Conclusions and perspectives

5.1 Conclusions

In the food industry, surfaces contaminated with microorganisms are a major source of crosse-contamination in food products (DeFlorio et al., 2021; Midelet et al., 2024). Contamination of food with microorganisms can lead to two major problems: foodborne illness and food waste. Contamination of food with microorganisms can lead to two major problems: foodborne illnesses and food waste. To mitigate these issues, it is essential to implement thorough cleaning and disinfection processes to maintain surface hygiene. However, despite these efforts, the incidence of foodborne illnesses continues to rise each year, indicating that current practices may not be adequate. This underscores the need for ongoing improvements in sanitation protocols, enhanced monitoring, and the adoption of innovative technologies to ensure food safety and reduce waste (Sarno et al., 2021). Furthermore, the cleaning processes used in the food industry consume substantial resources, including vast amounts of water, energy, and chemicals. These resource-intensive practices not only have a significant environmental impact but also contribute to the operational costs of food production. The high consumption of water and energy raises concerns about sustainability, particularly in regions facing water scarcity and high energy costs. Additionally, the use of chemicals, while essential for effective sanitation, can pose risks to both human health and the environment if not managed properly. To address these challenges, the industry is increasingly exploring more sustainable cleaning technologies and practices. Innovations such as dry-cleaning methods, the use of environmentally friendly cleaning agents, and advanced monitoring systems can help reduce resource usage while maintaining high standards of hygiene. Implementing these practices not only helps in minimizing the environmental footprint but also promotes a more sustainable and cost-effective approach to food safety. (Dallagi, 2022). One potential alternative is the use of foam for cleaning closed surfaces, similar to its application on open surfaces. Foams are widely utilized in the food industry for applying cleaning chemicals to open surfaces (EHEDG, 2021). However, the specific mechanisms by which foams clean are not fully understood. Despite this, foams offer promising environmental benefits, as they can potentially reduce the consumption

of water, energy, and chemicals required for cleaning (Dallagi et al., 2022). The objective of this thesis was to investigate the properties of foams that contribute to the removal of microorganisms on both open and closed surfaces, aiming to utilize foams as an environmentally friendly cleaning method. Additionally, the research sought to propose alternative and innovative cleaning techniques. By advancing our understanding of foam cleaning mechanisms and optimizing their application, this work could pave the way for more sustainable and efficient cleaning methods in the food industry.

Foams have on their own a cleaning action on open surfaces contaminated with spores under static conditions.

Based on our results on two different foam systems and comparisons with existing literature, we estimate that when spores are strongly adhered to surfaces, foams can achieve a maximum removal rate of about 2 logs for hydrophilic spores. The removal efficiency is lower for hydrophobic spores due to the presence of clusters, which complicates the cleaning process. We suppose that the main mechanism of foam-based removal is wiping. Bubble size appears to play a crucial role, with smaller bubbles (around 20-50 µm) providing better cleaning efficiency compared to larger bubbles (above 100 µm). The liquid fraction of the foam does not seem to significantly influence the cleaning efficiency on its own. The effectiveness of foam cleaning improves significantly when spores are dispersed in a liquid and not strongly adhered to surfaces. In such cases, the foam's imbibition mechanism becomes effective, achieving a high removal efficiency of around 4 logs for both hydrophilic and hydrophobic spores.

Additionally, we demonstrated that foams can be formulated with bio-based surfactants, such as 10-HSA soap and SCI surfactant. Our research provided valuable insights into the self-assembly properties of these surfactants, which are crucial for formulation purposes. We showed that aqueous dispersions of 10-HSA soap can produce foams with a destabilization threshold temperature triggered by the tube-to-micelle transition. For SCI surfactant, we

demonstrated that it forms crystals below the Kraft temperature and self-assembles into negatively charged micelles above this temperature.

Foams flow cleaning can be achieved with various bio-based surfactants, leading to a decrease of environmental footprint.

We demonstrate that foams based on SDS and APGs at their respective CMC concentrations can effectively remove hydrophilic spores from pipes. Furthermore, our findings indicate that foams formulated with alkyl polyglucosides exhibit superior stability when passing through pipes compared to those produced with SDS. This stability could be advantageous when cleaning more complex installations. Additionally, through a life cycle assessment (LCA), we show that foams based on alkyl polyglucosides contribute to a reduction in environmental impacts during the cleaning process compared to those based on SDS. Finally, we demonstrated that filtration can effectively remove spores from the surfactant solutions of both SDS and APGs, allowing for the surfactant to be reused.

Water-in-water emulsions and foamulsion can be stabilized by lamellar gel networks and could be used as possible alternative and innovative cleaning methods

We demonstrated that W/W emulsions can be stabilized using mixtures of APGs and long-chain fatty alcohols. These mixtures form lamellar phases both in the bulk and at the interface surrounding the droplets. By varying the concentration of APGs and the molar ratio between the fatty alcohol and the APGs, we achieved emulsions with different droplet sizes. Additionally, we showed that the long-term stability of the emulsions depends on the type of APG used, maintaining stability for at least 42 days. These findings, supported by centrifugation tests, highlight the robustness of APG and decanol-based lamellar gel networks (LGNs) in stabilizing the droplets. Moreover, our preliminary results demonstrate, for the first time, the production of a foamulsion with a w/W emulsion as the continuous phase. This foamulsion exhibits enhanced stability compared to foams of the same composition without the w/W emulsion stabilized by LGNs. W/W emulsions are an emerging field, with new stabilization

methods continually leading to novel applications. Singh et al, have demonstrated the encapsulation of bacteria in W/W emulsions (Singh et al., 2018). In addition, we did some preliminary tests showing different affinities of bacteria for the W/W emulsion phases (**Figure 5.1.1**); that is why we believe that using this two phase system could be an innovative way to remove spores and bacteria.

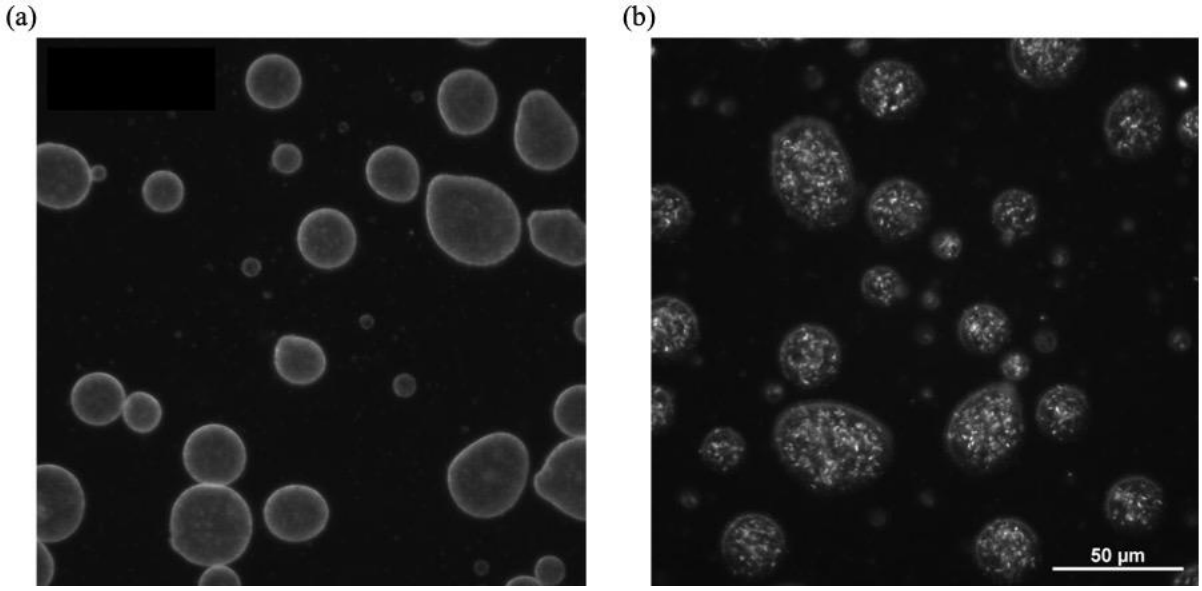

Figure 5.1.1. (a) *Escheria coli* at the interface surrounding the droplets of a dextran-in-PEG emulsion. (b) *Bacillus subtilis* encapsulated inside the droplets of dextran-in-PEG emulsion.

5.2 Perspectives

Effect of the surface and contamination types:

For both static and dynamic cleaning conditions, the influence of surface nature and roughness on cleaning effectiveness is well-established (Faille et al., 2002; Deleplace et al., 2022). Future studies could explore the cleaning efficiency on surfaces differing in roughness and hydrophobicity from stainless steel, such as glass or polypropylene (Deleplace et al., 2022). Additionally, further research could investigate cleaning efficacy against various types of microbial contamination, including biofilms. Given the diverse compositions of biofilms, it would be valuable to assess how cleaning efficiency varies across different biofilm types (Dallagi et al., 2022). In this thesis, we only focused on static foam cleaning on horizontal surfaces. Future studies could examine the effectiveness of cleaning on vertically surfaces, where the foam might behave differently, potentially affecting its cleaning efficiency (Le Toquin, 2018). In our experiments, we used foams with no drainage to remove this parameter. However, as demonstrated in other studies, the drainage has an effect on cleaning. Future experiments could be conducted with foam with different drainage rate to study the effect of the drained liquid on the removal of spores and biofilms.

Improving the foam cleaning efficacy trough the foam formulation:

In foam flow, friction occurs in the film between the bubbles and the surface (Denkov et al., 2006). Dame et al, demonstrated that the addition of co-surfactant to the foam formulation extends the film life and that decontamination is improved in foam flows for nuclear decontamination (Dame et al., 2005). In our work, it would be interesting to investigate different formulations that include the addition of co-surfactant to improve cleaning efficiency. The addition of co-surfactants allows to modify the surface mobility of the bubbles from moving to immobile surfaces, which results in an increase in the viscous stress. Moreover, the next step would be to combine the physical action of the foam with a chemical action to improve foam cleaning by adding disinfectant such as: Sodium hypochlorite (NaOCl) and hydrogen peroxide

(H2O2) (Le Toquin, 2018). Following the line of interface-based cleaning methods, it would be interesting to investigate the effects of incorporating a water-in-water emulsion into foam, creating a foamulsion, and to evaluate its efficacy in cleaning surfaces contaminated with microorganisms.

5.3 References

Dallagi, H. (2022). Numerical and experimental investigations of the rheological behavior of foam flow: application to the cleaning of surfaces contaminated by microorganisms in the food industries.

Dallagi, H., Faille, C., Gruescu, C., Aloui, F., and Benezech, T. (2022). Foam flow cleaning, an effective and environmentally friendly method for controlling the hygiene of closed surfaces contaminated with biofilms. Food and Bioproducts Processing, S0960308522001134. doi: 10.1016/j.fbp.2022.09.014

Dame, C., Fritz, C., Pitois, O., and Faure, S. (2005). Relations between physicochemical properties and instability of decontamination foams. Colloids and Surfaces A: Physicochemical and Engineering Aspects 263, 210–218. doi: 10.1016/j.colsurfa.2004.12.053

DeFlorio, W., Liu, S., White, A. R., Taylor, T. M., Cisneros-Zevallos, L., Min, Y., et al. (2021). Recent developments in antimicrobial and antifouling coatings to reduce or prevent contamination and cross-contamination of food contact surfaces by bacteria. Comp Rev Food Sci Food Safe 20, 3093–3134. doi: 10.1111/1541-4337.12750

Deleplace, M., Dallagi, H., Dubois, T., Richard, E., Ipatova, A., Bénézech, T., et al. (2022). Structure of deposits formed by drying of droplets contaminated with Bacillus spores determines their resistance to rinsing and cleaning. Journal of Food Engineering 318, 110873. doi: 10.1016/j.jfoodeng.2021.110873

Denkov, N. D., Tcholakova, S., Golemanov, K., Subramanian, V., and Lips, A. (2006). Foam–wall friction: Effect of air volume fraction for tangentially immobile bubble surface. Colloids and Surfaces A: Physicochemical and Engineering Aspects 282–283, 329–347. doi: 10.1016/j.colsurfa.2006.04.028

EHEDG (2021). Doc. 52 Basic Principles of Cleaning and Disinfection in Food Manufacturing.

Faille, C., Jullien, C., Fontaine, F., Bellon-Fontaine, M.-N., Slomianny, C., and Benezech, T. (2002). Adhesion of Bacillus spores and Escherichia coli cells to inert surfaces: role of surface hydrophobicity. Can. J. Microbiol. 48, 728–738. doi: 10.1139/w02-063

Le Toquin, E. (2018). Mode d'action biocide de nouveaux procédés de décontamination sur deux formes de résistances bactériennes. Normandie. Available at: https://theses.fr/2018NORMR103 (Accessed April 12, 2024).

Midelet, G., Brauge, T., and Faille, C. (2024). "Contamination croisée des aliments par des surfaces contaminées," in Contrôle et Prévention des Risques Biologiques Associés à la Contamination des Aliments : Transformation, Distribution et Utilisation par le Consommateur, (ISTE Editions). Available at: https://hal.univ-lille.fr/hal-04456514 (Accessed February 14, 2024).

Sarno, E., Pezzutto, D., Rossi, M., Liebana, E., and Rizzi, V. (2021). A Review of Significant European Foodborne Outbreaks in the Last Decade. Journal of Food Protection 84, 2059–2070. doi: 10.4315/JFP-21-096

Singh, P., Medronho, B., Miguel, M. G., and Esquena, J. (2018). On the encapsulation and viability of probiotic bacteria in edible carboxymethyl cellulose-gelatin water-in-water emulsions. Food Hydrocolloids 75, 41–50. doi: 10.1016/j.foodhyd.2017.09.014